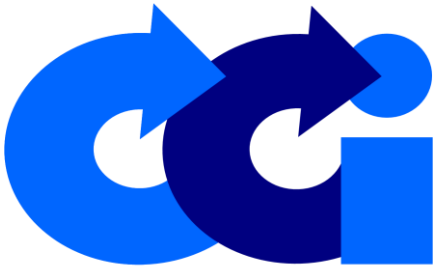

Investigations into the Direct Synthesis of Hydrogen Peroxide and CO Oxidation Using Precious Metal Catalysts

Thesis submitted in accordance with the requirements of the University of Cardiff for the degree of doctor of philosophy by

Simon James Freakley

School Of Chemistry

Cardiff University

2012

DECLARATION

This work has not been submitted in substance for any other degree or award at this or any other university or place of learning, nor is being submitted concurrently in candidature for any degree or other award.

Signed …… (candidate) Date ……

STATEMENT 1

This thesis is being submitted in partial fulfilment of the requirements for the degree of ……

Signed …… (candidate) Date ……

STATEMENT 2

This thesis is the result of my own independent work/investigation, except where otherwise stated.

Other sources are acknowledged by explicit references. The views expressed are my own.

Signed …… (candidate) Date ……

STATEMENT 3

I hereby give consent for my thesis, if accepted, to be available for photocopying and for inter-library loan, and for the title and summary to be made available to outside organisations.

Signed …… (candidate) Date ……

STATEMENT 4: PREVIOUSLY APPROVED BAR ON ACCESS

I hereby give consent for my thesis, if accepted, to be available for photocopying and for inter-library loans **after expiry of a bar on access previously approved by the Academic Standards & Quality Committee.**

Signed …… (candidate) Date ……

Summary

The direct synthesis of hydrogen peroxide from molecular hydrogen and oxygen represents an attractive atom efficient alternative to the current industrial auto-oxidation process which relies on the sequential oxidation and reduction of an anthraquinone. The first and most widely studied catalysts for this reaction were palladium based however over-hydrogenation of the synthesised hydrogen peroxide is a problem. Recent advances demonstrate that the addition of gold to the catalyst has been shown to significantly improve the productivity of the catalysts by suppressing the hydrogenation and decomposition activity. The work in this thesis shows that tin can be used as a catalyst additive as a direct replacement for gold by a simple impregnation method. By tuning the heat treatments of these bimetallic tin-palladium catalysts it was possible to switch off the competing hydrogenation and decomposition reactions. The construction of a small scale flow system has allowed the independent study of reaction variables and the determination of global kinetics and rate constants for the synthesis and subsequent reactions. It was shown that in a flow system it was the decomposition reaction that had a greater limiting effect on the production of hydrogen peroxide than the hydrogenation reaction. A study was also carried out into CO oxidation using gold / iron oxide catalyst prepared in Cardiff and by Prof. Haruta's group in Tokyo. These catalysts underwent extensive tests to try and identify the active species of the catalyst. Detailed testing and STEM characterisation of the samples identified the possibility of different mechanisms operating at different temperatures and no correlation between the nanoparticle population and activity at sub ambient temperature could be made which challenges the hypothesis that nanoparticles are the most active species and that sub nanometer clusters may be the active species at low temperatures.

Abstract

The research presented in this thesis describes investigations into two precious metal catalysed reactions; the direct synthesis of hydrogen peroxide from molecular hydrogen and oxygen and the oxidation of carbon monoxide.

The direct synthesis of hydrogen peroxide from molecular hydrogen and oxygen offers a much greener and sustainable approach when compared to the current industrial anthraquinone process and the work presented in this thesis examines some of the key factors in determining if the process will be viable, with the study focussing on producing a cheaper catalyst and also understanding the reaction in a continuous flow system.

The first part of this thesis aims to identify a replacement for Au in the typical Au-Pd bimetallic catalysts used for this reaction. The work carried out in this thesis shows that tin can be used as a catalyst additive as a direct replacement for gold. By tuning the heat treatments of catalysts prepared by a simple impregnation method the activity of bimetallic tin-palladium catalysts could be tuned to switch off the competing hydrogenation and decomposition reactions. The development of these low hydrogenation catalysts which were comparable in activity to the Au-Pd analogues and stable on commercial supports such as TiO_2 and SiO_2 represents a major milestone.

The second part of this thesis reports the construction and operation of a small continuous flow reactor to study independently the reaction variables and also allow the the determination of global kinetics and rate constants for the synthesis and subsequent reactions using a standard Au-Pd catalyst. It was shown that in a flow system is was the decomposition reaction that had a greater limiting effect on the production of hydrogen peroxide than the hydrogenation reaction and a global kinetic model was shown to agree well with experimental results

The third section of this thesis reports an investigation into Au / FeO_x catalysts for CO oxidation in collaboration with Prof. Haruta and Prof Kiely. STEM analysis of a range of catalysts was carried out along with kinetic studies and it was identified that different mechanisms may be operating at different temperatures. No correlation between the nanoparticle population and activity at sub ambient temperature could be made which challenges the hypothesis that nanoparticles are the most active species and actually sub nanometer clusters may be the active species at sub ambient temperatures.

Acknowledgements

First of all I would like to thank Professor Graham Hutchings for his advice, guidance and support during the 3 years of my PhD.

I would also like to thank Dr Edwin Ntainjua for helping me to get started in Cardiff, teaching me the basics in the lab and instilling me with a small percentage of his work ethic. I would also like to thank Dr Jennifer Edwards for her supervision, advice and careful corrections of this thesis. I would like to thank Dr Albert Carley and Dr Dave Morgan for their running and interpretation of XPS data along with Prof Chris Kiely and his staff, especially Qian He, for the amazing STEM images. I would like to gratefully acknowledge Prof. Jacob Moulijn for his advice regarding flow reactors and to Prof. Masatake Haruta for helping me to work in and explore Japan during my PhD.

I would like to thank all of the PhDs and post docs who have worked alongside me, I'm sure you have all answered my questions at some point. I would especially like to thank the hydrogen peroxide team, especially my predecessors Marco and James for all of your help in the lab.

I gratefully acknowledge everybody from the workshop who showed extreme patience in fixing and explaining any equipment that I broke or didn't understand. Especially Steve Morris who was able to build things from my scribbled drawings and repair things quicker than I thought possible.

Many thanks to all my friends and housemates in Cardiff for the laughs and nights out, especially the residents of 86 North Road, who made for an interesting first year in Cardiff.

A special thanks to Kaz, firstly for putting up with me talking about chemistry and finally for proof reading most of this thesis to make sure it made sense.

Most importantly I would like to thank my family, my grandparents and especially my parents who have supported me all the way through my university life, even when you thought what I was learning looked like an alien language.

Table of Contents

Chapter 4 - Direct Synthesis of H_2O_2 in a Gas Liquid Flow System

Chapter 1

1. Introduction

In this chapter the principles of catalysis are introduced along with the catalytic systems subsequently discussed and investigated in this thesis.

1.1 - Catalysis: Definitions and Basic Concepts

Catalysis is vital to modern society in many ways, for example without the production of ammonia by the Haber-Bosch process which leads to the manufacture of artificial fertilisers, the world's food production would only be able to sustain half of the current population.[1] The chemical industry is heavily reliant on the field of catalysis as the vast majority of chemical products are produced using some form of catalytic process.

A high proportion of these catalysed reactions are carried out using an heterogeneous catalyst, this means that the catalyst is in a different phase than the reactants. Typically this involves a solid catalyst with the reactant and products in the gas or liquid phase. The definition of a catalyst is a substance that increases the rate of a reaction without affecting the overall change in standard Gibbs energy of the reaction.[2] The ability of a catalyst to increase this reaction rate is of enormous benefit to industry as the rate of many reactions is essentially zero under conditions where the reaction is thermodynamically favourable. The rate of these reactions is essentially zero because of a large energy barrier associated with a reaction intermediate or transition state,

called the activation energy (E_a). The catalyst can enhance the reaction rate by reducing this activation barrier by means of providing a lower energy pathway for the reaction to take place, possibly through several intermediates or transition states as seen in figure 1.1.

.

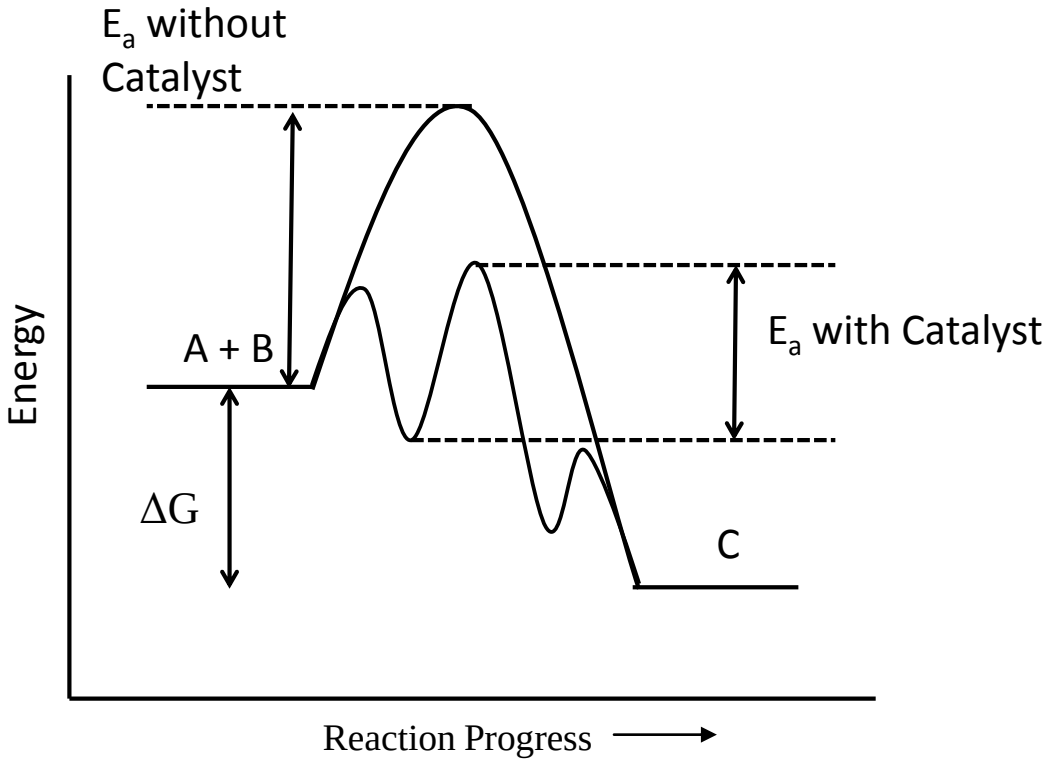

Figure 1.1 – Energy level diagram to compare the difference in activation energy between a catalysed and un-catalysed reaction of A + B to give product C.

E_a = activation energy ΔG = change in Gibbs free energy

As shown in figure 1.1 the catalysed reaction pathway is more energetically favourable because of the lower activation barriers, however this pathway may contain more reaction steps and intermediates than the un-catalysed reaction. The activation barrier in all these steps is significantly lower than the activation barrier of the un-catalysed reaction which is the reason for the much higher reaction rate in the presence of a catalyst. As can be seen from figure 1.1, a catalyst does not alter the thermodynamics of a reaction. The overall Gibbs free energy (ΔG) of a reaction is the same for catalysed and un-catalysed reactions, it is only the rate of reaction that is enhanced by a catalyst.

The overall catalytic process can typically be divided into a number of elementary steps, including adsorption of the reactants onto the catalyst surface, breaking or weakening of reactant bonds, reaction to form products and finally desorption of the products, which ideally leaves the catalyst unaltered and ready for a new reaction cycle. These steps are shown on the energy diagram in figure 1.2.

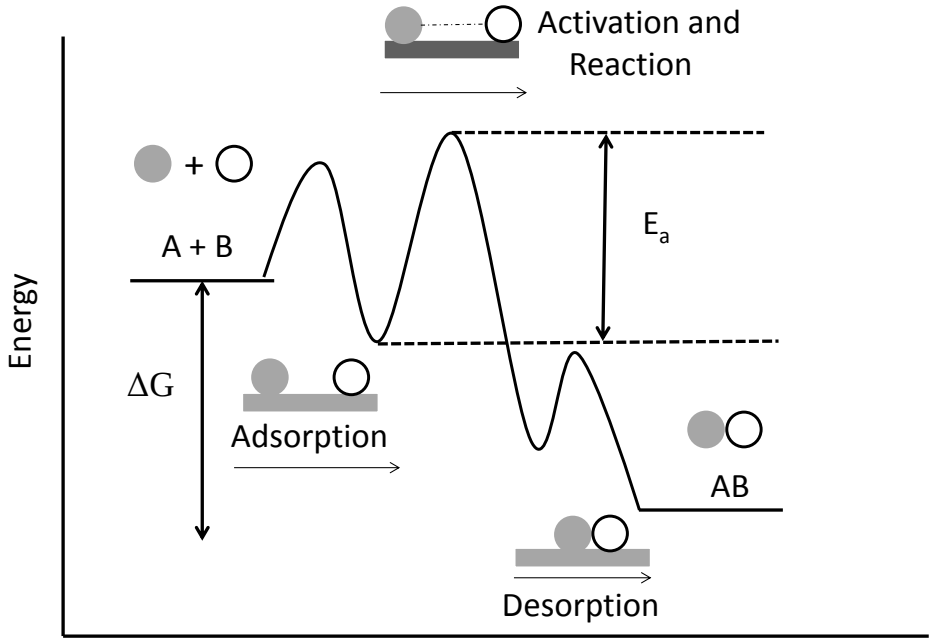

Figure 1.2 - Energy level diagram to show the possible steps in a catalysed reaction of A + B to give AB.

A heterogeneous catalyst provides a surface or active site on which the reactants can be brought together in such a way so as to react to give the desired product and consequently the activity of a catalyst scales with the number of active sites. These active sites are often provided by a precious metal such as platinum or palladium. To achieve a high number of active sites and to keep the total amount of precious metal low, the precious metals are often dispersed as nanoparticles on high surface area supports, such as alumina or silica.

1.2 - Hydrogen Peroxide

Hydrogen peroxide is a simple inorganic molecule and since its discovery by Louis Jacques Thénard in 1818, hydrogen peroxide (H_2O_2) has become an extremely important commodity chemical with both industrial and domestic uses. Domestically, H_2O_2 is contained in household bleaches and hair dyes at around 5 wt% and can also be used in lower concentrations as a

sterilant for cleaning wounds and water purification. In 2006 the annual production of H_2O_2 stood at around 4 million metric tonnes increasing by 4% annually.[3] Around 40% of H_2O_2 is used in the pulp and paper industry as an alternative to chlorine containing oxidants such as chlorine dioxide and sodium chlorate.[4] H_2O_2 is also used as an oxidant in the synthesis of a number of organic and inorganic chemicals and since the development of TS-1, a titanium silicate catalyst, several oxidation reactions using H_2O_2 in bulk processes have now been achieved, such as the oxidation of thioethers and sulfoxides[5], epoxidation of propene[6, 7] and cyclohexane oxidation.[8] Another major use is in water purification where H_2O_2 has been shown to destroy thiocyanate, nitrate, chlorine, hypochlorite and other potentially toxic chemicals which may be present in waste water.[9] Oxidation by H_2O_2 is considered to be a greener alternative compared to other bulky oxygen donors such as sodium perborate, metallic peroxides and percarboxylic acids which are less atom-efficient and have less environmentally friendly by-products. As the only by-product of oxidation by H_2O_2 is water it can be seen as an atom efficient environmentally friendly oxidant.

1.3 – Auto-oxidation (Anthraquinone) Process

Over 90% of the world's H_2O_2 is manufactured by the indirect anthraquinone process, otherwise known as the auto-oxidation process, which was developed during the 1930's to meet increasing H_2O_2 demand. The indirect synthesis of H_2O_2 by the sequential oxidation and hydrogenation of alkyl anthraquinones was first developed by Ridel and Pfleiderer in 1939.[10-12] The anthraquinone process involves the hydrogenation of a substituted anthraquinone using a nickel or palladium catalyst to form a diol. The diol is then oxidised by an O_2 rich air feed to reform the original anthraquinone and give H_2O_2 as a by-product. The process is based on the work of Manchot[13] who showed that hydroquinone and hydrobenzenes undergo auto-oxidation in alkaline conditions to produce peroxides. The process is summarised in the scheme shown in figure 1.3.

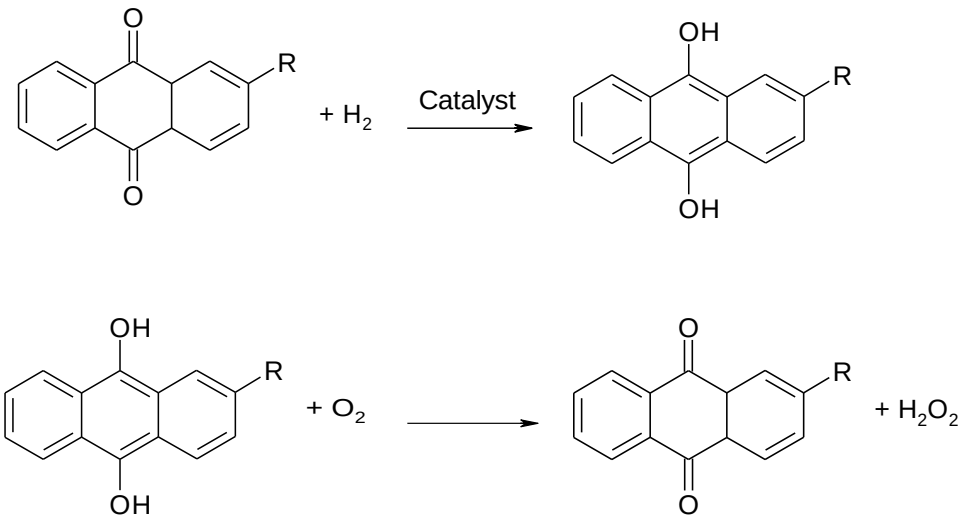

Figure 1.3 - Schematic of the industrially used auto-oxidation process to make H_2O_2.

Currently the anthraquinone process accounts for the majority of H_2O_2 produced industrially, with plants capable of producing up to 120,000 metric tonnes of concentrated H_2O_2 per year.[14] While this process is now large scale and energy efficient, there remain a number of problems associated with the anthraquinone process. The anthraquinone process is only viable on a large scale which means that concentrated H_2O_2 (70 wt%) solutions need to be stored and transported which can be hazardous, and the solutions may require the addition of acid or halide as stabilisers. While the process is operated at mild temperature and pressure, anthraquinone derivatives can be formed irreversibly which do not participate in the formation of H_2O_2. This means that the original anthraquinone molecule needs to be continually added to maintain the efficiency of the system. The use of a highly active hydrogenation catalyst can also result in the decomposition of the anthraquinone again reducing the efficiency of the system. In terms of the safety of the process the relatively mild conditions and the facility to keep H_2 and O_2 apart greatly reduces the chance of working in the explosive region.

The fact that an environmentally friendly oxidant is made this way when typical applications require 3-5 wt% H_2O_2 solutions has prompted research and development into more efficient, small-scale widespread synthesis routes to produce H_2O_2 at lower market value.

1.4. Direct Synthesis of H_2O_2

The direct synthesis of H_2O_2 by the combination of molecular H_2 and O_2, removing the need for an anthraquinone intermediate would provide a much greener route to H_2O_2 as the reaction would be 100% atom efficient. The first patent for the direct synthesis of H_2O_2 was granted to Henkel and Weber in 1914,[15] however the process has not yet been commercialised. While the combination of molecular H_2 and O_2 seems conceptually a simple reaction there are inherent problems associated with the process. The biggest of these problems is that catalysts which are active for the synthesis of H_2O_2 (1) also tend to be active for the hydrogenation (2) of H_2O_2 and the direct combustion of H_2 and O_2 (4), both reactions producing water as shown in figure 1.4. Also as H_2O_2 is an unstable molecule the product can decompose (3) into water after being synthesised. This decomposition reaction can also be catalysed by the same catalyst used to synthesise the H_2O_2.

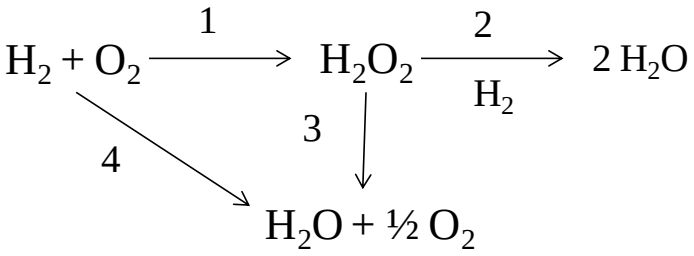

Figure 1.4 - Reaction scheme for the direct synthesis of H_2O_2.

$\Delta G_1 = -120$ kJ mol^{-1}

$\Delta G_2 = -354$ kJ mol^{-1}

$\Delta G_3 = -117$ kJ mol^{-1}

$\Delta G_4 = -237$ kJ mol^{-1}

The parallel combustion and subsequent hydrogenation and decomposition reactions all form water meaning that the efficient utilisation of H_2 towards the synthesis of H_2O_2 in this process represents a major problem. The subsequent hydrogenation and combustion reactions are also catalysed by the same catalyst that activates H_2 for the synthesis reaction.[16,17] Stopping the competing reactions to improve H_2 efficiency represents a major challenge. There are a number of ways to overcome the problem of selectivity in the direct synthesis of H_2O_2, for example

decreasing the reaction temperature or contact time with the catalyst. Also the addition of chemical additives such as acid and halide can decrease the rates of subsequent and competing water forming reactions and these approaches will be discussed later in this chapter.

Another reason that the process has not been commercialised nearly 100 years after its discovery is that H_2 / O_2 high pressure gas mixtures carry an inherent hazard because they are explosive over a wide range of compositions (5 – 95% vol H_2 at ambient temperature). To improve safety the reactant gases need to be diluted with an inert gas, such as N_2, to allow work below the lower explosive limit. This dilution of reactants can limit the amount of H_2O_2 it is possible to make.

1.4.1 - Direct Synthesis of H_2O_2 using Palladium Catalysts

Many research groups have worked on the development of catalysts for the direct synthesis of H_2O_2 so it is hard to standardise and compare results due to the different reaction set ups. The variable factors include reactor type (batch or flow), temperature, solvent system (organic or aqueous), pressure, ratio of H_2 to O_2, additives (acid or halide) and reaction time. All these variables need to be considered before attempting to assess the effectiveness of different catalysts and preparation methods on the direct synthesis of H_2O_2. Despite this, general trends can be extrapolated from various data sets and general conclusions drawn about effective catalyst systems.

Since 1914 when it was first shown that Pd could be used as an effective catalyst for the direct synthesis of H_2O_2[15] the vast majority of catalytic studies have remained focused on Pd as the catalytic species. Early studies tended to use gas compositions that were in the explosive region to produce as much H_2O_2 as possible at a high rate. Using these explosive gas mixtures at elevated pressure in the presence of a palladium catalyst meant that high concentrations of H_2O_2 could be made (35 wt%) however the operation of such a process commercially would be extremely problematic in terms of safety.[18]

1.4.1.1 - Acid Addition

In 1961 Pospelova showed in a seminal study that the addition of acids such as HCl and HNO_3 were essential to achieve high productivities when using palladium catalysts to synthesise

H_2O_2.[19-21] The addition of acid to the reaction medium improves the yield of H_2O_2 by suppressing the base catalysed decomposition reaction.

A study by Choudhary compared a series of acids as reaction stabilisers to suppress the decomposition activity for a 5 wt% Pd / C catalyst in an aqueous reaction medium.[22] The acids tested included mineral acids, such as phosphoric acid, and a series of halide acids and it was suggested that the nature of the anion present resulted in an increase in H_2O_2 productivity for different reasons. Non-coordinating ions such as phosphate, nitrate and sulphate are thought not to block any active palladium sites during the reaction, so only a decrease in the decomposition reaction was seen leading to higher selectivity. Conversely direct synthesis in a reaction medium containing a halide acid showed a decrease in H_2 conversion but an increased selectivity towards H_2O_2. This indicates an additional role being played by the halide ion in solution by the additional suppression of the hydrogenation reaction.

1.4.1.2 - Halide Addition

The effect of adding halide into the reaction medium and by incorporation into the catalyst during preparation has been extensively studied.[22-34] Studies with Pd catalysts on a range of supports: ZrO_2, Ga_2O_3, CeO_2, SiO_2 and Al_2O_3 showed that the addition of halides, in particular Cl^- and Br^- had a beneficial effect (at low concentrations) on the direct synthesis of H_2O_2 when acid was also present in the reaction medium. The improved productivity and selectivity caused by halide incorporation as a metal salt in the reaction medium were shown to be of similar magnitude to catalysts with halide incorporated into the catalyst preparation. The nature of the halide in the reaction medium was found to reduce H_2 conversion in the descending order KF > no halide > KCl > KBr for a Pd / CeO_2 catalyst.[35] This order was reversed when selectivity was examined showing reducing selectivity in the order KBr > KCl > no halide > KF. This order of decreasing selectivity showed that F^- additives, whilst increasing H_2 conversion gave the lowest H_2O_2 selectivity, indicating that F^- acts as a promoter for the competing combustion and hydrogenation reactions. The presence of iodide ions was shown to be detrimental to the catalyst activity due to co-ordination of iodide to palladium resulting in surface poisoning.

The increase in selectivity and decrease in H_2 conversion with the addition of a small amount of halide, especially Br^-, is thought to occur through the selective poisoning of the very reactive hydrogenation sites of palladium particles. Burch noted that this trend in catalytic behaviour did

not linearly correlate with electronegativity of the halide series and suggested the reason is due to sigma/pi donation effects with overall co-ordination ability increasing down group 7.[36] Iodide should form strong sigma bonds and fluoride is the best π-donor of the halides. Halides with intermediate sigma/pi donation ability such as Br^- and Cl^- have been shown to enhance transition metal catalysed oxidation reactions. An optimum amount of Br^- is crucial for achieving the maximum yield of H_2O_2 as shown in figure 1.5. Excess Br^- can cause indiscriminate blocking of the remaining catalytic sites, which are still active for the direct synthesis of H_2O_2.

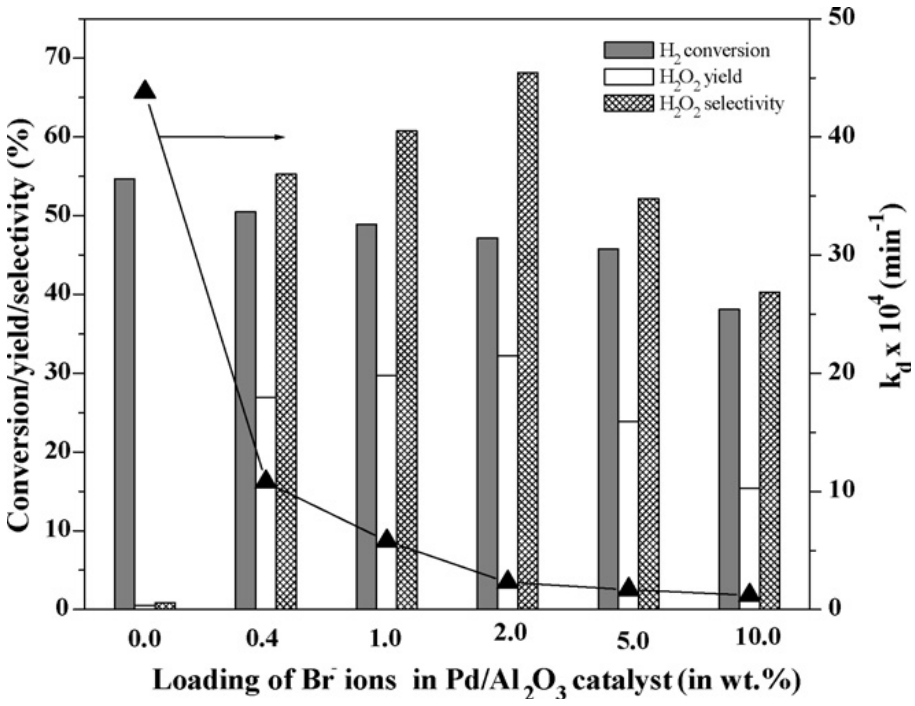

Figure 1.5 - Effect of bromide concentration on H_2O_2 synthesis reaction taken from reference 28.

1.4.1.3 - Palladium Oxidation State

Choudhary *et al.* have extensively studied Pd catalysts for the direct synthesis of H_2O_2.[22-30, 32-34, 37-41] Initial findings showed that reduced palladium catalysts were inactive for the synthesis of H_2O_2 with the combustion reaction being responsible for the high H_2 conversion observed.[23] Subsequent treatment with an oxidising species showed improved H_2O_2 yield due to a higher selectivity towards H_2O_2. The competing decomposition reaction was studied over reduced and oxidised Pd and it was shown that the catalysts with the highest yield tended to be the catalysts

that showed the lowest decomposition rate. The low decomposition rate after oxidation is thought to be due to the presence of PdO on the surface of the particles. It was also shown that to achieve high yields using reduced Pd catalysts it is essential to use halide promoters and an acidic reaction medium as described previously.

Choudhary postulated that the homolytic fission of H_2O_2 over Pd^0 is inhibited by halides. Choudhary demonstrated that oxidised catalysts were less active for the decomposition of H_2O_2 when compared to the reduced palladium catalysts. Hence, the formation of metallic Pd on catalysts during a reaction when under a partial pressure of H_2 could be responsible for the deactivation of the catalyst between catalyst tests. The identification of PdO as the most selective phase is in contrast to the work of Burch and Ellis who reported that Pd^0 was responsible for high selectivity and conversion.[36] The identification of the active species as oxidised or reduced palladium is inherently difficult as the catalyst is under a partial pressure of both H_2 and O_2 during the reaction so it is feasible that both species could co-exist during a reaction.

1.4.1.4 - Colloidal Palladium

While the addition of acid and halide into the reaction mixture has been shown to be necessary to enhance the H_2O_2 selectivity and productivity the acidic nature of the reaction medium may cause the dissolution of Pd from the catalyst support. Work by Lunsford showed that when high concentrations (0.1-1 M) of HCl were added to the reaction mixture $[PdCl_4]^{2-}$ and colloidal Pd were formed by the leaching of Pd from a silica supported catalyst.[42-44] It was shown that even after the catalyst was removed from the system H_2O_2 was still being produced, indicating that the colloidal Pd formed was active for the reaction as a homogeneous catalyst by the mechanism proposed in figure 1.6.

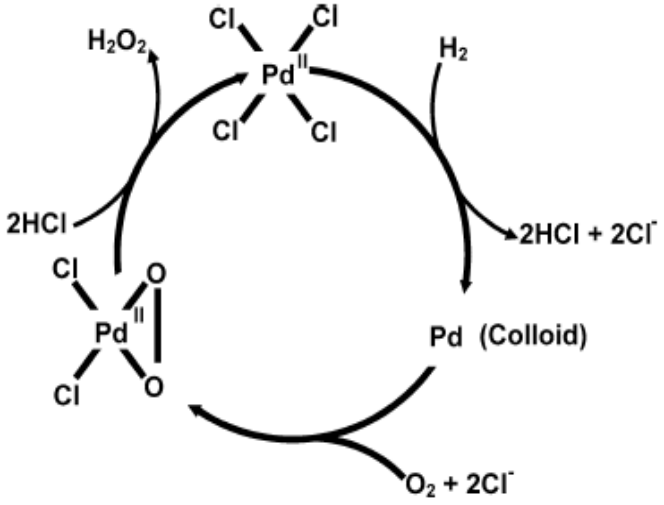

Figure 1.6 - Proposed reaction mechanism for the synthesis of H_2O_2 by colloidal palladium.

The presence of an acid in the reaction medium which could cause dissolution of the active phase along with the reactor internals should be avoided to keep the reaction strictly heterogeneously catalysed. Acidic properties can be introduced to the reaction by other means such as highly acidic catalyst supports including hetropolyacids[45-47] or through surface modification of common catalyst supports like SiO_2 and TiO_2 by groups such as SO_3H[48, 49] which leads to a higher selectivity and yield of H_2O_2 than similar systems containing no acid source.

1.5 - Summary of Critical Factors and Mechanism for H_2O_2 Direct Synthesis

A linear relationship between colloid concentration and H_2O_2 formation rate was observed during time on stream studies, while $^{16}O_2$ / $^{18}O_2$ isotope experiments and Raman spectroscopy confirmed that H_2O_2 is derived from molecularly adsorbed O_2 on the palladium surface.[44] Further testing of different O_2 / H_2 ratios using the colloidal catalytic system indicated that the formation of H_2O_2 was first-order with respect to H_2 and zero-order with respect to O_2. This shows H_2 activation as being the rate limiting step in the synthesis of H_2O_2.[50] Lunsford and Liu also showed that the role of chloride ions in solution is to prevent the O – O bond cleavage. This observation is advantageous for two reasons, firstly it prevents the direct combustion of H_2 and O_2 to form water and secondly it prevents the dissociation of the O – O bond of H_2O_2, hence reducing the hydrogenation and decomposition reactions and increasing selectivity towards H_2O_2.

The solvent system used in the direct synthesis reaction is also critical to the yields of H_2O_2. In the absence of an organic component such as methanol, the reaction proceeds at a very slow rate even if the water is acidified.[51, 52] The slow reaction rates in water only solvents are due to mass transport effects whereby low solubility of H_2 and O_2 limit the concentration of reactants in contact with the catalyst surface therefore limiting the maximum reaction rate. However, the use of an alcohol as the reaction medium can result in high hydrogenation rates at long reaction times due to the high concentration of H_2 in the alcohol. To produce high reaction rates and selectivity towards H_2O_2, careful control of the solvent composition and reaction time is needed.

1.6. Direct Synthesis of H_2O_2 using Gold - Palladium based Catalysts

To commercialise a direct synthesis process to produce H_2O_2 using a palladium catalyst would be problematic because of the additives needed to attain a high reaction rate and selectivity. The palladium catalyst system requires the addition of acid and halide which might be undesirable in the final solution of H_2O_2 if it is to be used in further chemical processes. Therefore a new catalyst system had to be developed that would improve on the efficiency of palladium catalysts. Hutchings *et al.* were the first to demonstrate that Au could be used as a catalyst to synthesise H_2O_2 and in the first case Au / Al_2O_3 was used as a catalyst.[53, 54] The key advance in the design of new catalysts came when it was shown that Au and Pd have a synergistic effect when used to catalyse the direct synthesis of H_2O_2. The addition of other metal additives to Pd / ZrO_2 and Pd / Ga_2O_3 catalysts has been studied by Choudhary *et al.*.[23, 33] They revealed that the addition of Ru and Rh metals decreased H_2O_2 yield, while enhancement was observed for Pt and Au, although the effect of Pt was not as pronounced. The observation that the addition of Au to Pd produced more active catalysts agrees with the observation by Corma[55, 56] that hydroperoxy species have been observed experimentally, and therefore stabilised with respect to Pd, on gold catalysts. This hydroperoxy species is likely to act as a key intermediate in H_2O_2 synthesis and if this is stabilised by the presence of Au in the catalyst, a higher rate of synthesis should be expected.[57] H_2O_2 synthesis using Au-based catalysts was also reported by Haruta[58] and Ishihara.[59]

Since the discovery of the synergistic effect between Au and Pd for the direct synthesis of H_2O_2 an extensive study has been carried out into the nature of this effect on a series of oxides.[60-70] TiO_2[67], SiO_2[62], Al_2O_3[66], Fe_2O_3[68] and Carbon[70] supports have been used and the synergistic effect of adding Au to Pd was observed for all these systems when catalysts were prepared by an

impregnation methodology, as shown in table 1.1. Typically the addition of Au leads to lower H_2 conversion but a more selective catalyst giving a higher yield of H_2O_2.

	Productivity / mol H_2O_2 kg^{-1} h^{-1} (Selectivity %)		
Catalyst Support	5% Au	2.5% Au 2.5% Pd	5% Pd
Fe_2O_3	1	16	4
TiO_2	7	64	30
	(n.d.)	(70)	(21)
SiO_2	1	108	80
	(n.d)	(80)	(80)
Al_2O_3	3	15	9
Carbon	1	110	55
	(n.d.)	(80)	(34)

Table 1.1 - Comparison on mono and bimetallic catalysts on various supports for the direct synthesis of H_2O_2.

Reaction Conditions - 5% H_2/CO_2 (2.9 MPa) and 25% O_2/CO_2 (1.1 MPa) , 8.5 g solvent (5.6 g MeOH + 2.9 g H_2O), 0.01 g catalyst, 2 ^oC , 1200 rpm, 30 mins

Hutchings *et al.* studied the direct synthesis of H_2O_2 at 2 °C whilst using dilute H_2 to stay well below the lower flammability limit. The solvent system was free from any acid and halide additives and consisted of 66% MeOH and 34% H_2O. The choice of CO_2 as a diluent for H_2 has been shown to act as an *in-situ* promoter for the reaction. Under pressure of CO_2, carbonic acid forms in the solvent mixture, and this acts as a stabiliser for the H_2O_2 during the reaction. Further studies have shown that the addition of stabilisers such as Br^- were deleterious for the highly active Au – Pd catalysts. The addition of Br^- to highly active Au-Pd / C catalyst only gave a subtle enhancement in the yield of H_2O_2 in marked contrast to monometallic Pd catalysts which need halide additives to achieve high yields.[71]

1.6.1 - Support effects

Table 1.1 shows that the H_2O_2 synthesis activity over Au-Pd catalysts also depends on the nature of support, this was studied by Ntainjua *et al.* [72] and Edwards *et al.*.[65] The activity of the Au-Pd bimetallic catalysts followed the order C > SiO_2 > TiO_2 > Al_2O_3 ~ Fe_2O_3. Subsequent hydrogenation and decomposition are the main pathways for the loss of selectivity and yield in the direct synthesis of H_2O_2. Studies have shown that the choice of support is crucial in limiting these subsequent reactions. In particular the acidity and isoelectric point of the supports was determined to be crucial in achieving high yields. As shown in Figure 1.a and b the productivity of bimetallic Au-Pd catalysts is highly dependent on the support chosen. Acidic supports such as carbon and SiO_2 show the highest H_2O_2 productivity whereas basic supports such as MgO and Al_2O_3 show much lower productivity. The trend generally follows the trend in isoelectric points of the supports. The isoelectric point of the support controls the surface charge and clearly high isoelectric point supports lead to the catalysis of non-desired sequential hydrogenation and decomposition of H_2O_2. These trends are similar to those observed for Pd catalysts in that adding acid into the reaction medium helps to improve the selectivity towards H_2O_2. Relative to Pd catalysts, selectivity is generally increased by the acidic nature of the support and the addition of Au.

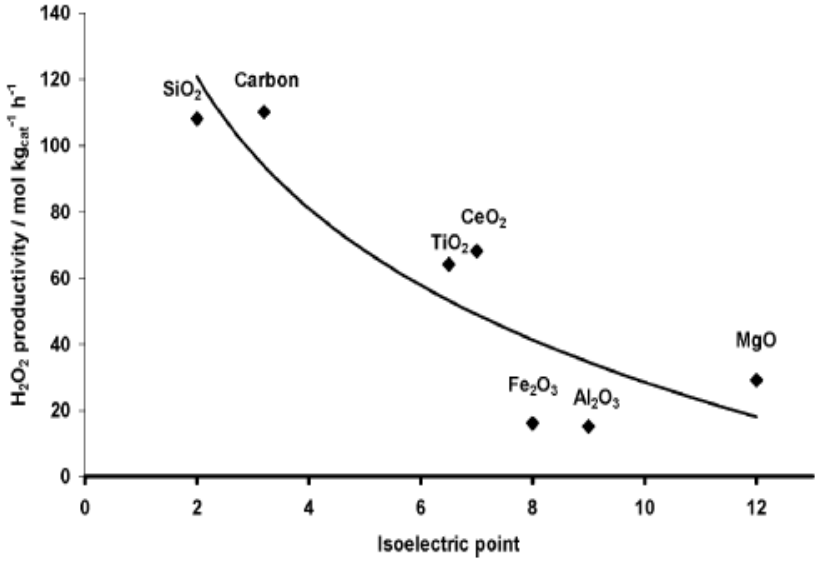

a)

Figure 1.7a) - Shows the dependence of H_2O_2 productivity on isoelectric point for Au – Pd catalysts.[73]

b)

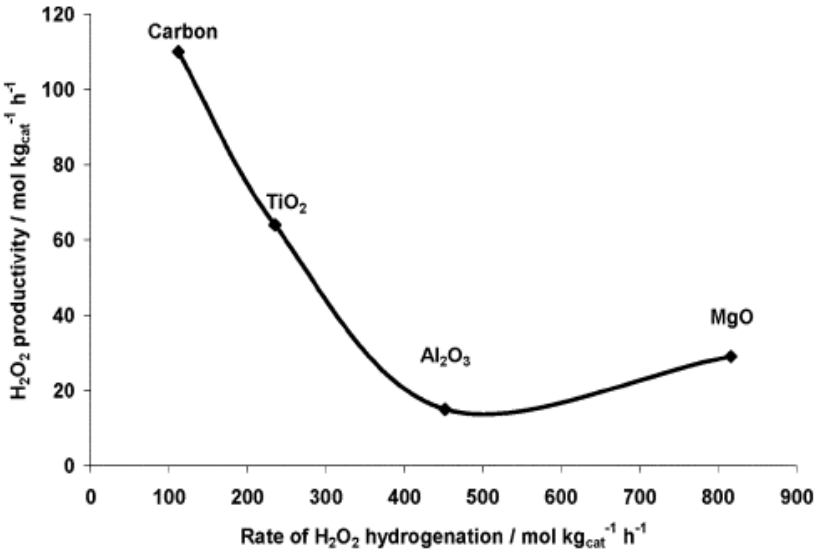

Figure 1.7 b) Graph to show productivity increases as hydrogenation decreases for various supports.[73]

1.6.2 - Particle morphology

A common feature of these bimetallic catalysts is that careful control of heat treatment is crucial in producing active stable catalysts. For all of the oxide supported materials the Pd and Au – Pd catalysts were most active after just a drying step. After drying, Pd catalysts have a very high conversion, 80% for Pd / TiO_2 and Au-Pd catalysts show very high selectivity, almost 90% for 2.5% Au 2.5% Pd / TiO_2.[74] However these catalysts are unstable and have been shown to lose up to 90% of their metal after reaction. After calcination at a temperature of 400 ºC these catalysts lose activity but remain stable after multiple reaction cycles. XPS and STEM studies have shown that dried bimetallic catalysts on oxide supports consist of homogeneous alloys of Au and Pd. During calcination to improve the catalysts stability the particles change morphology, forming core shell structures consisting of a Au core surrounded by a Pd shell. HAADF images of core shell structures of bimetallic particles on TiO_2 and Al_2O_3 catalysts are shown in figure 1.8.

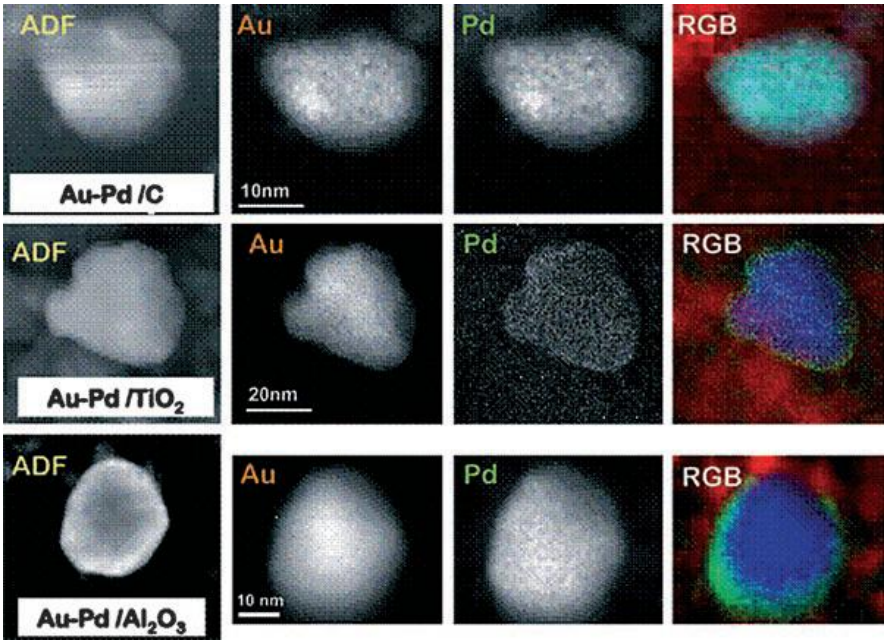

Figure 1.8 - HAADF images of bimetallic particle showing homogeneous Au-Pd alloy on carbon and core shell structures on TiO_2 and Al_2O_3.

The homogeneous alloys of Au – Pd present on dried samples are more active than the core shell structures formed after calcination on oxide supports. Interestingly carbon maintains a homogenous alloy after calcination, as shown in figure 1.8, and this may explain why carbon is the most active support for Au – Pd catalysts for the synthesis of H_2O_2. The strong tendency for palladium surface segregation, observed after calcination, was thought to be brought about by the preferential formation of Pd–O bonds at the alloy surface, because palladium oxidises more readily than gold in this temperature range. A composition dependence on size was also noted during the STEM study of these catalysts. The dried 2.5% Au / 2.5% Pd / TiO_2 catalyst consisted of a bimodal particle size distribution. Small particles were observed, 1-5 nm, consisting of pure Au with a smaller amount of pure Pd particles whereas the larger particles consisted of Au –Pd alloys. After calcination the same bimodal distribution was seen with the larger particles being core shell alloys; however no small Au particles were observed. Comparing the calcined and uncalcined catalysts, the most striking difference was the composition of the smaller particles. This can be explained by the fact that at the nm scale the melting point of a metal is much lower than the bulk metal. At the calcination temperature used small Au particles would be much more mobile than small Pd particles and these small Au particles can sinter with Pd particles to form

the larger alloyed particles which are thought to be responsible for the synergistic effect of Au and Pd for the synthesis of H_2O_2.

1.6.3 - Acid treatment

The observation that acidic supports tend to give higher H_2O_2 yields led to studies into the acid pre-treatments of supports prior to and during catalyst preparation. An important contribution by Edwards *et al.*[70] observed that by using a carbon supported Au – Pd catalyst, it was possible to switch off the hydrogenation activity by using an acid washing pre-treatment of the support prior to impregnation of the precious metals. The pre-treatment step consists of suspending the catalyst support in a 2 wt% aqueous HNO_3 solution for three hours followed by subsequent washing (thoroughly with approximately 1 L H_2O) and then drying (120 ºC). This reduction in hydrogenation activity resulted in a significant enhancement in the selectivity of the catalyst, in some cases reaching + 95% as shown in table 1.2.

Pretreatment	Selectivity %	Productivity mol H_2O_2 kg^{-1} h^{-1}
None	80	110
Water	80	110
2% HNO_3	+ 95%	160

Table 1.2 - Comparison of selectivities and productivities of 2.5% Au 2.5% Pd / C after various pre-treatments

The acid pre-treatment did not alter the previously seen particle morphology with homogeneous Au-Pd alloys observed in the stable samples after calcination. The beneficial effect of acid pre-treatment was to enhance the Au dispersion generating smaller Au-Pd nanoparticles between 1-5 nm that retained the homogeneous alloy previously observed on carbon supports. The increase in activity for the direct synthesis of H_2O_2 is therefore thought to be due to the formation of many smaller active alloy nanoparticles which block support sites that are active for the hydrogenation and decomposition of H_2O_2 which leads to higher selectivities towards H_2O_2. A similar effect was seen when using TiO_2 as a catalyst support with selectivities of up to 95% observed with a greater population of particles in the 1- 4 nm range when compared to the untreated catalysts.[69] To date the acid treated catalysts are the most active and selective catalysts to be reported in the literature.

1.7 - Reactor Types for the Direct Synthesis of H_2O_2

1.7.1 - Batch

By far the most common method of testing catalysts for the direct synthesis of H_2O_2 is a batch autoclave. This means that the catalyst will be in contact with the H_2O_2 produced for an extended period of time. When testing a catalyst for synthesis activity in a batch system it is difficult to achieve very short residence times, with the shortest feasible reaction being 1 min. By testing in the batch system you are only able to measure the H_2O_2 concentration at a certain time after the reaction has started, which makes it very difficult to measure the absolute rate of H_2O_2 synthesis due to the contribution of the subsequent reactions. This means that any measure of rate will only be an observed rate, k_{obs}, which is made up of contributions from the synthesis, hydrogenation and decomposition reactions whilst measure of conversion by H_2 consumption must take into account the direct combustion reaction.

1.7.2 - Flow Reactors

An important reaction parameter to consider when dealing with a process which has subsequent and competing reactions is the time the reaction product is in contact with the catalyst. By carefully controlling the time that the reactants are in contact with the catalyst it is possible to control and suppress the subsequent hydrogenation and decomposition reactions. By using a fixed bed reactor it is possible to flow gas and liquid through the system to give a well defined residence time over the catalyst to study synthesis of H_2O_2 along with hydrogenation and decomposition reactions.[75, 76] Using this reactor setup to limit the sequential reactions, reaction conditions such as pressure, temperature, gas ratios and solvent composition can easily be varied and studied along with the long term stability of the catalyst in a flow system. A common feature with the studies carried out in the literature is the use of halogen and acid promoters to suppress the side reactions and enhance selectivity towards H_2O_2.

1.7.3 - Membrane

To avoid the inherent hazards involved in the direct reaction of H_2 and O_2, a number of attempts have been described to run the reaction in an inherently safe membrane reactor. In a reactor of this type, where O_2 and H_2 are physically separated, only a small flux of H_2 can reach the catalytic sites where it immediately reacts to create H_2O_2, allowing high concentrations of gases

to be used. The reactor setup shown in figure 1.9 involves feeding H_2 gas from an internal section of the membrane to an O_2 saturated reactant solution; since the palladium membrane is permeable to H atoms and not molecular H_2 this gives improved safety. Work by Abate has indicated that defective surface sites on the Pd-catalyst surface are responsible for parallel and sequential unselective reaction taking place to different extents (confirmed by kinetic studies) under the adopted reactor setup.[77, 78] This suggests that while this reactor setup may be a safer alternative to work with higher gas concentrations, unwanted side reactions still pose a problem.

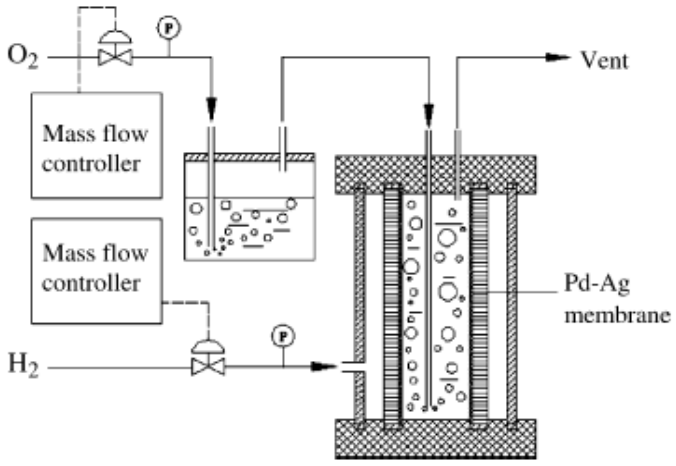

Figure 1.9 - Schematic setup of a membrane reactor taken from reference 77.

1.8 - Summary of the Background of H_2O_2 Synthesis

Many advances have been made towards a feasible process for the direct synthesis of H_2O_2, however the problem of low selectivities because of subsequent hydrogenation and decomposition reactions remain a major obstacle. The addition of Au to Pd has helped to address the problem of low selectivity however a pressure for catalysts to have cheaper and simpler preparation methods and use cheaper reagents remains a driving force for further developments. Research into new approaches to catalyst design including using less expensive metals and investigating optimum reaction conditions in different reactor configurations may provide further developments that could help the commercialisation of the process.

1.9 - Carbon Monoxide Oxidation

Bulk gold has limited use as a catalyst due to its inability to activate molecules such as H_2, O_2 and CO. However when gold particles on the nano scale are synthesised and supported on transition metal oxides, gold catalysts show high catalytic activity in a number of industrially useful reactions. Breakthroughs in gold catalysis came from Haruta's work on CO oxidation at ambient and sub ambient temperatures,[79,80] and Hutchings' work on catalysing ethyne hydrochlorination.[81,82] Since these observations the number of publications concerning gold catalysis has risen substantially, with over 1200 research articles being published up to 2007.[57] Since the discovery by Haruta *et al.*[79,80] that Au nanoparticles were exceptionally active for the oxidation of CO at sub-ambient temperatures, CO oxidation has become possibly the most studied reaction in heterogeneous catalysis. This conceptually simple reaction has fascinated scientists for nearly 30 years mainly because high reaction rates can be achieved at very low temperatures. Haruta reported in the first examples of CO oxidation by Au catalysts that catalysts were still highly active at -78 °C,[79, 80] and more recently model catalysts such as Au /Ni (111) have been shown to be active at temperatures as low as -203 °C.[83]

1.9.1 - Preparation Methods

Preparation methods have now been published that show active catalysts can be made using a number of metal oxides as supports including Fe_2O_3,[80, 84-90] TiO_2[79, 91-96] and CeO_2.[97, 98] High activity catalysts on a variety of supports are typically prepared by deposition and co-precipitation methods. This preparation methodology is needed to generate small Au nano particles which are active for CO oxidation. Au / TiO_2 catalysts prepared by impregnation show almost no activity for CO oxidation in contrast to H_2O_2 synthesis where impregnation has been shown to be an effective preparation methodology. The impregnation of Au onto oxide supports may be problematic because of the tendency of Au to sinter into larger inactive nanoparticles. Also, during heat treatments of Au catalysts where $HAuCl_{4(aq)}$ is used as a precursor, the presence of chloride greatly enhances the tendency of the Au particles to sinter. To achieve high reaction rates and Au particles below 10 nm it is important to choose the appropriate methodology for preparation and this may depend on the nature of the support being used.

1.9.2 - Particle Size effects

A common theory in the literature regarding CO oxidation is that small Au nanoparticles are needed for high catalytic activity. Lopez *et al.*[99] collated data from published literature regarding Au catalysts on a variety of supports and this showed the general trend that activity increased with decreasing particle size, shown in figure 1.10. The authors concluded that the most important factor controlling activity is particle size and that the nature of the support and support-particle interaction played a smaller role. However, there is a considerable error associated when trying to estimate particle sizes at the lower end of the scale and the fact that the particle size is only an averaged particle size must not be ignored. Many species smaller than the particle size given may be present in the catalyst but these, due to their size, do not contain many gold atoms and can therefore be overlooked using some characterisation techniques.

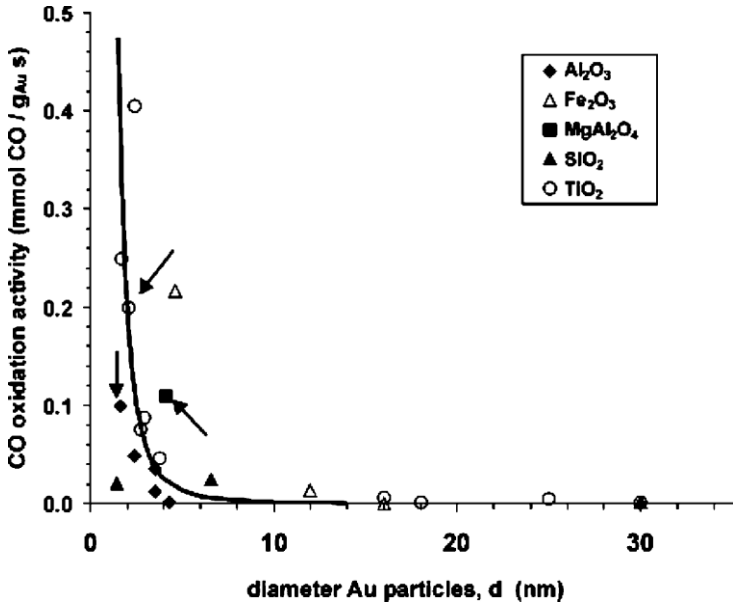

Figure 1.8 - Data collated by Lopez et al.[99] correlating CO oxidation activity with Au particle size for a variety of supports.

Haruta *et al.*[100] report that an FT-IR spectra for CO adsorption at 90 K over Au / TiO_2 having a mean particle diameter of 2.4 nm exhibits a large peak intensity at 2110 -2120 cm^{-1}. This can be attributed to the linear adsorption of CO on the metallic Au sites. When the diameter of the Au particles is increased to 10 nm by calcination at high temperatures, the intensity of the peak reduces remarkably, indicating that CO adsorption might preferentially occur on the high energy

steps, edges, and corners of the Au particles and not on the smooth surfaces. This may indicate that the adsorption of molecules onto the surface of Au may change with decreasing particles size which may affect the reaction pathway.

Hutchings and co-workers reported a HAADF STEM study which undertook a statistical analysis of gold particle size and type, comparing an extremely active CO oxidation catalyst and an inactive CO oxidation catalyst at a range of calcination temperatures.[101] They classified Au species into 4 main groups, isolated atoms, monolayer structures, bilayer structures and species above 1 nm, figure 1.11 shows a high resolution image of a dried Au / FeO_x catalyst with individual atoms indicated by white circles and bilayer structures indicated by black circles. On increasing calcination temperature they found that catalytic activity dropped from 100% conversion after drying to 0% conversion after calcination at 600 °C for 3 h. They found that on heat treatment, the number of isolated atoms decreased, the number of monolayers remained relatively constant and the number of bilayers decreased where as the number of species above 1 nm increased. This means that the active catalysts contained a higher number of bilayers and fewer clusters above 1 nm. They concluded that these bilayer structures consisting of ~8-10 Au atoms were the source of the high activity in the dried sample. Theoretical studies have shown that the activity of a Au surface is maximised when the Au structures are two atomic layers thick[102] which is in agreement with the findings of Hutchings *et al.* and the theoretically reported TOF for a bilayer structure is in close agreement with that of the experimental results when it is assumed that all of the activity comes from these bilayer structures present in the catalyst, which only accounted for 0.6 atomic % of Au present.

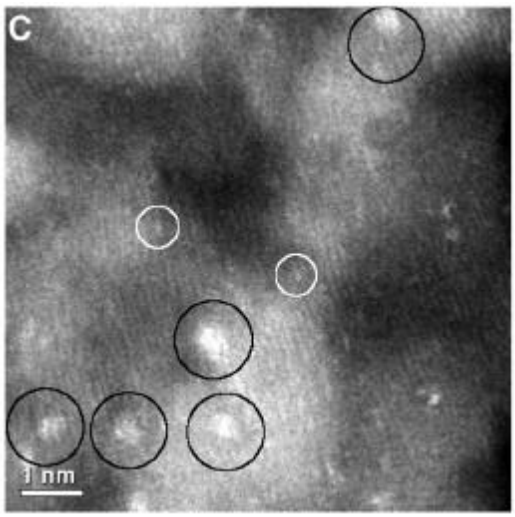

Figure 1.9 - A high resolution image of a dried Au / FeO_x catalyst with individual atoms indicated by white circles and bilayer structures indicated by black circles.

1.9.3 - Mechanism

Despite the CO oxidation reaction being extensively studied over the last 30 years a conclusive identification of the reaction mechanism and active site has not yet been made. A reason for this is that in reality the conceptually simple reaction may be occurring by a variety of mechanisms at a variety of active sites, as catalysts prepared in the laboratory by precipitation methods contain a large variety of gold nanoparticles. The large variety in Au particle size and morphology contributing towards experimental results also makes modelling the reaction very difficult.

Bond and Thompson[103] proposed a model where Au atoms at the interface between the Au particles and oxide support are the active oxidation species. The periphery of a Au nanoparticle has exposed Au atoms that can interact with the oxide support. The smaller the Au nanoparticles the higher the proportion of Au atoms which will be able to interact with the oxide support, leading to a higher reaction rate. Bond and Thompson[103] proposed that the atoms at the periphery could be cationic and that these atoms were responsible for the activation of O_2 in the reaction mechanism. They postulated that a hydroxyl group migrates to one of the cationic periphery Au atoms leaving an anion vacancy in the support. This hydroxyl then reacts with an adsorbed CO molecule to form a carboxylate species on the periphery, while the anion vacancy is filled by an O_2 molecule to form O_2^- as shown in figure 1.12. The O_2^- can then oxidise the carboxylate by abstracting the hydrogen atom to form CO_2 and OOH^- which can then oxidise another carboxylate and restore the hydroxyl to the catalyst surface.

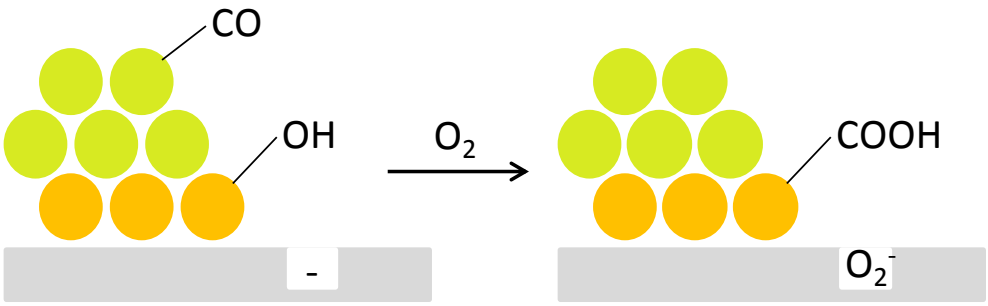

Figure 1.10 - Schematic of part of the reaction scheme proposed by Bond and Thompson

Kung *et al.*[104] also proposed a reaction mechanism which involves cationic gold at the periphery of gold nanoparticles. They favoured the formation of a bicarbonate species with the involvement of a hydroxyl species activated by the $Au^{\delta+}$ that is stabilized at the peripheral position. The idea that CO is activated by adsorption on the surface of the gold nanoparticles and that O_2 is activated by cationic Au atoms at the periphery between the support and the gold nano crystals has yet to be conclusively proven, however a unique feature of Au catalysts is that apparent activation energies are very low for CO oxidation using Au / TiO_2 catalysts prepared by deposition precipitation with typical values of 20 - 40 kJ mol^{-1} below 300 K and nearly 0 kJ mol^{-1} above 300 K. At room temperature, Au is more active by 1-4 orders of magnitude for CO oxidation when compared to Pt group metal catalysts prepared by similar methods.[100] These two very distinct activation energies may even suggest that different mechanisms operate at different reaction temperatures. Recent work has shown that at low temperature the support can play a key part in the reaction by delivering CO to the periphery gold sites to react with O_2. A study by Green *et al.* [105] observed by *in-situ* IR using a Au / TiO_2 catalyst that the CO adsorbed onto the TiO_2 surface was the first to react with activated O_2 at the periphery of the Au nano particles at temperatures of 120 K. At this low temperature the CO that was adsorbed on the Au was stuck due to a high diffusion barrier. This example of CO supply from the support and not the CO that was adsorbed on Au shows that this reaction is very complicated and the presence multiple active sites and mechanisms are likely.

1.9.4 - CO Oxidation using Gold Iron Oxide Catalysts

During the seminal study by Haruta in the 1980's, gold supported on iron oxide was identified as an extremely active catalysts for CO oxidation.[79, 80] The study of FeO_x supported Au for this reaction is still ongoing in the literature and still contains many discrepancies that need to be

addressed with regard to the most active state of the support, the most desired Au particle size and the active site present. [57, 84-86, 101, 106-108]

The preparation method of Au / FeO_x catalysts has been shown to drastically effect the CO oxidation activity.[68] Catalysts prepared by impregnation show very little activity whereas catalysts prepared by deposition precipitation and co-precipitation are much more active, with the preferred preparation method being co-precipitation. The effect on the gold particle size distribution with different preparation method is thought to be the reason for this, with impregnation producing mostly particles above 4-5 nm whereas as co-precipitation has been shown to produce particles from 2-4 nm particles down to isolated Au atoms, and it has been shown by many groups that activity is highly dependent on particle size. Hutchings and co-workers[101] postulated that Au bilayer structures were responsible for the high activity on iron oxide. In contrast Schuth and co-workers[108] have prepared catalysts with a tight 2 nm particle size distribution and they were still highly active. This may suggest that a number of gold species could be responsible for the activity with competing rates and mechanisms.

Another area of uncertainty in the Au / FeO_x system is the nature of the support. Many studies report that the nature of the support after a co-precipitation procedure is amorphous, iron oxyhydroxide phase.[84, 85] These catalysts on calcination at higher temperatures, up to 400 °C, become more crystalline and lose Au dispersion by sintering processes and Au can also become trapped within the support as it crystallises. This results in lower catalytic activity the higher the heat treatment prior to testing. This is in contrast to Haruta who reports that after preparation of the catalysts by the same methods it results in a crystalline iron oxide catalyst, which becomes more active with calcination up to 300 °C and then rapidly loses activity.[79,80] This clear difference in support phases and heat treatment between Au / FeO_x illustrates that there are many differing observations in the literature regarding Au / FeO_x catalysts for CO oxidation that are yet to be resolved, with a major challenge still being identification of the most likely active site.

1.10 - Thesis Aims

The aims of this thesis are outlined below:

1. It has been shown that Au addition to Pd can enhance H_2O_2 productivity by suppressing the subsequent hydrogenation and decomposition reactions. However for a process to be commercialised the cost of the catalyst must be taken into account. Investigation into the addition of less expensive second metals to Pd will be carried out with the aim of matching the activity of Au-Pd catalysts with catalyst that contain no or much less Au.
2. A fixed bed gas liquid reactor is to be designed and operated for the direct synthesis of H_2O_2 with the aim of investigating reaction parameters in a continuous flow system. This will allow the determination of kinetic parameters for each of the synthesis, hydrogenation and decomposition reaction to be explored and kinetic models to be proposed.
3. Further investigation into the active site for CO oxidation using Au / FeO_x catalysts will be carried out by undertaking kinetic studies of catalytic activity along with extensive characterisation using STEM to attempt to determine complete particle size distributions ranging from 10 nm particles down to single atoms.

1.11 - References

1. V. Smil, *Nature*, **1999**, *400*, 415.
2. A. McNaught and A. Wilkinson, *The IUPAC Compendium of Chemical Terminology*, Blackwell Science, Cambridge, **2003**.
3. G. J. Hutchings, *Chem. Commun.*, **2008**, *10*, 1148-1164.
4. P. B. Walsh, *Tappi J.*, **1991**, *74*, 81 - 83.
5. D. J. Robinson, L. Davies, N. McGuire, D. F. Lee, P. McMorn, D. J. Willock, G. W. Watson, P. C. B. Page, D. Bethell and G. J. Hutchings, *Phys. Chem. Chem. Phys.*, **2000**, *2*, 1523-1529.
6. S. Shin and D. Chadwick, *Ind. Eng. Chem. Res.*, **2010**, 49, 8125-8134.
7. E. Klemm, E. Dietzsch, T. Schwarz, T. Kruppa, A. de Oliveira, F. Becker, G. Markowz, S. Schirrmeister, R. Schutte, K. Caspary, F. Schuth and D. Honicke, *Ind. Eng. Chem. Res.*, **2008**, *47*, 2086-2090.
8. U. Schuchards, H. Pastore and E. Spinace, *Zeolites and Related Microporous Materials: State of the Art 1994*, **1994**, *84*, 1877-1882.
9. C. W. Jones, *Application of Hydrogen Peroxide and Derivatives*, Royal Society of Chemistry, London, **1990**.
10. G. Pfleiderer, H. J. Riedl and W. Deuschel, *BASF*, **1950**, DE 801840.
11. G. Pfleiderer and H. J. Riedl, *Alien Property Custodian*, **1945**, US 2369912.
12. H. J. Riedl and G. Pfleiderer, *I.G. Farbenindustrie AG*, **1939**, US 2158525.
13. W. Manchot, *Liebigs. Ann. Chim.*, **1901**, 314, 317.
14. J. M. Campos-Martin, G. Blanco-Brieva and J. L. G. Fierro, *Ang. Chem. Int. Ed.*, **2006**, *45*, 6962-6984.
15. S. Jacobson, *The BOC Group*, **1914**, US 1108752.
16. S. Chinta and J. H. Lunsford, *J. Catal.*, **2004**, *225*, 249-255.
17. S. Chinta and J. H. Lunsford, *Abstracts of Papers of the American Chemical Society*, 2004, *227*.
18. B. Zhou and L. K. Lee, *Hydrocarbon Technologies USA Inc.*, **2001**, US 6168775.
19. T. A. Pospelova and N. I. Kobozev, *Russ. J. Phys. Chem.*, **1961**, *35*, 1192-1197.
20. T. A. Pospelova, N. I. Kobozev and E. N. Eremin, *Russ. J. Phys. Chem.*, **1961**, *35*, 298-305.
21. T. A. Pospelova and N. I. Kobozev, *Russ. J. Phys. Chem.*, **1961**, *35*, 535-542.

22. V. R. Choudhary, C. Samanta and T. V. Choudhary, *J. Mol. Catl. A: Chem.*, **2006**, *260*, 115-120.
23. V. R. Choudhary, C. Samanta and T. V. Choudhary, *Appl. Catal. A: Gen.*, **2006**, *308*, 128-133.
24. V. R. Choudhary, C. Samanta and P. Jana, *Appl. Catal. A: Gen.*, **2007**, *332*, 70-78.
25. V. R. Choudhary and P. Jana, *Appl. Catal. A: Gen.*, **2007**, *329*, 79-85.
26. V. R. Choudhary, C. Samanta and P. Jana, *Appl. Catal. A: Gen.*, **2007**, *317*, 234-243.
27. V. R. Choudhary and P. Jana, *Catal. Commun.*, **2007**, *8*, 1578-1582.
28. V. R. Choudhary and P. Jana, *J. Catal.*, **2007**, *246*, 434-439.
29. V. R. Choudhary and P. Jana, *Catal. Commun.*, **2008**, *9*, 1624-1629.
30. V. R. Choudhary, P. Jana and S. K. Bhargava, *Catal. Commun.*, **2007**, *8*, 811-816.
31. V. R. Choudhary and P. Jana, *Catal. Commun.*, **2008**, *9*, 2371-2375.
32. C. Samanta and V. R. Choudhary, *Catal. Commun.*, **2007**, *8*, 2222-2228.
33. C. Samanta and V. R. Choudhary, *Appl. Catal. A: Gen.*, **2007**, *326*, 28-36.
34. C. Samanta and V. R. Choudhary, *Catal. Commun.*, **2007**, *8*, 73-79.
35. C. Samanta and V. R. Choudhary, *Chem. Eng. J.*, **2008**, *136*, 126-132.
36. R. Burch and P. R. Ellis, *Appl. Catal. B: Environ.*, **2003**, *42*, 203-211.
37. V. R. Choudhary, C. Samanta and P. Jana, *Chem. Commun.*, **2005**, *43*, 5399-5401.
38. V. R. Choudhary and C. Samanta, *J. Catal.*, **2006**, *238*, 28-38.
39. V. R. Choudhary, P. Jana and C. Samanta, *Appl. Catal. A: Gen.* , **2007**, *323*, 202-209.
40. V. R. Choudhary, C. Samanta and T. V. Choudhary, *Catal. Commun.*, **2007**, *8*, 1310-1316.
41. C. Samanta and V. R. Choudhary, *Appl. Catal. A: Gen*, **2007**, *330*, 23-32.
42. D. P. Dissanayake and J. H. Lunsford, *J. Catal.*, **2003**, *214*, 113-120.
43. J. H. Lunsford, *J. Catal.*, **2003**, *216*, 455-460.
44. D. P. Dissanayake and J. H. Lunsford, *J. Catal.*, **2002**, *206*, 173-176.
45. S. Park, T. J. Kim, Y. M. Chung, S. H. Oh and I. K. Song, *Res. Chem. Intermed.*, **2010**, *36*, 639-646.
46. S. Park, D. R. Park, J. H. Choi, T. J. Kim, Y. M. Chung, S. H. Oh and I. K. Song, *J. Mol. Catal. A: Chem.*, **2010**, *332*, 76-83.
47. S. Park, S. H. Lee, S. H. Song, D. R. Park, S. H. Baeck, T. J. Kim, Y. M. Chung, S. H. Oh and I. K. Song, *Catal. Commun.*, **2009**, *10*, 391-394.
48. S. Park, S. H. Baeck, T. J. Kim, Y. M. Chung, S. H. Oh and I. K. Song, *J. Mol. Catal. A: Chem.*, **2010**, *319*, 98-107.
49. S. Park, T. J. Kim, Y. M. Chung, S. H. Oh and I. K. Song, *Catal. Lett.*, **2009**, *130*, 296-300.

50. Q. S. Liu and J. H. Lunsford, *Appl. Catal. A: Gen*, **2006**, *314*, 94-100.
51. Y. F. Han and J. H. Lunsford, *J. Catal.*, **2005**, *230*, 313-316.
52. V. V. Krishnan, A. G. Dokoutchaev and M. E. Thompson, *J. Catal*, **2000**, *196*, 366 - 375.
53. P. Landon, P. J. Collier, A. J. Papworth, C. J. Kiely and G. J. Hutchings, *Chem. Commun.*, **2002**, 2058-2059.
54. P. Landon, P. J. Collier, A. F. Carley, D. Chadwick, A. J. Papworth, A. Burrows, C. J. Kiely and G. J. Hutchings, *Phys. Chem. Chem. Phys.*, **2003**, *5*, 1917-1923.
55. A. Abad, P. Concepcion, A. Corma and H. Garcia, *Ang. Chem. Int. Ed.* , **2005**, *44*, 4066-4069.
56. A. Corma and M. E. Domine, *Chem. Commun.*, **2005**, 4042-4044.
57. G. Hutchings, *Dalton Trans.*, **2008**, *41*, 5513-5560.
58. M. Okumura, Y. Kitagawa, K. Yagamuchi, T. Akita, S. Tsubota and M. Haruta, *Chem. Lett.*, **2003**, *82*, 822-823.
59. T. Ishihara, Y. Ohura, S. Yoshida, Y. Hata, H. Nishiguchi and Y. Takita, *Appl. Catal. A: Gen.*, **2005,** *291*, 215-221.
60. J. A. Lopez-Sanchez, N. Dimitratos, P. Miedziak, E. Ntainjua, J. K. Edwards, D. Morgan, A. F. Carley, R. Tiruvalam, C. J. Kiely and G. J. Hutchings, *Phys. Chem. Chem. Phys*, **2008**, *10*, 1921-1930.
61. A. A. Herzing, A. F. Carley, J. K. Edwards, G. J. Hutchings and C. J. Kiely, *Chem. Mater.*, **2008**, *20*, 1492-1501.
62. J. K. Edwards, A. Thomas, A. F. Carley, A. A. Herzing, C. J. Kiely and G. J. Hutchings, *Green Chem.*, **2008**, *10*, 388-394.
63. J. K. Edwards, A. F. Carley, A. A. Herzing, C. J. Kiely and G. J. Hutchings, *Faraday Discuss.*, **2008**, *138*, 225-239.
64. G. Li, J. Edwards, A. F. Carley and G. J. Hutchings, *Catal. Commun.*, **2007**, *8*, 247-250.
65. J. K. Edwards, A. Thomas, B. E. Solsona, P. Landon, A. F. Carley and G. J. Hutchings, *Catal. Today*, **2007**, *122*, 397-402.
66. B. E. Solsona, J. K. Edwards, P. Landon, A. F. Carley, A. Herzing, C. J. Kiely and G. J. Hutchings, *Chem. Mater.*, **2006**, *18*, 2689-2695.
67. J. K. Edwards, B. E. Solsona, P. Landon, A. F. Carley, A. Herzing, C. J. Kiely and G. J. Hutchings, *J. Catal.*, **2005**, *236*, 69-79.
68. J. K. Edwards, B. Solsona, P. Landon, A. F. Carley, A. Herzing, M. Watanabe, C. J. Kiely and G. J. Hutchings, *J. Mater. Chem.*, **2005**, *15*, 4595-4600.

69. J. K. Edwards, E. Ntainjua, A. F. Carley, A. A. Herzing, C. J. Kiely and G. J. Hutchings, *Ange. Chem. Int. Ed.*, **2009**, *48*, 8512-8515.
70. J. K. Edwards, B. Solsona, E. N. N, A. F. Carley, A. A. Herzing, C. J. Kiely and G. J. Hutchings, *Science*, **2009**, *323*, 1037-1041.
71. E. Ntainjua, M. Piccinini, J. C. Pritchard, Q. He, J. K. Edwards, A. F. Carley, J. A. Moulijn, C. J. Kiely and G. J. Hutchings, *Chem. Cat. Chem.*, **2009**, *1*, 479-484.
72. N. N. Edwin, M. Piccinini, J. C. A. Pritchard, J. K. Edwards, A. F. Carley, J. A. Moulijn and G. J. Hutchings, *ChemSusChem*, **2009**, *2*, 575-580.
73. N. N. Edwin, J. K. Edwards, A. F. Carley, J. A. Lopez-Sanchez, J. A. Moulijn, A. A. Herzing, C. J. Kiely and G. J. Hutchings, *Green Chem.*, **2008**, *10*, 1162-1169.
74. J. K. Edwards and G. J. Hutchings, *Ange. Chem. Int. Ed.*, **2008**, *47*, 9192-9198.
75. Y. Voloshin and A. Lawal, *Appl. Catal. A: Gen.*, **2009**, *353*, 9-16.
76. Y. Voloshin, R. Halder and A. Lawal, *Catal. Today*, **2007**, *125*, 40-47.
77. S. Abate, S. Melada, G. Centi, S. Perathoner, F. Pinna and G. Strukul, *Catal. Today*, **2006**, *117*, 193-198.
78. S. Abate, G. Centi, S. Melada, S. Perathoner, F. Pinna and G. Strukul, *Catal. Today*, **2005**, *104*, 323-328.
79. M. Haruta, T. Kobayashi, H. Sano and N. Yamada, *Chem. Lett.*, **1987**, 405-408.
80. M. Haruta and H. Sano, *Abstracts of Papers of the American Chemical Society*, **1985**, 189.
81. G. J. Hutchings and D. T. Grady, *Appl. Catal.*, **1985**, *17*, 155-160.
82. G. J. Hutchings, *J. Catal.*, **1985**, *96*, 292-295.
83. D. L. Lahr and S. T. Ceyer, *J. Am. Chem. Soc*, **2006**, *128*, 1800.
84. R. Finch, N. Hodge, G. Hutchings, A. Meagher, Q. Pankhurst, M. Siddiqui, F. Wagner and R. Whyman, *Phys. Chem. Chem. Phys.*, **1999**, *1*, 485-489.
85. S. Golunski, R. Rajaram, N. Hodge, G. Hutchings and C. Kiely, *Catal. Today*, **2002**, *72*, 107-113.
86. N. Hodge, C. Kiely, R. Whyman, M. Siddiqui, G. Hutchings, Q. Pankhurst, F. Wagner, R. Rajaram and S. Golunski, *Catal. Today*, **2002**, *72*, 133-144.
87. M. Kahlich, H. Gasteiger and R. Behm, *J. Catal.*, **1999**, *182*, 430-440.
88. G. Avgouropoulos, T. Ioannides, C. Papadopoulou, J. Batista, S. Hocevar and H. Matralis, *Catal. Today*, **2002**, *75*, 157-167.
89. P. Landon, J. Ferguson, B. Solsona, T. Garcia, A. Carley, A. Herzing, C. Kiely, S. Golunski and G. Hutchings, *Chem. Commun.*, **2005**, 3385-3387.

90. P. Landon, J. Ferguson, B. Solsona, T. Garcia, S. Al-Sayari, A. Carley, A. Herzing, C. Kiely, M. Makkee, J. Moulijn, A. Overweg, S. Golunski and G. Hutchings, *J. Mater. Chem.*, **2006**, *16*, 199-208.
91. F. Moreau, G. C. Bond and A. O. Taylor, *J. Catal.*, **2005**, *231*, 105-114.
92. F. Moreau and G. C. Bond, *Appl. Catal. A: Gen*, **2006**, *302*, 110-117.
93. F. Moreau and G. C. Bond, *Catal. Today*, **2007**, *122*, 215-221.
94. F. Moreau and G. C. Bond, *Catal. Today*, **2007**, *122*, 260-265.
95. R. Zanella, S. Giorgio, C. H. Shin, C. R. Henry and C. Louis, *J. Catal.*, **2004**, *222*, 357-367.
96. R. Zanella and C. Louis, *Catal. Today*, **2005**, *107*, 768-777.
97. J. Guzman, S. Carrettin, J. Fierro-Gonzalez, Y. Hao, B. Gates and A. Corma, *Ange. Chem. Int. Ed.*, **2005**, *44*, 4778-4781.
98. J. Guzman, S. Carrettin and A. Corma, *J. Am. Chem. Soc.*, **2005**, *127*, 3286-3287.
99. N. Lopez, T. Janssens, B. Clausen, Y. Xu, M. Mavrikakis, T. Bligaard and J. Norskov, *J. Catal.*, **2004**, *223*, 232-235.
100. M. Haruta, *Gold Bull.*, **2004**, *37*, 27-36.
101. A. Herzing, C. Kiely, A. Carley, P. Landon and G. Hutchings, *Science*, **2008**, *321*, 1331-1335.
102. H. Hakkinen, W. Abbet, A. Sanchez, U. Heiz and U. Landman, *Ange. Chem. Int. Ed.*, **2003**, *42*, 1297-1300.
103. G. C. Bond and D. T. Thompson, *Gold Bull.*, **2000**, *33*, 41-51.
104. C. Costello, J. Yang, H. Law, Y. Wang, J. Lin, L. Marks, M. Kung and H. Kung, *Appl. Catal. A: Gen.*, **2003**, *243*, 15-24.
105. I. Green, W. Tang, M. Neurock and J. Yates, *Science*, **2011**, *333*, 736-739.
106. G. J. Hutchings, M. S. Hall, A. F. Carley, P. Landon, B. E. Solsona, C. J. Kiely, A. Herzing, M. Makkee, J. A. Moulijn, A. Overweg, J. C. Fierro-Gonzalez, J. Guzman and B. C. Gates, *J. Catal.*, **2006**, *242*, 71-81.
107. G. Neri, A. Visco, S. Galvagno, A. Donato and M. Panzalorto, *Thermochim. Acta*, **1999**, *329*, 39-46.
108. Y. Liu, C. Jia, J. Yamasaki, O. Terasaki and F. Schuth, *Ange. Chem. Int. Ed.*, **2010**, *49*, 5771-5775.

Chapter 2

2. Experimental

This chapter outlines the experimental procedures followed when preparing, testing and characterising the materials subsequently discussed in this thesis.

2.1 - Materials Used

$PdCl_2$ – Johnson Matthey

$Pd(NO_3)_2.2H_2O$ – Sigma Aldrich (40% Pd assay)

$HAuCl_4$ – Johnson Matthey

$SnCl_4.5H_2O$ – Sigma Aldrich (> 98%)

$Fe(NO_3)_3.9H_2O$ – Sigma Aldrich (99.99% trace metal basis)

Na_2CO_3 – Sigma Aldrich (99.995% trace metal basis)

TiO_2 – Degussa p25 (99.5% trace metal basis, 20-30 nm particle size)

SiO_2 – Matrex 60

MeOH – Sigma Aldrich (HPLC Grade)

Water – Sigma Aldrich (HPLC Grade)

50 % H_2O_2 – Sigma Aldrich (Stabilised)

$(NH_4)_2Fe(SO_4)_2.6H_2O$ – Sigma Aldrich (98%)

$Ce(SO_4)_2$ – Sigma Aldrich (> 98%)

2.2 - Catalyst Preparation

2.2.1 – Gold, Palladium and Gold-Palladium Catalysts prepared by Impregnation

Monometallic and bimetallic gold palladium catalysts were prepared by impregnating or co-impregnating the appropriate catalyst support with solutions of $PdCl_2$ and $HAuCl_4$. The catalysts contained a nominal metal content of 5 wt% unless otherwise stated. A typical preparation for 1 g of 2.5% Pd / 2.5% Au / TiO_2 was carried out according to the following procedure which has been previously reported in the literature.[1] 0.042 g of $PdCl_2$ was added to 2.04 ml of $HAuCl_4$ (12.25 g Au / 1000 ml) and heated to 80 °C with stirring and left until the $PdCl_2$ had completely dissolved. 0.95 g of the desired support was then added to the solution and the water allowed to evaporate until the mixture formed a paste like consistency. The samples were dried at 110 ºC for 16 h and then calcined in static air at various temperatures, typically 400 ºC for 3 h with a ramp rate of 20 ºC min^{-1}. To prepare pelletised catalysts the samples were pressed after calcination into discs using a hydraulic press at a pressure of 10 tonnes for 10 minutes. The sample disks were then ground and sieved to the desired particle size, typically 450-225 micron.

2.2.2 – Tin, Palladium and Tin-Palladium Catalysts prepared by Impregnation

Tin and palladium monometallic and bimetallic catalysts were prepared by impregnating or co-impregnating aqueous solutions of metal salts onto the appropriate catalyst support which included TiO_2 and SiO_2. The catalysts prepared had a nominal total metal loading of 5 wt% unless otherwise stated. A typical preparation for 1 g of 2.5 % Pd / 2.5% Sn / TiO_2 was carried out as follows; 0.063 g $Pd(NO_3)_2.2H_2O$ was first dissolved in 2 ml of de-ionised water and heated to 80 ºC with stirring. 0.074 g of $SnCl_4.5H_2O$ was dissolved in a minimal amount of water and added to the aqueous palladium solution and left for 15 min. 0.95 g of the support was then added to the solution and the water allowed to evaporate until the mixture had formed a paste like consistency. Samples were then dried at 110 ºC for 16 h and calcined in static air at various temperatures for 3 h with a ramp rate of 20 ºC min^{-1}. Samples were also calcined at other conditions to evaluate their effects on catalyst performance and stability. Selected samples were reduced at various temperatures under a flow of 5% H_2/Ar for 2 h with a ramp rate of 20 ºC min^{-1}.

2.2.3 - Au / Fe_2O_3 Co-precipitated Catalysts

Gold supported on iron oxide was prepared by co-precipitation of $HAuCl_4$ and $Fe(NO_3)_3.9H_2O$ using Na_2CO_3. A typical preparation of 5 wt% Au / Fe_2O_3 was carried out according to the following procedure which has been reported previously in the literature.[2] 4.807 g of $Fe(NO_3)_3.9H_2O$ was dissolved in 200 ml of de-ionised water, 4.08 ml of $HAuCl_4$ (12.25 g Au in 1000 ml) was added to this solution and stirred vigorously while the solution was heated to 80 ºC. The solution had an initial pH of around 0.8. The pH of the solution was increased by adding Na_2CO_3 until the pH reached 8.5. The solution was then left for 1 h under continuous stirring. During this time the pH of the solution rose from 8.5 to approximately 9.2. The solution was then suction filtered and washed with 2 L of warm water at around 80 ºC. The solid was then dried in a GC oven under flowing air at 120 ºC for 16 h. Parts of the sample were then calcined at 200, 300, 400 and 500 ºC for 3 h with a ramp rate of 20 ºC min^{-1}.

The catalyst preparation procedure was varied according to the methods listed below:

- *Method 1* - Na_2CO_3 was added drop wise, over 30 min, to the solution of $HAuCl_4$ and $Fe(NO_3)_2.9H_2O$.
- *Method 2* - Na_2CO_3 was added quickly, over 2 min, to the solution of $HAuCl_4$ and $Fe(NO_3)_2.9H_2O$.
- *Method 3* - $HAuCl_4$ and $Fe(NO_3)_2.9H_2O$ solution was added drop wise, over 30 min, to the Na_2CO_3 solution.
- *Method 4* - $HAuCl_4$ and $Fe(NO_3)_2.9H_2O$ solution was added quickly, over 2 min, to the Na_2CO_3 solution.

2.2.4 - Au / Fe_2O_3 Catalysts Prepared by Deposition Precipitation

Gold supported on iron oxide was also prepared by a deposition precipitation method.[3] A typical preparation of 1 g of 5 wt% Au / iron oxide is outlined by the following procedure. 0.95 g of a pre-prepared iron oxide support was suspended in 200 ml of de-ionised water and held at 60 °C whilst stirring the solution. 4.08 ml of $HAuCl_4$ (12.25 g Au in 1000 ml) was added to this solution and stirred for 15 min. A Na_2CO_3 solution was then added drop wise until the pH of the solution stabilised at 8.5. The preparation was then left for 1 h before filtration and washing with

1 L of hot deionised water (80 °C). The sample was then dried at 110 °C for 16 h followed by calcination at various temperatures between 200 – 500 °C in static air.

2.3 - Catalyst Testing

2.3.1 - H_2O_2 Synthesis in a Batch System

The performance of each catalyst for the direct synthesis of H_2O_2 from H_2 and O_2 was determined using a Parr Instruments stainless-steel autoclave (equipped with an overhead stirrer and temperature/pressure sensors) with a nominal volume of 100 ml and a maximum working pressure of 14 MPa. During a standard synthesis test the autoclave was charged with 5.6 g of MeOH, 2.9 g of HPLC grade H_2O and 10 mg of catalyst. The autoclave was pressurised with 2.9 MPa 5% H_2/CO_2 and 1.1 MPa 25% O_2/CO_2 to give a total reaction pressure of 4 MPa. The autoclave was cooled to 2 °C and then stirred at 1200 rpm for 30 min. After the reaction was complete the solvents were filtered from the catalyst and 0.25 g aliquots of the solvent were titrated against a diluted $Ce(SO_4)_2$ solution acidified with 2% H_2SO_4 using ferroin as an indicator. The exact concentration of the $Ce(SO_4)_2$ solution was determined by titration of a known amount of $(NH_4)_2Fe(SO_4)_2.6H_2O$ again using ferroin as an indicator.

To compare the performance of the catalysts over the 30 min reaction the average rate of H_2O_2 production was calculated and normalised to catalyst mass to give a productivity value which is presented as $mol_{H2O2}\ h^{-1}\ kg_{cat}^{-1}$. The wt % of H_2O_2 was also determined for each reaction using the following calculations:

$$\text{Volume } Ce(SO_4) \text{ to titrate whole reaction solution} = \frac{\text{Titre} \times 8.5}{\text{Sample mass}} \quad (2.1)$$

$$\text{Moles } Ce(SO_4) = \frac{\text{Vol. } Ce(SO_4) \text{ to titrate reaction solution} \times [Ce(SO_4)_2]}{1000} \quad (2.2)$$

$$\text{Moles } H_2O_2 = \frac{\text{Moles } Ce(SO_4)_2}{2} \quad (2.3)$$

$$\text{Productivity} = \frac{\text{Mol } H_2O_2}{\text{Catalyst mass (kg) x Reaction Time (h)}} \quad (2.4)$$

$$\text{wt\% } H_2O_2 = \frac{\text{Moles } H_2O_2 \text{ x Mr } H_2O_2}{8.5} \quad (2.5)$$

2.3.2 - H_2O_2 Hydrogenation in a Batch System

The hydrogenation activity of a catalyst was tested in a similar way to the direct synthesis activity. The autoclave was charged with 5.6 g of MeOH, 0.67 g 50 wt% H_2O_2 and 2.23 g of HPLC grade H_2O (Aldrich) and thoroughly mixed, after which 10 mg of catalyst was added. This solvent composition is equivalent of a 4 wt% H_2O_2 solution of the same volume used previously in the H_2O_2 synthesis experiments. 2 drops of the solvent solution each weighing around 0.04 g were removed and titrated with the acidified $Ce(SO_4)_2$ solution using ferroin as an indicator to determine accurately the initial H_2O_2 concentration. The autoclave was pressurised with 2.9 MPa 5% H_2/CO_2 and cooled to 2 °C and the reaction was carried out for 30 min at 1200 rpm stirring speed. After the reaction was complete the solvents were filtered from the catalyst and two ~0.04 g aliquots of the solvent were titrated against an acidified dilute $Ce(SO_4)_2$ solution using ferroin as an indicator. The hydrogenation activity was calculated as $mol_{H2O2}\ h^{-1}\ kg_{cat}^{-1}$ along with the percentage of the initial H_2O_2 which was present at the end of the reaction.

2.3.3 - Catalyst Re-use in a Batch System

Catalyst reusability was tested by running a synthesis reaction as outlined above but increasing the amount of catalyst to 70 mg. After the reaction was complete the solvent was filtered from the catalyst, and the catalyst was allowed to dry overnight on the filter paper. Before being retested the catalyst was dried at 110 °C in an oven for 1 h to ensure the sample was completely dry. Following this procedure a synthesis reaction was run as previously described.

2.3.4 - H_2O_2 Synthesis in a Flow System

A reactor was designed to allow testing of catalysts for H_2O_2 synthesis in a continuous flow system, the schematic of which is shown in figure 2.1. The reactor was constructed using Swagelok which had an internal diameter of 1/8 inch. Gas flows were controlled using three Brooks mass flow controllers and the pressure maintained using a back pressure regulator at the end of the system. Solvent was pumped through the system using an Agilent HPLC pump.

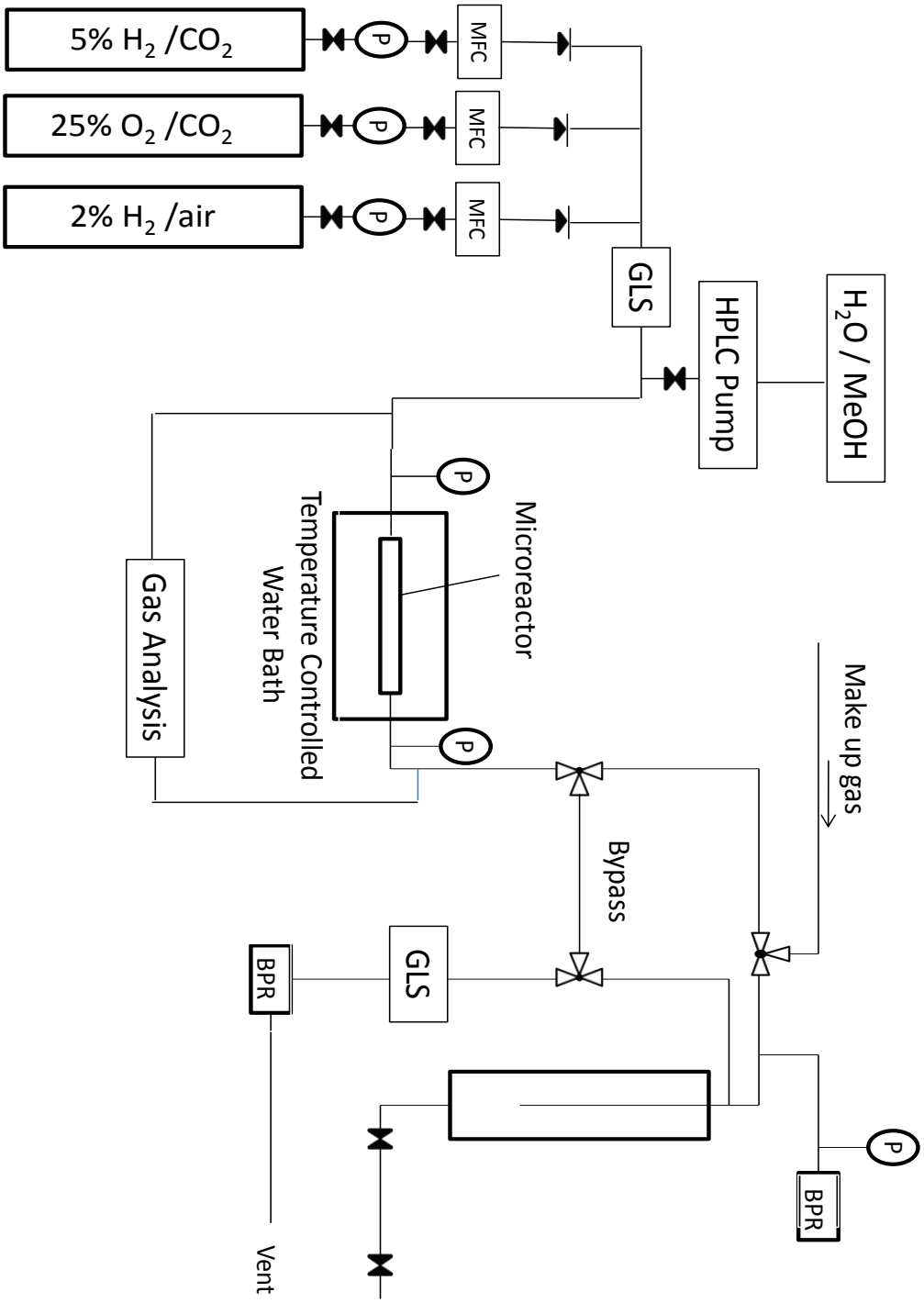

Figure 2.1 - Schematic of the flow reactor designed to test H_2O_2 synthesis.

P = pressure gauge, MFC = Mass flow controller, GLS = gas liquid separator, BPR = back pressure regulator.

A gas liquid separator (GLS) and one way valves were placed before the reactor bed to prevent any liquid from flowing back and entering the mass flow controllers. A schematic of the GLS is shown in figure 2.2. Pressure gauges were placed before and after the catalyst bed to monitor

pressure drops through the bed and to indicate if a blockage had formed in the system. Liquid was collected downstream before the back pressure regulator by emptying a 150 ml GLS fitted with a valve which acted as a sample bomb.

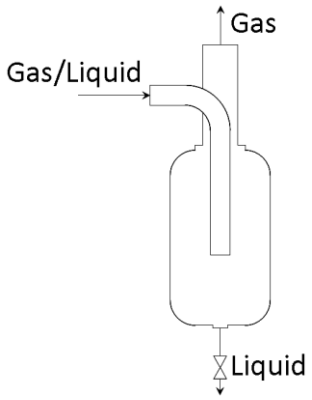

Figure 2.2– Schematic of a gas liquid separator used to sample from the flow system.

The sampling system was designed to allow liquid sampling with minimal disruption to the gas flow through the catalyst bed and therefore residence time of the gas in the catalyst bed. To sample, the gas was routed through a bypass loop which isolated the sample bomb from the gas and liquid flow. Any pressure drop when taking a liquid sample was restricted to the sample loop and the lost pressure was restored using a makeup gas before the bypass loop was closed. The gas and liquid flow can then be restored through the sample bomb. A typical pressure drop during sampling was 2 bar, and using this bypass system the flow could be restored within 5 min of the sample being taken.

Typically 30 – 120 mg of pelleted catalyst was packed into the microreactor between two pieces of glass wool to prevent any catalyst particles from blocking the filters after the reactor tube. The reactor was then cooled by the water bath to 2 ºC. The system was pressurised to the desired pressure using the ratio of H_2 and O_2 desired for the reaction. Typical total gas flows used varied between 6 – 45 ml min^{-1}. Once the system was pressurised the solvent was pumped through the system at 0.2 ml min^{-1}. Liquid samples were taken from the sample bomb every 60 minutes and the concentration of H_2O_2 was determined by titration against an acidified dilute $Ce(SO_4)_2$ solution using ferroin as an indicator.

H_2O_2 hydrogenation experiments were carried out in the flow reactor by replacing the 25% O_2 / CO_2 feed with 100 % CO_2 to maintain the flow rate through the catalyst bed. As a solvent, 500

ppm H_2O_2 solution was passed through the catalyst and by titrating the solution before and after passing through the catalyst bed it was possible to determine loss in H_2O_2 due to hydrogenation. H_2O_2 decomposition experiments were carried out by replacing both the H_2 and O_2 feeds with 100% CO_2 and passing a 500 ppm H_2O_2 solution through the catalyst and determining the loss in H_2O_2 by titration.

2.3.4.1 - Calculation of Residence Time

The residence time of the gas and liquid passing through the catalyst bed was calculated based on the total liquid and gas flow rate and the volume of the catalyst bed. The volume of the catalyst bed was calculated using the diameter of the reactor tube and the catalyst bed length obtained from the calibration plot shown in figure 2.3 based on various amount of 0.5% Au / 0.5% Pd / TiO_2 formed into pellets between 450 – 225 micron.

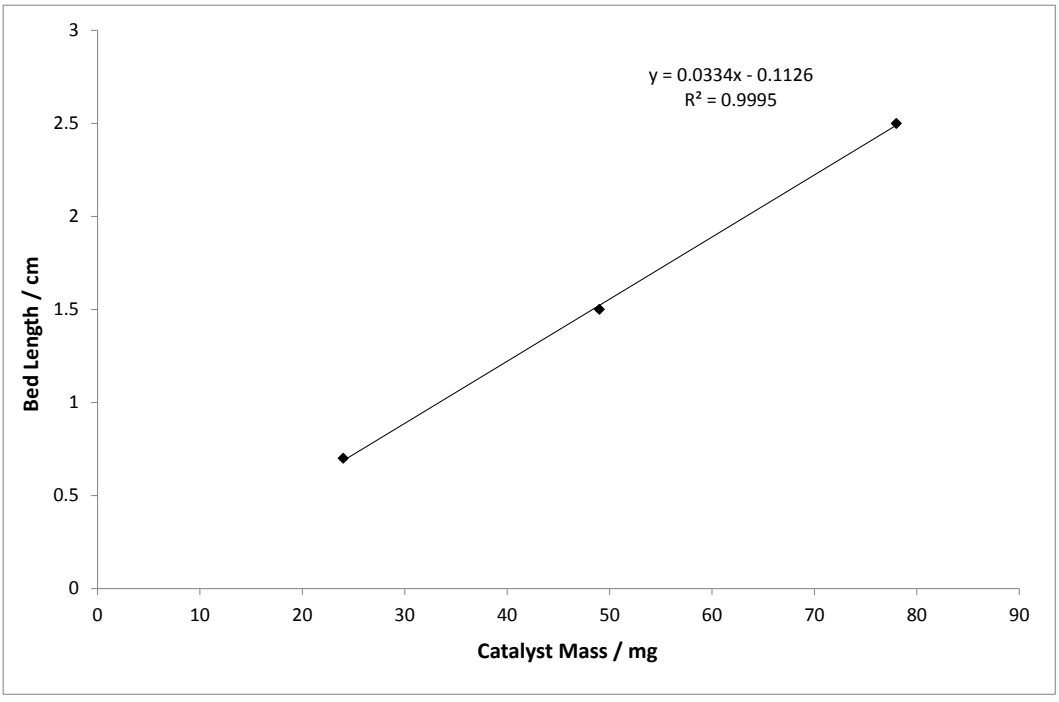

Figure 2.3 - Calibration plot to determine catalyst bed length for various catalyst masses of 0.5% Au / 0.5% Pd / TiO_2 formed into pellets between 450 – 225 micron.

The contact time of the system was calculated using following equations:

$$\text{Gas Hourly Space Velocity (GHSV)} = \frac{\text{Total flow (cm}^3\text{ min}^{-1})}{\text{Volume of catalyst bed (cm}^3)} \quad (2.6)$$

$$\text{Residence Time } (\tau) = \frac{1}{\text{GHSV}} \quad (2.7)$$

2.3.5 - Gas Chromatography

2.3.5.1 - Introduction and Theory

Chromatography is a technique used to separate a mixture of chemical substances. It relies on differences in partitioning behaviour between a flowing mobile phase and a stationary phase. Gas chromatography (GC) is one of the most common analytical techniques used to analyse mixtures of gases or compounds that can be easily vaporised. Gas chromatography can provide both qualitative and quantitative information about gaseous mixtures and also indentify impurities in the mixture.[4] A GC system typically involves introducing a sample of the mixture to be analysed into a mobile phase, called the carrier gas. The carrier gas containing the mixture is passed through a sample loop and is injected into a column, which is the stationary phase and held at a specific temperature by an oven.

Volatile samples are vaporised before entering the column for analysis. The separation of the mixture occurs as each component is carried through the column by the carrier gas at a different speed. If the component has a strong interaction with the column it will remain in the column for longer than a component that has a weak interaction. The components then leave the column at different times, known as the retention time, and enter the detector. A schematic of a typical gas chromatography system is shown in figure 2.4.

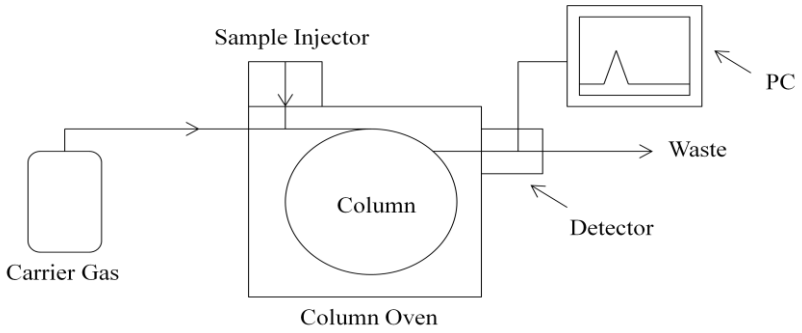

Figure 2.4 - Schematic of a typical gas chromatography system.

Many factors affect the separation of components, these include carrier gas flow rate, column temperature and column type which can all be optimised to give the most effective separation of components. Typical carrier gases used are helium, nitrogen and argon with the gas that is used depending on the detector and the components that are to be identified. The carrier gas should typically be inert and of high purity and a molecular sieve is usually used to filter any moisture before it enters the GC system. The carrier gas flow rate can significantly affect the analysis because it effects how long the components are retained by the column. The higher the flow rate the faster the analysis, but the lower the separation between analytes. Selecting the flow rate is therefore a compromise between the level of separation and length of analysis. Samples enter the column by passing through an injection port, which is held at a high enough temperature to vaporise the components of the mixture if they are not already in the gas phase.

The column is the stationary phase that the components of the system interact with and leads to elution from the column at different times. There are two main types of separation column for gas chromatography, packed columns and capillary columns. Packed columns are typically 1-10 m in length and have an internal diameter of 2-5 mm. The tube is usually made of glass or stainless steel and contains finely divided inert solid support material, which is coated with the stationary phase. This stationary phase can be varied to provide effective separation of components and many columns are readily available to separate the desired mixture of compounds. Capillary columns are usually made of flexible materials so column lengths can be very long, up to 50 m. The internal diameter of these columns is usually tenths of millimetres and the stationary phase is coated on to the internal walls of the column. The temperature that the column is held at is important; as a low column temperature produces the greatest level of separation, but can result in very long elution times, whereas a high temperature gives fast analysis times but shorter retention times and less product separation.

A thermal conductivity detector (TCD) is the most commonly used detector for GC. The detector relies on the difference in thermal conductivity of the carrier gas and the component being eluted from the column. The detector contains two sample cells one has pure carrier gas passing through it and the other has the gas from the column which will contain the components of the mixture after a certain retention time has elapsed. When these components pass through the TCD a difference in heat conductivities is detected between the reference cell and the sample cell and this gives rise to the signal.

2.3.5.2 - GC setup for Analysis of Gas from H_2O_2 Flow Reactor

A Varian 3800 GC fitted with a TCD was used to analyse the gas stream exiting from the H_2O_2 flow reactor. The reactor was fitted with a 4 m molecular sieve 5 Å column and Ar used as a carrier gas at a flow rate of 30 ml min^{-1}. As an internal standard 1% of the total gas flow was nitrogen, this provided an easy to separate peak to which the integrated area of H_2 and O_2 could be compared before and after the reaction. The column oven was held at 40 ºC for 6 min which allowed separation of H_2, O_2 and N_2. The oven was then ramped at 25 ºC min^{-1} up to 200 ºC to ensure all CO_2 and moisture was removed from the column. The retention times of the components analysed during a H_2O_2 synthesis reaction is shown in table 2.1.

Component	Retention time / min
H_2	1.4
O_2	2.7
N_2	4.5
CO_2	7.2

Table 2.1 – Retention times of components analysed during flow reactor experiments to determine H_2O_2 synthesis activity.

Hydrogen conversion was measured by calculating the difference between the H_2 : N_2 ratio before and after the reaction. H_2 selectivity was calculated based on the rate of H_2O_2 produced per min and the rate of hydrogen converted per min.

2.3.6 - CO Oxidation Testing

2.3.6.1 - Cardiff University

Au / Fe_2O_3 catalysts were tested for CO oxidation using a glass micro-reactor with i.d. 0.5 cm shown schematically in figure 2.5. Typically 10 mg of catalyst was packed between two small pieces of glass wool to prevent the catalyst from being carried out of the reactor by the gas flow. The reactor was fixed inside a thermostatic water bath which was held at 25 °C for the duration of the reaction. The gas feed, 5000 ppm CO in synthetic air, was passed through the catalyst bed

at various flow rates (25 – 100 ml min^{-1}) controlled by a mass flow controller (MFC) giving a possible range of gas hourly space velocity (GHSV) of 150,000 – 600,000 h^{-1}. The reaction products were analysed by on-line GC with a 1.5 m Carbosieve Column.

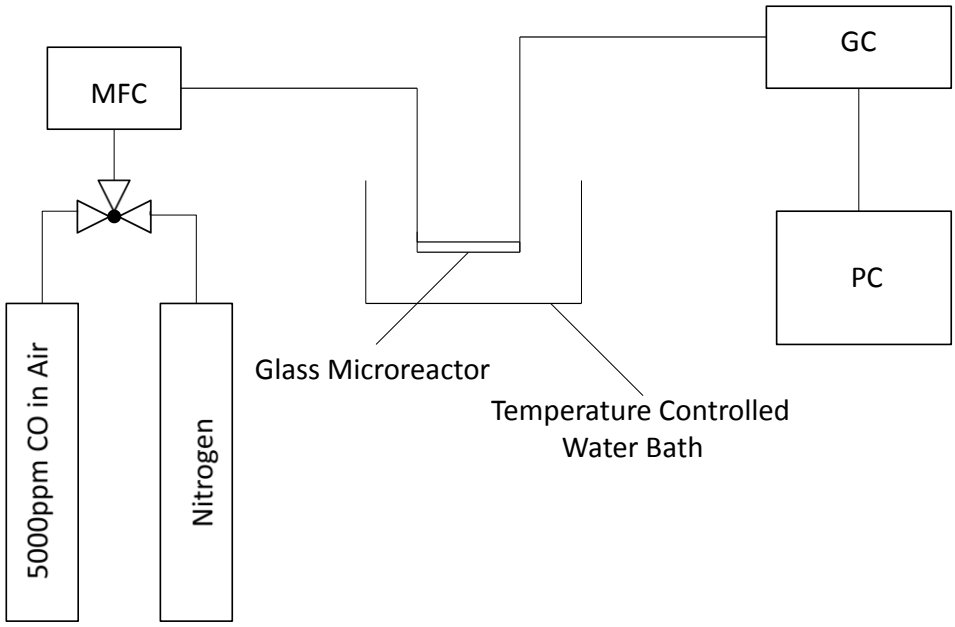

Figure 2.5 - Schematic of the CO oxidation testing system

A Varian 3800 GC was used to analyse the gas stream exiting from the CO oxidation reactions. He was used as a carrier gas at a flow rate of 30 ml min^{-1} and the GC was set up to inject a sample every 4 min into a carbosieve 1.5 m column which was held at 195 °C. This set up provided good separation of the CO_2 from un-reacted CO and synthetic air, however it did not separate the CO from the synthetic air. The components were detected using a TCD detector. The retention times of the components are listed in table 2.2;

Component	Retention time / min
CO + synthetic air	0.4
CO_2	1.4
Moisture	3.0

Table 2.2 – Retention times of the components analysed by GC during CO oxidation tests.

Each reaction was allowed to continue for a minimum of 4 hours with a data point being collected every 4 min. Each catalyst test was repeated twice to confirm the result. The GC was calibrated with varying concentrations of CO_2 in air, up to 5000 ppm CO_2 which corresponds to 100 % CO conversion. The conversion of CO was determined by the integrated area under the CO_2 peaks which corresponds to the total amount of CO that has been oxidised. The percentage of CO conversion was determined using the following equation:

$$\text{CO Conversion \%} = \frac{\text{Area under } CO_2 \text{ peak from reaction x 100}}{\text{Area under } CO_2 \text{ peak for 5000 ppm calibration}} \qquad (2.8)$$

2.3.6.2 - Tokyo Metropolitan University

Catalytic CO oxidation experiments were also carried out at Tokyo Metropolitan University using a similar but more flexible experimental set up. Typically between 10-50 mg of catalyst was diluted with between 150 – 190 mg of α-alumina to give a total sample mass of 200 mg. This was packed between two pieces of glass wool in a 6 mm diameter u-shaped glass reactor. Using 3 flow controllers to mix gases it was possible to use 0.5 – 10 vol% CO and 1 – 20 % O_2 at flow rates 10-100 ml min^{-1} with the balance of the gas being made up by He. Using water and oil baths the reactions were able to be carried out between 10 – 120 °C.

2.3.6.3 - Kinetic Measurements

Experiments were carried out to determine reaction orders and activation energies of CO oxidation catalysts using Arrhenius plots. To determine reaction rates more accurately conditions were chosen to make it possible to model the reactor system as a differential plug flow reactor. These conditions used were:

1. Small catalyst amounts – to allow the assumption that the reaction rate is constant throughout the bed.
2. Slow reactions – low conversion was achieved by high flow rates which allows the assumption that there is no concentration gradients through the catalyst bed.

By modelling the reactor as a differential reactor it is possible to determine the reaction rate by using the equation:

$$\text{Reaction rate} = \frac{\text{CO Flow rate x Conversion}}{\text{Catalyst Bed Volume}} \quad (2.9)$$

A derivation of the reaction rate equation for a differential reactor is shown in Appendix 1.

2.4 - Catalyst Characterisation

2.4.1 - Temperature Programmed Reduction

Temperature programmed reduction (TPR) is a thermal analysis technique that allows H_2 consumption to be measured while the sample undergoes a heating profile therefore indicating the temperatures at which the sample consumes H_2 and has been used extensively to study catalytic systems.[5] During a temperature programmed reduction the sample is heated under a flow of H_2 containing gas and H_2 consumption by the sample can be monitored using a TCD to analyse the gas that has passed through the sample cell. A plot of TCD signal against temperature can indicate at which temperature the sample undergoes reduction. A positive peak in the TCD signal indicates H_2 consumption. TPR can give an indication as to what temperature a sample needs to be reduced at to generate the desired species on a catalyst and can also give an indication of the initial species present on the catalyst.

TPR profiles were recorded using a Thermo 1100 series TPDRO. 0.1 g of sample was packed into the sample tube between quartz wool. Argon (15 ml min^{-1}) was then passed through the system while it was heated from room temperature to 110 °C at 5 °C min^{-1}, where it was held for 60 min. The sample was allowed to cool to room temperature and following this the gas was switched to 10% H_2 / Ar (15 ml min^{-1}) and the sample was heated at 5 °C min^{-1} up to 800 °C. The profile was recorded using a TCD with positive polarity.

2.4.2 - BET Adsorption Isotherms

The measurement of surface area by N_2 adsorption using the BET equation has been used as a characterisation tool in catalysis for many years.[6] The BET isotherm is an extension of the Langmuir isotherm that takes into account multiple layer adsorption, making a number of

assumptions, firstly gas layers physisorb onto a solid in layers infinitely, secondly there is no interaction between the layers and thirdly the Langmuir adsorption isotherm can be applied to each layer. This results in the BET equation shown below:

$$\frac{p}{v(p_o-1)} = \frac{c-1}{v_m c}\left(\frac{p}{p_o}\right) + \frac{1}{v_m c} \qquad (2.10)$$

p is the gas partial pressure, p_o is the saturation pressure, v is the volume of gas adsorbed at the relative pressure, v_m is the monolayer volume and c is the BET constant defined as:

$$c = \exp\left(\frac{E_1 - E_2}{RT}\right) \qquad (2.11)$$

where E_1 and E_2 are the heat of adsorption of the first and second layer respectively, R is the gas constant and T the temperature at which the adsorption is carried out.

At low pressure the surface of the solid is only partially covered by the adsorbing gas, at higher pressures the monolayer is filled and the isotherm reaches a plateau. This part of the isotherm from zero pressure to the pressure of point B is equivalent to the Langmuir isotherm shown in figure 2.6. At higher pressures a second layer starts to form followed by multilayer formation as the pressure approaches the saturation pressure.

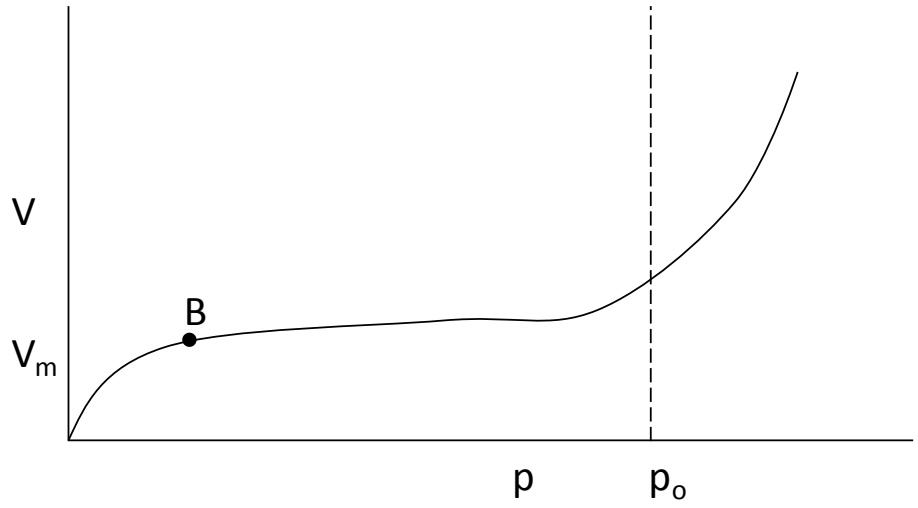

Figure 2.6 – Plot to show the variation in volume of adsorbed gas with increasing partial pressure.

Surface area analysis was determined using a Micromeritics Gemini 2360 analyser. A known amount of sample, 100-200 mg, was placed into a straight walled tube and degassed for 1 h at 120 °C under a flow of N_2 to remove any physisorbed material before surface area analysis was carried out. The sample was re-weighed after degassing to account for the slight weight change caused by removing physisorbed material. The surface area was analysed using a single point analysis typically taking 5 points between $P/P^o = 0.05 – 0.1$

2.4.3 - X-Ray Diffraction

X-Ray diffraction (XRD) is a technique which can give information about the averaged bulk structure of crystallite phases present in the material and also to estimate crystallite sizes. XRD is a non-destructive technique which has a detection limit of around 5 wt% and can detect crystallite phases down to a size of around 5 nm.[7] X-rays are generated by bombarding a copper target with high energy electrons. As the electrons are slowed by the target they produce a broad X-ray background which has superimposed onto it characteristic narrow energies, known as K_α and K_β, which arise from energy released by electrons falling from high energy shells to fill gaps in core shells generated by bombardment with primary electrons. The X-rays generated are filtered to give a monochromatic source and as these X-rays hit the sample they are scattered by the atomic planes present in the crystalline materials. Figure 2.7 shows scattered X-rays exiting the sample where they can constructively interfere when the distance between the lattice planes is equal to an integer number of wavelengths or when $AB + BC = n\lambda$,

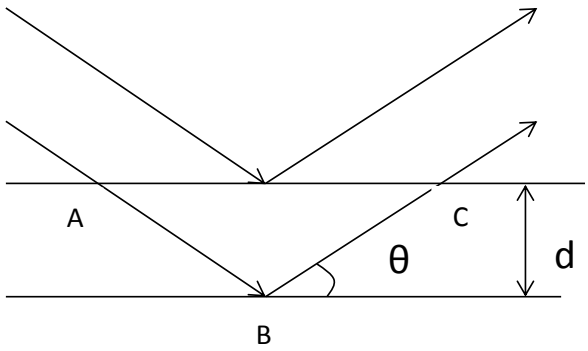

Figure 2.7 - Diagram to show diffraction of X-rays from successive lattice planes of a crystallite where d is the lattice spacing and θ is the angle between incident and normal to the plane.

By maintaining a stationary X-ray source and using a movable detector to measure the angle at which constructive interference occurs (θ) it is possible to calculate the lattice spacing of the crystallite using the Bragg relationship shown as equation 2.12. Each different crystallite has reflections at a unique set of angles, θ.

$$n\lambda = 2d \sin\theta \quad (2.12)$$

n = an integer, λ = X-ray wavelength, d = lattice spacing, θ = angle between incident and normal to the plane.

For small crystallites, for example supported metal nanoparticles, incomplete destructive interference gives rise to line broadening. This means that information about crystallite size can be extracted from the shape of the peaks. Smaller crystallites have fewer lattice planes giving rise to broader peaks, whereas large crystallites which have many lattice planes give rise to very narrow peaks. Using the Scherrer equation, shown as equation 2.13, is it possible to estimate the crystallite size of a supported metal particle:

$$n = \frac{k\lambda}{\beta \cos\theta} \quad (2.13)$$

n = crystallite size, k = form factor, λ = X-ray wavelength β = full width half maximum of the peak, θ = diffraction angle.

Investigation of the bulk structure of the catalytic materials was carried out using a (θ-θ) PANalytical X'pert Pro powder diffractometer using a Cu Kα radiation source operating at 40 KeV and 40 mA. Standard analysis was performed using a 40 min scan between 2θ values of 10-80° with the samples supported on an amorphous silicon wafer. Diffraction patterns of phases were identified using the ICDD data base.

2.4.4 - *In-Situ* X-ray Diffraction

An extension of standard XRD is *in-situ* XRD which allows the study of the bulk phase to be monitored continuously as the sample is heated, pressurised or exposed to reaction conditions or a pressure of gas. Investigation of the bulk properties of the catalysts was carried out while increasing the temperature of the sample to mimic calcination conditions. An X'pert Pro XRD fitted with an Anton-Parr XRK900 *in-situ* cell (internal volume of 0.5 L) was used with XRD

patterns recorded between 10-55° 2θ at various temperatures as the sample was heated under static air. Diffraction patterns of phases were identified using the ICDD data base.

2.4.5 - X-ray Photoelectron Spectroscopy

X-ray photoelectron spectroscopy (XPS) is a characterisation technique which can give information such as composition and oxidation state of species on the surface of the catalyst to a depth of around 10 nm.[8] XPS is based on the photoelectric effect, whereby an atom absorbs high energy X-ray radiation and as a consequence ejects a core electron with a characteristic amount of kinetic energy. The kinetic energy of the ejected electron depends on the energy of the incident X-rays, the binding energy of the core electron and the work function of the spectrometer being used. Each element has a specific binding energy for each of its core electrons, and this also depends on the oxidation state of the sample. The higher the oxidation state of the sample the higher the binding energy of its core electrons. To eject an electron from a core level the incident energy of the X-rays has to be greater than this binding energy. The work function of the spectrometer is the energy needed to eject an electron from the Fermi level into a vacuum and therefore to detect an electron the incident X-rays have to be higher in energy than the binding energy and the work function combined with the excess energy being measured as the kinetic energy of the electron. Based on the conservation of energy the equation below describes the process,

$$E_k = h\nu - E_b - \varphi \quad (2.14)$$

E_k – kinetic energy of electron, $h\nu$ – photon energy, E_b – binding energy, φ – work function

By keeping the energy of the incident X-ray photons constant and with the binding energy and work function being characteristic and constant for each element it is possible to record XPS spectra as either intensity of detected photoelectrons vs kinetic energy or by only detecting electrons of a certain kinetic energy, intensity of photoelectrons detected vs binding energy. The simplified energy level diagram of equation 2.14 is shown in figure 2.8. This shows that to eject an electron from a core level the photon energy of the incident x-ray beam is equal to the binding energy, work function and kinetic energy combined.

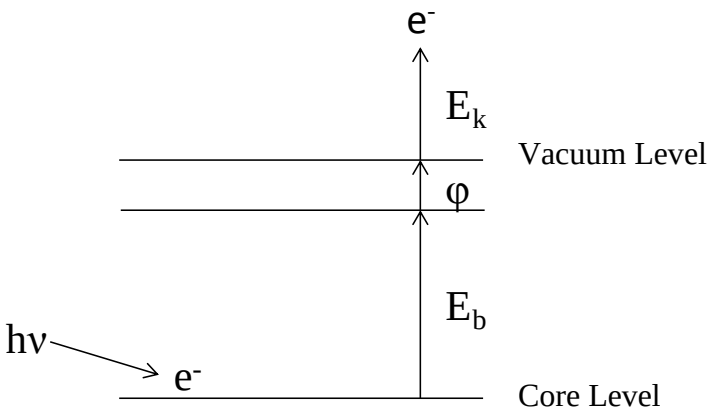

Figure 2.8 - Energy level diagram to illustrate the energy barriers associated with the photoelectric effect, where E_b is the binding energy of the core electron, φ is the work function and E_k is the residual kinetic energy associated with the electron.

XPS was performed using a VG EscaLab 220i spectrometer, using a standard Al-Kα X-ray source (300 W) and an analyser pass energy of 20 eV. Samples were mounted using double-sided adhesive tape, and binding energies were referenced to the C 1s binding energy of adventitious carbon contamination, which was taken to be 284.7 eV.

2.4.6 - Scanning Transmission Electron Microscopy

To image structures on the nm scale optical microscopy cannot be used because the wavelength of light is greater than the structures trying to be imaged. To image structures 10 nm and below, electron microscopy is used. Scanning transmission electron microscopy, STEM, is a technique that can give information about the morphology of catalyst particles at the atomic scale.[9]

STEM employs a high energy electron beam which is focused onto a small area of the sample. Detectors positioned around the sample can produce a number of images, a bright field image is generated by detecting the electrons which pass straight through and are therefore unaffected by the sample. As the beam attenuation is related to the density and thickness of the sample along with diffraction of the electron beam, bright field imaging can give a 2 dimensional projection of where metal particles are located. Dark field images are created by the diffracted electron beam which is detected slightly off angle to the incident beam. The diffracted electrons can only be detected when the electron beam passes through a crystalline species such as an oxide support or supported metal particle. By detecting at even higher angles electrons scattered by the presence

of heavy elements such as supported metal particles can be detected, this is known as high angle annular dark field, HAADF imaging and the detection regions are shown in figure 2.9.

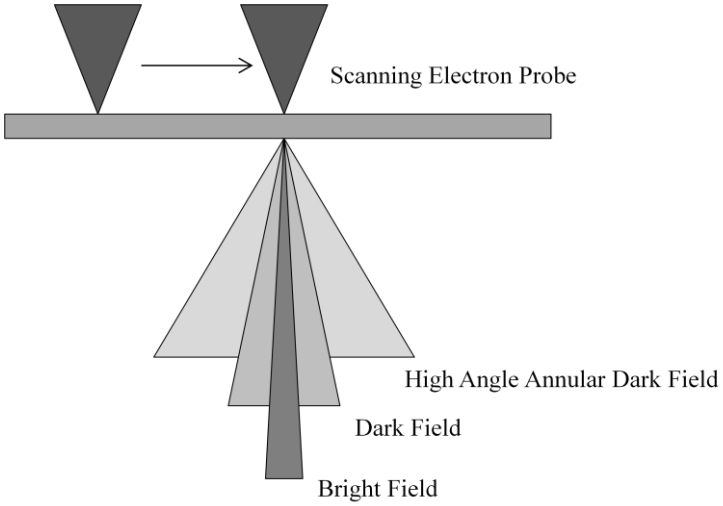

Figure 2.9– Schematic of the detection regions of a STEM microscope

STEM was carried out by Prof. Chris Kiley's group at Lehigh University. Samples of each catalyst were prepared for examination by STEM by dispersing the catalyst powder in high-purity ethanol. A drop of the suspension was then allowed to evaporate on a holey-carbon film supported by a 300-mesh copper TEM grid. Atomic-resolution, high-angle annular dark field (HAADF) scanning transmission electron microscopy was carried out using a JEOL 2200FS TEM/STEM and an FEI Titan 80-300 TEM/STEM, both equipped with CEOS spherical aberration correctors. All STEM-HAADF images were medium low-pass filtered using a 3x3 kernel in order to reduce high-frequency noise.

In addition to STEM electron microscopy electron energy-loss spectroscopy (EELS) was carried out. EELS involves analysing the energy distribution of electrons that have transmitted through the specimen. Compared to X-ray energy dispersive spectroscopy (XEDS), EELS not only provides elemental information from the specimen, it also gives information about the chemistry and the electronic structure of the specimen atoms, which in turn reveals details of their bonding/valence state, the nearest-neighbor atomic structure, and the specimen thickness.

Aberration-corrected STEM imaging and EEL spectrum-imaging experiments were performed with a Nion UltraSTEM100 at Oak Ridge National Lab, equipped with a cold field emission electron source and a corrector of 3^{rd} and 5^{th} order aberrations. The microscope was operated at 100 kV accelerating voltage. EEL spectra were collected using a Gatan Enfina spectrometer.

2.5 - References

1. J. K. Edwards, B. E. Solsona, P. Landon, A. F. Carley, A. Herzing, C. J. Kiely and G. J. Hutchings, *J. Catal.*, **2005**, *236*, 69-79.
2. A. Herzing, C. Kiely, A. Carley, P. Landon and G. Hutchings, *Science*, **2008**, *321*, 1331-1335.
3. M. Haruta, S. Tsubota, T. Kobayashi, H. Kegeyama, M. J. Gent, B. Delmon, *J. Catal*, **1993**, *144*, 175-192.
4. G. Schwedt, *Essential Guide To Analytical Chemistry*, Wiley and Sons, **1997,** 142-173.
5. U. S. Ozkan, M.W. Kumthekar and G. Karakas, *Catal Today*, **1998**, 40, 3.
6. S. Brunauer, P. H. Emmett and E. Teller, *J. Am. Chem. Soc.*, **1938**, *60*, 309.
7. J. W. Niemantsverdriet, *Spectroscopy in Catalysis 3rd Edition*, Wiley, **2007,** 148-154.
8. J. W. Niemantsverdriet, *Spectroscopy in Catalysis 3rd Edition*, Wiley, **2007,** 39-80.
9. S. Amelinckx, D. V. Dyck, J. V. Landuyt, *Handbook of Microscopy – Applications in Materials Science, Solid State Physics and ChemistryMethods II*. **1997**.
10. D. B. Williams and B.C Carter, *Transmission Electron Microscopy: A Textbook for Materials Science*, **2009.**

Chapter 3

Direct Synthesis of H_2O_2 Using Supported Palladium Tin Catalysts

3.1 - Introduction

Many studies[1-19] have been carried out in order to develop heterogeneous catalysts capable of producing H_2O_2 effectively from molecular H_2 and O_2. Supported monometallic Pd catalysts are the most widely studied catalysts in the literature for the direct synthesis of H_2O_2. However Pd catalysts which are active for H_2O_2 synthesis also tend to be active for the subsequent hydrogenation and decomposition of H_2O_2 resulting in lower overall yield and reduced H_2O_2 selectivity. The addition of halides and acids, either added to the reaction solution or incorporated into the catalyst, have been used to suppress the competing hydrogenation and decomposition reactions leading to improved yields of H_2O_2.[5-9] It has been previously shown that Au-Pd bimetallic catalysts are significantly more active and selective for the direct synthesis of H_2O_2 than monometallic palladium catalysts.[10-17] Furthermore, no acid or halide additives are needed when using these more active catalysts.[18]

In order to scale up the direct process to an economically viable size, catalyst cost is an important factor that has to be taken into account and any reduction in the cost, while still maintaining the efficiency of the system, would be very advantageous. There are various ways to achieve this including decreasing the amount of the active precious metals present in the catalyst. Another way would be to develop alternative Pd-based bimetallic catalysts containing an inexpensive second metal as a replacement for Au. However, to date, there are no such bimetallic catalysts reported that can compete with the best Au-Pd bimetallic catalysts for the direct synthesis of H_2O_2. As one of the main problems with the Pd based catalyst systems is the over hydrogenation of O_2 to form water a means of altering the hydrogenation activity of Pd might provide a route to a more effective catalyst for the direct synthesis of H_2O_2.

Recently a number of papers have appeared in the literature investigating the effect of the addition of Sn to Pd in hydrogenation reactions. For example, a study of Pd and Pd-Sn catalysts for the hydrogenation of 1-3 butadiene has been reported by Pattamakomsan *et al.*[20] They showed that for monometallic Pd catalysts, butane was formed and 1-butene was isomerised at high conversion of 1,3-butadiene. In contrast, the bimetallic Pd–Sn catalysts showed 100% butene selectivity at the relatively high 1,3-butadiene conversion (80%) without any loss of 1-butene to butane (via hydrogenation) or 2-butene (via isomerisation). CO–IR experiments confirmed that Sn addition played an important role in modifying the nature of surface sites and the electronic properties of the Pd and hence changing the catalytic properties.

Another similar study carried out by Sales *et al.* [21] on the liquid phase hydrogenation of hexa-1-3-diene and hexa-1-5-diene using Pd and Sn-Pd catalysts. In the case of hexa-1,5-diene hydrogenation, monometallic palladium catalysts give mainly 1-hexene at conversions lower than 80% and hex-2-ene by isomerisation at higher conversions. The selectivity to 1-hexene at higher conversions is significantly improved by addition of Sn to Pd. In the hydrogenation of hexa-1,3-diene, hex-1-ene is preferentially formed on monometallic palladium catalysts with low metal dispersion; on bimetallic Pd–Sn the selectivity to hex-3-ene is enhanced and this isomer is even predominant up to 100% conversion using Pd–Sn catalysts. These results are explained by the geometric effect of the dilution of Pd atoms, which reduces the palladium double-bond isomerisation ability. Both of these studies show that the addition of Sn to Pd catalysts can alter the behaviour of the catalyst during hydrogenation reactions and in particular may have an effect on subsequent reactions of the products with the catalyst.

The only example in the literature of Sn-Pd based catalysts being used in the direct synthesis of H_2O_2 is a patent granted to the Mitsubisi Gas Company and was authored by Tomita *et al*..[22] They claimed that palladium catalysts supported on various oxide supports including SiO_2, ZrO_2, TiO_2 and mixed oxides such as MoO_3-ZrO_2 and WO_3-ZrO_2 could be improved by impregnating a large amount of tin (II) acetate (15 wt%) onto the oxide support prior to impregnating Pd at a much lower loading (0.5 wt%), however no explanation of the effect was given in the article. We have therefore concentrated on the possibility of using supported Pd-Sn, with much lower Sn quantities than previously reported as a potential catalyst for the direct synthesis of H_2O_2 because of the possible ability of Sn to alter the hydrogenation behaviour of Pd. This work explores the potential use of TiO_2 and SiO_2 based catalysts prepared by conventional impregnation methods in the direct synthesis of H_2O_2.

3.2 - Results

Supported Sn-Pd catalysts were prepared on SiO_2 and TiO_2 by the standard impregnation methods explained in chapter 2 using $Pd(NO_3)_2$ and $SnCl_4$ as metal precursors because of their high solubility in water. All H_2O_2 synthesis and hydrogenation tests were carried out according to the testing procedures outlined in chapter 2 unless otherwise stated. A summary of the testing conditions is given below:

- Rate of H_2O_2 production determined after reaction using the standard reaction conditions: 5% H_2/CO_2 (2.9 MPa) and 25% O_2/CO_2 (1.1 MPa) , 8.5 g solvent (5.6 g MeOH + 2.9 g H_2O), 0.01 g catalyst, 2 ^oC , 1200 rpm, 30 mins.
- Rate of hydrogenation of H_2O_2 calculated from the amount of H_2O_2 hydrogenated using standard reaction conditions: 2.9 MPa 5%H_2/CO_2, 8.5 g solvent (5.6 g MeOH, 2.22 g H_2O and 0.68 g 50%H_2O_2), 0.01 g catalyst, 2 ^oC, 1200 rpm, 30 mins.

3.2.1 - Catalyst Testing

3.2.1.1 – H_2O_2 synthesis testing of monometallic and bimetallic Sn-Pd catalysts supported on TiO_2 and SiO_2

Monometallic catalysts were prepared by impregnation containing 5 wt% Pd and 5 wt% Sn using both SiO_2 and TiO_2 as support materials and calcined at 500 °C for 3 h in static air. Table 3.1 shows that the supported 5 wt% Pd catalyst was active, as expected, for the direct synthesis of H_2O_2 under our standard reaction conditions. Table 3.1 also shows that the monometallic 5 wt%

Sn catalysts were active for H_2O_2 synthesis however much less active than the monometallic Pd catalysts. Bimetallic catalysts were prepared containing 2.5 wt% Pd / 2.5 wt% Sn on both SiO_2 and TiO_2, table 3.1 shows that these bimetallic catalysts had enhanced activity when compared to the monometallic Pd and Sn catalysts on both supports, indicating a synergistic effect between Pd and Sn for the synthesis of H_2O_2. In the case of SiO_2 the bimetallic catalyst has an activity of 40 mol kg_{cat}^{-1} h^{-1} compared to monometallic Pd which had an activity of 12 mol kg_{cat}^{-1} h^{-1}. On TiO_2 a smaller improvement was observed with the productivity increasing from 41 mol kg_{cat}^{-1} h^{-1} for the monometallic Pd catalyst to 62 mol kg_{cat}^{-1} h^{-1} for the bimetallic catalyst.

Catalyst	**H_2O_2 productivity / mol kg_{cat}^{-1} h^{-1} TiO_2**	**H_2O_2 productivity / mol kg_{cat}^{-1} h^{-1} SiO_2**
5 % Pd	41	12
5 % Sn	18	7
2.5 % Pd / 2.5 % Sn	62	40
2.5 % Pd	20	8
2.5 % Sn	6	5

Table 3.1 - H_2O_2 productivity of monometallic and bimetallic Sn-Pd catalysts supported on SiO_2 and TiO_2 showing synergy between Sn and Pd. All catalysts calcined in static air at 500 °C for 3 h.

Comparing the sum of the H_2O_2 productivity of the supported monometallic 2.5 wt% Pd, 2.5 wt% Sn with the bimetallic 2.5 wt% Pd / 2.5 wt% Sn catalysts, a clear synergistic effect between Pd and Sn when supported on both TiO_2 and SiO_2 is observed. This effect is similar to the synergistic effect previously reported for supported Au-Pd catalysts on identical support materials.[10-17]

3.2.1.2 – H_2O_2 Synthesis and Hydrogenation Activity of Sn-Pd Catalysts with Various Metal Ratios

To investigate the effect of Sn : Pd ratio on both the synthesis and hydrogenation activity of these materials a series of catalysts were prepared on SiO_2 and TiO_2 containing a total nominal metal content of 5 wt% with varying Sn and Pd contents. The H_2O_2 synthesis results of the catalysts containing various Sn : Pd are shown in figure 3.1.

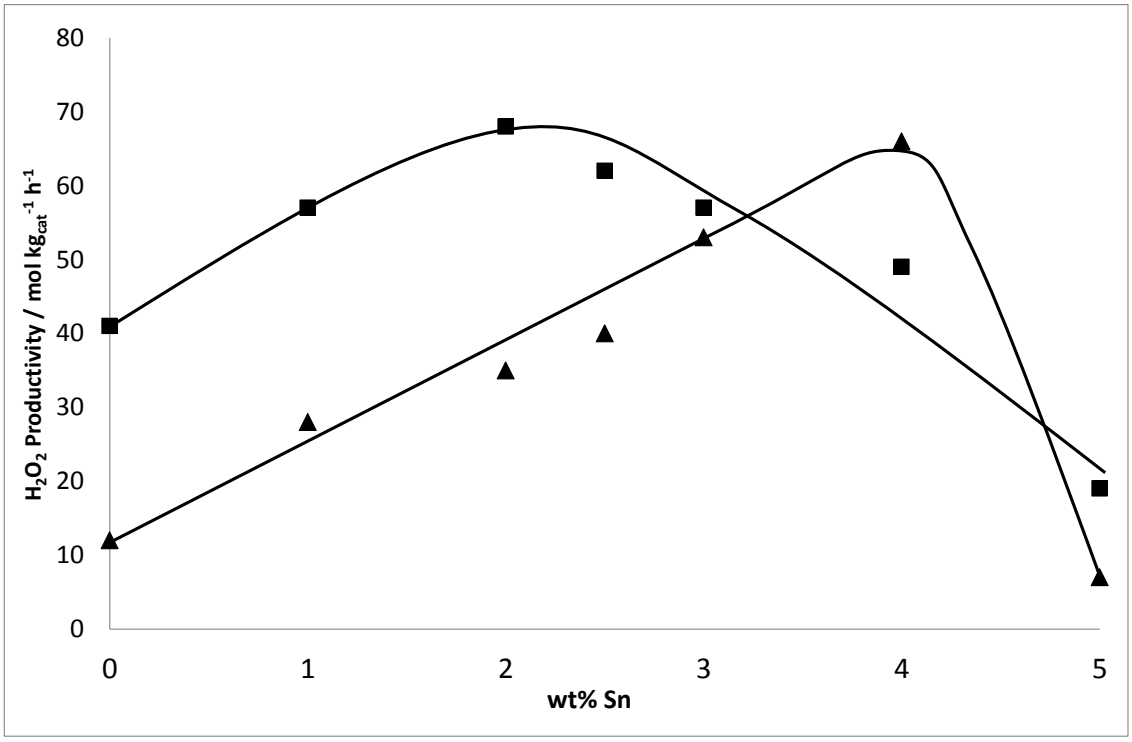

Figure 3.1 - Effect of Pd-Sn composition on the synthesis of H_2O_2 using SiO_2 (▲) and TiO_2 (■) supported catalysts. All catalysts calcined in static air at 500 °C for 3 h.

The results show that for both the SiO_2 and TiO_2 supported materials the Pd-Sn bimetallic catalysts, irrespective of the Pd : Sn ratio were considerably more active than their corresponding monometallic Pd or Sn counterparts containing the same total metal loading (5 wt %). The results also show that the Sn : Pd ratio had a significant effect on the activity of the catalyst. For both supports it was found that 2.5 % Pd / 2.5 % Sn was not the optimum composition and interestingly the optimum ratio was different on SiO_2 than on TiO_2, with the optimum SiO_2 catalyst containing 1 wt% Pd / 4 wt % Sn which had a H_2O_2 synthesis activity of 65 mol kg_{cat}^{-1} h^{-1} , whereas when TiO_2 was used as the support the optimum ratio was 3 wt% Pd / 2 wt% Sn which had a productivity of 68 mol kg_{cat}^{-1} h^{-1}. With the exception of the 1% Pd / 4% Sn catalyst, all other TiO_2-supported bimetallic Pd-Sn catalysts showed higher H_2O_2 synthesis activities than the corresponding SiO_2 supported catalysts with the same Pd : Sn ratio. These observations suggest that the optimum metal ratio is support dependant for this system, with the SiO_2 support appearing to utilise the Pd better than the TiO_2 system. This is in contrast to the analogous Au-Pd system where 2.5% Au 2.5% Pd has been shown to be the most active catalysts on both supports.[12]

Table 3.2 shows the results of the H_2O_2 hydrogenation tests carried out on the same catalysts with varying Sn : Pd ratios. The results show that irrespective of the Pd : Sn ratio, all Pd-Sn

bimetallic TiO_2 or SiO_2 supported catalysts were less active for H_2O_2 hydrogenation/decomposition than the corresponding Pd monometallic catalysts. On both supports the monometallic Sn catalysts showed very low hydrogenation activity especially on SiO_2 where no hydrogenation activity was measured. It is interesting to note that on TiO_2 the catalyst with the lowest hydrogenation activity, 2 % wt Pd / 3 wt % Sn, is not the most active for direct synthesis of H_2O_2. Similarly on SiO_2 the sample with the lowest hydrogenation activity (3 % wt Pd / 2 wt% Sn) is not the most active for the synthesis of H_2O_2. This indicates that the addition of Sn lowers the hydrogenation activity of Pd catalysts but at the cost of some synthesis activity, meaning that the hydrogenation reaction cannot be switched off independently of the synthesis reaction.

Catalyst	**H_2O_2 hydrogenation rate /** mol kg_{cat}^{-1} h^{-1} **TiO_2**	**H_2O_2 hydrogenation rate /** mol kg_{cat}^{-1} h^{-1} **SiO_2**
5 % Pd	126	113
5 % Sn	32	0
4 % Pd / 1 % Sn	83	75
3 % Pd / 2% Sn	65	50
2.5 % Pd / 2.5 % Sn	41	53
2 % Pd / 3 % Sn	12	60
1 % Pd / 4 % Sn	65	66

Table 3.2- H_2O_2 hydrogenation over monometallic and bimetallic Sn-Pd catalysts supported on SiO_2 and TiO_2 containing various metal ratios. All catalysts calcined in static air at 500 °C for 3 h.

These results indicate that Sn as a catalyst component may play an analogous role to that identified for Au in previous studies[10-17], by helping to suppress the H_2O_2 hydrogenation/decomposition which results in an enhancement of the H_2O_2 yield in the calcined catalysts compared to the monometallic samples.

3.2.1.3 – Effect of catalyst reduction on H_2O_2 synthesis and hydrogenation over Pd-Sn catalysts

Having identified the optimum Pd : Sn ratios for the TiO_2-supported (3% Pd / 2% Sn / TiO_2) and SiO_2-supported (1% Pd / 4% Sn / SiO_2) bimetallic catalysts, the effect of reducing the catalysts to investigate if the catalysts could be made more active by generating metallic Pd species after calcination at 500 °C for 3 h was investigated. Reductions were carried out on the calcined samples using 5% H_2 in Ar at a range of temperatures (100 – 500 ^oC, for 2 h) on H_2O_2 synthesis and hydrogenation.

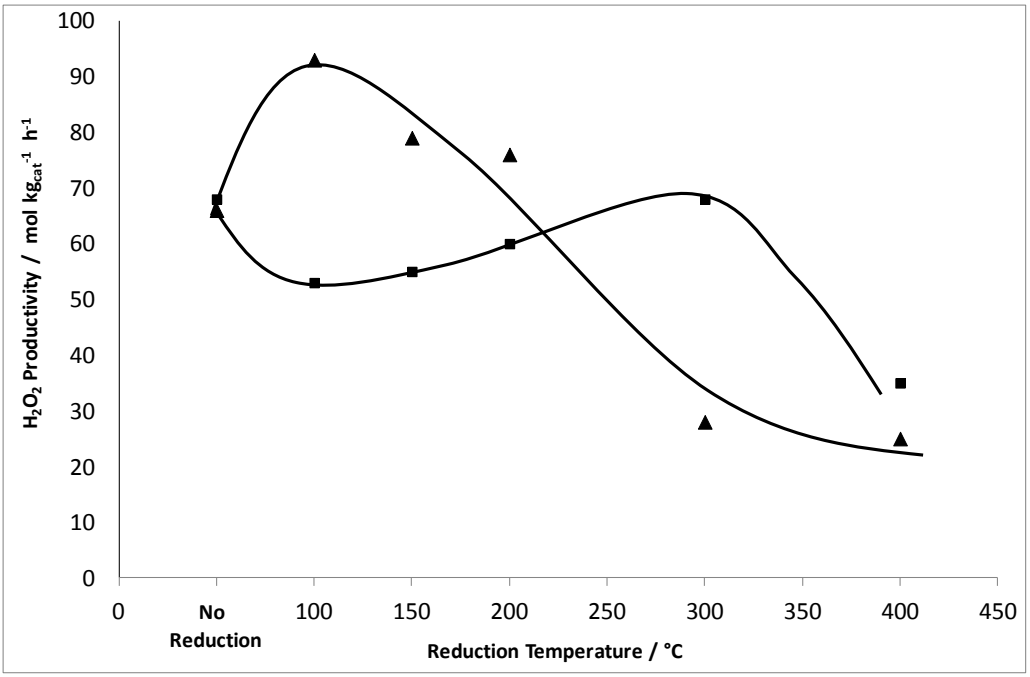

Figure 3.2 - Effect of reduction at varying temperatures of 3 % Pd / 2 % Sn / TiO_2, ■ and 1 % Pd / 4 % Sn / SiO_2, ▲, on their H_2O_2 synthesis activity. All catalysts calcined in static air at 500 °C for 3h followed by a subsequent reduction at various temperatures for 2 h under a flow of 5% H_2 / Ar.

Figure 3.2 shows H_2O_2 productivity as a function of reduction temperature. Reduction of the 1% Pd / 4% Sn / SiO_2 catalyst resulted in enhanced H_2O_2 productivities at lower reduction temperatures (100 – 200 ^oC) increasing from 65 mol kg_{cat}^{-1} h^{-1} to 93 mol kg_{cat}^{-1} h^{-1} after a reduction at 100 °C however this falls to 72 mol kg_{cat}^{-1} h^{-1} after reduction at 200 °C. The relationship between H_2O_2 productivity and the reduction temperature for the SiO_2-based catalyst shows that the activity decreases dramatically if the reduction temperature is increased beyond 300 °C, with the productivity decreasing to ~ 30 mol kg_{cat}^{-1} h^{-1} after reduction at these higher

temperatures. The H_2O_2 productivity of the optimum bimetallic Sn Pd catalyst supported on TiO_2 did not show any improvement on reduction at 100 °C but a slight decrease in activity from 68 mol kg_{cat}^{-1} h^{-1} to 58 mol kg_{cat}^{-1} h^{-1}. At temperatures from 100 – 300 °C the catalyst showed very little change in H_2O_2 productivity and similarly to the SiO_2 samples at reduction temperatures higher than 300 °C the activity reduces dramatically

Figure 3.3 shows the catalyst hydrogenation activity of the Pd-Sn catalysts as a function of reduction temperature. For the SiO_2 catalyst (1 % Pd / 4 % Sn / SiO_2) and TiO_2 catalyst (3 % Pd / 2 % Sn / TiO_2) it can be seen that the low temperature reduction greatly enhances the catalysts H_2O_2 hydrogenation activity which is detrimental in terms of H_2O_2 selectivity. Figure 3.3 also shows that catalyst reduction at high temperatures increases the H_2O_2 hydrogenation activity for both the TiO_2 and SiO_2-based catalysts when compared to the calcined catalyst; however the increase was to a lesser extent than reduction at low temperatures. This observation suggests that the positive effect on the H_2O_2 productivity of reducing the SiO_2-based Pd-Sn catalysts is related to the generation of species that promote the overall hydrogenation of both O_2 and H_2O_2. For the bimetallic TiO_2 supported catalyst to retain a similar observed synthesis activity (figure 3.2) while the hydrogenation activity increases dramatically after reduction at 100 °C also suggests that the synthesis activity must also have increased after a low temperature reduction however was masked by the increase in the hydrogenation activity.

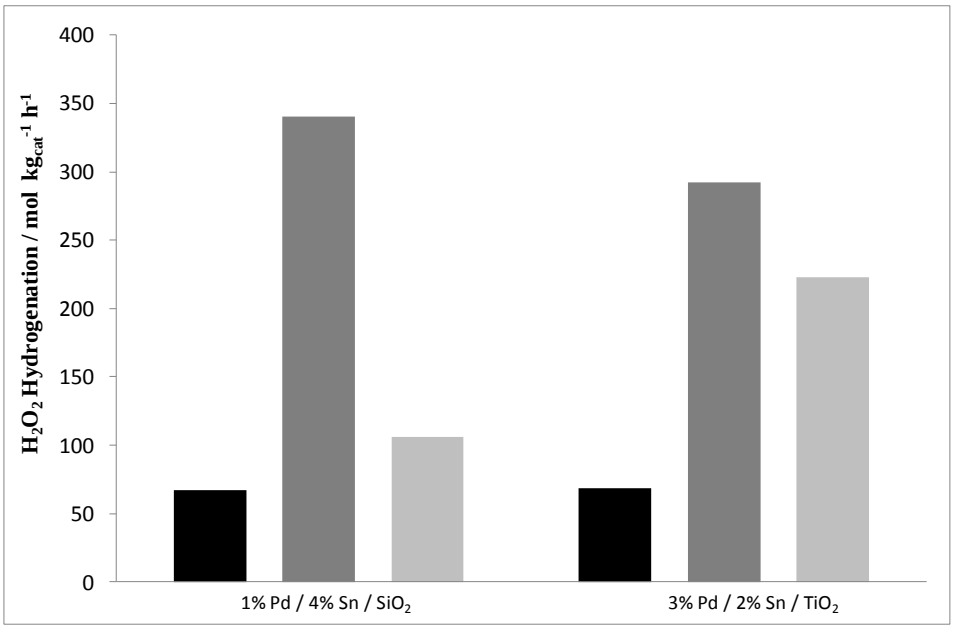

Figure 3.3 - Effect of reduction temperature on H_2O_2 hydrogenation over 4 % Sn / 1 % Pd / SiO_2 and 3 % Pd / 2 % Sn / TiO_2. ■ Calcined 500 °C / 3 h in air, ■ Calcined 500 °C / 3 h + Reduced 100 °C 2 h in 5% H_2/Ar, ■ Calcined 500 °C / 3 h + reduced 300 °C 2 h in 5% H_2/Ar.

Figure 3.4 compares the H_2O_2 synthesis activity of unreduced mono-metallic Pd / SiO_2 and Sn / SiO_2 and the optimum Pd-Sn / SiO_2 catalyst, with the activity of the analogous catalysts which have been reduced at the optimum reduction temperature, 100 ^oC for 2 h. The Pd-only and Pd-Sn bimetallic catalysts both showed marked increases in H_2O_2 synthesis activity with catalyst reduction, while the Sn-only catalyst did not show any significant improvement upon reduction at 100 °C. While the reduced 1% Pd / 4% Sn / SiO_2 bimetallic catalyst was the best H_2O_2 synthesis catalyst amongst all catalysts investigated, reduction of the Pd-only catalyst led to the highest degree of enhancement, with H_2O_2 productivity increasing from 12 to 67 mol kg_{cat}^{-1} h^{-1} compared to an increase from 66 to 93 mol kg_{cat}^{-1} h^{-1} for the 1% Pd / 4 % Sn / SiO_2 bimetallic catalyst. Although normalised to the amount of Pd the bimetallic catalyst shows a higher improvement per weight % of Pd which could indicate an increased dispersion of Pd in the bimetallic sample.

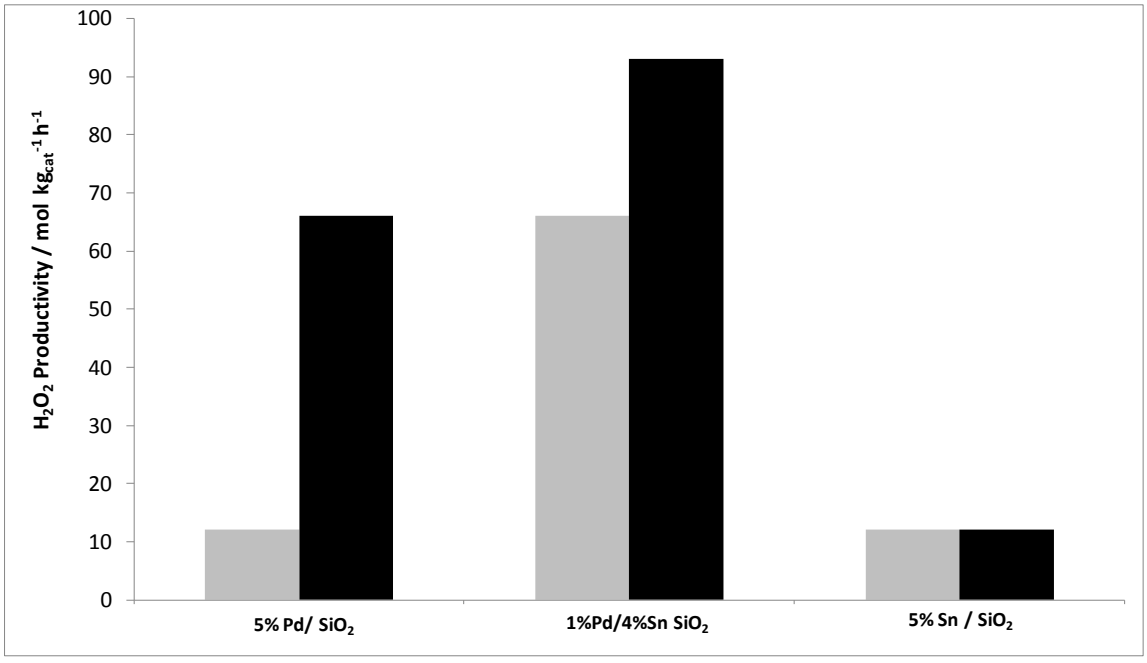

Figure 3.4 - Effect of optimum reduction temperature (at 100 ^oC) on the H_2O_2 synthesis activity of SiO_2-based Pd-only, Sn-only and 4 % Sn / 1% Pd catalysts. ■ Calcined 500 °C / 3 h in air, ■ calcined 500 °C / 3 h + reduced 100 °C 2 h in 5% H_2/Ar.

The synthesis enhancement due to catalyst reduction demonstrated by the Pd-only catalyst, coupled with the observation that the reduction of the Sn-only catalyst did not promote H_2O_2 synthesis activity and the large increase in the hydrogenation activity after reduction, suggests that the promotional effect observed upon reduction of the SiO_2-based bimetallic Pd-Sn catalysts is much more likely to be related to a reduction of Pd rather than Sn species.

3.2.1.4 – Effect of catalyst preparation method on the H_2O_2 synthesis activity of Sn-Pd catalysts.

The effect of catalyst preparation route was investigated for the optimum catalyst composition on both SiO_2 and TiO_2. Variations in the preparation method were investigated including co-impregnation or sequential impregnation and the number of heat treatments applied during these preparation was also investigated with the results being shown in table 3.3. The nomenclature used in the table relates to the order of the metal impregnation, for example 1 % Pd @ 4 % Sn / SiO_2, catalysts are denoted metal 2 @ metal 1 / support, where metal 1 was impregnated onto the support first and then dried at 110 ºC for 16 h followed by either calcination at 500 ºC for 3 h before the impregnation of metal 2 followed by the same drying and calcination procedure, or a second drying step followed by one calcination.

Catalyst	**Heat Tretments**	**H_2O_2 productivity /** mol kg_{cat}^{-1} h^{-1}
1 % Pd / 4 % Sn / SiO_2	500 °C / 3 h	65
1 % Pd @ 4 % Sn / SiO_2	500 °C / 3 h	32
1 % Pd @ 4 % Sn / SiO_2	500 °C / 3 h x 2	7
3% Pd / 2% Sn / TiO_2	500 °C / 3 h	68
3% Pd @ 2% Sn / TiO_2	500 °C / 3 h	38
3% Pd @ 2% Sn / TiO_2	500 °C / 3 h x 2	12

Table 3.3 - Effect of catalyst preparation method on the H_2O_2 synthesis activity of 1 % Pd / 4 % Sn / SiO_2 and 3% Pd / 2% Sn / TiO_2.

The results in table 3.3 show that a similar trend is followed by both SiO_2 and TiO_2 systems. Both co-impregnated catalysts showed the highest activity when compared to the catalysts prepared by sequential impregnation with a drying step in between metal impregnation before calcination. The lowest activity catalyst for both TiO_2 and SiO_2 supported materials were those prepared by sequential impregnation with a calcination between the impregnation of each metal. All further experiments were carried out on catalysts prepared by co-impregnation of Sn and Pd as this was shown to be the best impregnation method to provide high activity catalysts.

3.2.1.5 – Effect of various heat treatments on the H_2O_2 synthesis activity and stability of bimetallic Sn – Pd catalysts.

The effect of a range of heat treatments on the H_2O_2 synthesis performance and stability of the best bimetallic Sn-Pd catalysts supported on SiO_2 and TiO_2 was investigated and is reported in tables 3.4 and 3.5. For any industrial catalytic process to be viable a stable catalyst is essential to prevent the constant need to replace the catalyst and maintain a high yield of the desired product over time. The optimum SiO_2 based Sn-Pd bimetallic catalyst, 1% Pd / 4% Sn / SiO_2, was shown to be unstable after calcination at 500 °C for 3 h with the H_2O_2 productivity dropping from 66 to 22 mol kg_{cat}^{-1} h^{-1} on catalyst re-use. Increasing the calcination temperature to 600 °C for 3 h produced catalysts with much lower activity and it was shown to be similarly unstable on re-use.

Heat Treatment	**1st Use H_2O_2 productivity /** mol kg_{cat}^{-1} h^{-1}	**2nd Use H_2O_2 productivity /** mol kg_{cat}^{-1} h^{-1}	**3rd Use H_2O_2 productivity /** mol kg_{cat}^{-1} h^{-1}
500 °C / 3 h / air	66	22	n.d.
600 °C / 3 h / air	25	12	n.d.
500 °C / 3 h / air + Reduced 100 °C / 2 h	93	69	n.d.
500 °C / 3 h / air + Reduced 100 °C / 4 h	53	42	40
500 °C / 3 h / air + Reduced 200 °C / 2 h	76	76	74
500 °C / 3 h / air + Reduced 200 °C / 4 h	32	28	28

Table 3.4 – Table to show the effect of heat treatment on H_2O_2 productivity and stability over a 1% Pd / 4% Sn / SiO_2 catalyst. n.d. – not determined

After reduction in 5% H_2/Ar at 100 °C for 2 h, the H_2O_2 synthesis activity of the catalyst increased from 66 to 93 mol kg_{cat}^{-1} h^{-1} as has been shown previously. The stability of the catalyst also improved after this reductive treatment, giving H_2O_2 productivity of 69 mol kg_{cat}^{-1} h^{-1} on the second use, a much smaller drop than the catalysts which had been calcined only. Increasing the reduction time from 2 to 4 h lowered the activity of the catalyst, but did increase is stability

relative to the calcined catalyst. Increasing the reduction temperature from 100 to 200 °C for 2 h reduced the activity of the catalyst to 76 mol kg_{cat}^{-1} h^{-1}, but the catalyst then retained its activity on second and third reaction cycles. Increasing the reduction treatment time to 4 h at 200 °C significantly decreased the activity of the catalyst however the stability of the catalyst remained. These findings point to the heat treatment being crucial in developing a stable catalyst for H_2O_2 synthesis and that a reduction temperature of 200 °C is necessary to impart stability onto the calcined Sn-Pd / SiO_2 system. However these stable catalysts have a much higher hydrogenation activity than the calcined only catalysts which is detrimental in achieving high H_2O_2 selectivity.

Table 3.5 shows the effect of heat treatment on the optimum bimetallic Sn-Pd / TiO_2 catalyst, 3% Pd / 2 % Sn / TiO_2. Calcination in air at 600 and 700 °C produced catalysts which had a lower H_2O_2 synthesis activity than those calcined at 500 °C.

Heat Treatment	**1st Use H_2O_2 productivity /** mol kg_{cat}^{-1} h^{-1}	**2nd Use H_2O_2 productivity /** mol kg_{cat}^{-1} h^{-1}	**3rd Use H_2O_2 productivity /** mol kg_{cat}^{-1} h
500 °C / 3 h / air	68	14	n.d.
600 °C / 3 h / air	56	33	26
700 °C / 3 h / air	25	18	18
500 °C / 3 h / air + Reduced 200 °C / 2 h	60	58	60
500°C / 3 h / air + Reduced 300 °C / 2 h	68	51	50

Table 3.5 - Investigation of the effect of heat treatment on H_2O_2 productivity and stability of 3 % Pd / 2 % Sn / TiO_2.n.d. – not determined

All catalysts calcined in air showed poor re-usability similar to the SiO_2 samples, with their H_2O_2 synthesis activity decreasing considerably on the second use. Reduction of 3% Pd / 2 % Sn / TiO_2 material in 5 % H_2 / Ar at 200 °C for 2 h after calcination at 500 °C led to a catalyst that consistently maintains a H_2O_2 synthesis activity of 60 mol kg_{cat}^{-1} h^{-1} which could be re-used at least three times without significant loss of activity. Reduction of the calcined catalyst in 5% H_2/Ar at 300 °C for 2 h led to a catalyst that lost activity after first use, with its productivity

dropping from 68 to 50 mol kg_{cat}^{-1} h^{-1}, but on third use maintained an activity level of 50 mol kg_{cat}^{-1} h^{-1}. Again this set of results suggest that the heat treatment is crucial and the species present on the catalysts need to be reduced at a temperature of 200 °C or above to become stable to multiple reaction recycles. Again in the case of the TiO_2 supported materials the reductive treatment caused an increase in hydrogenation activity. These results (table 3.4 and 3.5) support previous findings when working with Au-Pd systems[15] in showing that optimising the catalyst heat treatment is a critical step in producing active stable catalysts.

3.2.1.6 – Effect of subsequent heat treatments on stable Sn-Pd catalysts

The observation that the catalyst hydrogenation and synthesis activity increases on reduction is consistent with the work of Choudhary and Samanta[23] who observed that metallic Pd is a more active catalyst for the direct synthesis and hydrogenation of H_2O_2 than PdO. The Sn-Pd catalyst system appears to have an inherent compromise between hydrogenation activity and stability. A stable catalyst can be prepared however it has a relatively high hydrogenation activity imparted by the reduction step. If by following this preparation method some of the Pd is not used in forming Sn-Pd alloys this would result in the formation of metallic Pd nanoparticles which will show a high hydrogenation activity or alternatively Sn-Pd alloy or mixed oxides formed in the preparation could be reduced to generate metallic Pd species. To try and lower the hydrogenation activity of the reduced catalysts a subsequent heat treatment in air was added to the preparation to try and re-oxidise these particles and lower the hydrogenation activity. The results are shown for the best SiO_2 catalyst, 1% Pd / 4% Sn / SiO_2 in table 3.6 below.

The results in table 3.6 show that after an initial calcination of 500 °C / 3 h / air gave an active catalyst with low hydrogenation activity however is unstable to re-use. After reduction at 200 °C / 2 h using 5% H_2 / Ar the catalyst produced was much more active and stable but showed a high hydrogenation activity, presumably due to the presence of metallic Pd either in the alloy particles or as isolated nanoparticles. The addition of a third heat treatment by way of calcination in air for various times firstly showed a decrease in activity at short calcination times of 1 h however the hydrogenation activity also reduced. On increasing the time of this third calcination the hydrogenation activity continued to decrease and the synthesis activity began to increase, presumably due to the reduction in hydrogenation activity of the catalyst on the re-oxidation of Pd to PdO. It may also be possible that this third calcination could generate a different distribution of Sn-Pd alloys. The optimum calcination treatment was to calcine the reduced

sample at 400 °C for 3 h in air, this gave an active stable catalyst that had no hydrogenation activity.

Heat Treatment	**1st Use H_2O_2 productivity /** mol kg_{cat}^{-1} h^{-1}	**2nd Use H_2O_2 productivity /** mol kg_{cat}^{-1} h^{-1}	**H_2O_2 hydrogenated/** mol kg_{cat}^{-1} h^{-1}
500 °C / 3 h / air	66	22	66 (2%)
500 °C / 3 h / air + Reduced 200 °C / 2 h	76	76	340 (10%)
500 °C / 3 h / air + Reduced 200 °C / 2 h + 400 °C / 1h / air	27	28	113 (3.5%)
500 °C / 3 h / air + Reduced 200 °C / 2 h + 400 °C / 2h / air	35	32	38 (1%)
500 °C / 3 h / air + Reduced 200 °C / 2 h + 400 °C / 3h / air	50	50	0
500 °C / 3 h / air + Reduced 200 °C / 2 h + 400 °C / 4h / air	22	20	0

Table 3.6 - Investigation of the effect of subsequent heat treatments on H_2O_2 productivity and stability over a 1% Pd / 4% Sn / SiO_2 catalyst.

The same calcination procedures were applied to the best TiO_2 supported catalyst and showed similar effects and the results are shown in table 3.7. On calcination at 400 °C in air the hydrogenation activity of the catalyst reduced with increasing calcination time. The hydrogenation activity reduced from 292 to 15 mol kg_{cat}^{-1} h^{-1} after calcination for 4 h, while still maintaining the synthesis activity of the calcined and reduced catalyst. This sample shows optimum performance at a slightly longer time than the SiO_2 catalyst which could be down to the higher Pd content in this catalyst requiring a longer time to re-oxidise the Pd or stronger interactions between the metal particles and the TiO_2 support. The sample shows that the H_2O_2 synthesis activity decreases slightly on subsequent calcinations for 1-4 h while the hydrogenation activity reduces more quickly to around 15 mol kg^{-1} h^{-1}, this indicates a fine balance between the synthesis and hydrogenation activity of the reduced and re-oxidised catalysts. The catalyst

subsequently calcined for 4 h at 400 ºC showed very low hydrogenation activity was stable to re-use and showed comparable activity to the well-studied 2.5% Au / 2.5% Pd / TiO_2 catalyst which has a H_2O_2 productivity of 64 mol kg_{cat}^{-1} h^1. The Au containing catalyst has a much higher hydrogenation activity of 235 mol kg_{cat}^{-1} h^1 and as thus the development of a catalyst with Au replaced by Sn which is stable and showed very little hydrogenation activity represents a big step forward in the development of catalysts for the direct synthesis of H_2O_2.

Heat Treatment	**1st Use H_2O_2 productivity /** mol kg_{cat}^{-1} h^{-1}	**2nd Use H_2O_2 productivity /** mol kg_{cat}^{-1} h^{-1}	**H_2O_2 hydrogenated/** mol kg_{cat}^{-1} h^{-1}
500 °C / 3 h / air	68	14	65 (2%)
500 °C / 3 h / air + Reduced 200 °C / 2 h	60	58	292 (8.5%)
500 °C / 3 h / air + Reduced 200 °C / 2 h + 400 °C / 1h / air	73	70	237 (7.5 %)
500 °C / 3 h / air + Reduced 200 °C / 2 h + 400 °C / 2h / air	65	63	159 (5%)
500 °C / 3 h / air + Reduced 200 °C / 2 h + 400 °C / 3h / air	59	60	34 (1%)
500 °C / 3 h / air + Reduced 200 °C / 2 h + 400 °C / 4h / air	61	60	15 (0.5%)

Table 3.7 - Investigation of the effect of subsequent heat treatments on H_2O_2 productivity and stability over a 3% Pd / 2% Sn / TiO_2 catalyst.

3.2.2 – Catalyst Characterisation

3.2.2.1 – Temperature Programmed Reduction

As a reductive heat treatment has been shown to be crucial in obtaining stable Sn-Pd catalysts for the direct synthesis of H_2O_2 temperature programmed reduction (TPR) of the catalysts was carried out following calcination at 500 °C. This allowed the investigation of the reducibility of the catalysts and to try and identify the metal species present on the bimetallic samples that may be responsible for the enhanced H_2O_2 synthesis activity. Figure 3.5 shows the TPR profiles of the monometallic Sn and Pd catalysts supported on TiO_2 and also the bare TiO_2 support after an identical calcination treatment at 500 °C for 3 h. As expected, the TPR profile of the bare TiO_2 support after being calcined at 500 °C showed no major reduction peaks in the temperature range 50-800 °C.

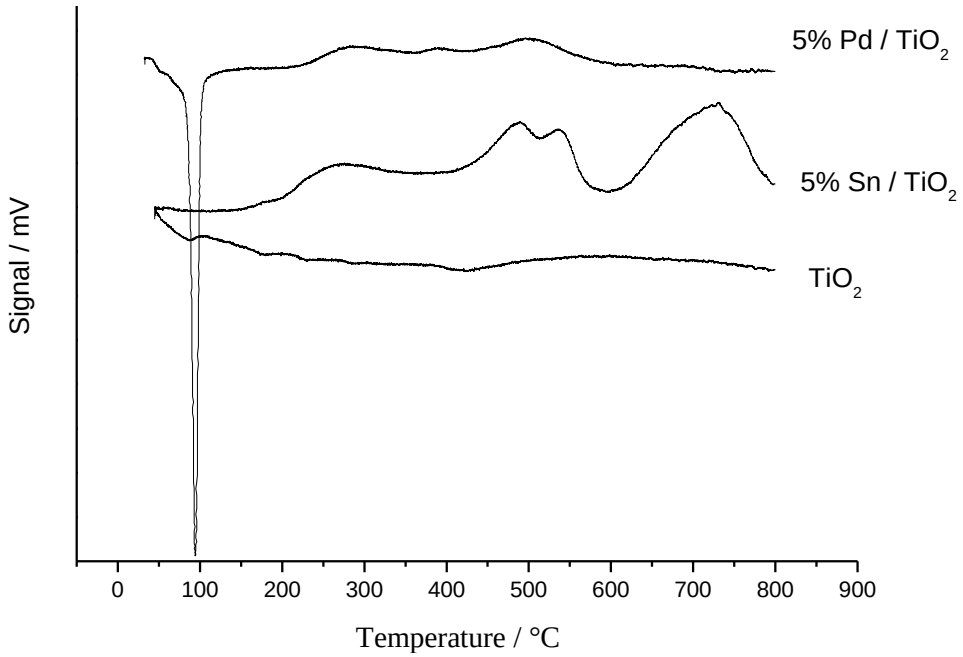

Figure 3.5 -TPR profiles of monometallic Pd and Sn supported on TiO_2 after calcination at 500 °C for 3 h in static air.

The monometallic 5% Pd / TiO_2 catalyst TPR profile is also shown in figure 3.5. A large negative response at 90 °C can be attributed to the evolution of hydrogen from the sample resulting from the decomposition of palladium-β-hydride which is consistent with literature examples.[24] The TPR profiles for Pd / TiO_2 recorded at sub-ambient temperatures have been reported in the literature to show reduction of palladium oxide to Pd metal at temperatures as low as 5 °C; this would allow hydrogen to absorb into the metallic palladium particles and form the

palladium-β-hydride phase which is seen in this profile. The monometallic Pd catalyst also showed small reduction bands at 275 and 500 °C which may be attributed to strongly bound palladium nanoparticles.[24] The TPR profile of the monometallic 5% Sn / TiO_2 catalyst (figure 3.5) showed a number of features between 200 and 800 °C. The onset of reduction is seen at 200 °C with bulk reduction beginning at around 450 °C. The large signal present at 450 °C correspond to bulk reduction of Sn (IV) to Sn (II) and the features present at lower temperatures have been assigned to the reduction of small surface Sn species. A high temperature reduction peak is centred at 720°C, which can be attributed to the reduction of Sn (II) to metallic Sn.[25]

The TPR profiles of the bimetallic catalysts, shown below in figure 3.6, show very different features compared to either of the monometallic Pd and Sn catalysts. All samples show a response at 90 °C attributed to the decomposition of palladium-β-hydride; however the intensity of this signal decreased considerably and non-linearly with increasing Sn content (*i.e.* decreasing Pd content). This could either suggest that the presence of Sn inhibits the formation of palladium-β-hydride or that the Pd is present in a different form, such as a Pd-Sn alloy, which prevents it from forming palladium-β-hydride. This observation is important as it indicates that the addition of Sn may decrease the hydrogenation activity of the bimetallic catalysts by stopping the formation of Pd-β-hydride.

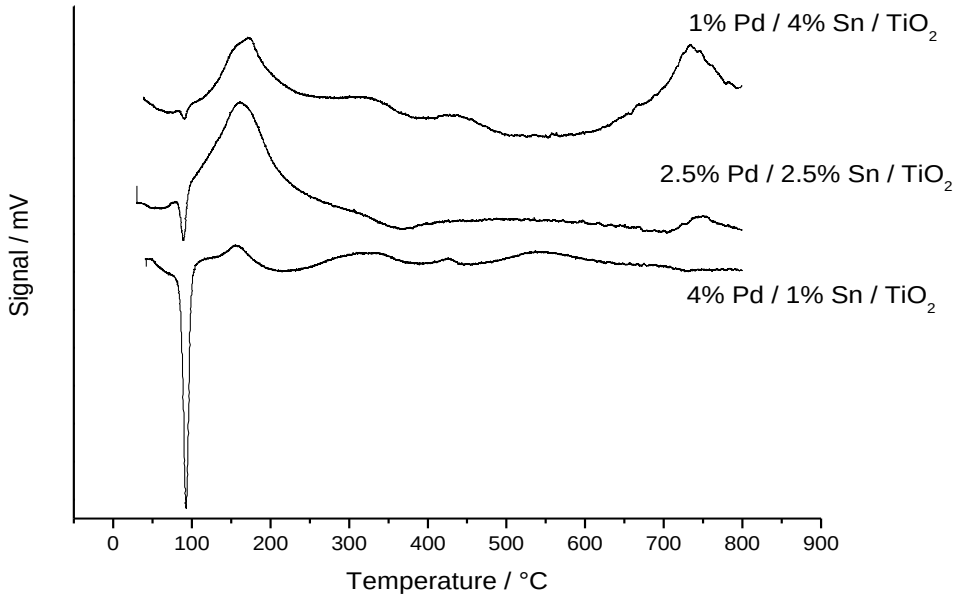

Figure 3.6 - TPR profiles of bimetallic Pd-Sn catalysts with various metal ratios supported on TiO_2 after calcination at 500 °C for 3 h in static air.

The Pd-Sn bimetallic catalysts showed additional high temperature reduction peaks (above 300 ^{o}C) which are related to Sn reduction. Interestingly the TPR profiles of the bimetallic catalysts show a new unique feature at *ca.* 150 °C. This feature is not present in the TPR profiles of either the monometallic Pd or Sn catalysts and may be related to a lowering of the reduction temperature for the Sn species which occurred at 450 °C in the monometallic Sn catalyst. However the position of the highest temperature Sn reduction peak (700 ^{o}C) is unaffected by the Pd content which may suggest that Sn reduction is independent of the presence of Pd. This new feature in the TPR profiles of the Pd-Sn bimetallic catalysts varies in intensity with varying Sn : Pd, with the 2.5 % Sn / 2.5 % Pd / TiO_2 the most active of the three catalysts showing the largest intensity for this feature. If this reduction feature was solely associated with Sn reduction, then it would be expected to give the highest signal for the sample containing the most Sn, but this is not the case. Also, if this feature indicates a lowering of the reduction temperature of Sn, then the observed temperature of the reduction should decrease as more Pd is added to the catalyst.

The presence of this feature also coincides with the decrease in the intensity of the palladium-β-hydride signal, which may suggest that the some of the Pd surfaces are no longer readily available to form palladium-β-hydride. These observations suggest that this unique TPR feature at 150 ^{o}C present in the TiO_2-based Pd-Sn bimetallic catalysts is likely to be related to a mixed Pd-Sn species, presumably a Pd-Sn alloy phase which may be active for the direct synthesis of H_2O_2. TPR profiles were also recorded for the equivalent monometallic Sn and Pd and bimetallic Sn-Pd catalysts supported on SiO_2 and are shown in figure 3.7. The monometallic 5% Pd / SiO_2 catalyst also showed a significant response at 90 °C which can be assigned to the evolution of hydrogen from the sample resulting from the decomposition of palladium-β-hydride. The monometallic Sn catalyst showed a broad reduction feature beginning at 200 °C with the highest intensity signal at 450 °C, with no features above 600 °C. According to Mossbauer studies by Nava *et al.* with Sn / SiO_2 systems [24] after reduction above 600 °C all the Sn is present as metallic Sn.

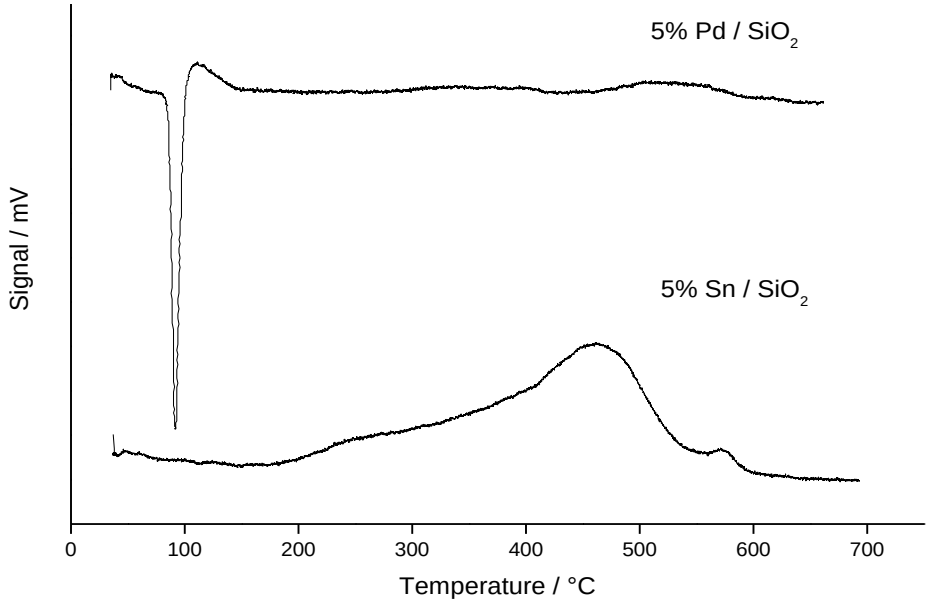

Figure 3.7 - TPR profiles of monometallic Pd and Sn supported on SiO_2 after calcination at 500 °C for 3 h in static air.

The TPR profiles of the bimetallic catalysts supported on SiO_2 are shown in figure 3.8. They show different features depending on the ratio of the two metals. The bimetallic 4 % Pd / 1 % Sn / SiO_2 catalyst shows a small negative peak due to palladium-β-hydride decomposition, which is much less intense than that expected when compared to the 5% Pd-only catalyst, which implies that the presence of Sn is limiting the formation of this hydrogen containing Pd phase. No other major features were seen in this TPR profile. In direct contrast, the 2.5 % Pd / 2.5 % Sn / SiO_2 material did not show this feature at 90°C. Instead a positive peak was seen at 100 °C, as was observed for the TiO_2-supported samples with higher Sn loadings, but with no palladium-β-hydride decomposition peak. This reduction feature was split into a doublet which might indicate either the presence of two mixed phases or two closely separated reduction steps of a single species. A broad but weak peak is also present between 300 and 400 °C which can be assigned to Sn reduction. The catalyst with a higher Sn content, i.e. 4 % Sn / 1 % Pd / SiO_2, also showed a broad reduction feature between 300 and 400 °C, and the low temperature reduction peak which only consists of a single peak in this profile. In contrast to the reduction profiles of the TiO_2-supported catalysts, no palladium-β-hydride decomposition peak was observed for the catalysts containing 2.5 % and 4 % Sn. This could indicate that if Sn-Pd alloy species are the cause of the decrease in the formation of palladium-β-hydride, they may form more readily on the SiO_2 support.

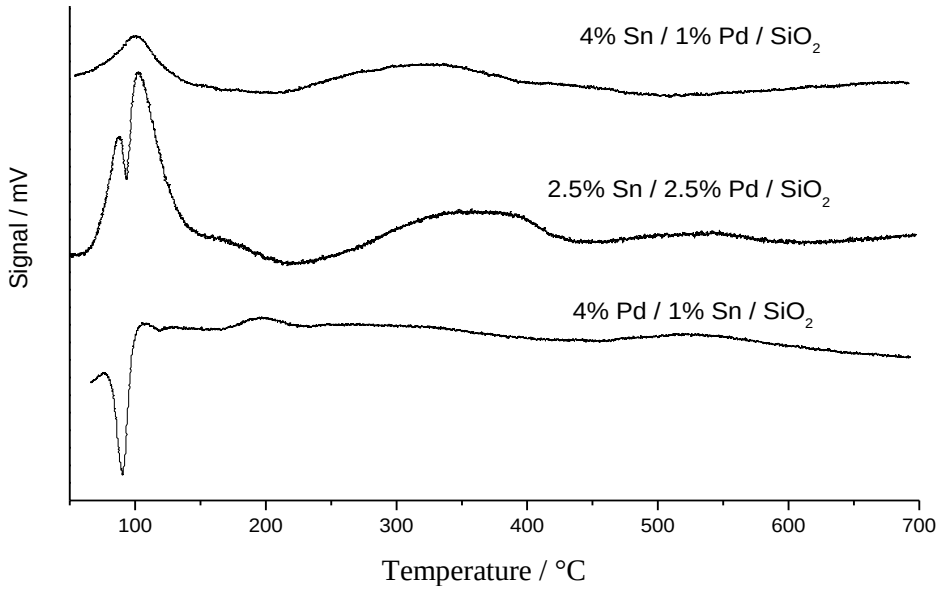

Figure 3.8 - TPR profiles of bimetallic Pd-Sn catalysts with various metal ratios supported on SiO_2 after calcination at 500 °C for 3 h in static air.

From the TPR profiles of the monometallic Pd and Sn catalysts it can be seen that the reduction temperatures of the two profiles do not overlap, with all Pd features being present below 200 °C whereas all Sn reduction features are present between 200 - 600 °C. An obvious feature of the TPR containing both Sn and Pd is the lower area of the Sn reduction peaks above 200 °C when compared to the monometallic sample even when the differences in loading are taken into account. Table 3.8 shows the integration values of the monometallic and bimetallic TPR profiles of the SiO_2 supported catalysts between 200 and 600 °C after they have been normalised with regard to sample mass, then signal per weight percent of Sn in the catalyst was calculated for comparison between samples.

% Pd Content	% Sn Content	Sample weight normalised signal area between 200 – 600 °C	Normalised Signal area between 200 – 600 °C per % of Sn	Normalised Signal with respect to 5% Sn	Catalyst Productivity mol kg_{cat}^{-1} h
5	0	0	0	-	12
0	5	246446	49289	1	7
1	4	66076	16519	0.33	68
2.5	2.5	96411	38565	0.78	36
4	1	46466	46466	0.94	24

Table 3.8 - Table showing the integration values of the SiO_2 supported catalyst TPR profiles.

As can be seen from the table above the monometallic Pd catalysts shows no signal above 200 °C, whereas the monometallic Sn catalyst shows a large signal between 200 and 600 °C. When 1% Pd is added to the catalyst, the Sn signal between 200 – 600 °C dramatically reduces and is accompanied by emergence of the positive TPR feature below 200 °C. When 1% of the Sn is replaced by Pd it would be expected to see a reduction of 20% of the Sn signal between 200 and 600 °C if there was no interaction or alloying between the two metals. In fact the signal reduces by more than 65% with respect to the monometallic Sn catalyst which suggests that there is a strong interaction between the Sn and Pd in the bimetallic catalysts. On increasing the Pd content the Sn signal between 200 – 600 °C still indicates that the Sn and Pd are interacting by a lower than expected signal corresponding to Sn reduction. The catalysts containing 4% Pd and only 1% Sn shows only a small deviation from the expected value for the reduction of 1% Sn, and this catalyst only showed a small improvement when compared to the monometallic palladium catalyst which may indicate only a small interaction between the Pd and Sn. The normalised signal between 200 – 600 °C with respect to the monometallic Sn catalysts is a good indication of the amount of interaction between the two metals and it follows that the more interaction there is the higher the activity of the catalyst.

Due to the higher reduction temperature of Sn on TiO_2, as seen in figure 3.5, the same analysis cannot be carried out on the Sn-Pd / TiO_2 TPR profiles although a similar effect can be seen on the addition of Pd to Sn. With the 2.5% Sn / 2.5% Pd catalysts showing almost no signal at high reduction temperatures where it is expected to see a Sn reduction peak with the area of half the monometallic sample. This indicates that nearly all the Sn is interacting with the Pd in either alloy formation of in close proximity to the Pd species. This ratio corresponds to the best catalyst formulation found on TiO_2 after calcination at 500 °C with an activity of 68 mol kg_{cat}^{-1} h^{-1}. This catalyst also shows the biggest positive signal between 100 - 200 °C which may represent the reduction of a Sn-Pd species, this sample also shows a small palladium-β-hydride which indicates that there is some small Pd only particles present in the sample which may be responsible for the high hydrogenation activity of the catalysts after reduction to make the catalyst stable.

Figure 3.9 shows both the TPR profile and the H_2O_2 productivity of the 4 % Sn / 1 % Pd / SiO_2 catalyst. It can be clearly seen that as the reduction temperature is increased beyond the temperature needed to reduce the feature observed at 100 °C, the productivity increases to its maximum value of 93 mol kg_{cat}^{-1} h^{-1}. As the temperature is further increased beyond this point (*i.e.* 150 and 200 °C) the productivity decreases slightly to 76 and 72 mol kg_{cat}^{-1} h^{-1}, with the

200 °C reduction giving a stable catalyst. This indicates that complete reduction of this species may be needed to form stable catalysts. Increasing the reduction temperature even further to 300 and 400 °C produced low activity catalysts based on the TPR results it is considered that reduction at these high temperatures results in Sn reduction which may be responsible for the lower catalytic activity.

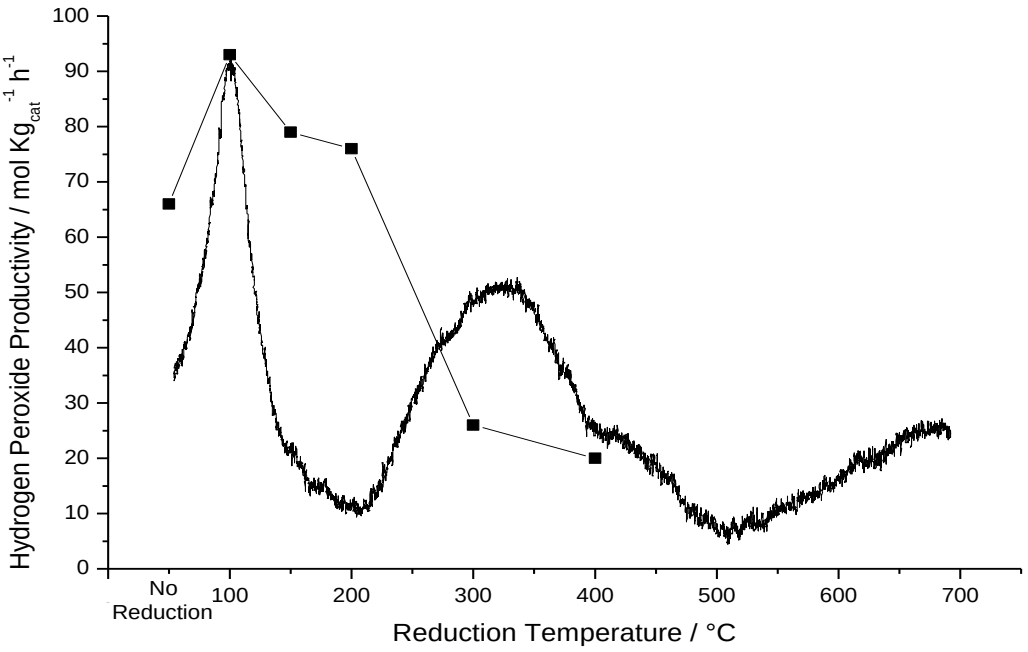

Figure 3.9 - Combined TPR profile and H_2O_2 productivity after various reduction temperatures of 4 % Sn / 1 % Pd / SiO_2.

Figure 3.10 shows the TPR profiles of the 4 % Sn / 1 % Pd / SiO_2 prepared by various impregnation methods, including co-impregnation methods and sequential impregnation methods. The TPR profiles show very different features depending on the preparation methods used. The 1 % Pd @ 4 % Sn / SiO_2 catalyst which as has been calcined between the impregnation of Sn and Pd shows a TPR profile with a large negative peak at 80 °C which indicates a palladium-β-hydride phase which means that Pd is present in the catalyst which is not associated with Sn. This TPR profile looks most like a combination of the monometallic Pd and Sn catalyst TPR profiles and is the least active catalyst. The catalysts prepared with one calcination but sequential impregnation of the metals showed a large positive reduction peak that was split into a doublet which might indicate either the presence of two Sn-Pd species indicating that the metals may not be as intimately mixed Sn-Pd species as the catalyst prepared by co-

impregnation. There is also a large signal at higher reduction temperatures indicating a large amount of isolated Sn still present in the catalyst when compared to the catalyst prepared by co-impregnation.

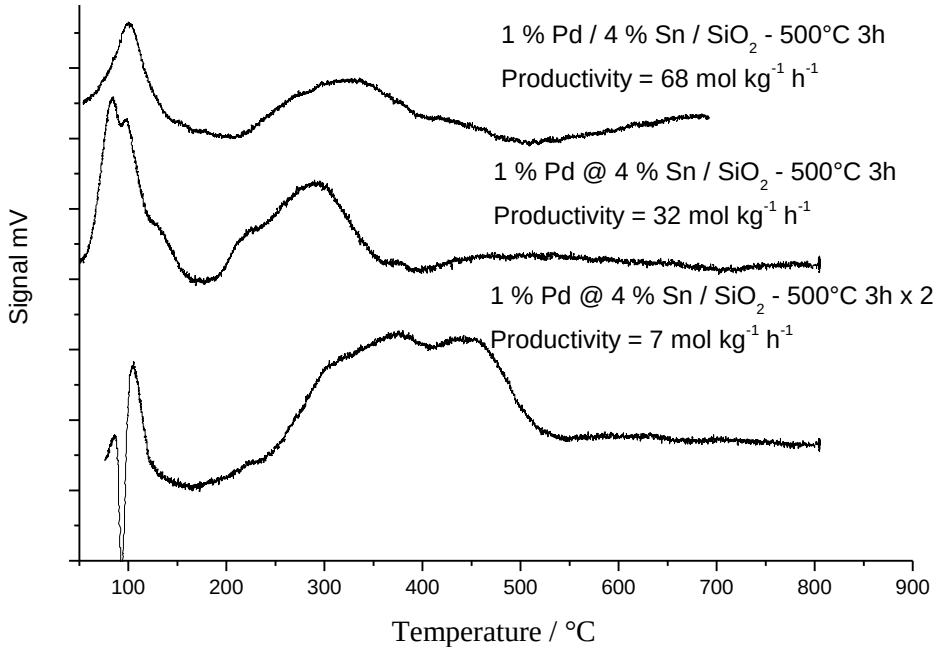

Figure 3.10 – TPR profiles of 1% Pd / 4% Sn / SiO_2 prepared by various impregnation methods.

3.2.2.2 – X-Ray Diffraction

X-ray diffraction patterns were obtained for selected Sn-Pd bimetallic catalysts supported on SiO_2 and TiO_2. Figure 3.11 shows XRD of the monometallic 5% Pd, 5% Sn and bimetallic 2.5% Pd 2.5% Sn supported on silica after calcination at 500 °C for 3 h. The 5% Pd and 5% Sn materials both show a broad reflection at 22° from the poorly crystalline silica support. The monometallic Pd and Sn catalysts both show reflections characteristic of the PdO and SnO_2 phases respectively. The bimetallic catalyst shows weak features of both PdO and SnO_2 indicating that while synergy is observed when adding Sn to Pd a small amount of PdO is retained in the bimetallic sample.

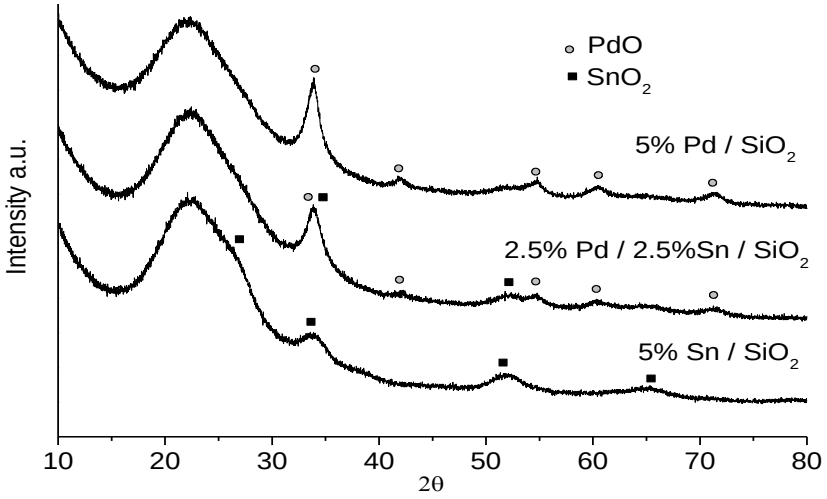

Figure 3.11 - XRD profiles of monometallic and bimetallic catalyst supported on SiO_2 after calcination at 500 °C for 3 h.

Figure 3.12 illustrates how the XRD pattern varies when the Sn : Pd ratio is changed. PdO features are indicated by the dashed line and as the Pd content is decreased from 5% the features become less intense as expected. The same can be seen with the SnO_2 reflections indicated by the dotted lines. The reflection at 34° is a combination of both SnO_2 and PdO reflections and the shape of this reflection does not change regularly with increasing Pd content. Interestingly the intensity of this reflection for the catalyst containing 1% Pd / 4% Sn is lower and broader than for 5% Sn. This could indicate an enhanced dispersion of the Pd or Sn when the metals are present at this composition. There are also no features visible which relate to PdO at higher angles in this catalyst.

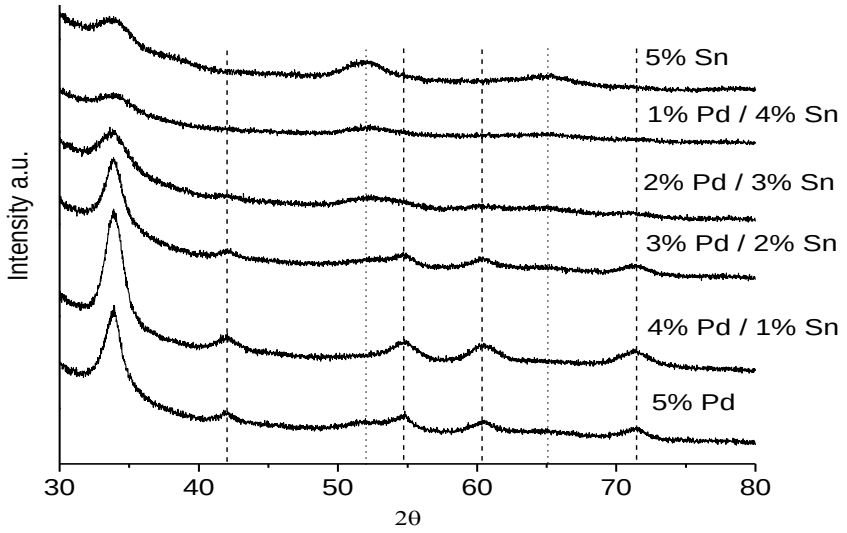

Figure 3.12 - XRD profiles of monometallic and bimetallic catalysts supported on SiO_2 containing varying ratios of Pd and Sn after calcination at 500 °C for 3 h.

To check that the absence of PdO peaks in the XRD pattern was not due to the Pd being below the detection limits of the technique, standard samples were prepared with 1% Pd and calcined at 500 °C for 3 h, identical to that employed for the catalyst containing 1% Pd / 4% Sn / SiO_2. The XRD patterns are shown in figure 3.13. The catalysts containing 1% Pd with no Sn clearly show PdO reflections at 34°, with an average particle size of 9 nm. After reduction at 100 °C, the catalyst clearly showed reflections of Pd metal with similar particle sizes. These features are not present in the catalyst containing 1% Pd / 4% Sn either after calcination or calcination and subsequent reduction at 100-300 °C, implying that Sn enhances the dispersion of Pd in the bimetallic catalysts or the Pd is incorporated into the Sn as an alloy, especially in the lower Pd content catalysts. After subsequent calcination after reduction of the catalyst no discernable features could be detected above the SiO_2 diffraction patterns indicating that the metals are in a highly dispersed state. The observation of a reduction in the average particles size seen when Sn and Pd are both present in the catalyst is consistent with the observations from TEM performed by Vicente *et al.* who studied Sn-Pd catalysts for the hydrogenation of citral. [26]

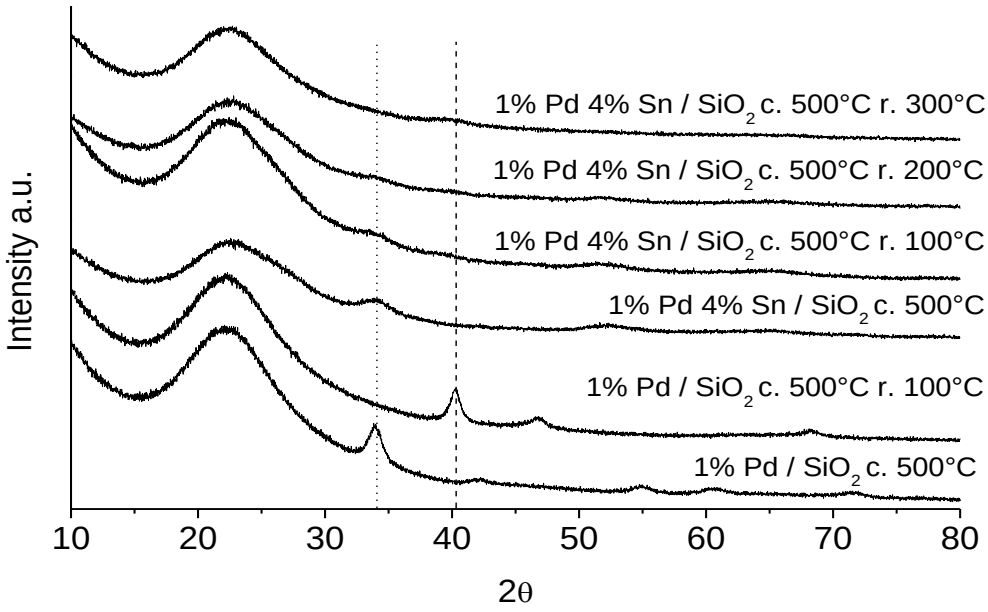

Figure 3.13 - XRD profiles of 1% Pd 4% Sn / SiO_2 after various calcination and reduction treatments. PdO indicated by the dotted lines and metallic Pd by the dashed line.

XRD patterns were recorded for the equivalent TiO_2 samples however no reflections corresponding to Sn or Pd could be seen over the intense anatase and rutile peaks of the TiO_2 used as the support material for the catalyst.

3.2.2.3 –Electron Microscopy

The metal dispersion of several key catalysts was investigated using STEM and SEM analysis by Prof Kiely's group at Lehigh University. Analysis combined the use of these two techniques to try and observe the very broad range of particle sizes typically encountered in samples prepared by impregnation methods. For comparison with the bimetallic catalyst STEM-HAADF images of the calcined monometallic samples (*i.e.* 5% Pd / SiO_2 calcined 500 ^oC for 3h in air and 5% Sn / SiO_2 calcined for 500 ^oC in air) are shown in Figures 3.14 and 3.15, in both of these samples nanoparticles of Pd and Sn can be seen in the respective samlpes. Figure 3.14 shows SEM data obtained from the 5% Sn / SiO_2 sample in which µm-scale Sn-rich particles can be found along with nanoparticles of varying size.

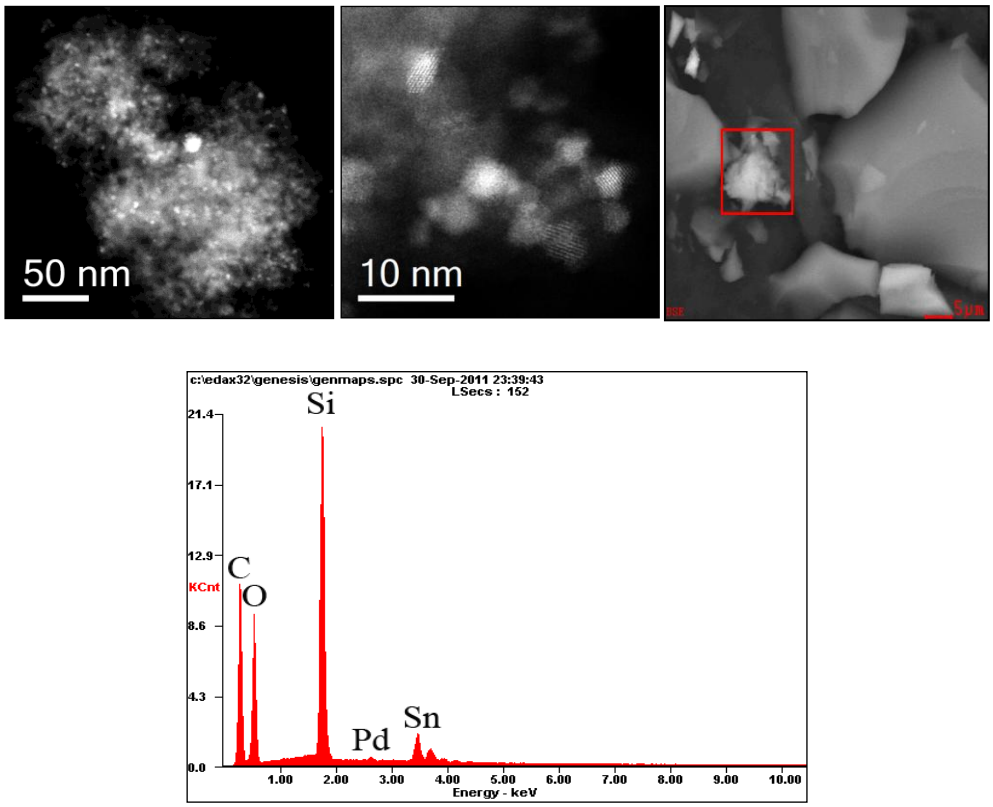

Figure 3.14 - STEM-HAADF images of the monometallic sample 5% Sn / SiO_2 calcined 500 °C for 3 h in air.

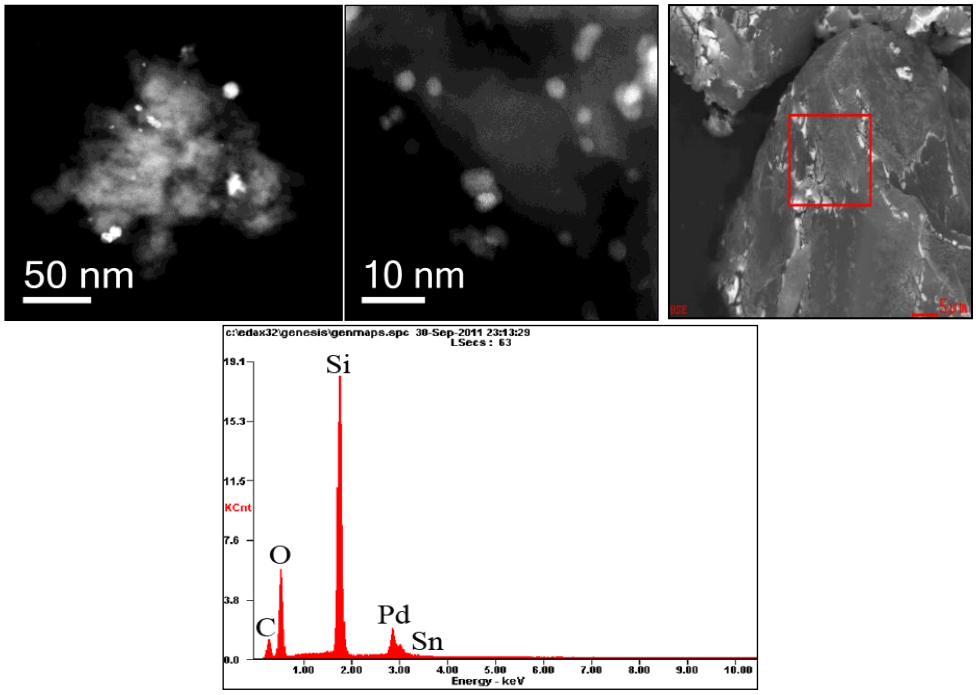

Figure 3.15 - STEM-HAADF images of the monometallic sample 5% Pd / SiO_2 calcined 500 °C for 3 h in air.

Interestingly, SEM images of the 5% Pd / SiO_2 sample, figure 3.15 did not show any µm-scale Pd particles, but instead exhibited extended thin film regions that were Pd-rich and showed characteristic cracking patterns along with Pd nanoparticles around 5-10 nm. This particle size corresponds to the particles size estimated using the Scherrer equation from XRD patterns of the calcined monometallic Pd catalyst.

Representative high angle annular dark field (HAADF) STEM images of the fresh 1% Pd / 4% Sn / SiO_2 catalyst after calcination for 3 h at 500 ^{o}C in air are presented in figure 3.16. Numerous finely dispersed nanoparticles in the 2-5 nm size range are present indicating a reduced average particle size on addition of Sn, although occasional larger scale (10-20 nm) particles can also be found. STEM-XEDS was used to probe the composition of individual particles.. The particles in the 2-5 nm size range were generally found to contain both Pd-Sn, although their compositions were very variable from particle-to-particle. Furthermore, there was no systematic correlation between the size of a particle and its composition. Indeed, very few of these particles actually exhibited a composition corresponding to the nominal loading (*i.e.* 1% Pd : 4 % Sn weight ratio). No comparable features to the monometallic Pd catalyst were found in the bimetallic 1% Pd / 4% Sn / SiO_2 sample in terms of the cracking patterns observed during SEM analysis, probably because of the lower overall Pd loading.

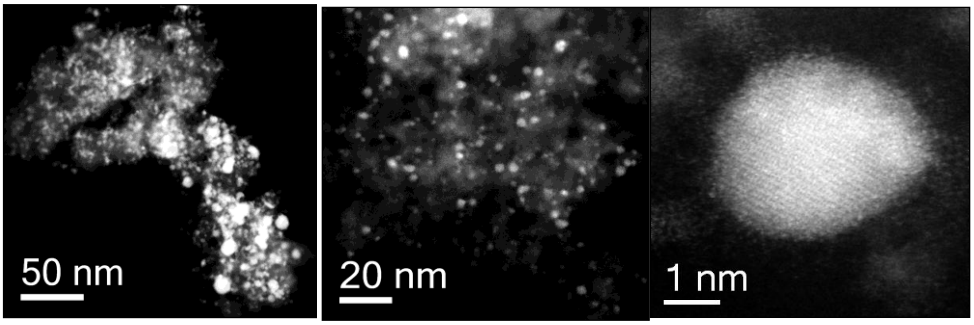

Figure 3.16 - HAADF images of 1% Pd / 4% Sn / SiO_2 catalyst after calcination for 3 h at 500 ^oC in air and then subsequently reduced at 200 ^oC for 2 h in 5% H_2 / Ar.

Shown in figures 3.17 and 3.18 are representative HAADF images of both the optimum SiO_2 and TiO_2 catalysts after calcination and subsequent reduction to give stable catalysts with high hydrogenation activity. Also shown are images of the best catalysts which are stable and show no hydrogenation activity after the calcination-reduction-calcination cycle described earlier.

The HAADF images of both catalysts show that there is a high density of nanoparticles between 2-5 nm. The high dispersion retained after two high temperature heat treatments shows that these nanoparticles are particularly resistant to sintering at high temperatures. This is confirmed by observing that the samples that have undergone three heat treatments have retained a high density of small particles. EDX analysis of the samples shows that the small nanoparticles are composed of Sn-Pd alloys in the samples after calcination-reduction and calcination-reduction-calcination. This may indicate that the change in hydrogenation activity and stability with heat treatments is likely due to a chemical change, *e.g.* oxidation states of Pd, rather than a change in particle size distribution of the particles observed. All small particles were observed to contain both Sn and Pd although no uniform composition was observed in the particles and no dependence on the composition on the size was observed. Due to the many possible Sn-Pd alloys that could exist in these samples it is not possible to identify a specific alloy responsible for the activity. As Sn and Pd have similar atomics masses it is difficult to differentiate the metals in electron microscopy images due to similar observed contrast.

a)

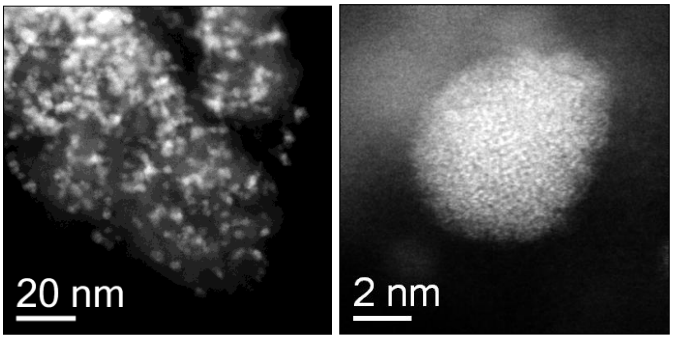

b)

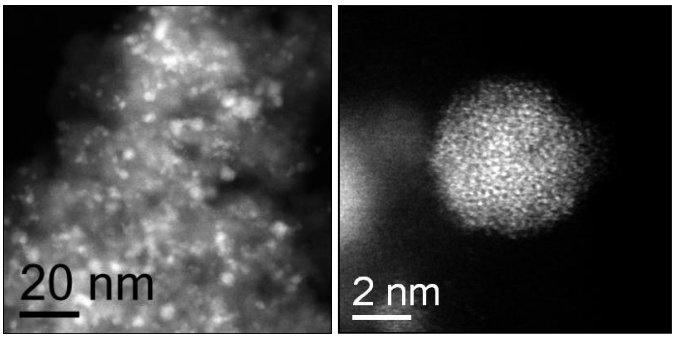

Figure 3.17 - HAADF images of 1% Pd / 4% Sn / SiO_2 after a) Calcination at 500 ºC 3 h + Reduction 200 ºC 2 h and b) Calcination 500 ºC 3 h + Reduction 200 ºC 2 h + Calcination 400 ºC 3 h.

a)

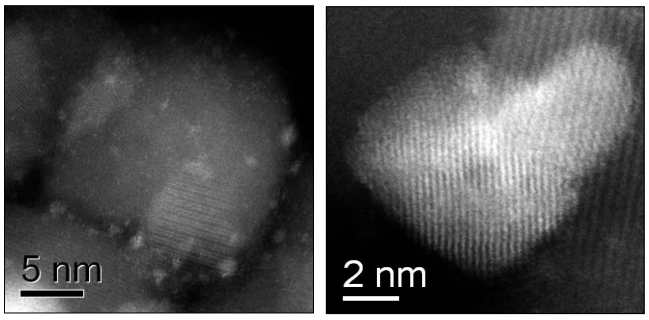

b)

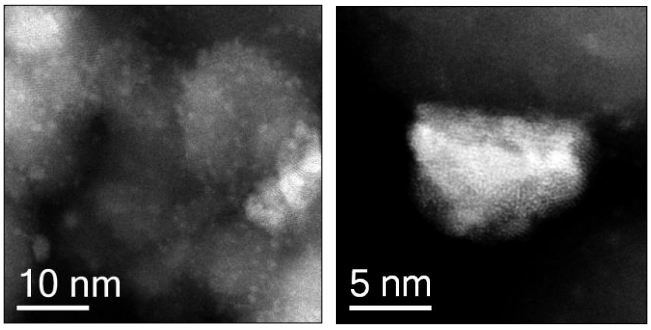

Figure 3.18- HAADF images of 3% Pd / 2% Sn / TiO_2 after a) Calcination at 500 ºC 3 h + Reduction 200 ºC 2 h and b) Calcination 500 ºC 3 h + Reduction 200 ºC 2 h + Calcination 400 ºC 3 h.

The microscopy study confirms that co-impregnation is an efficient and simple method to produce bimetallic Pd-Sn alloy catalysts, but at present it provides limited control of the alloy particle composition and size distribution however similar trends were seen on both TiO_2 and SiO_2 supports. On incorporation of Sn a lower average particle size was observed in the bimetallic catalysts when compared to the monometallic samples. The particle size and density of particles remained during all three heat treatments indicating that these particles are more resistant to sintering than supported Au catalysts which are known to sinter easily during high temperature heat treatments.

3.2.2.4 – X-ray Photoemission Spectroscopy

XPS spectra were recorded for the best catalysts supported on SiO_2 after various heat treatments and also for the monometallic catalysts, TiO_2 samples were not investigated due to the presence of a higher concentration of isolated Pd as shown by the TPR profiles. Figure 3.19 shows the Pd(3d) XPS spectra of monometallic and bimetallic catalysts after calcination at 500 ºC for 3 h. The monometallic Pd sample shows peaks indicating the Pd is present in the 2+ oxidation state which agrees with the observation of PdO in the XRD analysis. The Pd(3d) XPS spectra of the bimetallic catalysts shows a shift to higher binding energy relative to the monometallic catalysts which indicates that the Pd is in a more oxidised state, possibly indicating electron transfer from Pd to Sn.

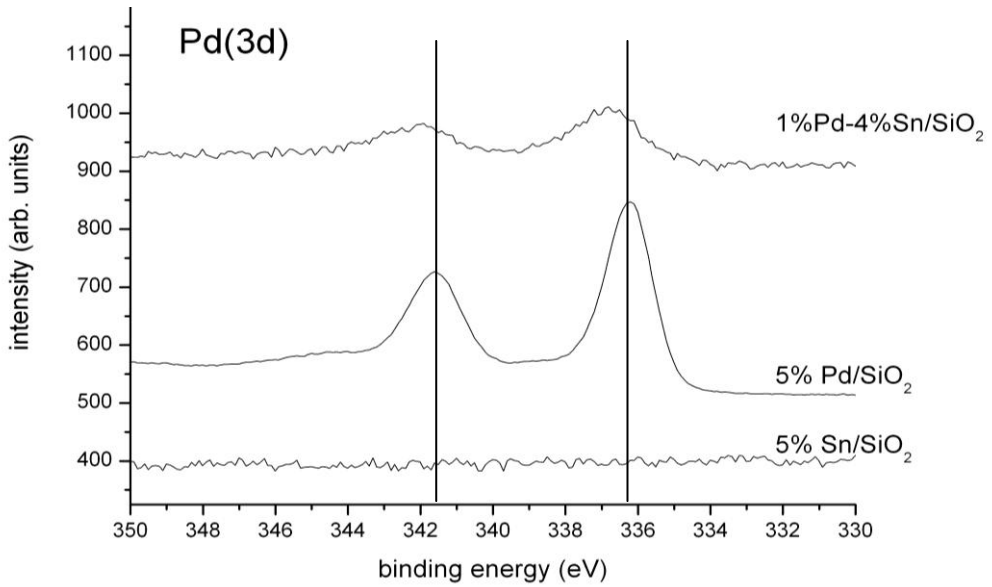

Figure 3.19 – Pd(3d) XPS spectra of monometallic and bimetallic Pd and Sn catalysts after calcination at 500 ºC for 3 h.

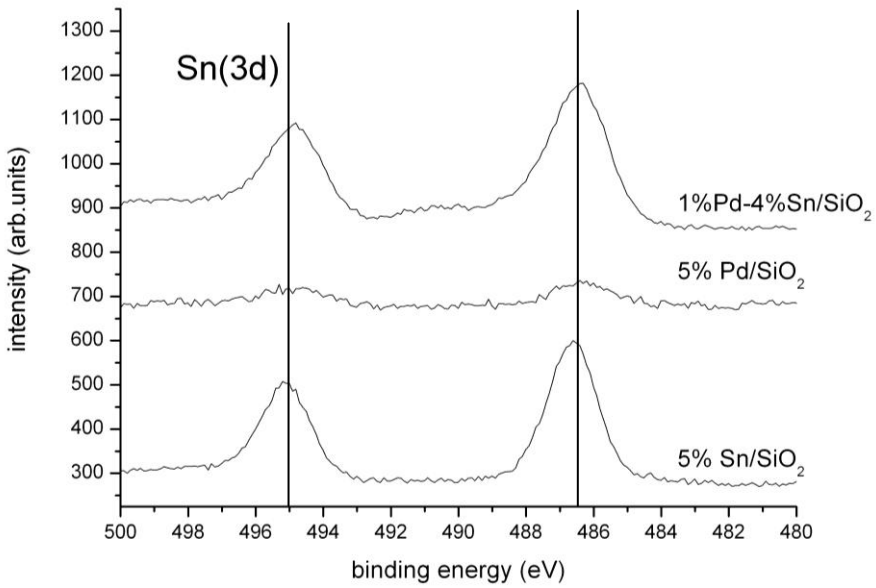

Figure 3.20 – Sn(3d) XPS spectra of monometallic and bimetallic Pd and Sn catalysts after calcination at 500 ºC for 3 h.

Figure 3.20 shows the Sn(3d) XPS spectra of monometallic and bimetallic catalysts after calcination at 500 ºC for 3 h. The monometallic catalyst shows peaks associated with the Sn(IV) oxidation state which again agrees with the XRD analysis. Again a shift is seen in the position of the peaks in the bimetallic catalysts but in this case the shift to lower binding energy indicating a more reduced Sn species. Following the observations from the STEM analysis observed particles that contained both Sn and Pd coupled with the observation that the binding energy of the Sn and Pd shift in opposite directions in the bimetallic catalysts relative to the monometallic samples indicates a strong possibility that the Sn and Pd have formed alloy particles with electron density moving from Pd to Sn in the particles. On inspection of the metal to Si ratios when compared to the monometallic samples both the Sn and Pd ratio to Si are much lower than expected; this could be consistent with sintering of the metal particles or the dilution of the metals indicating alloy formation. The fact that the XRD indicates better Pd dispersion when in a bimetallic catalyst and the shifts indicating electron transfer between the metals suggests that alloy particles have been formed. The ratios also show that both metal to Si ratios decrease by roughly the same amount which is consistent with a homogeneous alloy has been formed between the Sn and Pd in contrast the core shell structures observed in Au-Pd analogues.[16] The presence of Sn-Pd bond formation is also supported by the observation that the addition of Sn stops the formation of palladium-β-hydride.

Figure 3.21 shows the Pd(3d) XPS spectra for the of 1% Pd / 4% Sn / SiO_2 after calcination at 500 ºC for 3 h and subsequent reduction at various temperautres for 2 h under 5% H_2 / Ar. A clear shift from Pd(II) to metallic Pd can be seen after reduction at 100 °C and remains unchanged during reduction upto 400 °C. The Sn(3d) spectra show no indication of Sn reduction during reduciton upto 400 °C. The productivity of the catalyst increases after reduction up to 200 °C then reduces after reduction at 400 °C with a increase in hydrogenation acitvity for all reduced catalysts which can be correlated with the presence of metallic Pd.

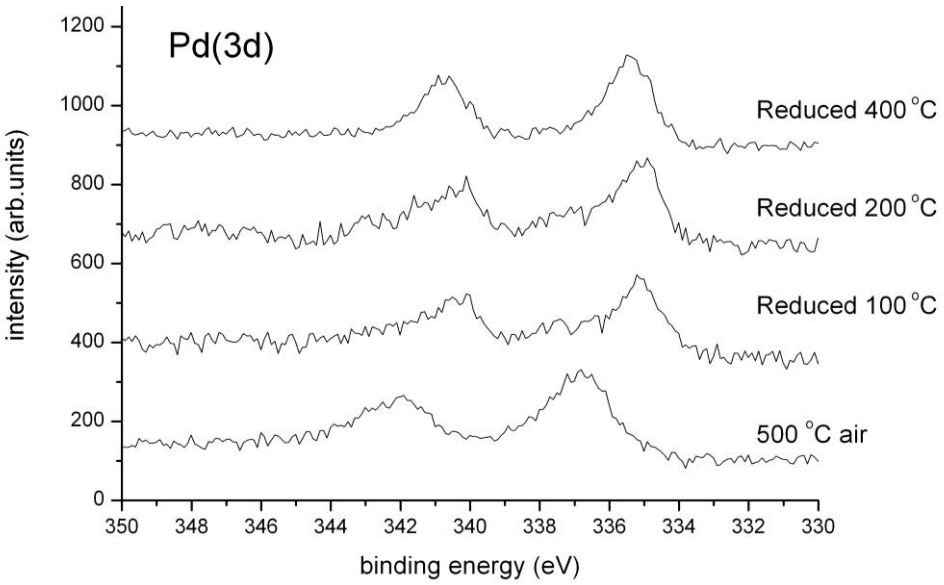

Figure 3.21 - Pd(3d) XPS spectra of 1% Pd / 4% Sn / SiO_2 after calcination at 500 ºC for 3 h and subsequent reduction at various temperautres for 2 h under 5% H_2 / Ar.

After reduction at 400 °C the Sn : Si ratio was observed to increase by around three times while the Pd : Si ratio doubled which could indicate the re-dispersion of the metals and the segregation of the alloy into Pd and Sn particles which could account for the low productivity of the samples after reduction at this temperature.

Figure 3.22 shows the Pd(3d) spectra of the reduced 1% Pd / 4% Sn / SiO_2 after subsequent calcination at 400 °C in air for various times. The spectra show that on heating under air at high temperatures for various times the Pd returns to the Pd(II) oxidation state and the Pd(0) species begins to disappear, after 3 h the catalyst predominantly contains Pd(II), no change to the Sn species was seen in the XPS spectra meaning that Sn is still present as Sn(IV). The observation that after a reduction and oxidation following calcination switches off the hydrogenation activity must indicate a change in particle morphology or surface composition as the catalyst is returned to its starting state in terms of oxidation state.

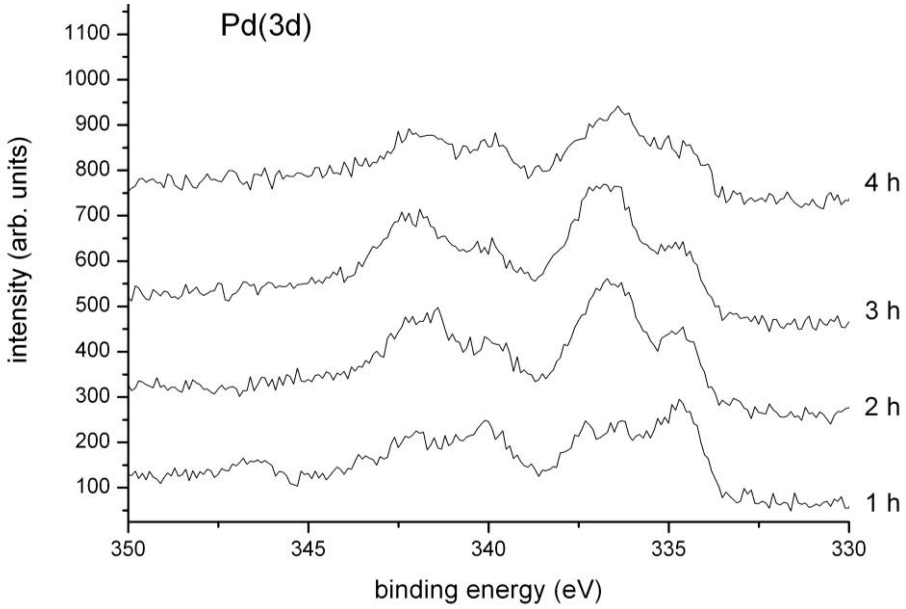

Figure 3.22 - Pd(3d) XPS spectra of 1% Pd / 4% Sn / SiO_2 after calcination at 500 ºC for 3 h and subsequent reduction at 200 °C for 2 h under 5% H_2 / Ar folowed by recalcination at 400 °C for various times.

Inspection of the Pd : Si and Sn : Si on calcination at various times up to the point where the hydrogenation is switched off (400 °C for 3 h) indcates that both metal ratios increase realtive to the Si with the Sn : Si ratio increasing dramatically after 3 h at elevated temperatures, shown in table 3.9. As the Pd(II) state still shows a shift indicating electron transfer to the Sn it can be speculated that the particles still contain both Sn and Pd in close porximity (confirmed by the STEM analysis), the incease in Pd and Sn ratio to Si could be a result of the partial segregation of Pd and Sn on the reoxidation of Pd.

Calcination time	Atomic ratios			
	O/Si	Pd/Sn	Pd/Si	Sn/Si
1 h	2.7	0.20	0.011	0.054
2 h	2.7	0.21	0.015	0.073
3 h	2.8	0.15	0.018	0.12

Table 3.9 – XPS-derived surface atomic ratios for a silica-supported 4% Sn-1% Pd catalyst calcined (500 ^{o}C, 3 h, air), reduced (200 ^{o}C 2 h) and then re-oxidised at 400 ^{o}C for the times indicated.

After heat treatments for 4 h the ratios drop dramatically which could indicate the sintering of particles, this also coincides with a big drop in activity from 50 to 20 mol_{H2O2} kg^{-1} h^{-1}.

XPS spectra were recorded for the calcined only catalyst to investigate the reason for the deactivation on second use. From the XPS surface Si : Sn and Si : Pd no change was seen between the first and second use however the oxidation state of the Pd was seen to change from PdO to Pd on use as shown in figure 3.23. No change was seen in the Sn spectra. The observed stability after reduction suggests that metallic Pd is much more stable on SiO_2 than PdO during the reaction and the reduction step forms a strong metal to support interaction as on re-oxidation the catalysts remain stable despite PdO being the predominant Pd species in the catalysts that do no hydrogenate H_2O_2.

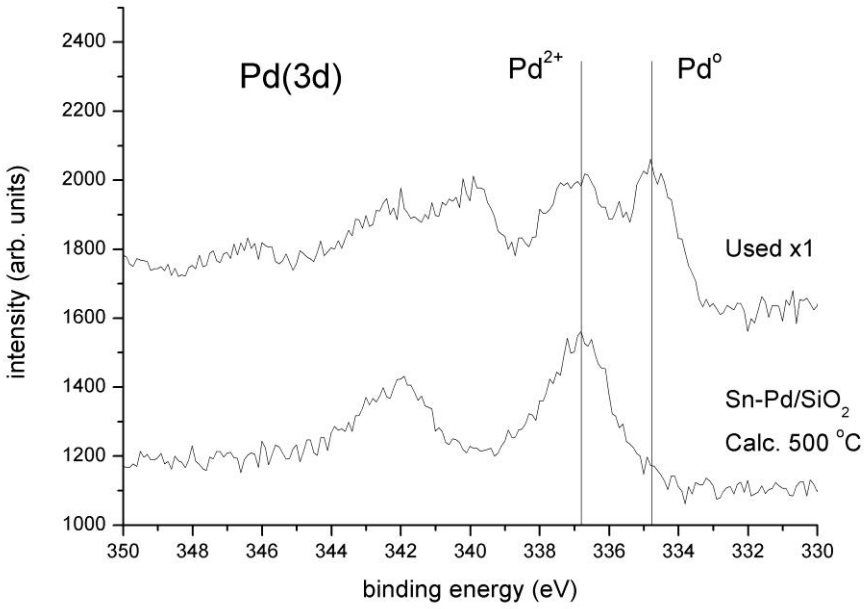

Figure 3.23 - Pd(3d) XPS spectra of 1% Pd / 4% Sn / SiO_2 after calcination at 500 ºC for 3 h fresh and used once.

3.3 - Discussion

In order to scale up a direct synthesis process the cost of the catalyst components especially the active metals is very important. To date the most active catalysts for H_2O_2 synthesis contain Pd and Au which are far more expensive than base metals such as Sn. The results shown indicate that, similar to Au, there is a synergistic effect for the direct synthesis of H_2O_2 between Sn and Pd and this is the first time this has been seen in a co-impregnated catalyst with 5 wt% metal loading. This effect is observed when the metals are supported on both SiO_2 and TiO_2 which are two common catalyst supports that are already extensively used in industry. Bimetallic catalysts

containing 2.5% Sn and 2.5% Pd have been shown to be more active than the equivalent monometallic catalysts and also more active than monometallic catalysts containing 2.5% Pd or Sn confirming that the effect is a synergistic effect rather than an enhancement in dispersion achieved by having less metal in the catalyst.

Unlike the analogous Au-Pd / TiO_2[12] system the 2.5% Sn 2.5% Pd metal ratio is not the optimum ratio for Sn-Pd and it is seen that the optimum ratio is dependent on the support with the optimum composition on the SiO_2 support containing only 1% Pd. This support dependence on optimum Sn : Pd may come from the strength of interaction between the support surface and the metal particles. A strong particle surface interaction may inhibit the formation of catalytically active alloys or prevent certain alloys from forming. This may explain why more Pd is needed in the TiO_2 system to achieve an active catalyst whereas on SiO_2 the structures can form more readily. All of the catalysts that have been calcined once showed very low hydrogenation activity, this indicates that Sn as a catalyst component may play an analogous role to that identified for Au in our previous studies, by helping to suppress the H_2O_2 hydrogenation/decomposition which results in an enhancement of the H_2O_2 yield in the calcined catalysts. More importantly, these Pd-Sn bimetallic catalysts showed considerably lower H_2O_2 hydrogenation activities (1 - 4 wt% H_2O_2 hydrogenation) and comparable H_2O_2 synthesis activity to those previously reported for the Au-Pd / TiO_2 catalysts (H_2O_2 hydrogenation = 12 wt%, H_2O_2 productivity = 64 mol kg_{cat}^{-1} h^{-1}). However after just one calcination the catalysts are unstable and show much lower activity for H_2O_2 synthesis on re-use.

The TPR profiles of the catalysts show that a new feature is present in the bimetallic samples and the absence of a Pd-β-hydride decomposition feature indicates that there is a strong interaction between the Sn and Pd in these catalysts. STEM analysis confirms that both Sn and Pd are present in the particles and that the addition of Sn to Pd results in a high particle density of 2-5 nm particles. XPS analysis also suggests the possibility of alloy formation with electron transfer occurring form Pd to Sn.

Both catalyst systems show the same trends with regard to subsequent reduction making the catalysts stable to re-use after reduction at temperatures of 200 ºC and above. After reduction both sets of catalysts show high hydrogenation activity, due to the higher Pd content of the TiO_2 samples the increase in hydrogenation results in a slightly lower observed H_2O_2 synthesis activity due to the increased hydrogenation. The SiO_2 samples shows a slight increase because a higher percentage of the Pd may be involved in forming alloys and leaving less free Pd on the

surface of the catalyst. XPS analysis of the SiO_2 samples show that the reduction treatment results in the formation of Pd(0) and at a reduction temperature of 200 ºC no reduction of the Sn species is observed, which is consistent with the TPR results.

The possible presence of alloys in the SiO_2 system is shown by the XRD analysis of the samples where only a small Pd or PdO reflection can be seen when compared to a catalyst containing 1 % Pd indicating that the Pd is no longer present as metallic or PdO nanoparticles of ~ 9 nm as in the monometallic samples that have been calcined and reduced. The possible alloys were also detected in the STEM analysis of the reduced samples which observed a range of compositions for the nanoparticles that contained both Sn-Pd although no correlation between size and composition could be found with XPS also suggesting the presence of Sn-Pd alloys in the reduced samples.

In order to reduce the hydrogenation activity of the stable catalysts after they have been reduced a third heat treatment was added to try and re-oxidise any metallic Pd that had been formed during the reduction step. It was found that a heat treatment at 400 °C for 3-4 h was suitable to substantially reduce the hydrogenation activity with XPS showing the reoxidation of Pd(0) to Pd(II) during this heat treatment. Using this methodology it was possible to generate catalysts that showed no hydrogenation activity on both SiO_2 and TiO_2. No differing features in particle size or morphology could be detected using STEM analysis after these heat treatments. However as the STEM analysis points towards the vast majority of the small catalytically interesting particles as being Pd-Sn alloys and these species show very low hydrogenation activity after the heat treatments developed it may be the dilution of the Pd particles with Sn that suppresses this subsequent reaction. Due to the many possible Sn-Pd alloys that could exist in these samples it is not possible to identify a specific alloy responsible for the activity. As Sn and Pd have similar atomic masses it is difficult to differentiate the metals in electron microscopy images due to similar observed contrast. XPS shows an increase in surface concentration of both Sn and Pd on re-oxidation which may suggest surface segregation as the Pd is reoxidised.

Figure 3.24 shows a postulated evolution of the Sn-Pd particles through the various heat treatments based on the characterisation carried out of the SiO_2 samples. STEM analysis shows that at each stage the 2 – 5 nm particles contain both Sn and Pd. After initial calcination XPS suggests a homogeneous alloy of Sn and Pd with electron transfer from Pd to Sn, however XRD still shows the presence a small amount of PdO. TPR shows the Sn – Pd are likely to be mixed as the addition of Sn hinders the formation of Pd-β-hydride. After the initial oxidative heat

treatment Sn is likely to be present as SnO_2 so it is postulated that the particles are a mixed oxide at this point. STEM analysis was unable to detect oxygen in the structure of the particles because of its low contrast compared to the much heavier metals. On reduction the TPR shows a reduction feature at 150 °C, which may be the reduction of the PdO involved in the mixed oxide as no Sn reduction was seen until much higher temperature were reached. XPS shows a decrease in the amount of surface Pd which may suggest that the Pd is able to migrate into the SnO_2 to generate a Pd-SnO_2 particle. The generation of metallic Pd either in the alloy particles or isolated nanoparticles is thought to be responsible for the higher observed hydrogenation activity.

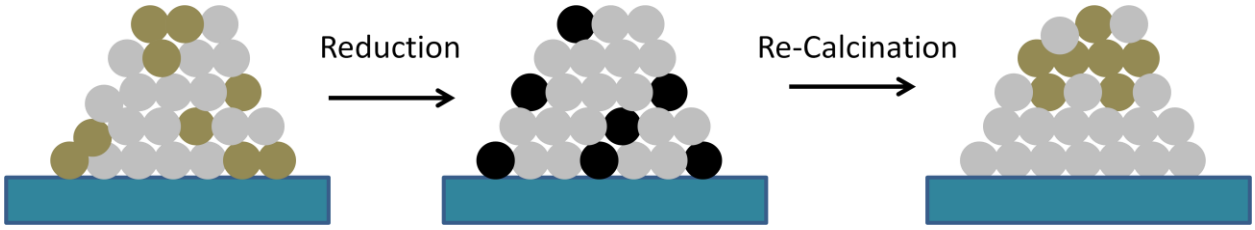

Figure 3.24 – Postulated evolution of Sn-Pd particles through the oxidation – reduction – oxidation treatments to generate a stable low hydrogenation activity catalyst. ● Pd (II) ● Pd ● Sn(IV)

On re-calcination of the oxidised samples no features of sintering were observed in the XRD, with the STEM analysis confirming that there was no obvious change in particle size of the Sn-Pd particles. Inspection of the Pd : Si and Sn : Si on calcination at various times up to the point where the hydrogenation is switched off (400 °C for 3 h) indcates that both metal ratios increase realtive to the Si with the Sn : Si ratio increasing dramatically after 3 h at elevated temperatures. As the Pd(II) state still shows a shift indicating electron transfer to the Sn it can be speculated that the particles still contain both Sn and Pd in close porximity (confirmed by the STEM analysis), the increase in Pd and Sn ratio to Si could be a result of the partial segregation of Pd and Sn on the reoxidation of Pd. One possible morphology that aggress with this is the surface segreagation of PdO from SnO_2. This morphology would provide a palladium oxide surface that would be heavily influenced by the SnO_2 below, increasing the binding energy of the Pd electrons and therefore reducing its ability to dissociate the O-O bond of both O_2 and H_2O_2.

It must be stressed that at this point the scheme is only postulated and more extensive structural characterisation of a wider range of samples is needed as the system seems to be highly responsive to small changes in the composition of the nanoparticle surface.

3.4 - Conclusions

The methodology employed in the catalyst preparations of Sn-Pd outlined here show a big step forward in the development of catalysts for the direct synthesis of H_2O_2 and a number of key milestones have been achieved. Firstly the synthesis of catalysts that show activity of similar magnitude to analogue Au-Pd catalysts but have replaced Au with a cheap base metal like Sn makes the system much more attractive form an industrial perspective. Also the observation that Au is not unique in promoting the reaction could lead to extensive research into other metals that could show similar effects or even replace Pd as the hydrogenation component of the system to produce a catalyst made of only base metals.

The use of Sn - Pd to prepare a catalyst on SiO_2 which is stable to multiple uses represents an advantage over using the Au-Pd system which has been shown to lose Au during reaction meaning the catalyst is unstable to the reaction conditions. The heat treatment cycles developed during this research have been able generate Sn-Pd species that are stable on SiO_2 to the reaction conditions and multiple cycles of the reaction conditions along with the most active TiO_2 catalyst which is also stable. The preparation methods developed in the research have most importantly developed catalysts which show no hydrogenation activity towards H_2O_2 under our reaction conditions. These catalysts are only the second example of this to be reported and the first example on SiO_2 and TiO_2 supports to be reported. The fact that the catalysts do not include Au as the means of increasing the selectivity towards H_2O_2 which represents a big milestone in the process. This research shows that Au is not essential and may not be the most effective metal in switching off the subsequent hydrogenation of H_2O_2 and more work should be carried out into the effects of base metals in the H_2O_2 synthesis reaction.

References

1. V.R. Choudhary, A. G Gaikwad, S.D. Sansare, *Catal. Lett.*, **2002**, 83, 235.
2. J. H. Lunsford, *J. Catal.*, **2003**, 216, 455.
3. V.R. Choudhary and C. Samanta, *Catal. Lett.* **2005**, 99, 79.
4. S. Chinta and J. H. Lunsford, *J. Catal.*, **2004**, 225, 249.
5. Q. S. Liu and J. H. Lunsford, *J. Catal.*, **2006**, 239, 237.
6. V.R. Choudhary and C. Samanta, *J. Catal.*, **2006**, 238, 28.
7. S. Chinta and J.H. Lunsford, *J. Catal*., **2005**, 230, 313.
8. V. R. Choudhary and P. Jena, *J. Catal.*, **2007**, 246, 434.
9. C. Samanta and V.R. Choudhary, *Catal. Commun.*, **2007**, 8, 73.
10. G. Li, J. Edwards, A. F. Carley and G. J. Hutchings, J. *Catal.*, **2006**, 114, 369.
11. B. E. Solsona, J. K. Edwards, P. Landon, A. F. Carley, A. Herzing, C. J. Kiely and G. J. Hutchings, *Chem. Mater.*, **2006**, 18, 2689.
12. J. K. Edwards, B. E. Solsona, P. Landon, A. F. Carley, A. Herzing, C. J. Kiely and G. J. Hutchings, *J. Catal.*, **2005**, 236, 69.
13. J. K. Edwards, B. Solsona, P. Landon, A. F. Carley, A. Herzing, M. Watanabe, C. J. Kiely and G. J. Hutchings, *J. Mater. Chem.*, **2005**, 15, 4595.
14. J. K. Edwards, B. Solsona, E. Ntainjua N. N, A. F. Carley, A. A. Herzing, C. J. Kiely and G. J. Hutchings, *Science*, **2009**, 323, 1037.
15. J. K. Edwards, A. F. Carley, A. Herzing, C. J. Kiely, G. J. Hutchings, *Faraday Discuss.*, **2008**, 138, 225.
16. J. K. Edwards and G. J. Hutchings, *Angew. Chem. Int. Ed.*, **2008**, 47, 9192.
17. J. K. Edwards, E. Ntainjua N., A. F. Carley, A. A. Herzing, C. J. Kiely and G. J. Hutchings, *Angew.Chem. Int. Ed.*, **2009**, 48, 8512.
18. E. Ntainjua N., M. Piccinini, J.C. Pritchard, J.K. Edwards, A. F. Carley, J.A. Moulijn and G. J. Hutchings, *Chem. Sus. Chem*,, **2009**, 2, 575.
19. G. Bernardotto, F. Menegazzo, F. Pinna, M. Signoretto, G. Cruciani and G. Strukul, *Appl. Catal. A.*, **2009**, 358, 129.
20. K. Pattamakomsan, E. Ehret, F. Morfin, P. Gélin, Y. Jugnet, S. Prakash, J.Claude Bertolini, J. Panpranot and F. J. C. S. Aires, *Catal. Today*, **2011**, 1, *28.*
21. E. A. Sales, M. Mendes and F. Bozon-Verduraz, *J. Catal.*, **2000**, 195, 96.
22. T. Tomita, Y. Ishiuchi, M. Kawakami and H. Nagashima., US Patent 5378450, 1995
23. C. Samanta, *Appl. Catal. A: Gen.*, **2008**, *350*, 113-149.

24. U. S. Ozkan, M.W. Kumthekar and G. Karakas, *Catal Today*, **1998**, 40, 3.

25. N. Nava and T. Viveros, *J. Radioanal. Nucl. Chem.*, **2000**, 243, 683.

26. A. Vicente, G. Lafaye, C. Especel, P. Marecot, C. T. Williams, *J. Catal.*, **2011**, 283, 133-142.

27. J. K. Edwards, S. F. Parker, J. Pritchard, M. Piccinini, S. J. Freakley, A. F. Carley, Q. He, C. J. Kiely and G. J. Hutchings, *Chem. Sci.*, **2012**, submitted for publication.

Chapter 4

Direct Synthesis of H_2O_2 in a Gas Liquid Flow System

4.1 - Introduction

As previously discussed in the first chapter, many different approaches have been explored in order to find suitable methods for producing H_2O_2 in a much greener way compared to the current industrially used anthraquinone process. These include membrane reactors[1,2] microreactors[3-4] and fixed bed reactors[5-7].

Requirements for industrial scale direct synthesis plants, such as high H_2O_2 concentrations and high H_2 selectivities are yet to be achieved. Although the direct synthesis from H_2 and O_2 seems to be a viable candidate to succeed, most of the catalysts active for H_2O_2 synthesis are also active for its subsequent decomposition/hydrogenation reactions leading to low H_2 selectivities. A possible solution to this problem may lie in the use of continuous flow reactors for the direct synthesis of H_2O_2. The advantage of using these particular reactors is that it may be possible to

minimise the subsequent hydrogenation and decomposition reactions which are shown as k_2 and k_3 in the reaction scheme shown in figure 4.1.

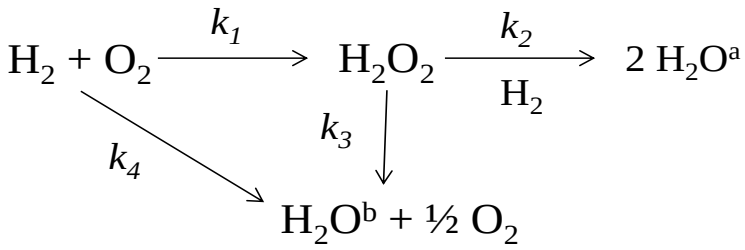

Figure 4.1 - Reaction Scheme for the Direct Synthesis of H_2O_2.

k_1 – Synthesis rate constant, k_2 – Hydrogenation rate constant, k_3– Decomposition rate constant, k_4 – Combustion rate constant, H_2O^a – water from hydrogenation reaction and H_2O^b – water from decomposition and combustion reaction.

Even though it is not possible to completely minimise the loss in H_2 and increase in H_2 conversion due to the direct combustion of H_2 and O_2 to form H_2O, subsequent hydrogenation / decomposition of H_2O_2 can be diminished by carefully choosing an appropriate reaction condition and catalyst.

Lawal *et al.* have extensively studied the direct synthesis of H_2O_2 using a gas liquid flow reactor a 1 wt% solution of H_2O_2 was synthesised in a microreactor (i.d. 765 μm)[5-7] using deionised water as a solvent. Although the reaction medium contained 1 wt% H_2SO_4 and 10 ppm of NaBr as promoters using a 2% Pd / SiO_2 catalyst at 20 bar pressure at 40- 50 ºC. Jaenicke *et al.* synthesised a 1.4 wt% solution of H_2O_2 using a Pd catalyst in a MeOH / HCl / KBr solvent system. Although these systems are capable of producing high concentrations of H_2O_2, they rely heavily on the presence of acid and halide promoters to suppress the subsequent hydrogenation and decomposition reactions and to increase selectivity. The addition of promoters and stabilisers is undesirable in a large scale process because it requires further product purification downstream. Also the addition of acid can lead to degradation of the reactor over extended periods of time.

This study will look at the use of a Au-Pd catalyst to produce H_2O_2 using a flow reactor, in a reaction medium free from acid and halide promoters therefore in the presence of the subsequent non selective reactions (H_2O_2 hydrogenation and decomposition). The aim is to investigate the

reaction parameters for the direct synthesis of H_2O_2 under flow conditions and try to identify the conditions which suppress these subsequent reactions.

4.1.1 - H_2O_2 Synthesis Reaction Profile

As shown in figure 4.1 the direct synthesis of H_2O_2 from H_2 and O_2 is a challenging reaction with a number of competing side reactions which destroy the H_2O_2 that has been synthesised. Another complication is that catalysts which are active for the synthesis of H_2O_2 are also active for the hydrogenation and decomposition reactions. The balance between these reactions can be tailored by designing catalysts to give high selectivities to H_2O_2 whilst suppressing the decomposition and particularly the hydrogenation reaction. The aim of this study is to optimise the design of the reaction process through the use of a flow reactor to provide a system capable of producing H_2O_2 at high selectivities whilst operating under conditions which minimise the non selective side reactions.

An important reaction parameter to consider when dealing with a process which has subsequent and competing reactions is residence time (τ). By carefully controlling the time that the reactants are in contact with the catalyst it is possible to control and suppress the subsequent reactions. Figure 4.2 shows theoretically how the concentration of various reactants and products vary with residence time. As can be seen at short residence times H_2 conversion is low, however at these residence times the main reaction is the synthesis of H_2O_2 leading to high H_2 selectivity. A small amount of water is also made by the direct combustion of H_2 at these residence times. This is because the synthesis and combustion reactions are independent of the concentration of H_2O_2 and can be assumed to be first order with respect to H_2 and O_2 concentrations. Therefore at low residence times, where only a small amount of H_2O_2 is synthesised the contribution from the subsequent hydrogenation and decomposition is small.

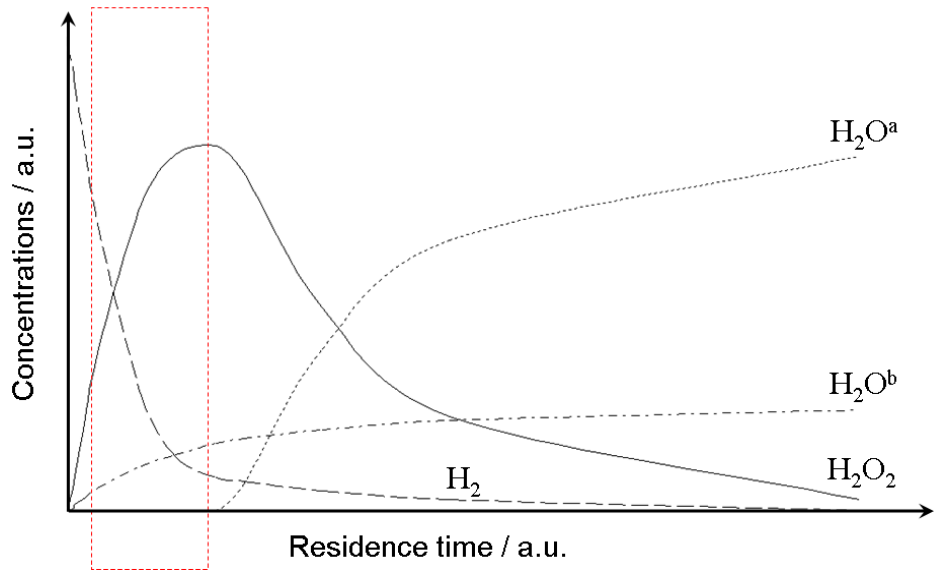

Figure 4.2 - Theoretical reactant and product profiles at various residence times.

H_2O^a – water from hydrogenation reaction and H_2O^b – water from decomposition and combustion reaction.

At longer residence times the concentration of H_2O_2 begins to build and the contribution from the hydrogenation and decomposition reactions becomes more pronounced and causes an increase in H_2 conversion and a decrease in selectivity. These reactions become more prominent at longer residence times because they can be assumed to be first order in H_2O_2, meaning that as the synthesis reaction produces H_2O_2 the rates of the subsequent hydrogenation and decomposition increase reducing the overall yield of H_2O_2.

As can be seen in figure 4.2, the residence time is crucial in achieving high yields of H_2O_2. Ideally the residence time should be low enough to stop the subsequent hydrogenation and decomposition reactions as shown by the red area highlighted in figure 4.2. However at these very short residence times, which give high H_2O_2 selectivities, the H_2 conversions will be low which industrially would not be very attractive without gas recycling being incorporated into the process.

4.1.2 - Implications of Testing in a Batch System

When testing a catalyst for H_2O_2 synthesis activity in a batch system it is difficult to achieve very short residence times, with the shortest feasible reaction being 1 min. By testing in a batch reactor the H_2O_2 productivity can only be measured as a “snap shot” sum of the reaction profiles of both the synthesis and the competing hydrogenation/decomposition reactions. This makes it

very difficult to measure the absolute rate of H_2O_2 synthesis due to the contribution of the subsequent reactions. Meaning that any measure of rate will only be an observed rate, k_{obs}, which is made up of contributions from the synthesis, hydrogenation and decomposition reactions, as shown by equation 4.1.

$$k_{obs} = k_{synthesis} - k_{hydrogenation} - k_{decomposition} \quad (4.1)$$

The batch system also does not allow for measurements of catalyst deactivation during the reaction as the reaction must be repeated multiple times with the same residence time to test for catalyst stability. A flow system is a possible solution to this problem because the catalyst can be held at a steady residence time continuously for a set period of time. The rates of reaction can then be measured over extended periods of time under various experimental reaction conditions.

4.1.3 - Aims of the Study

The aim of the study is to set-up and operate a new liquid gas flow system to investigate the reaction parameters for the direct synthesis of H_2O_2 under flow conditions. The conditions investigated include residence time, pressure, temperature, H_2 : O_2, solvent composition and solvent flow rate. Also included in this study is an investigation into whether the synthesis, decomposition and hydrogenation rate constants can be extracted and combined into a kinetic model for this catalyst system.

4.2 - Reactor Setup

4.2.1 - Safety

In order to ensure the safety of the reactor when contacting a H_2 / O_2 mix, it is essential to ensure that the gas composition remains below the lower explosive limit of H_2, 5 % in air at room temperature. This is ensured by using intrinsically safe gas mixtures of 5 % H_2/CO_2, 25 % O_2/CO_2. Although the reaction is exothermic heat spots in the reactor are minimised by cooling the reactor throughout the reaction in a water bath. Another safety issue is the potential rapid pressure increase due to a block in the system, which could cause a failure in one of the reactor joints. The risk of this is controlled by fitting pressure relief valves before and after the catalyst bed and also using MFC inlet pressures of 15 bar were used which means that once the pressure of the reactor has equalled the inlet pressure of the MFCs no more gas will flow into the system.

4.2.2 – Evaluation of Blank Reactions

Before any synthesis experiments were carried out using the H_2O_2 flow reactor, it was important to check that the reactor itself did not catalyse the direct synthesis of H_2O_2 or the competing hydrogenation and decomposition reactions. These blank reactions were carried out by passing a H_2O_2 solution with a predetermined concentration through the system at various gas flows, liquid flows and pressures and measuring the concentration after it has passed through the reactor.

4.2.2.1 – Blank Decomposition Experiments

A 4.32 wt% H_2O_2 solution was pumped through the reactor at various flow rates to give various contact times with the reactor to check that the reactor did not catalyse the rapid decomposition of H_2O_2. The concentration at the end of the system was measured after giving 1 h to equilibrate between flow changes. The results are given in table 4.1;

Liquid Flow Rate ml / min	wt% H_2O_2
0	4.32
0.02	4.39
0.2	4.37
1	4.34
5	4.33

Table 4.1 - Table showing the measured concentration of H_2O_2 after passing through the reactor at various flow rates at atmospheric pressure. Initial H_2O_2 concentration = 4.32 wt%.

The results show that the concentration of H_2O_2 measured after it has passed through the reactor is within experimental error of the initial concentration. This indicates that importantly the reactor itself does not catalyse the decomposition of H_2O_2.

4.2.2.2. – Blank Hydrogenation Experiments

A 4 wt% H_2O_2 solution was pumped through the reactor at various flow rates in the presence of 2% H_2 / air to check that the reactor did not catalyse the hydrogenation of H_2O_2. The concentration at the end of the system was measured after giving 1 h to equilibrate between flow changes. The experiments were performed with and without filters in the system as it was thought that the 0.5 micron filters may act as a likely site for hydrogenation as the gas and H_2O_2 pass through, the results are shown in table 4.2.

Initial wt% H_2O_2 = 4.08

	Gas Flow ml / min	Liquid Flow Rate ml / min	wt% H_2O_2
With Filters	10	0.2	4.00
	10	0.8	4.09
	10	1.3	4.03
Without Filters	10	0.2	4.05
	10	0.8	4.04

Table 4.2 - Table showing the measured concentration of H_2O_2 after passing through the reactor at various flow rates at atmospheric pressure under a flow of 2% H_2 / air.

The hydrogenation experiments show that, within experimental error there is no loss of H_2O_2 as it passes through the reactor in the presence of H_2 at various contact times with the alloy. The same experiments were carried out using methanol as a solvent and 5 bar 5% H_2 / CO_2 to check for hydrogenation at conditions which should promote high H_2 solubility and still no appreciable hydrogenation activity was seen.

Experiments were also carried out under 10 bar pressure of an 1 : 1 H_2 / O_2 mix using H_2O/MeOH as a solvent to check that the reactor did not catalyse the direct synthesis of H_2O_2. No H_2O_2 was detected during these blank experiments.

4.2.3 - Flow Regime

To help understand the kinetic and mass transfer limitations inside the flow reactor it is important to determine how the gas and liquid flow through the system and which flow regime operates during the reaction. Visualisation experiments were carried out at atmospheric pressure with typical reaction flows of gas and liquid using a glass tube of the same diameter as the reactor. Schematics of the flow regime through an empty tube and a tube packed with catalyst and glass wool are shown in figure 4.3.

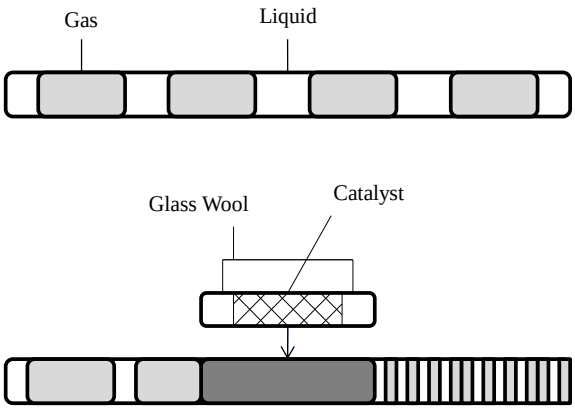

Figure 4.3 – Schematic representation of the flow regime at comparable gas and liquid flow rates to the reaction conditions.

The flow regime commonly seen in channels with diameters in the order of the reactor used in this study (⅛ inch internal diameter) is called Taylor flow[6], which was confirmed by the visualisation experiments. The flow consists of an alternating sequence of gas bubbles and liquid slugs where the length of the gas bubbles is larger than the diameter of the reactor. When a catalyst bed was placed into the tube, the flow exiting the bed still had distinct gas and liquid slugs but the flow was less regular after being broken up by the catalyst bed. The breaking of the gas and liquid slugs could be seen as the flow passed through the catalyst bed. The rate of mass transfer of reactants to the catalyst under Taylor flow can be assumed to be high for two reasons; firstly the liquid layer between the gas and catalyst particles is so thin that it forms a very low barrier to mass transfer of reactants to the catalyst, secondly, the liquid slugs in the reactor can circulate internally eliminating any radial concentration gradients. This flow regime, combined with the fact the reactants are highly soluble in the reaction solvent lead to the assumption that the system would not be limited by mass transfer.

4.3 - Initial Synthesis Experiments Using 0.5% Au / 0.5% Pd / TiO_2

Initial synthesis experiments were carried out using a 0.5% Au / 0.5% Pd / TiO_2 prepared by impregnation and reduced at 400 °C / 4 h with a ramp rate of 10 °C min^{-1}. This catalyst was developed using a modified impregnation procedure recently reported by Hutchings *et al.*[8] This low metal containing catalyst was chosen to try and avoid any metal leaching during the extended flow testing runs, as well has having been studied extensively in the batch system under similar conditions to the flow system. The catalyst was found to be stable for a number of runs when tested under batch conditions. The initial experiments preformed in the flow system employed conditions that were as analogous to the batch reactor as possible.[9] The typical conditions used for H_2O_2 synthesis in the batch and flow system are summarised in table 4.3.

Conditions	Batch Reactor	Flow Reactor
Catalyst Mass	10 mg	120 mg
Pressure	40 bar	10 bar
Temperature	2 ºC	2 ºC
Solvent Composition	66% MeOH, 34% H_2O	66% MeOH, 34% H_2O
Solvent Flow	(8.5 ml Total Volume)	0.2 ml / min
Gas Composition	H_2 : O_2 = 1 : 1 (3.5%)	H_2 : O_2 = 1 : 1 (3.5%)
Reaction / Residence Time	30 min	0.2-1 sec

Table 4.3 – Table of typical reaction conditions for the batch and flow systems to test H_2O_2 productivity.

Initial reactions were carried out using a horizontal reactor tube with the catalyst packed between two pieces of glass wool. A flow of H_2 and O_2 diluted in CO_2 with total flow rate 40 ml min^{-1} was passed over 120 mg of catalyst while at the same time flowing 0.2 ml min^{-1} of water / methanol solvent. This initial experiment was carried out to check the reproducibility of the results obtained and the average concentration of H_2O_2 is shown in table 4.4.

The results show that H_2O_2 was made under these reaction conditions however the results were not reproducible when the reactor tube was in the horizontal position. When packing the catalyst into a horizontal tube two pieces of glass wool are pressed into the tube to hold the catalyst in place. If these pieces of glass wool are too tight this will restrict flow and increase the pressure drop though the catalyst bed. If these pieces were packed too loosely the catalyst bed will split during reaction leaving a void above the catalyst bed for reactants to bypass. In order to achieve

reproducible results with a horizontal bed both the catalyst and the glass wool have to be packed identically each time the reactor tube is filled. This is very difficult and may account for the irreproducible results observed in table 4.4. By switching to a vertical catalyst bed, supporting the catalysts only at one point with gas and liquid flowing from top to bottom the experimental results became much more reproducible as seen in table 4.4. Using a vertical catalyst bed has other advantages in that the catalyst particles are distributed and packed more uniformly and better radial liquid distribution can be achieved which could contribute to the higher amount of H_2O_2 observed.

Catalyst	Test Number	Tube Orientation	ppm H_2O_2
0.5% Au / 0.5% Pd / TiO_2	1	Horizontal	320
	2	Horizontal	296
	3	Horizontal	265
0.5% Au / 0.5% Pd / TiO_2	1	Vertical	756
	2	Vertical	743
	3	Vertical	751

Table 4.4 - Results showing the effect of reactor orientation on the repeatability of H_2O_2 synthesis results. Reaction Conditions – 10 bar, 2 ºC, 40 ml / min gas flow, H_2 : O_2 = 1:1 (3.6 %), solvent MeOH / H_2O flow rate = 0.2 ml / min, 120 mg catalyst, τ = 0.25s.

4.4 – Results

4.4.1 - Effect of Gas Flow Rate on H_2O_2 Synthesis

The effect of total gas flow rate was investigated whilst keeping all other reaction conditions constant to determine the optimum residence time at which to carry out further reactions. Experiments were carried out at increasing total gas flow rate while keeping the reactant concentrations constant along with the catalyst mass. The results are shown in figure 4.4.

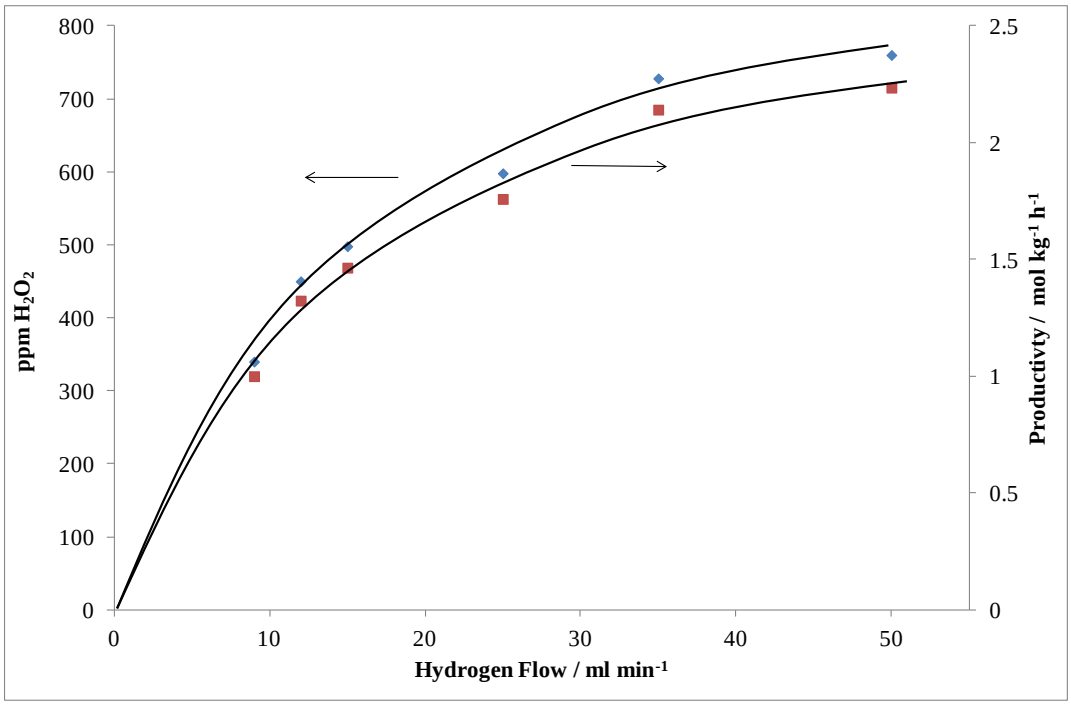

Figure 4.4 – H_2O_2 concentration (♦) and production rate (■) at various residence times. Reaction Conditions – 10 bar, 2 ºC, 40 ml / min gas flow, H_2 : O_2 = 1:1 (3.6 %), solvent MeOH / H_2O flow rate = 0.2 ml / min, 120 mg catalyst, τ = 0.25 s.

As the gas flow was increased so did the H_2O_2 concentration measured up to a maximum flow of around 40 ml min^{-1}, after which no further increase in H_2O_2 was seen with increasing gas flow rate which corresponded to a H_2O_2 productivity rate of 2.2 mol kg^{-1} h^{-1}. At higher flow rates the plateau may be attributed to gas bypassing the catalyst bed by flowing through the catalyst too quickly for a reaction to take place. Also at higher flow rates preferential routes through the catalyst bed, especially at the walls of the reactor tube, could also be responsible for no further increase in H_2O_2 being observed. The total flow rate used for all further experiments was 42 ml min^{-1} which corresponds to a residence time of 0.25 s.

The highest H_2O_2 productivity achieved in the flow system is of the same order of magnitude to the equivalent test in a batch reactor. This indicates that there are no significant mass transfer limitations in the flow system and the results can be confidently compared to results taken from the batch system.

The feed composition for the optimum condition identified above consists of equimolar hydrogen and oxygen (7 x 10^{-5} moles/min) and a liquid feed of equimolar H_2O to MeOH (4 x 10^{-3} moles/min) which H_2O_2 at a rate of 4 x 10^{-6} moles / min.

4.4.2- Effect of Catalyst Mass on H_2O_2 Synthesis

The effect of catalyst mass was investigated while holding other reaction variables constant, including residence time, pressure, temperature and $H_2 : O_2$ ratio. The results are shown in figure 4.5 using various catalyst masses from 50 – 120 mg;

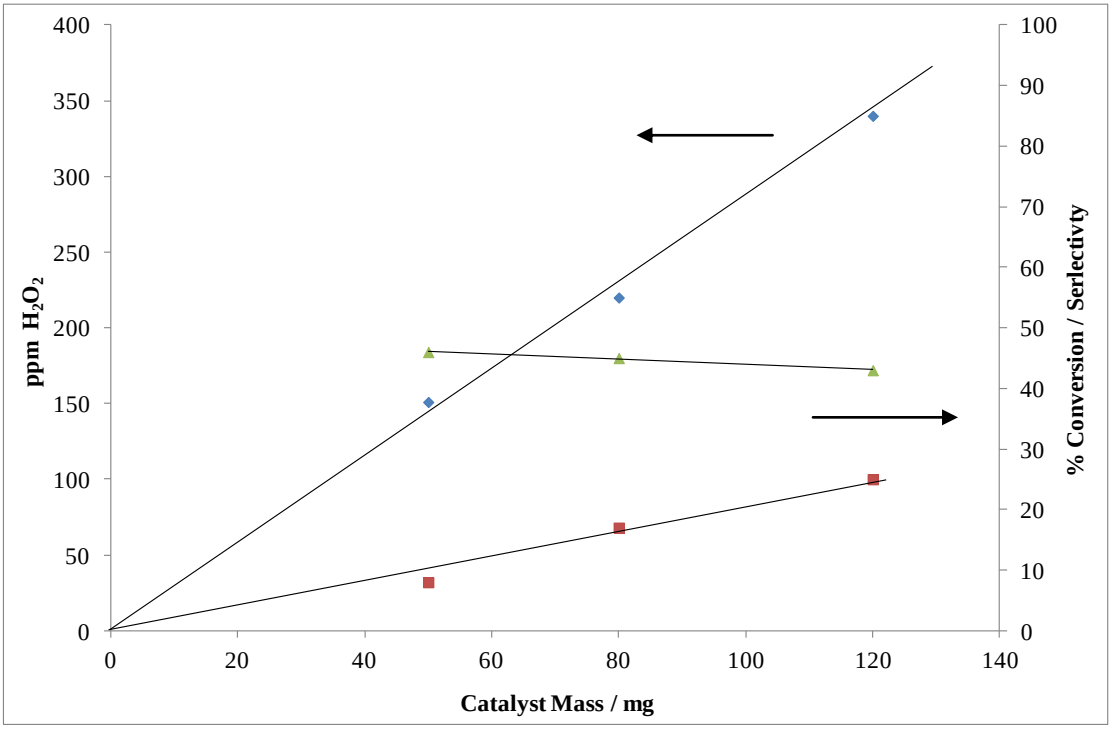

Figure 4.5 - Results obtained at various catalyst masses, showing H_2O_2 concentration (♦) H_2 conversion (■), and H_2O_2 selectivity (▲). Reaction Conditions – 10 bar, 2 ºC, 20 - 40ml / min gas flow, solvent MeOH / H_2O flow rate = 0.2 ml / min, 60 - 120 mg catalyst, τ = 0.75 s, $H_2 : O_2$ = 1.

The results show that as catalyst mass was increased at constant residence time the concentration of H_2O_2 increased linearly. The results also show that as catalyst mass increased, and therefore the length of the catalyst bed increased, H_2 conversion also increases which accounts for the increased H_2O_2 concentration obtained. As the catalyst mass was increased the gas flow was changed accordingly to hold the system at a constant residence time of 0.75 s, as the selectivity is determined by the residence time of the system. These experiments show that a constant selectivity can be achieved, regardless of the catalysts mass (and therefore the length of the catalyst bed), provided the residence time is adjusted accordingly by decreasing or increasing the flow of the reactant gases through the catalyst bed.

4.4.3 - Effect of Total Pressure on H_2O_2 Synthesis

The effect of total reaction pressure was investigated in the flow system while holding all other reaction variables constant including H_2 : O_2 ratio, residence time and solvent composition. The results are shown in figure 4.6,

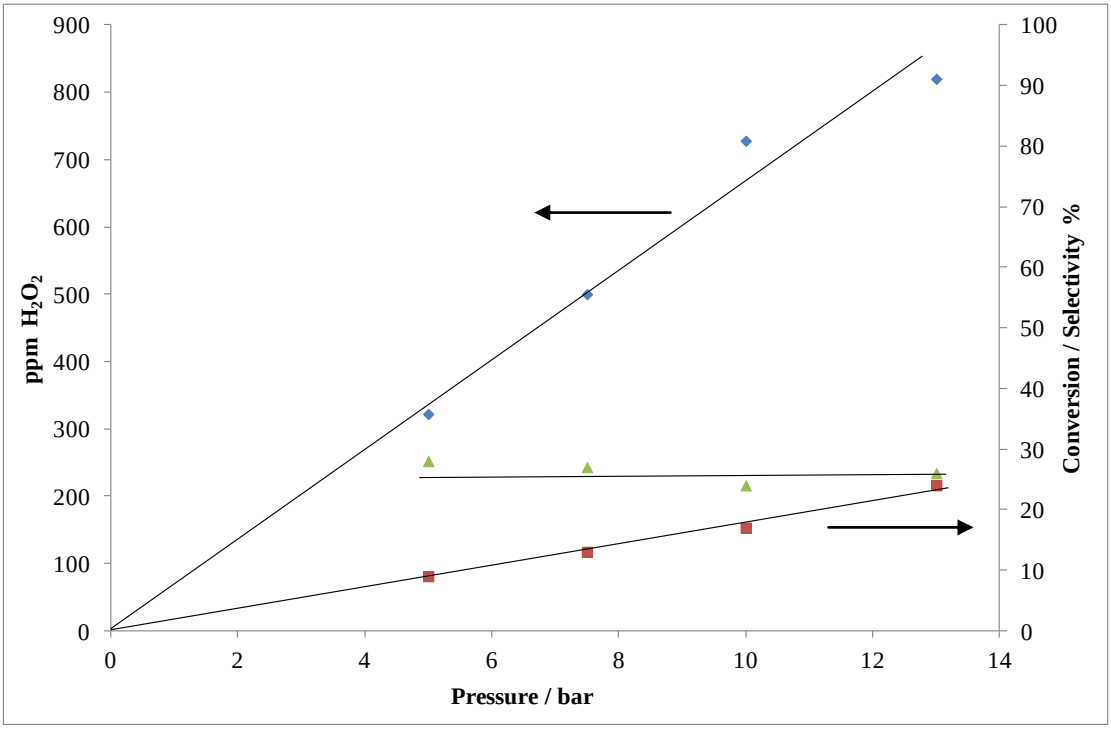

Figure 4.6 – Results obtained at various total pressure, showing H_2O_2 concentration (♦) H_2 conversion (■), and H_2O_2 selectivity (▲). Reaction Conditions – various pressure, 2 ºC, 40 ml / min gas flow, solvent MeOH / H_2O flow rate = 0.2 ml / min, 120 mg catalyst, τ = 0.25 s, H_2 : O_2 = 1.

As expected, an enhancement in the H_2O_2 concentration was observed with increasing pressure which would be expected due to higher gas solubility and smaller gas bubble size. As the pressure of the system increased the H_2 conversion also increased while the selectivity of the system remained constant at around 25%. If the synthesis reaction was assumed to be described by the kinetic expression shown as equation (4.2) a quadratic dependency on pressure would be expected.

$$\text{Synthesis Rate} = r_s = k_s[H_2][O_2] \qquad (4.2)$$

The linear dependency can be explained by assuming a number of things about the key reaction steps in the synthesis reaction. It has been postulated that the activation sites for H_2 and O_2 are

different[9], and if it is assumed that there is nearly full coverage of O_2 at the O_2 activation sites the rate of H_2O_2 synthesis will be proportional to the rate of H_2 activation, which in turn will be proportional to the H_2 partial pressure. By assuming this case to be true the linear dependence observed can be explained along with the linear increase in H_2 conversion. The results show that pressure had no effect on H_2O_2 selectivity indicating that the rate of synthesis and hydrogenation increase in proportion as both reactions are related to the H_2 partial pressure.

4.4.4 - Effect of Solvent Composition on H_2O_2 Synthesis

The effect of the solvent composition was investigated while keeping all the other reaction conditions constant including residence time, temperature, pressure, gas concentration and flow rate. As the methanol content was increased the amount of H_2O_2 produced also increased, with a maximum concentration of 1541 ppm being produced in a pure methanol solvent. The results are shown figure 4.7,

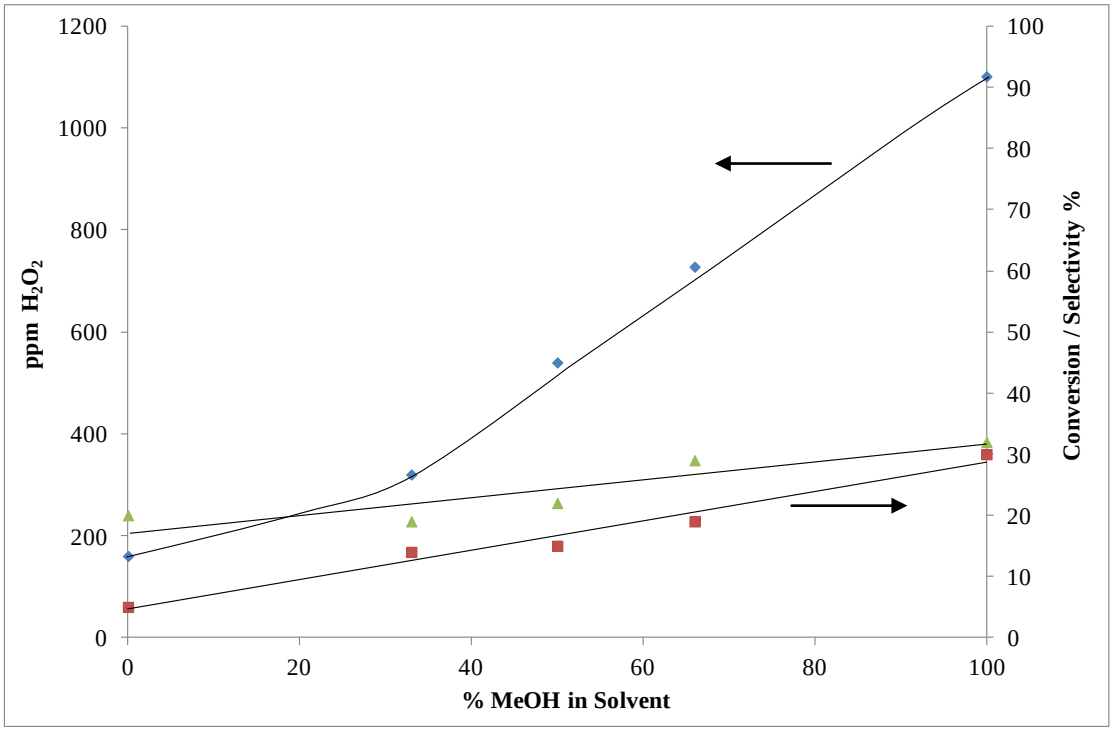

Figure 4.7 - H_2O_2 concentration obtained at various solvent compositions, showing H_2O_2 concentration (♦) H_2 conversion (■), and H_2O_2 selectivity (▲). Reaction Conditions – 10 bar, 2 - 20 ºC, 40 ml / min gas flow, solvent MeOH / H_2O flow rate = 0.2 ml / min, 120 mg catalyst, τ = 0.25 s, H_2 : O_2 = 1.

The increase in H_2O_2 concentration can be explained by the increase in H_2 and O_2 solubility with increasing methanol content and this can also be seen with increasing H_2 conversion with increasing methanol content. When increasing the methanol content selectivity rises slightly from about 22 % in water only to 32 % in methanol only. The rise in selectivity indicates that the rate of synthesis is higher than the rate of hydrogenation as the increase in solubility of both H_2 and O_2 results in an enhancement in the amount of H_2O_2 produced. If the hydrogenation rate was faster than the synthesis reaction more H_2 in the system would lead to a reduction in the amount of H_2O_2 observed.

4.4.5 - Effect of Solvent Flow Rate on H_2O_2 Synthesis

The effect of solvent flow rate was investigated in the flow system while holding all other reaction variables constant including, H_2 : O_2 ratio, residence time, pressure and solvent composition. The results of H_2O_2 concentration observed and moles of H_2O_2 formed are shown in figure 4.8,

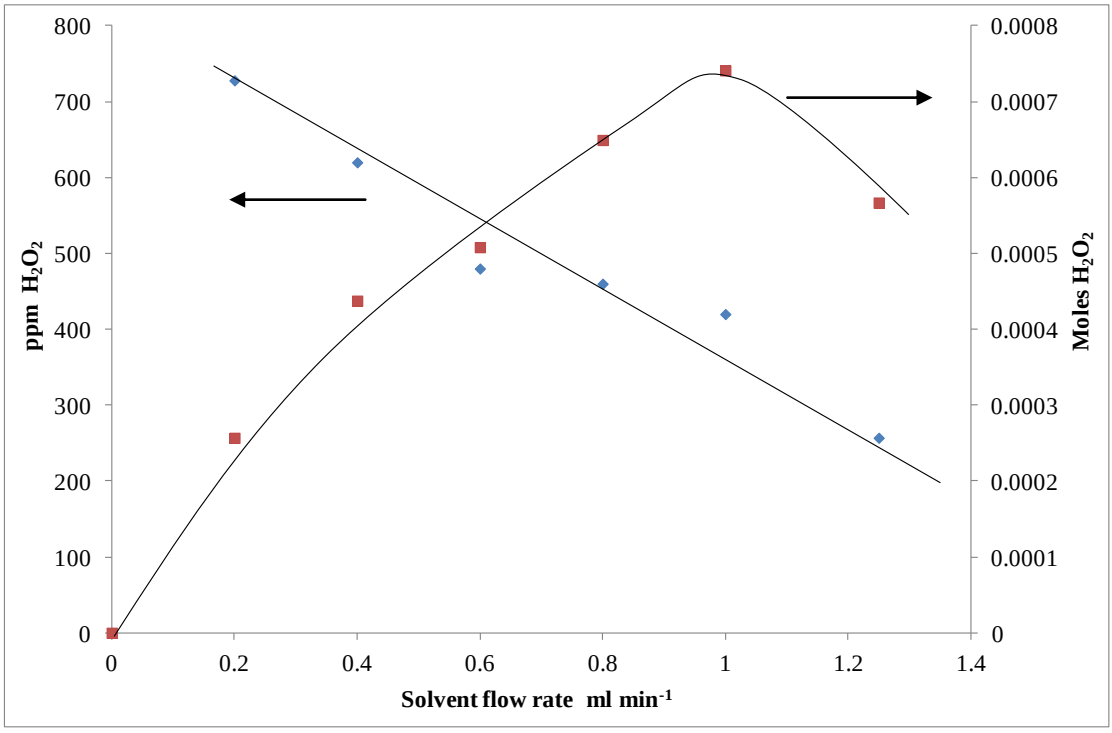

Figure 4.8 - H_2O_2 concentration obtained at various solvent flow rates, showing H_2O_2 concentration (♦) and moles of H_2O_2 formed (■). Reaction Conditions – 10 bar, 2 ºC, 40 ml / min gas flow, solvent MeOH / H_2O flow rate = 0.2 – 1.2 ml / min, 120 mg catalyst, τ = 0.25 s, H_2 : O_2 = 1.

The results obtained show that as the solvent flow rate through the catalyst bed is increased the concentration of H_2O_2 measured decreased. As ppm is a measure of H_2O_2 concentration it is expected that this would decrease with increasing solvent flow because there is more solvent to dilute the H_2O_2 produced. When considering the results in terms of total moles of H_2O_2 formed per hour, this increases with solvent flow, with a maximum of 7 x 10^{-4} moles achieved at 1 ml min^{-1} of solvent. To investigate the reason for this increase in moles H_2O_2 formed H_2 conversion and selectivity to H_2O_2 were measured and are shown in figure 4.9.

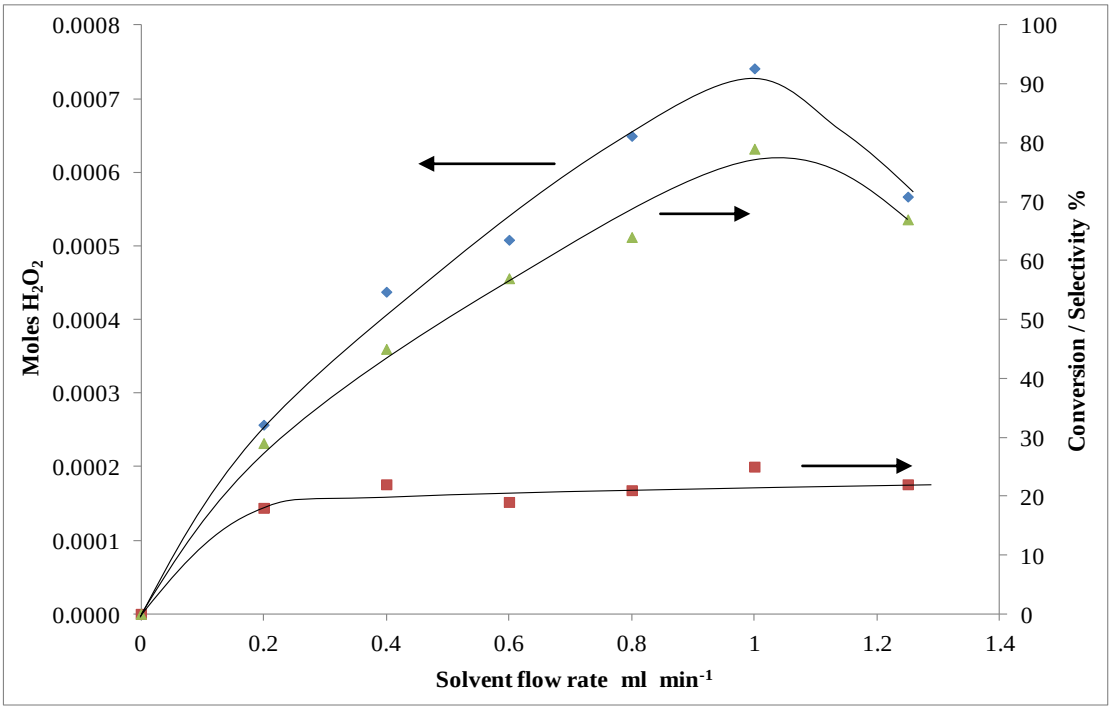

Figure 4.9 - H_2O_2 concentration obtained at various solvent flow rates, showing moles of H_2O_2 formed (♦), H_2 conversion (■), and H_2O_2 selectivity (▲). Reaction Conditions – 10 bar, 2 ºC, 40 ml / min gas flow, solvent MeOH / H_2O flow rate = 0.2 – 1.2 ml / min, 120 mg catalyst, τ = 0.25 s, H_2 : O_2 = 1.

The results show that at various solvent flow rates while the moles of H_2O_2 formed increase up to 1 ml min^{-1}, the H_2 conversion remained constant at 20 % while the selectivity towards H_2O_2 increased in a similar manner to the moles of H_2O_2 formed up to a selectivity of 80 %. This can be explained in terms of H_2O_2 concentration, as more solvent passes through the system the total concentration of H_2O_2 is reduced. As the rate of subsequent hydrogenation and decomposition reactions are proportional to the concentration of H_2O_2, the rate of these reactions will also reduce, increasing selectivity. These results show that hydrogenation and decomposition

reactions are responsible for reducing selectivity in the flow system despite short residence times, and the increased amount of solvent shields the synthesised H_2O_2 from the catalyst and prevents these subsequent reactions. This has implications in the challenge of making high concentrations of H_2O_2 using a catalyst that hydrogenates and decomposes H_2O_2.

4.4.6 - Effect of Reaction Temperature on H_2O_2 Synthesis

The effect of reaction temperature was investigated in the flow system while holding all other reaction variables constant including H_2 : O_2, residence time, pressure and solvent composition. The results are shown in figure 4.10,

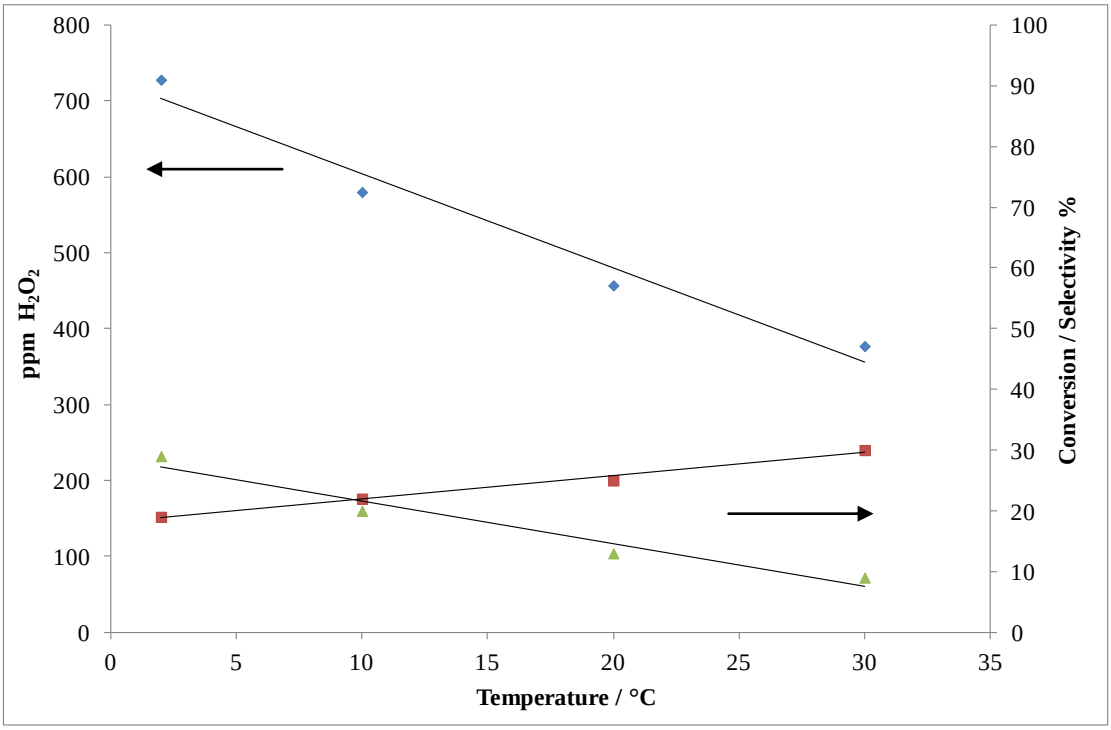

Figure 4.10 - H_2O_2 concentration obtained at various H_2 : O_2, showing H_2O_2 concentration (♦) H_2 conversion (■), and H_2O_2 selectivity (▲). Reaction Conditions – 10 bar, 2 - 20 ºC, 40 ml / min gas flow, solvent MeOH / H_2O flow rate = 0.2 ml / min, 120 mg catalyst, τ = 0.25 s, H_2 : O_2 = 1

Increasing the reaction temperature at a constant residence time resulted in a decrease in H_2O_2 concentration. The experiments show that as temperature increases the conversion of H_2 increases from 20% at 2 ºC to 30% at 30 ºC while the selectivity towards H_2O_2 decreased from 30% at 2 °C to 9% at 30 °C indicating that while more H_2 is consumed at higher temperature it is not being used to synthesise H_2O_2. When the temperature of the reaction is increased this changes the solubility of both reactant gases in the system. As the reaction temperature is

increased, O_2 solubility reduces in both water and methanol which reduces the rate of synthesis of H_2O_2. Conversely the solubility of H_2 increases in methanol at higher temperatures, therefore the rate of hydrogenation is expected to increase at higher temperatures which will increase H_2 conversion, which in turn decreases H_2O_2 selectivity through non selective H_2 utilisation. This means that lower H_2O_2 concentrations are obtained as seen in the results in figure 4.10, confirming that if a catalyst shows hydrogenation activity low temperatures are desirable to obtain higher H_2O_2 concentrations.

4.4.7 - The Effect of H_2 : O_2 on H_2O_2 Concentration

The impact of H_2 : O_2 molar ratio on H_2O_2 concentration was investigated in the flow system while all other reaction variables including temperature, residence time, pressure and solvent composition were held constant. Figure 4.11 shows that the stoichiometric 1 : 1 ratio was shown to be the optimum ratio to generate H_2O_2 with 758 ppm being observed at the end of the system. As expected the variation of this parameter was shown to have a major effect on the observed concentration of H_2O_2 with the optimum concentration being observed with equimolar gas concentration.

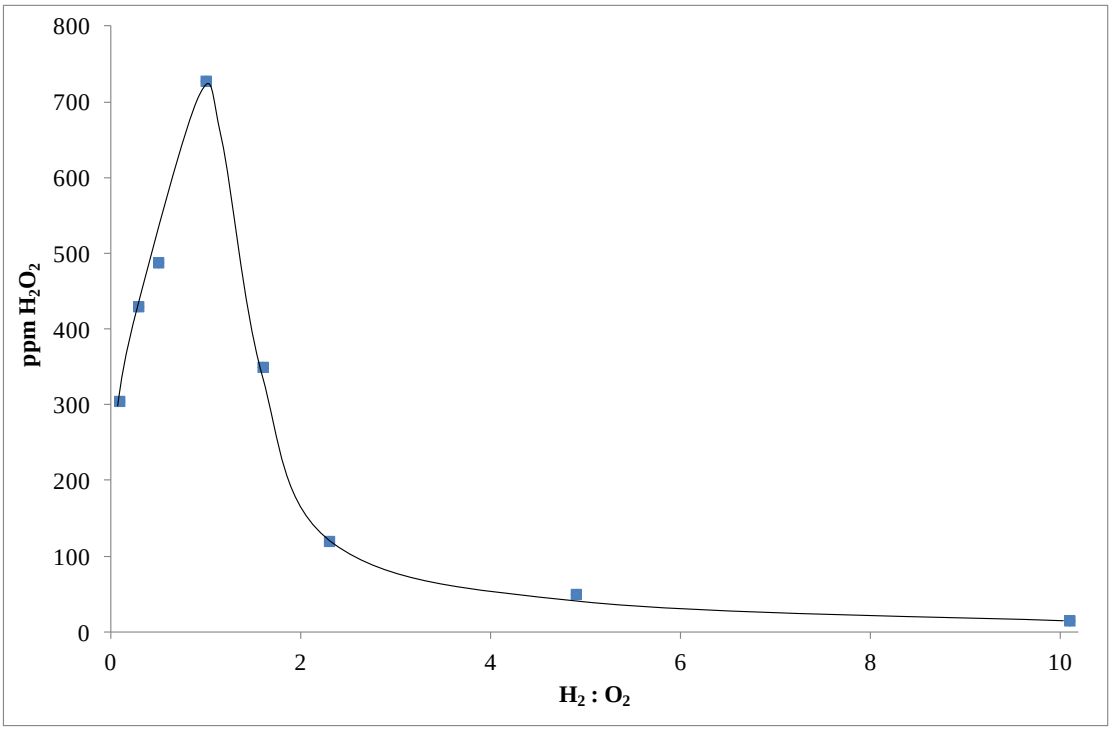

Figure 4.11 –H_2O_2 concentration obtained at various H_2 : O_2. Reaction Conditions – 10 bar, 2 ºC, 40 ml / min gas flow, solvent MeOH / H_2O flow rate = 0.2 ml / min, 120 mg catalyst, τ = 0.25 s.

The reaction gas contains CO_2 as a diluent which has been shown to form carbonic acid *in-situ* by dissolving in the solvent, lowering the pH of the reaction solution and increasing H_2O_2 by making the solvent slightly acidic.[10,11] However at a pressure of 10 bar the solvent solution can be assumed to be saturated with CO_2 meaning that the pH of the solvent is constant throughout the experiments and therefore the results show the true dependence of H_2O_2 concentration on H_2 : O_2. The decrease in H_2O_2 concentration at a deviation away from 1 : 1 can be explained in terms of limiting reagent. Due to the available gas cylinders, and lower explosive limits for H_2 the 1 : 1 data point is the maximum concentration at which a 1 : 1 ratio can be achieved. The data was then generated by reducing the concentration of one of the gases, limiting the reaction by the lower reactant concentration.

It might be expected that H_2O_2 concentration varies symmetrically around the 1 : 1 ratio and that decreasing H_2 concentration would have the same effect as decreasing O_2. In fact, as has already been seen in a similar study in a batch system[9] there is an asymmetry, with H_2O_2 concentration decreasing more rapidly with decreasing O_2 partial pressure than with decreasing H_2 partial pressure. This can be seen more clearly when H_2 : O_2 and O_2 : H_2 are plotted together in figure 4.12 .

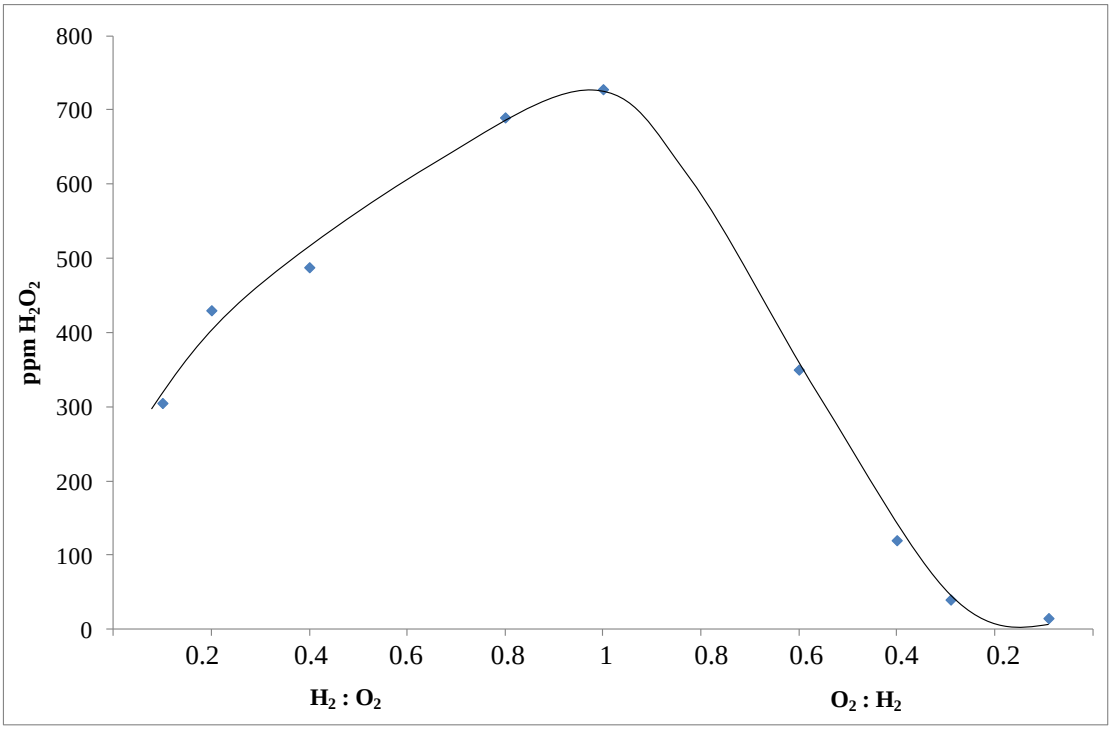

Figure 4.12 - H_2O_2 concentration obtained at various H_2 : O_2. Reaction Conditions – 10 bar, 2 ºC, 40 ml / min gas flow, solvent MeOH / H_2O flow rate = 0.2 ml / min, 120 mg catalyst, τ = 0.25 s.

As can be seen in figure 4.12 even when there is 10 times more O_2 than H_2 this only gives rise to a decrease in H_2O_2 concentration from 750 ppm to 300 ppm whereas with 10 times more H_2 than O_2 only around 20 ppm is observed. These results are similar to the result seen in the batch system and can be explained in much the same way by considering the key reaction steps involved. As has been previously postulated[9], all of the reactions steps share the same intermediate reaction species and H_2O_2 is formed by a 2-step hydrogenation of adsorbed O_2. The key reaction steps for the synthesis of H_2O_2 are shown below, where * denotes a vacant site on the catalyst surface,

$$H_2 + 2* \rightarrow 2H*$$

$$O_2 + * \rightarrow O_2*$$

$$H* + O_2* \rightarrow HO_2* + *$$

$$HO_2* + H* \rightarrow H_2O_2* + *$$

$$H_2O_2* \rightarrow H_2O_2 + *$$

Competing with this reaction scheme are the reactions that lead to the undesired formation of water which involve the hydrogenation of dissociated surface O_2 species

$$O_2 + 2* \rightarrow 2O* \text{ or } H_2O_2* + * \rightarrow H_2O + O*$$

$$H* + O* \rightarrow HO* + *$$

$$HO* + H* \rightarrow H_2O* + *$$

$$H_2O* \rightarrow H_2O + *$$

The asymmetry in figure 4.12 is predicted by this model, in that when H_2 partial pressure is low compared to O_2 (left side of figure 4.12) the concentration of H* will be low, meaning that less O* will be scavenged and therefore less hydrogenation will take place. In terms of kinetic equations, where the rate of hydrogenation is proportional to the H_2 partial pressure a lower H_2 rate would also be predicted when O_2 is in excess as well as a lower synthesis rate. If a catalyst was tested which showed no hydrogenation activity a much more symmetrical shape would be observed when investigating $H_2 : O_2$.

4.5 - Kinetic Analysis of Decomposition and Hydrogenation of H_2O_2

When using a solvent system that does not contain any acid or halide additives to suppress the subsequent decomposition and hydrogenation reactions, the observed concentration of H_2O_2 is a result of the combination of the synthesis reaction and the two subsequent reactions. In order to put together a kinetic model for the synthesis of H_2O_2 the decomposition and hydrogenation rates must be included in the overall rate equations for the system. To do this the rate constants for this system must be determined for the decomposition and hydrogenation reactions. The rate constants were determined using the residence time that resulted in the most amount of H_2O_2 being made, τ = 0.25 s, and using similar concentrations of H_2O_2 and H_2 than were used in the synthesis experiments.

4.5.1 - Decomposition Reaction

The decomposition rate constant was determined by pressurising the system to 10 bar with CO_2 and maintaining a flow of 42 ml min^{-1} through the system. A water-methanol solvent mixture containing various amounts of H_2O_2 was passed through the reactor with the catalyst in place and without the catalyst to determine the background activity of the reactor under reaction conditions. Assuming that the decomposition reaction is first order with H_2O_2 is can be described by the simple expression shown as equation (4.3) ;

$$\text{Decomposition Rate} = r_d = k_d[H_2O_2] \qquad (4.3)$$

Based on this expression, the decomposition rate should increase linearly as the concentration of H_2O_2 increases and should be independent of the total pressure of the system. Figure 4.13 shows the decomposition rate as a function of H_2O_2 concentration for both the catalyst and the reactor. The results show that in accordance with the first order kinetic expression the decomposition rate increases linearly with increasing H_2O_2 concentration. From this data it is clear to see that the reactor contributes a small amount to the decomposition activity however this is minimal when compared to the decomposition activity of the catalyst. From this data it is possible to obtain the rate constant for the catalyst at the reaction condition investigated. The gradient of this line gives this rate constant for the decomposition reaction which equals 68 dm^3 kg^{-1} h^{-1}. To confirm that the decomposition reaction was independent of pressure the experiment was repeated at various pressures of CO_2 in the presence of the catalyst. The results shown in figure 4.14 indicate that this is true, the decomposition rate remained constant at ~1.7 mol kg^{-1} h^{-1} over a pressure range of 0 -10 bar indicating that it is first order with respect to H_2O_2 only.

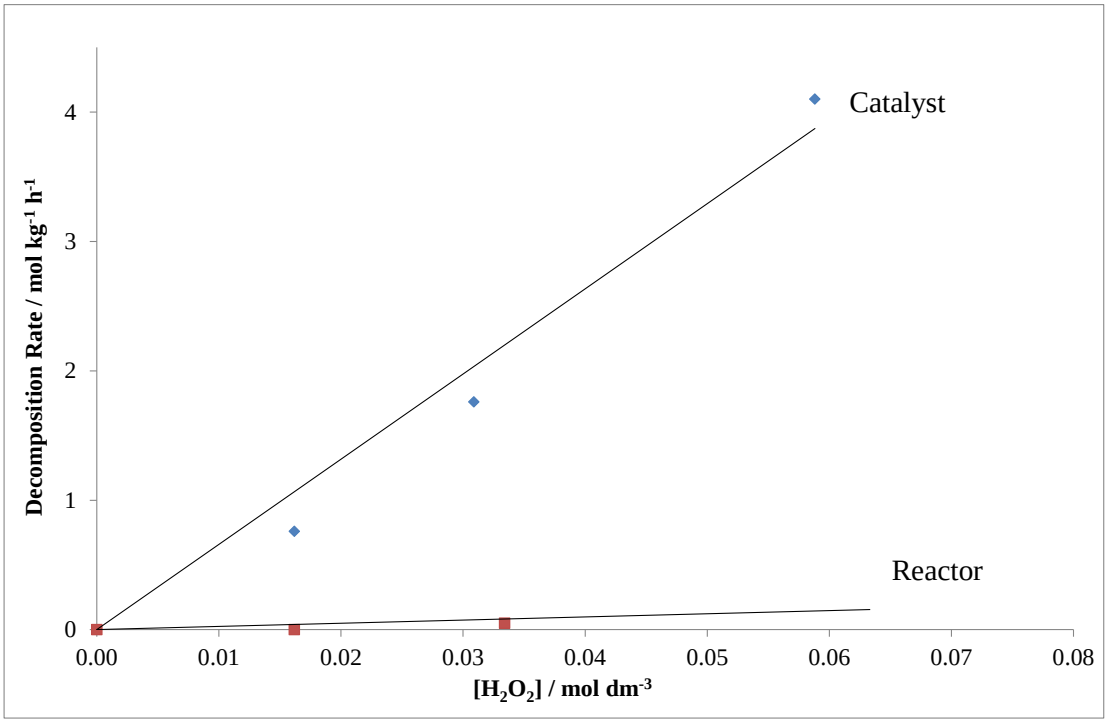

Figure 4.13 - Effect of H_2O_2 concentration on the decomposition rate of both the catalyst (♦) and the reactor (■). Reaction Conditions – 10 bar, 2 ºC, 40 ml / min gas flow, solvent MeOH / H_2O flow rate = 0.2 ml / min, 120 mg catalyst, τ = 0.25 s, $[H_2O_2]$ = 0 – 2000 ppm.

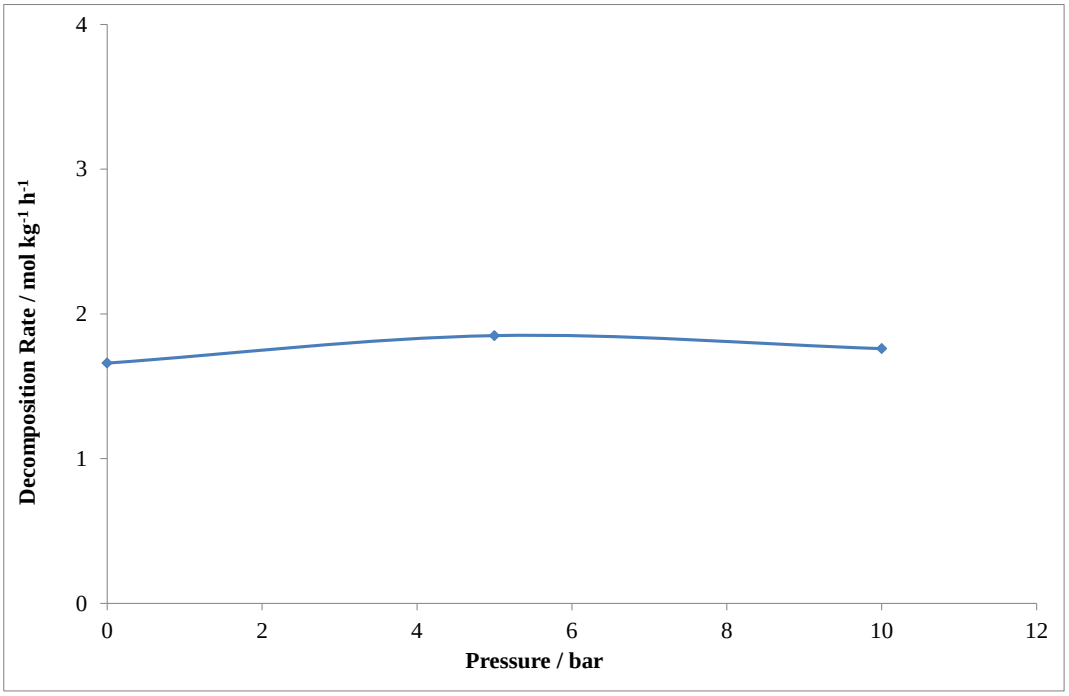

Figure 4.14 - Effect of reactor pressure on the decomposition rate at constant gas flow.

Reaction Conditions – 0 - 10 bar, 2 ºC, 40 ml / min gas flow, solvent MeOH / H_2O flow rate = 0.2 ml / min, 120 mg catalyst, τ = 0.25 s, $[H_2O_2]$ = 1000 ppm.

Decomposition constants were obtained for the system containing the catalyst, the catalyst support and the empty reactor and the results are shown in figure 4.15. From these results it is clear that the metals in the catalyst are responsible for the decomposition activity with the catalyst having a decomposition constant 10 times higher than the support alone. It can be seen that both the catalyst support and the reactor have a small amount of decomposition activity and it is the Au-Pd on the catalyst that is responsible for the subsequent decomposition of H_2O_2.

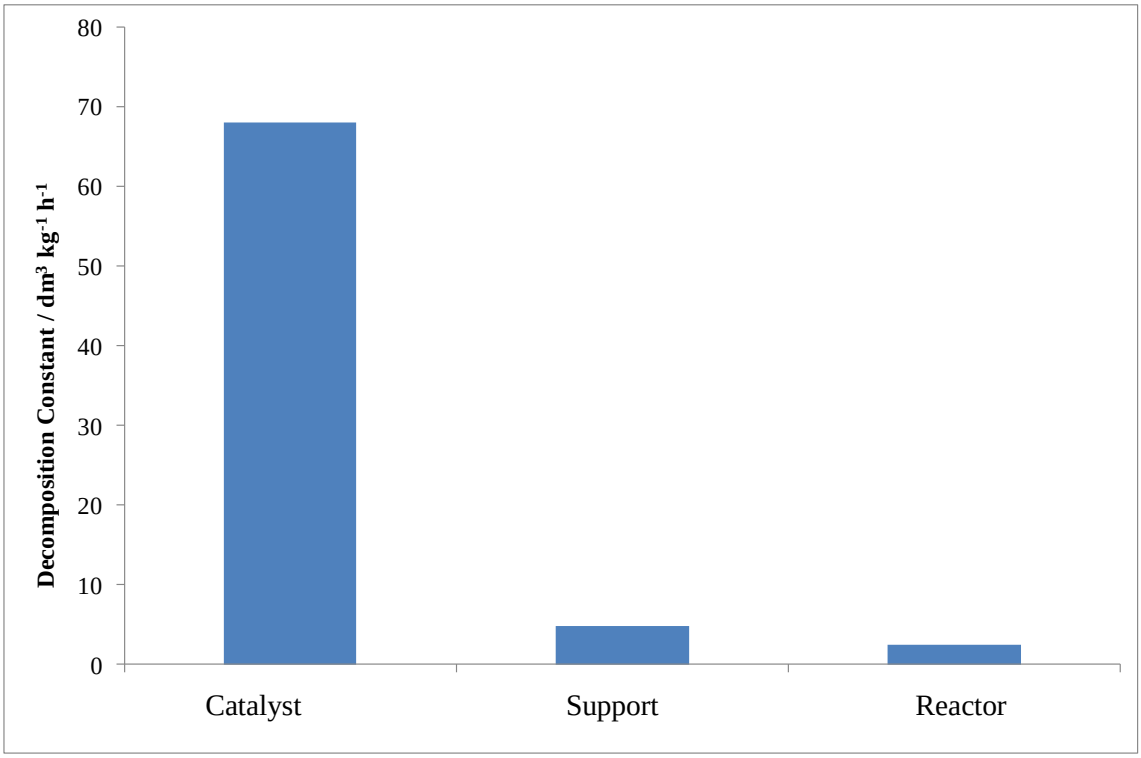

Figure 4.15 – Graph to show the decomposition rate constant of the catalyst, catalyst support and reactor. Reaction Conditions – 10 bar, 2 ºC, 40 ml / min gas flow, solvent MeOH / H_2O flow rate = 0.2 ml / min, 120 mg catalyst, τ = 0.25s, $[H_2O_2]$ = 1000 ppm.

4.5.2 - Hydrogenation Reaction

The hydrogenation rate constant was determined by pressurising the reactor with H_2 and CO_2 at various concentrations while maintaining the gas flow rate and also by passing various concentrations of H_2O_2 through the system, at a constant H_2 concentration and measuring the concentration of H_2O_2 exiting the reactor. The observed rate during these experiments is a combination of the hydrogenation and decomposition rates, so to extract the hydrogenation rate, the decomposition rate at the reaction condition also has to be determined and subtracted from the observed rate. All the hydrogenation rates presented have been deconvoluted from the

decomposition rates. Assuming that the hydrogenation reaction is first order with H_2O_2 and H_2 it can be described by the simple expression shown in equation (4.4);

$$\text{Hydrogenation Rate} = k_h = k_h[H_2][H_2O_2] \quad (4.4)$$

By holding one of the reactants constant whilst varying the other it is possible to determine k_h in two ways: by varying $[H_2O_2]$ while maintaining $[H_2]$ and vice versa. Both variables should be directly proportional to the hydrogenation rate so increasing one reactant should result in a linear response of the hydrogenation rate if the other reactant is held constant. Figure 4.16 shows how the hydrogenation rate varies linearly with increasing $[H_2]$ at constant $[H_2O_2]$ for the catalyst and an empty reactor tube.

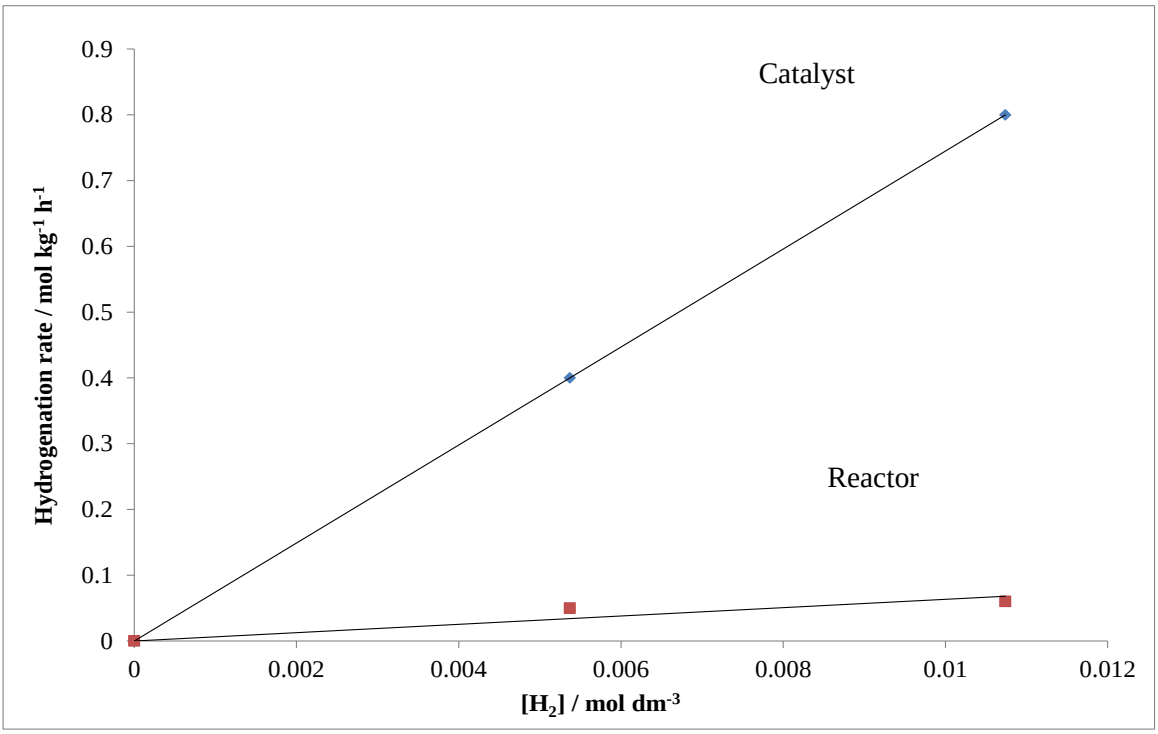

Figure 4.16 - Effect of H_2 concentration on the hydrogenation rate of both the catalyst (♦) and the reactor (■). Reaction Conditions – 10 bar, 2 ºC, 40 ml / min gas flow, solvent MeOH / H_2O flow rate = 0.2 ml / min, 120 mg catalyst, τ = 0.25 s, $[H_2O_2]$ = 1000 ppm.

From this data an hydrogenation constant can be extracted from the gradient of the graph which is equal to $k_h[H_2O_2]$ from this data a value of k_h of 1133 $dm^6\ kg^{-1}\ h^{-1}\ mol^{-1}$ can be obtained. From the results it is seen that the reactor has a small amount of hydrogenation activity but minimal when compared to the catalyst. To verify the results the same experiment was conducted but this time varying the H_2O_2 concentration, shown in figure 4.17.

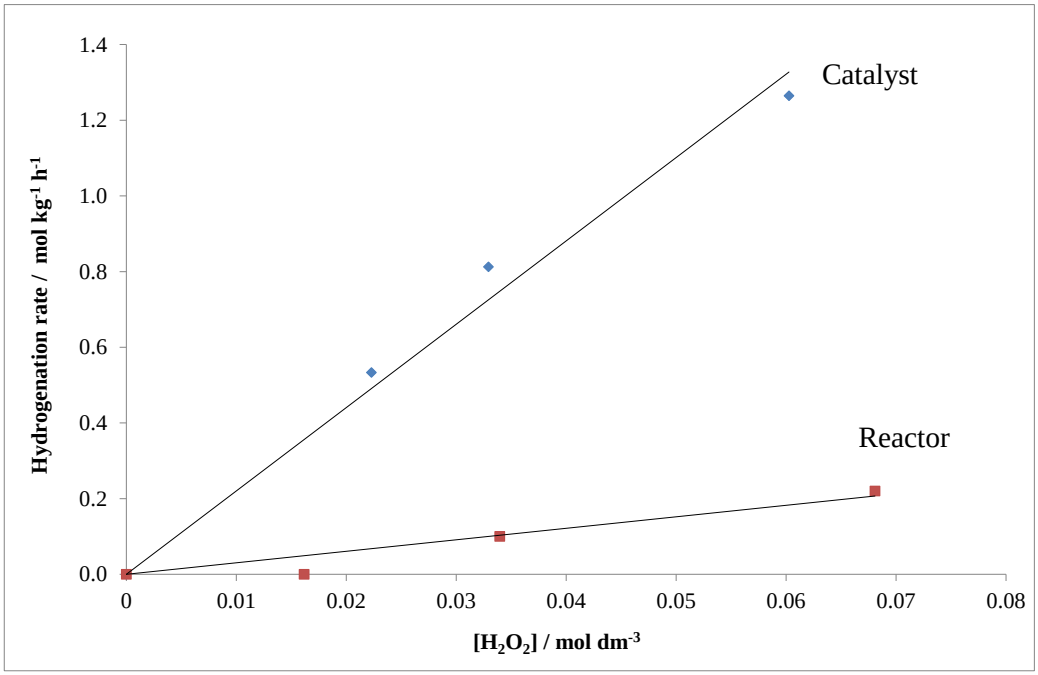

Figure 4.17 - Effect of H_2O_2 concentration on the hydrogenation rate of both the catalyst (♦) and the reactor (■). Reaction Conditions – 10 bar, 2 ºC, 40 ml / min gas flow, solvent MeOH / H_2O flow rate = 0.2 ml / min, 120 mg catalyst, τ = 0.25 s, [H_2] = 4 vol%.

From this data an hydrogenation constant can be extracted from the gradient of the graph which is equal to $k_h[H_2]$ meaning a value of k_h of 1079 dm^6 kg^{-1} h^{-1} mol^{-1} can be obtained which is in good agreement with the value obtained previously by varying the concentration of H_2.

As for the decomposition reaction the hydrogenation constants can be determined for each of the components of the catalyst system at identical reaction conditions. Figure 4.18 shows that, similar to decomposition, it is the precious metals on the catalyst support that are responsible for most of the hydrogenation activity. The reactor shows some background hydrogenation activity but much lower than the catalyst, whereas the TiO_2 support shows no hydrogenation activity at all.

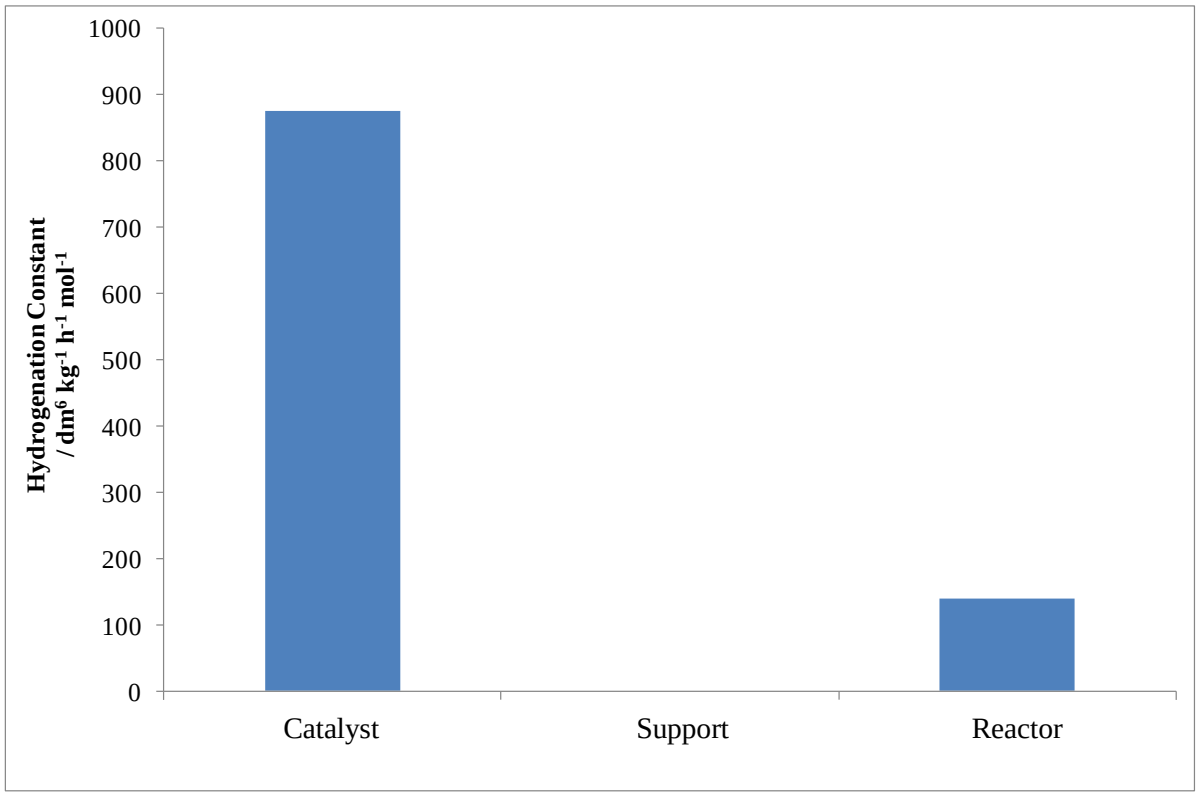

Figure 4.18 - Graph to show the hydrogenation rate constant of the catalyst, catalyst support and reactor. Reaction Conditions – 10 bar, 2 ºC, 40 ml / min 5% H_2 / CO_2 flow, solvent MeOH / H_2O flow rate = 0.2 ml / min, 120 mg catalyst, τ = 0.25 s, [H_2O_2] = 1000 ppm.

4.5.3 - Kinetic Analysis of Synthesis Reaction

As was shown previously the concentration of H_2O_2 synthesised does not depend symmetrically on the H_2 and O_2 concentration. Due to the H_2O_2 hydrogenation rate being proportional to the concentration of hydrogen, increasing the H_2 in the system decreases the observed H_2O_2 concentration more rapidly than an increase in O_2. Increasing the O_2 concentration in the system may increase the synthesis rate without increasing the hydrogenation rate. Due to the available gas cylinders the O_2 concentration could not be increased past the values used to obtain the maximum H_2O_2 concentration shown earlier, [O_2] = 3.6 vol%.

To model the synthesis reaction and to allow prediction of H_2O_2 concentration in O_2 and H_2 rich conditions a synthesis constant must be determined for both the O_2 and H_2 rich system. This was done by initially starting from H_2 : O_2 = 1 : 1 and gradually decreasing one of the reactants while maintaining the concentration of the other reactant. Following on from the analysis of the

decomposition and hydrogenation reactions a similar kinetic expression can be used to estimate the H_2O_2 synthesis rate. A simple equation shown as equation (4.5) assumes that the reaction rate is proportional to the H_2 and O_2 concentration and is first order with each reactant.

$$\text{Synthesis Rate} = r_s = k_s[H_2][O_2] \quad (4.5)$$

The effect of reducing the O_2 content in the reaction, and therefore carrying out the reaction in a H_2 rich atmosphere is shown in figure 4.19. It can be seen that the synthesis rate depends linearly on the O_2 concentration and therefore it can be assumed to be first order with respect to O_2 with observed rate constant = 81.6 dm^6 kg^{-1} h^{-1} mol^{-1} = $k_s[H_2]$. Therefore k_s = 4647 dm^6 kg^{-1} h^{-1} mol^{-1} when H_2 is in excess.

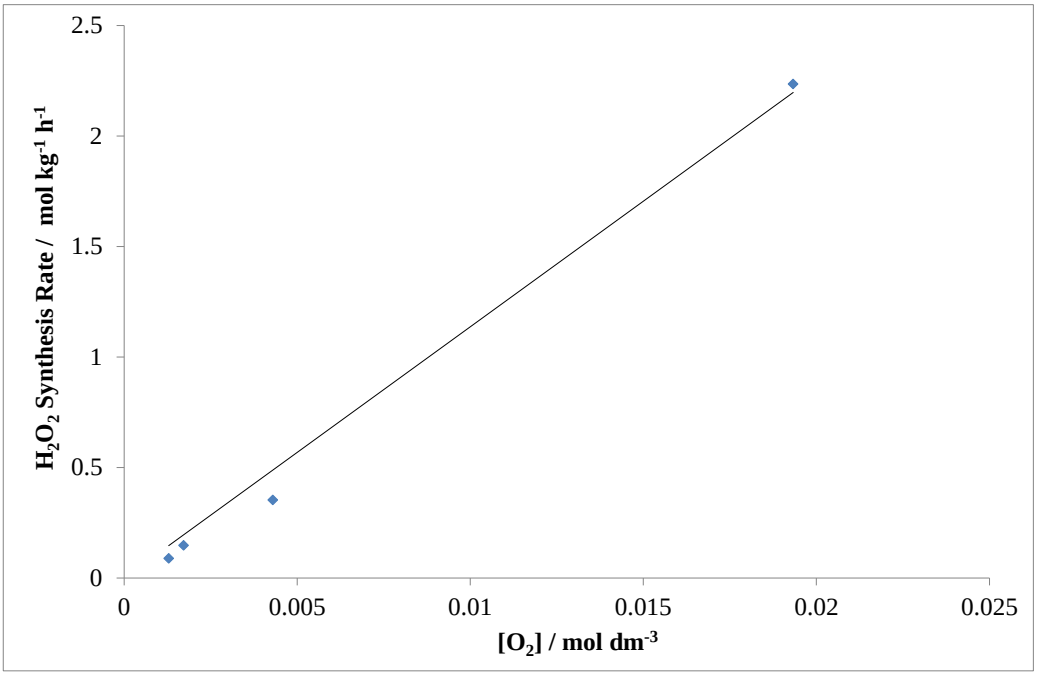

Figure 4.19 - Effect of O_2 concentration on synthesis rate at constant H_2 concentration and residence time. Reaction Conditions – 10 bar, 2 ºC, 40 ml / min gas flow, solvent MeOH / H_2O flow rate = 0.2 ml / min, 120 mg catalyst, τ = 0.25 s, $[H_2]$ = 0.017 mol dm^{-3}.

The effect of reducing the H_2 content in the reaction, and therefore carrying out the reaction in an O_2 rich atmosphere is shown in figure 4.20. It can be seen that the synthesis rate depends linearly on the H_2 concentration and therefore can be assumed to be first order with respect to H_2 with the gradient of the graph = 120 dm^6 kg^{-1} h^{-1} mol^{-1} = $k_s[O_2]$. Therefore k_s = 7000 dm^6 kg^{-1} h^{-1} mol^{-1} when O_2 is in excess.

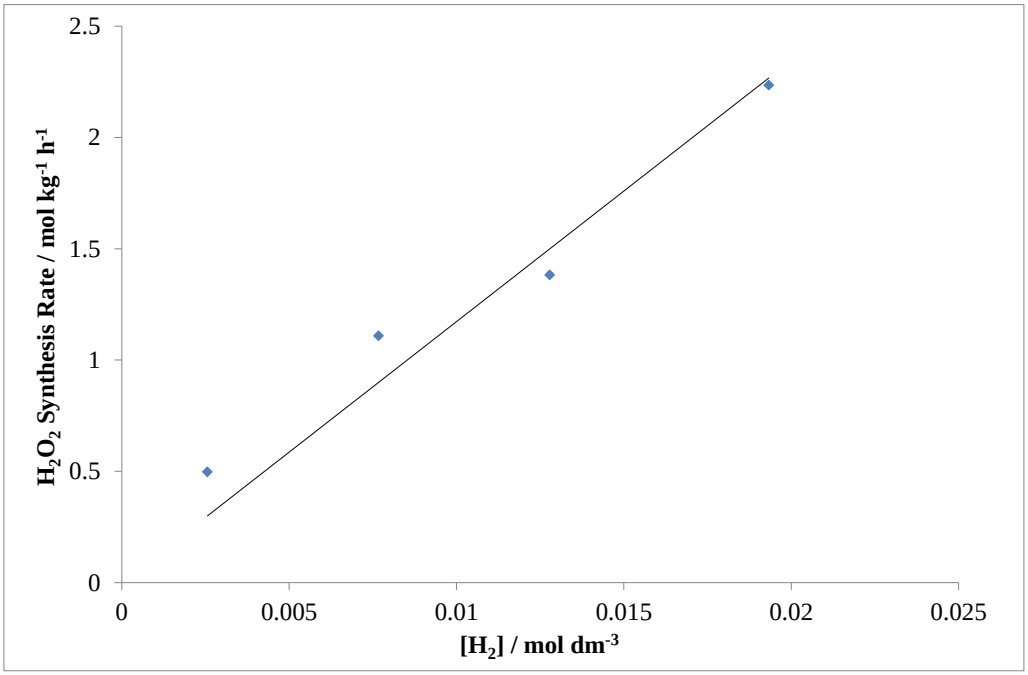

Figure 4.20 - Effect of H_2 concentration on synthesis rate at constant O_2 concentration and residence time. Reaction Conditions – 10 bar, 2 ºC, 40 ml / min gas flow, solvent MeOH / H_2O flow rate = 0.2 ml / min, 120 mg catalyst, τ = 0.25s , $[O_2]$ = 0.017 mol dm^{-3}.

The experiments carried out have allowed rate constants to be determined for all of the reactions that are taking place in the direct synthesis process and are summarised below. It is important to note that these rate constants are related to both the catalyst and the residence time of the experiments which were kept constant throughout. At higher residence times it would be expected that all of the rate constants would increase because of greater contact time with the catalyst and the reverse if the residence time was decreased.

$$k_d = 63.38\ dm^3\ kg^{-1}\ h^{-1}$$

$$k_h = 1133\ dm^6\ kg^{-1}\ h^{-1}\ mol^{-1}$$

$$k_s = 4647\ dm^6\ kg^{-1}\ h^{-1}\ mol^{-1}\ \text{when } H_2 \text{ is in excess}$$

$$k_s = 7000\ dm^6\ kg^{-1}\ h^{-1}\ mol^{-1}\ \text{when } O_2 \text{ is in excess}$$

4.5.4 - Combining Experimental Results into a Kinetic Model

From the experiments carried out so far it has been possible to establish rate constants for the H_2O_2 decomposition reaction, hydrogenation reaction and the synthesis reaction both in O_2 rich and H_2 rich conditions. Based on the simple kinetic equations that describe each reaction it is

possible to combine all of the rate constants into a single equation to predict the concentration of H_2O_2 that is expected to be produced, and then test this model containing the derived rate constants against the observed experimental results. Based on the assumption that all of the reaction rates are first order with respect to any one reactant the rates of reactions can be expressed as follows;

$$\text{Decomposition Rate} = r_d = k_d[H_2O_2] \quad (4.6)$$

$$\text{Hydrogenation Rate} = r_h = k_h[H_2][H_2O_2] \quad (4.7)$$

$$\text{Synthesis Rate} = r_s = k_s[H_2][O_2] \quad (4.8)$$

The rates of reaction are also dependent on the amount of catalyst in the system however the catalyst mass has been constant throughout the experiments and because the rate is calculated as mol kg_{cat}^{-1} hr^{-1} the amount of catalyst is incorporated into the calculated rate constants so is not included in these rate equations. The rate at which H_2O_2 is formed can be defined as the difference between the H_2O_2 forming rate and the H_2O_2 removal rate which can be described by equation (4.9) :

$$\frac{d[H_2O_2]}{dt} = r_s - r_h - r_d \quad (4.9)$$

And substituting the definitions of the rate equations for synthesis, hydrogenation and decomposition into the equation above results in the following equation (4. 10) that describes the rate of production of H_2O_2

$$\frac{d[H_2O_2]}{dt} = k_s[H_2][O_2] - k_h[H_2][H_2O_2] - k_d[H_2O_2] \quad (4.10)$$

If the system is assumed to be at steady state with no catalyst deactivation, meaning that the rate constants remain unchanged during the reaction, the concentration of H_2O_2 being produced is constant and the reaction time is defined as the residence time which is constant at 0.25 s for all the kinetic experiments the equation (4.11) can be written as

$$[H_2O_2] = k_s[H_2][O_2] - k_h[H_2][H_2O_2] - k_d[H_2O_2] \quad (4.11)$$

The equation can be re-arranged into the form

$$[H_2O_2] = \frac{k_s[H_2][O_2]}{1+k_d+k_h[H_2]} \quad (4.12)$$

All of the reaction constants that have been derived experimentally can now be substituted into the formula above to predict the concentration of H_2O_2 that is produced based on the H_2 and O_2 concentrations that are used in the experiment, assuming that the liquid flow remains constant at 0.2 ml min^{-1}. This equation was tested by comparing the results of the experiment to investigate the effect of ratio H_2 : O_2 and also the effect of catalyst mass. When using the equation to model the results of the experiment two values of k_s were used to reflect the asymmetry between the H_2 and O_2 rich reactions observed in the experimental work. Concentration of H_2O_2 produced in an H_2 rich reaction was predicted using k_s = 4647 dm^6 kg^{-1} h^{-1} mol^{-1} and when the reaction was carried out in an O_2 rich environment the value used was k_s = 7000 dm^6 kg^{-1} h^{-1} mol^{-1}. A selection of H_2 and O_2 concentrations that were in a similar range to the values used during the experimental study and the predicted results are shown in comparison to the experimental results in figure 4.21

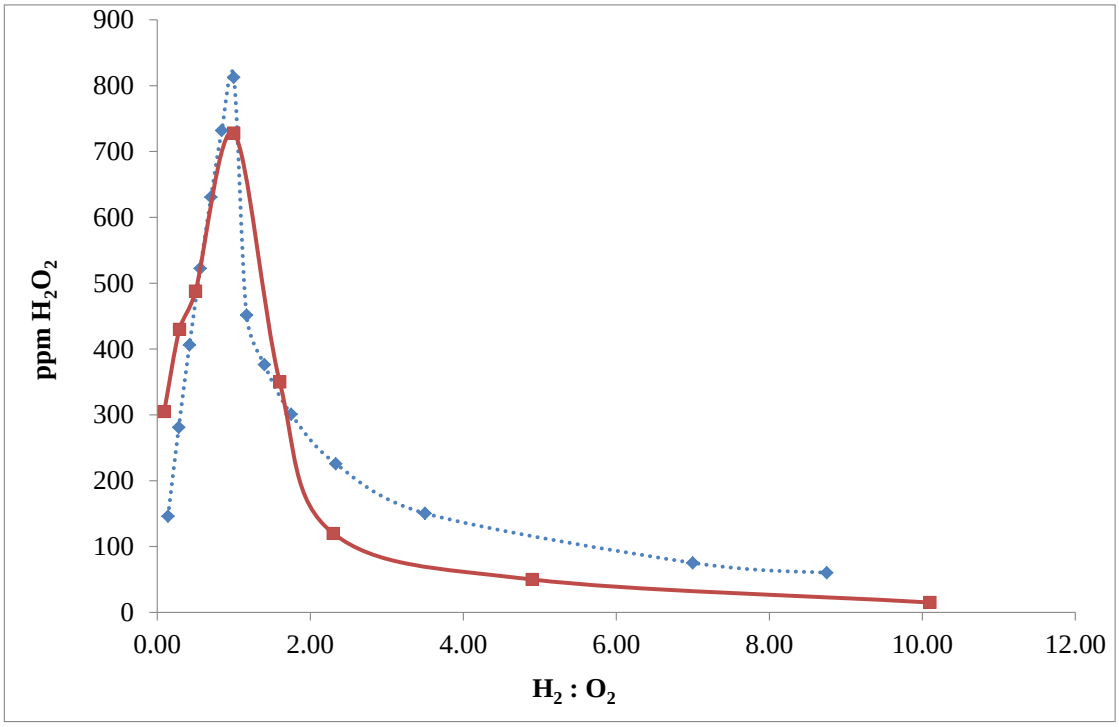

Figure 4.21 - Plot to compare experimental results to the values predicted by the derived kinetic model – dotted line shows predicted results and solid line shows experimental results.

Reaction Conditions – 10 bar, 2 ºC, 40 ml / min gas flow, H_2 : O_2 = various, solvent MeOH / H_2O flow rate = 0.2 ml / min, 120 mg catalyst, τ = 0.25 s.

The results in figure 4.21 show that the results predicted by the model agree well with the results obtained experimentally. The model containing the experimentally determined kinetic constants

predicts that the observed optimum H_2 : O_2 is 1 : 1 as was shown by experiment, it also shows that the predicted H_2O_2 concentration values are relatively close to the experimental concentration values, meaning that the kinetic constants obtained by experiment are reliable for this catalyst system at this residence time.

Now that a basic model has been obtained it is possible to predict the results of the reactions at various conditions such as various H_2 : O_2 for catalysts that have different rate constants. This will also allow the prediction H_2O_2 concentration that could be produced without the destruction of H_2O_2 by the subsequent decomposition and hydrogenation reactions. By setting the rate constants in the model to the background reactor values for decomposition and hydrogenation while leaving the synthesis rate constants unchanged it is possible to see which of the side reactions is hindering the production of high concentrations of H_2O_2 the most. Figure 4.22 shows the effect of reducing the decomposition rate constant to the background level of the reactor, k_d = 4 $dm^3\ kg^{-1}\ h^{-1}$, with the blue dashed line showing the values predicted by the model and the solid red line showing the previously obtained experimental results.

The results show that decomposition plays a large part in limiting the concentration of H_2O_2 produced. This would be expected from the rate equation for H_2O_2 decomposition because the decomposition rate is first order with respect to H_2O_2 and the use of the flow system to suppress decomposition seems not to have been effective. If decomposition was reduced to background levels the H_2O_2 concentration would increase four fold indicating that the decomposition reaction is still limiting this subsequent reaction. This may be to do with the reactor set-up in that to pass through the reactor H_2O_2 must pass through the tightly packed cylindrical catalyst bed meaning lots of contact with catalyst surface. As the reaction is only dependent on the concentration of H_2O_2 and therefore only on the diffusion of H_2O_2 to the catalyst surface a high decomposition rate for higher concentrations would be expected. This may be addressed in two ways, either through catalyst design to reduce the decomposition rate or through the design of the catalyst bed. Theoretically a disk shape catalyst bed instead of a cylindrical bed of the same volume would provide less subsequent chance for the H_2O_2 to decompose while still maintaining the residence time of the cylindrical bed which may lead to a lower decomposition rate and the possibility of producing higher concentrations.

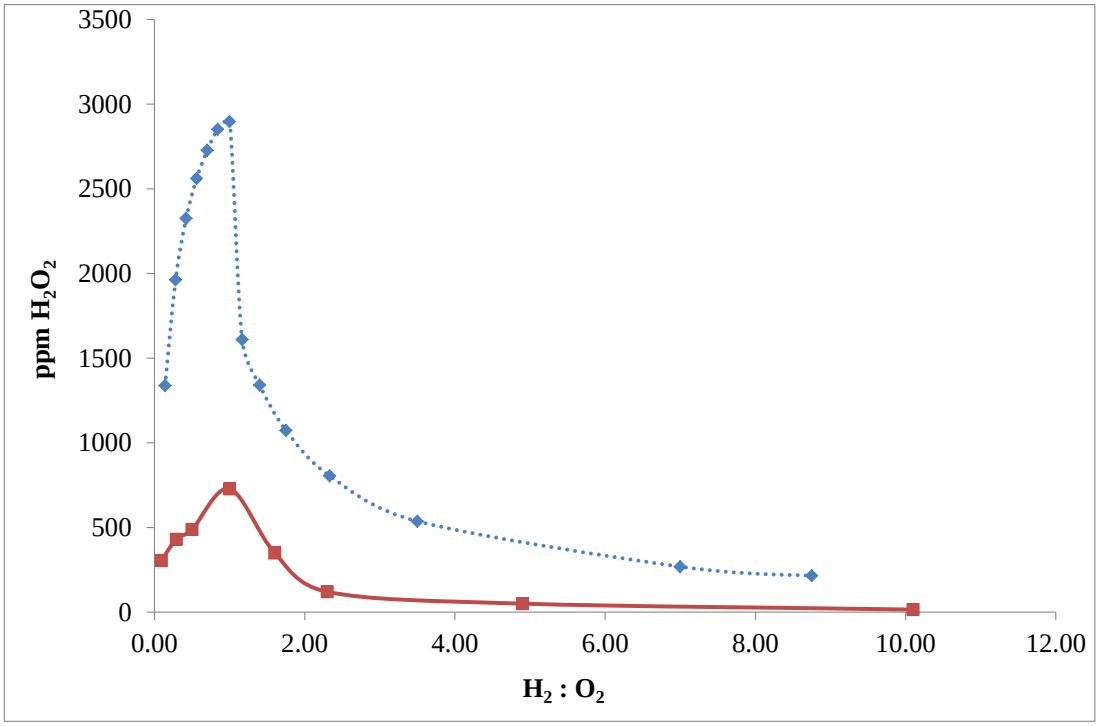

Figure 4.22 - Prediction of H_2O_2 concentration at various H_2 : O_2 assuming no decomposition from the catalyst – blue dashed line shows predicted results red solid line shows previous experimental results. Reaction Conditions – 10 bar, 2 ºC, 40 ml / min gas flow, H_2 : O_2 = various, solvent MeOH / H_2O flow rate = 0.2 ml / min, 120 mg catalyst, τ = 0.25s

The same process can be applied to investigate how the concentration of H_2O_2 would change if the hydrogenation rate constant was set to the background value for the reactor of 140 dm^6 kg^{-1} h^{-1} mol^{-1}, which is shown in figure 4.23 by the blue dashed line showing the predicted results and the red line showing the experimental results obtained previously.

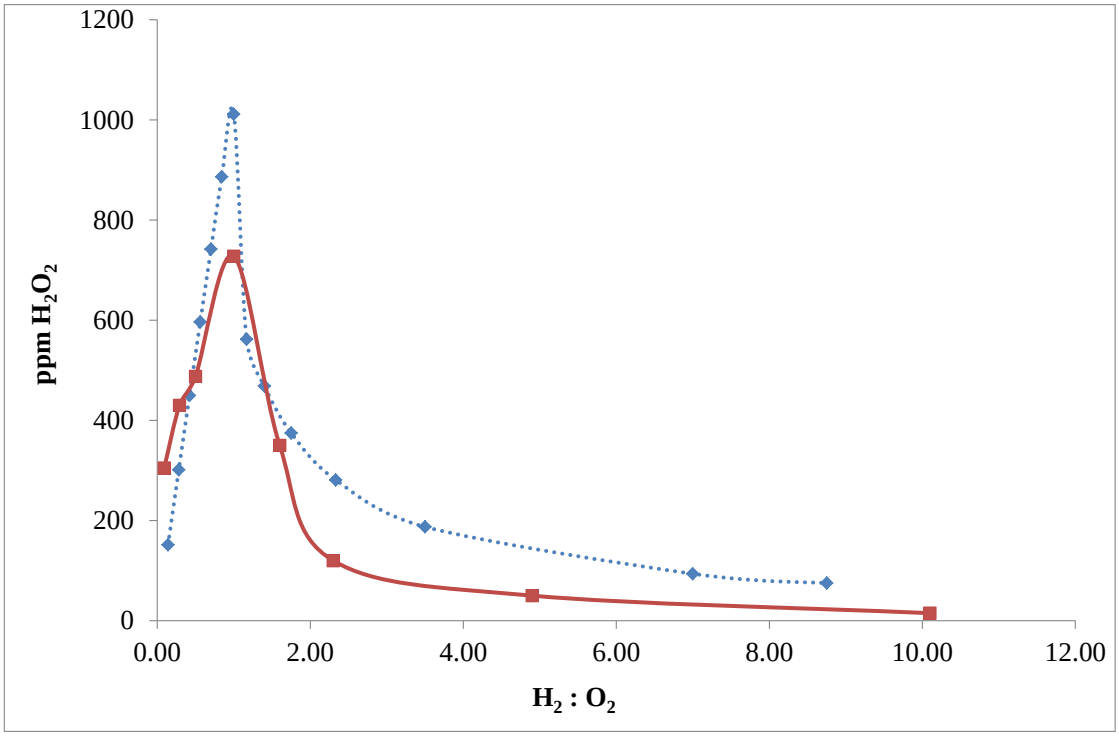

Figure 4.23 - Prediction of H_2O_2 concentration at various H_2 : O_2 assuming no hydrogenation from the catalyst – blue dashed line shows predicted results red solid line shows previous experimental results Reaction Conditions – 10 bar, 2 ºC, 40 ml / min gas flow, H_2 : O_2 = various, solvent MeOH / H_2O flow rate = 0.2 ml / min, 120 mg catalyst, τ = 0.25 s.

The results show that while the concentration of H_2O_2 increases slightly with the removal of subsequent hydrogenation it does not have as big as effect as the removal of decomposition. The maximum concentration obtained is still for the H_2 : O_2 of 1 :1 but there is only a 300 ppm improvement in H_2O_2 yield compared to the improvement of around 2000 ppm by the removal of the decomposition reaction. This indicates that to make higher concentrations of H_2O_2 it is the decomposition reaction which has the greater limiting effect on the yield of H_2O_2 and this should be addressed either through catalyst design or engineering developments.

4.5.5 - Predicted Effect of Catalyst Mass

The model can also be used to predict the effect of changing the catalyst mass on the amount of H_2O_2 formed in the reactor at the reaction conditions and residence time used previously. The amount of catalyst was previously included in the rate constants for synthesis, hydrogenation and

decomposition but by calculating the rate constants without including the catalyst mass the model can be expanded to equation (4.13) and various catalyst masses can be taken into account;

$$[H_2O_2] = \frac{k_s[H_2][O_2][cat]}{1 + k_d[cat] + k_h[H_2][cat]} \quad (4.13)$$

The predicted results are shown in the figure 4.24 as the concentration of H_2O_2 produced at various H_2 : O_2 while using different catalyst masses. The figure shows that when starting at low catalyst masses the H_2O_2 concentration increases quickly but as the catalyst mass increases the amount of H_2O_2 predicted does not continue to increase at the same rate. This is because the rate of the subsequent hydrogenation and decomposition reactions are also increased by the increasing catalyst concentration. The rates of these subsequent reactions also increase relative to the rate of H_2O_2 synthesis. This means that doubling the catalyst concentration does not result in twice as much H_2O_2 being formed beyond a certain catalyst mass and in fact the increase in H_2O_2 when adding additional catalyst will plateau at a certain point.

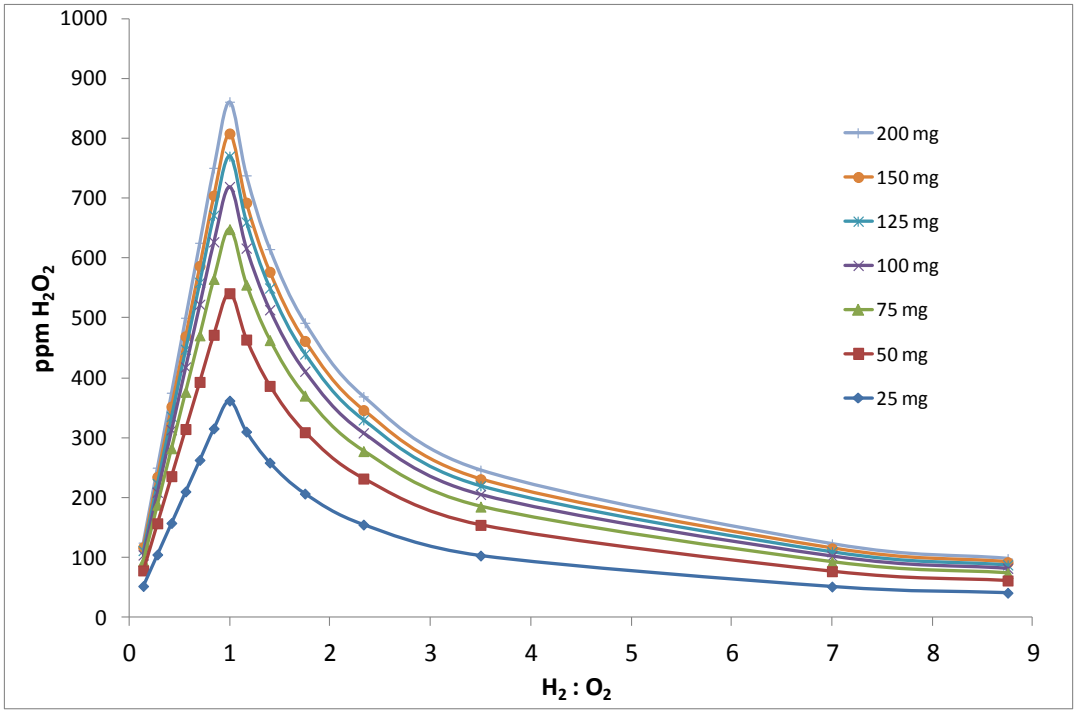

Figure 4.24 - Prediction of H_2O_2 concentration at various H_2 : O_2 at various catalyst masses.

Reaction Conditions – 10 bar, 2 ºC, 40 ml / min gas flow, H_2 : O_2 = various, solvent MeOH / H_2O flow rate = 0.2 ml / min, τ = 0.25 s.

The model can also be used to predict the H_2O_2 concentration if a catalyst was used with no decomposition or hydrogenation activity. By setting the rate constants for these two reactions to

the background reactor levels it is possible to see the effect of increasing catalyst mass without contributions from the catalyst to the subsequent reaction rates. Figure 4.25 shows the predicted data, when there is no contribution from hydrogenation the H_2O_2 concentration still plateaus with increasing catalyst mass indicating that it is the decomposition reaction that is limiting the concentration of H_2O_2 produced. The results with no contribution from decomposition rate included but still including the hydrogenation rate constant predict an almost linear increase in H_2O_2 concentration with catalyst mass. This emphasises the importance in designing catalysts that have low decomposition rates to make high concentrations of H_2O_2.

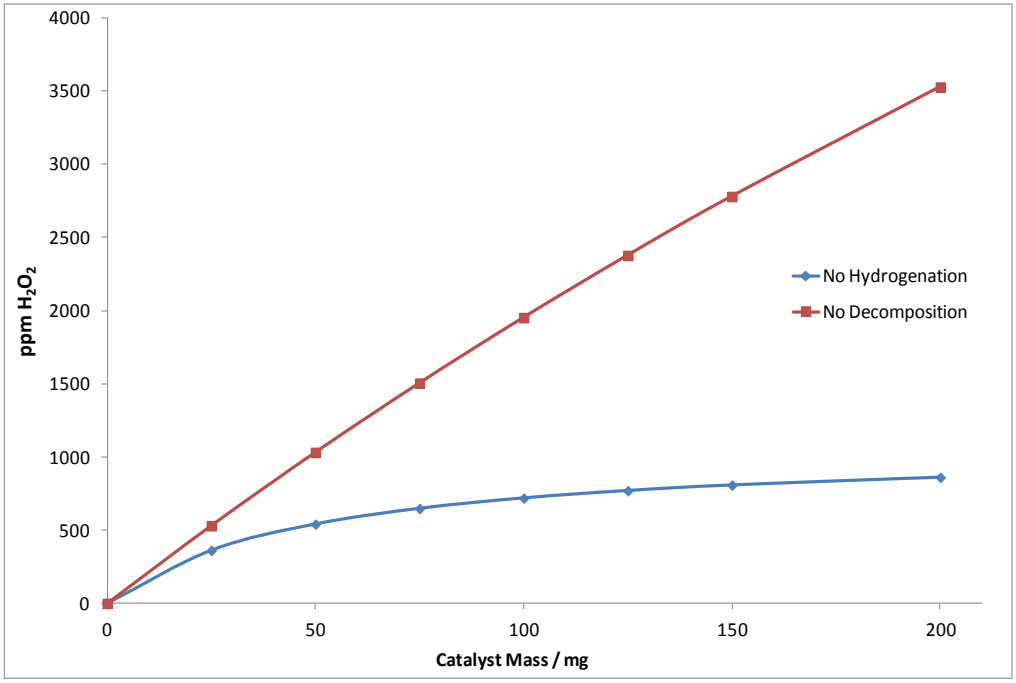

Figure 4.25 - Prediction of H_2O_2 concentration at various H_2 : O_2 at various catalyst masses assuming no hydrogenation (♦) or decomposition from the catalyst (■) Reaction Conditions – 10 bar, 2 ºC, 40 ml / min gas flow, H_2 : O_2 = various, solvent MeOH / H_2O flow rate = 0.2 ml / min, τ = 0.25 s.

4.6 - Conclusions

The direct synthesis of H_2O_2 is a challenging reaction with competing subsequent decomposition and hydrogenation reactions favouring the formation of water. When testing catalysts in a batch system only a snap shot of the reaction profiles can be determined. This makes it very difficult to measure the absolute rate of H_2O_2 synthesis due to the contribution of the subsequent reactions. The work described above firstly describes the construction and operation of a small scale flow reactor that could be used to for the direct synthesis of H_2O_2. It was observed that a vertical

reactor orientation was preferential in terms of H_2O_2 productivity and reproducibility of results. Reaction conditions were systematically studied with short residence times, low temperatures and high pressures being shown to be beneficial for H_2O_2 synthesis. H_2O_2 productivity showed an asymmetrical dependency on $H_2 : O_2$ as had been previously observed in the batch system as a result of the high hydrogenation activity of the catalyst at high H_2 concentrations. It was shown that high selectivity, 80 %, could be achieved by increasing the solvent flow through the catalyst bed by reducing the concentration of H_2O_2 and hence reducing the decomposition and hydrogenation rates. The reactor set-up also allowed rate constants to be determined for the decomposition, hydrogenation and synthesis reactions and these values were combined into a basic kinetic model to predict the H_2O_2 concentration that would be obtained. The model was able to give a good prediction of the effect of $H_2 : O_2$ which matched closely the experimental results. The model was also able to show that under the testing regime used it was the decomposition reaction that limits the concentration of H_2O_2 that is able to be obtained with the hydrogenation having less of an effect.

4.7 - References

1. S. Abate, S. Melada, G. Centi, S. Perathoner, F. Pinna and G. Strukul, *Catal. Today*, **2006**, *117*, 193-198.
2. S. Abate, G. Centi, S. Melada, S. Perathoner, F. Pinna and G. Strukul, *Catal. Today*, **2005**, *104*, 323-328.
3. X. Wang, Y. Nie, J. L. C. Lee, S. Jaenicke, *Appl. Catal. A: Gen.*, **2007**, *317*, 258-265.
4. J. F. Ng, Y. Nie, G. K. Chuah, S. Jaenicke, *J. Catal.*, **2007**, *269*, 302 – 308.
5. Y. Voloshin and A. Lawal, *Appl. Catal. A: Gen.*, **2009**, *353*, 9-16.
6. Y. Voloshin, R. Halder and A. Lawal, *Catal. Today*, **2007**, *125*, 40-47.
7. Y. Volshin and A. Lawal, *Chem. Eng. Sci.*, **2009**, *65*, 1028-1036.
8. M. Sankar, M. Morad, J. C. Pritchard, S. J. Freakley, Q. He, J. K. Edwards, S. Taylor, A. F. Carley, D. Knight, C. J. Kiely, and G.J. Hutchings, *ACS Nano*, **2012**, DOI: 10.1021/nn302299e
9. M. Piccinini, E. Ntanjua, J. K. Edwards, A. F. Carley, J. A. Moulijn and G. J. Hutchings, *Phys. Chem. Chem. Phys.*, **2010**, *10*, 2488-2492.
10. J. K. Edwards, A. Thomas, A. F. Carley, A. A. Herzing, C. J. Kiely and G. J. Hutchings, *Green Chem.*, **2008**, *10*, 388-394.
11. N. N. Edwin, M. Piccinini, J. C. A. Pritchard, J. K. Edwards, A. F. Carley, J. A. Moulijn and G. J. Hutchings, *ChemSusChem*, **2009**, *2*, 575-580.
12. N. N. Edwin, J. K. Edwards, A. F. Carley, J. A. Lopez-Sanchez, J. A. Moulijn, A. A. Herzing, C. J. Kiely and G. J. Hutchings, *Green Chem.*, **2008**, *10*, 1162-1169.

Chapter 5

Towards Identifying Active Gold Nano-clusters in FeO_x supported CO Oxidation Catalysts

5.1 - Introduction

In 1982, nearly 30 years ago, while studying transition metal composite oxides as catalysts for combustion reactions Masatake Haruta discovered that Au containing catalysts showed exceptional activity towards CO oxidation at sub-ambient temperatures.[1] Using the latest microscopy available at the time it was shown that the catalysts were in fact not composite oxides but highly dispersed Au species on the support material.[2] Since this discovery, CO oxidation has become possibly the most studied reaction in heterogeneous catalysis.

The preparation method of Au / FeO_x catalysts has been shown to drastically affect the CO oxidation activity.[3] Catalysts prepared by impregnation methods show very little activity whereas catalysts prepared by deposition precipitation and co-precipitation are much more active, with the preferred preparation method being co-precipitation.[3] The gold particle size distribution with different preparation methods is thought to be the reason for this, with impregnation

producing mostly large Au particles with few small species. In contrast, co-precipitation has been shown to produce particles ranging from 2-4 nm clusters down to isolated Au atoms, and it has been reported by many groups that activity is highly dependent on particle size.[4]

5.2 - Debate over the active site

A common theory in the literature regarding CO oxidation is that small Au nano particles are needed for high catalytic activity; however, there is still debate on what the optimum size of the Au nanoparticles should be. The debate was initiated by Bond and Thompson[5] who proposed a mechanism whereby Au atoms at the interface of the nanoparticle and the support are the active oxidation centres. This model predicted that the smaller the particles the higher proportion of atoms will be located at the periphery when compared to inactive Au in the bulk of the nanoparticle. Lopez *et al.*[4] collated published data regarding Au catalysts on a variety of supports, and this showed the general trend that activity increased with decreasing particle size. The authors concluded that the most important factor controlling activity is particle size and hence the number of periphery atoms, and that the nature of the support and support interaction played a smaller role. They observed that the optimum average particle size when available data was compared from the open literature was between 1-2 nm. However, there is a considerable error associated with trying to estimate particle sizes at the lower end of the scale, and the fact that the particle sizes used are only averaged particle size must not be ignored. Model studies by Goodman *et al.*[6] attempted to explain the role played by the periphery atoms by preparing model catalysts based on monolayers and bilayers of Au supported on a TiO_2 surface with the results shown in figure 5.1. They showed that the bilayer structures were much more active than the monolayer structures and that the active species in these model catalysts closely resemble the structures present in an active Au / TiO_2 catalyst.

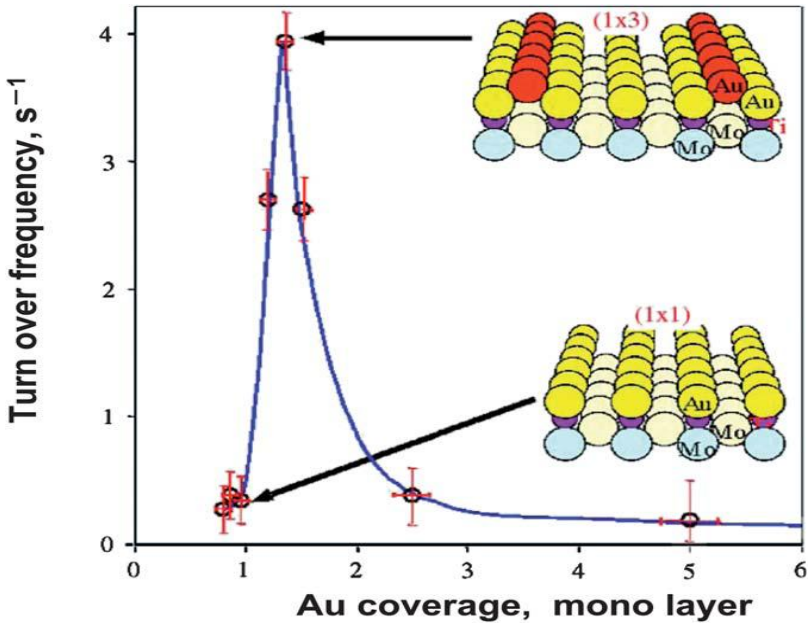

Figure 5.1 - CO oxidation turn-over frequencies (TOF) for different model Au structures, taken from the work of Goodman *et al.*[6]

Hutchings and co-workers reported a HAADF STEM study which undertook for the first time a statistical analysis of gold particle size and type, comparing an extremely active CO oxidation catalyst and an inactive CO oxidation catalyst at a range of calcination temperatures.[7] They classified Au species into 4 main groups: isolated atoms, monolayer structures, bilayer structures and species above 1 nm. They found that on heat treatment, the number of isolated atoms decreased, the number of monolayers remained relatively constant and the number of bilayers decreased, whereas the number of species above 1 nm increased. This suggested that the active catalysts contained a higher number of bilayers and fewer nanoparticles above 1 nm. They concluded that these bilayer structures consisting of ~8-10 Au atoms were the source of the high activity in the dried sample. These results agree well with the predictions of Goodman[6] and also with the observations of Arenz *et al.*[8] which show that a minimum of 8 atoms is needed to show catalytic activity, as 8 atom Au clusters can form stable surface structures. This work challenged the previous hypothesis that 2-5 nm particles were the active sites; however during this work the particle size distribution above 1 nm was not compared.

In a recent study by Schuth *et al.*[9] it was demonstrated that catalysts prepared by colloidal methods to have very tight particle size distributions could show high CO oxidation activity with no STEM evidence of small clusters below 1 nm. These data combined with the study of Hutchings[7] suggest that there may not be one active site for CO oxidation on Au nano particles and that in fact a large particle size range may be effective for the reaction; however different

particle morphologies may have vastly different activity. As there are a limited number of catalyst preparation methods that result in mono dispersed Au particles sizes, and due to equipment and time restraints, imaging the full range of particles is difficult. The full picture of the distribution of activity with Au particles size in real catalyst systems is thus hard to know. Catalytic activity results in the literature must be read with caution as they may represent a weighted average of activity due to different particle sizes and also average particle sizes may be quoted due to the large error in determining small particles below 1 nm with TEM imaging.

Another area of uncertainty in the Au / FeO_x system is the nature of the support. Many studies report that the nature of the support after a co-precipitation procedure is an amorphous iron oxyhydroxide phase.[10, 11] These catalysts on calcination at higher temperatures, up to 400 °C, become more crystalline and lose Au dispersion by sintering processes and also Au can be become trapped within the support as it crystallises. This results in lower catalytic activity the higher the heat treatment prior to testing. This is in contrast to Haruta who reports that preparation of the catalyst by a slightly different co-precipitation method results in a crystalline iron oxide catalyst, which becomes more active with calcination up to 300 °C and then rapidly loses activity.[1] This clear contrast in the support phase of the catalyst and behaviour on heat treatment between Au / FeO_x samples prepared by slightly different methods illustrates one of many properties regarding Au / FeO_x catalysts for CO oxidation that are yet to be fully understood, with a major challenge still being identification of the most likely active Au site.

5.3 - Aims of the study

The aim of this study is to carry out further investigation into the active site for CO oxidation using Au / FeO_x catalysts. This will involve undertaking kinetic studies of catalytic activity along with extensive characterisation using STEM in an attempt to determine complete particle size distributions ranging from 10 nm particles down to single atomic species for a number of catalysts. This investigation forms collaboration between three universities: Cardiff University, Tokyo Metropolitan University and Lehigh University. Cardiff University carried out catalyst preparations and testing of catalysts supplied by Tokyo Metropolitan University. Under the guidance of Prof. Haruta I was able to carry out kinetic investigations of the catalysts systems during a 1 month stay at Tokyo Metropolitan University. Prof. Kiely at Lehigh University carried out extensive STEM analysis of the catalysts to establish particle size distributions of the different Au species.

5.4 – Investigation of Catalysts Prepared in Cardiff

5.4.1 -Effect of Preparation Method on the Activity of CO Oxidation Catalysts

Based on the catalyst preparation method reported by Hutchings *et al.*[7] four catalyst samples of 5 wt% Au / FeO_x were prepared to investigate the effect of the preparation method on the catalytic activity and to further investigate structure property relationships of the materials. Catalysts were prepared by varying the order of addition of the acid and base and also the speed of addition, as previously outlined in chapter 2, with the results of CO conversion of the catalysts after drying at 110 °C for 16 h catalysts shown in table 5.1.

Catalyst Preparation Method	CO Conversion / %
Acid into base – slowly	66
Acid into base – quickly	51
Base into acid – slowly	99
Base into acid - quickly	85

Table 5.1- CO Conversion of 5% Au / FeO_x prepared by various methods after drying at 110 °C for 16 h. Testing conditions - 50 ml min^{-1} 0.5% CO / air, 10 mg catalyst, 25 ºC, GHSV = 300,000 h^{-1}.

The results show that the preparation method drastically affects the activity of the catalysts with the method previously employed in the study by Hutchings *et al.*[7] producing the most active catalyst. Both parameters investigated, the order of addition of acid and base and also the speed of addition, cause differences in activity of the catalysts. Catalysts that were prepared by adding base into acid were more active than catalysts prepared by adding acid into base and catalysts prepared by slow addition were more active than catalysts prepared by quick addition.

5.4.2 -Effect of Calcination Temperature on Activity of CO Oxidation Catalyst

The effect of calcination at various temperatures, ranging from 200 – 500 ºC, for 3 h were investigated for all of the preparation methods. The dependence of CO conversion on the calcination temperature for the catalysts prepared by adding base into acid is shown in figure 5.2.

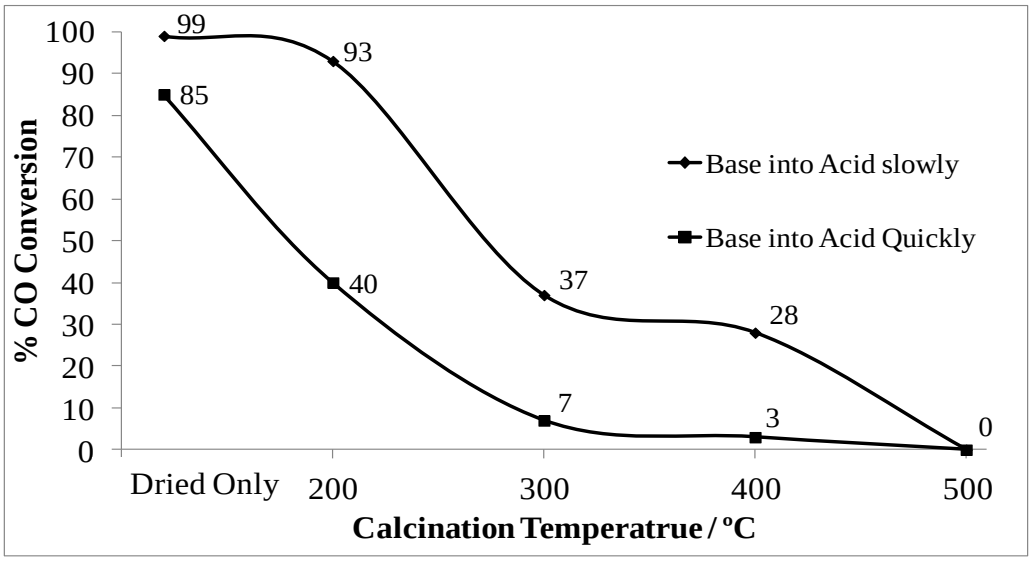

Figure 5.2 – Variation of CO Conversion of 5% Au / FeO_x prepared by two methods and after calcination at different temperatures. Testing conditions - 50 ml min^{-1} 0.5% CO / air, 10 mg catalyst, 25 ºC GHSV = 300,000 h^{-1}.

It was observed that the activity of both catalysts decreased as the calcination temperature increased, with the activity reducing more dramatically for the catalyst prepared by adding base into acid quickly when compared to the catalyst prepared by the slow addition of base into acid. After calcination at 500 ºC for 3 h both catalysts showed no activity towards CO oxidation irrespective of the preparation method. The catalysts prepared by adding acid into base showed lower activity than the catalysts prepared by adding base into acid but showed an identical trend with increasing calcination temperature.

5.4.3 - Catalyst Characterisation

5.4.3.1 - Surface Area Measurement

The surface area of the catalysts after various heat treatments were determined using nitrogen adsorption and the BET isotherm and the results are shown in table 5.2. The surface area analysis of the samples shows that the preparation method also affects the surface area of the material with base into acid preparation generating higher surface area materials than acid into base preparation. Quick addition of the reagents generates slightly higher surface area materials than the slow addition of the reagents. On calcination at increasing temperatures a dramatic loss in surface area was seen in the materials which could account for the loss in activity if the reduction in surface area either causes the encapsulation of Au during a change in the phase of support material or the promotion of Au sintering as the available surface area of the support reduces.

	Surface area / $m^2 g^{-1}$		
Preparation Method	**Dried only**	**300 ºC / 3 h**	**500 ºC / 3 h**
Acid into base – slowly	150	82	29
Acid into base – quickly	183	99	22
Base into acid – slowly	253	125	23
Base into acid - quickly	273	109	26

Table 5.2- BET surface areas of 5% Au / FeO_x prepared by various methods and after different calcination temperatures.

5.4.3.2 – X-ray Diffraction

The X-ray diffraction patterns for all of the dried catalysts are shown in figure 5.3. It was observed that the phase of the support material was dependent on the preparation method used. When catalysts were prepared by adding base in to acid either by fast or slow addition, an almost amorphous phase resulted which could be assigned to ferrihydrite ($Fe_2O_3.0.5H_2O$) which is shown in more detail later in figure 5.9. However when acid was added into base either slowly or quickly the resulting catalyst consists of a much more crystalline α-haematite phase, (α-Fe_2O_3).

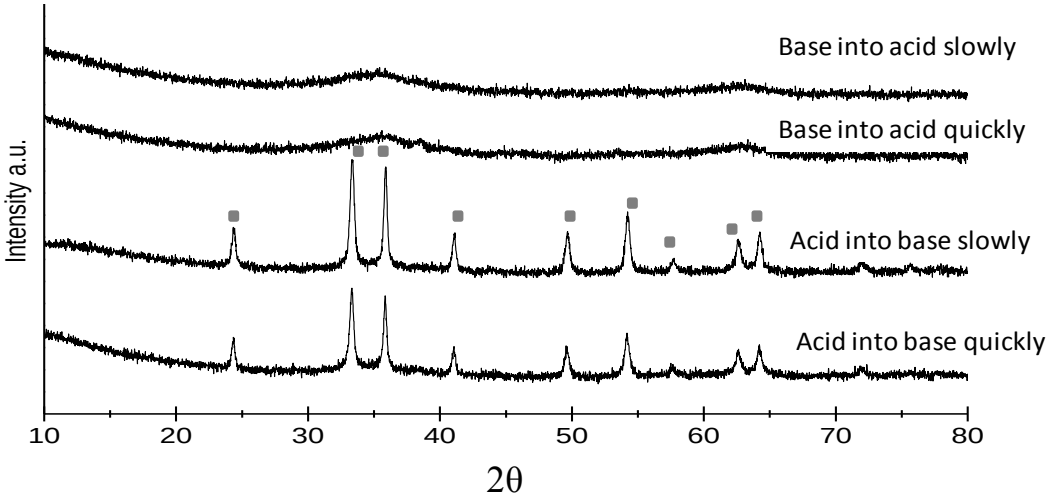

Figure 5.3 - XRD diffraction patterns of 5% Au / FeO_x prepared by various methods and after drying step of 100 ºC for 16 h. Haematite peaks are indicated by ■

The generation of a crystalline support from an acid into base method may arise from the $Fe(NO_3)_3$ being precipitated immediately on addition to a highly basic medium. The amorphous phase on the other hand will be precipitate gradually as the pH of the preparation is increased

from a starting value of ~0.8 up to 8.2 by addition of the base. From the surface area measurements it can be seen that the ferrihydrite phase generated by the base into acid preparation methods results in catalysts with higher surface areas than the acid into base methods which may be a reason for the higher activity seen towards CO oxidation if the Au can be more highly dispersed on this support material.

5.4.3.3 - X-ray Photoelectron Spectroscopy

XPS spectra of the catalysts after being calcined at a range of temperatures were carried out, and the spectra of the most active catalyst, base into acid slowly, are shown in figure 5.4.

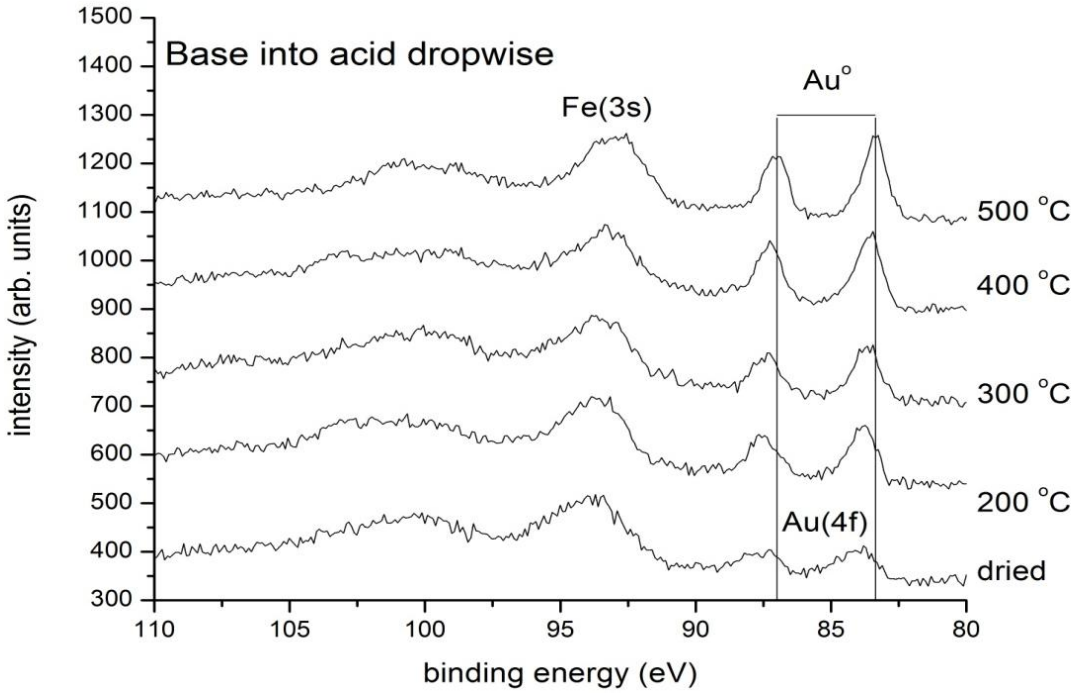

Figure 5.4 - XPS spectra of 5% Au / FeO_x prepared by a base into acid drop-wise (slow addition) method followed by drying and various calcinations.

The dried catalyst shows a similar trend to all of the other preparation methods in that the binding energy of Au is slightly shifted to higher binding energy than that expected for Au^0, suggesting that a small amount of the Au is present in an oxidic state. After heating above 300 ºC the binding energy matches more closely with the binding energies expected for metallic Au and these features are present in all of the catalysts characterised. In addition the intensity of the Au signal increases as the calcination temperature increases especially after 300 ºC, which indicates that there is an increase in surface Au concentration. This increase is highly unlikely to come from a re-dispersion of surface Au species as elevated temperatures aid Au mobility and will

cause small Au particles to sinter.[12] A more likely explanation is that subsurface Au can migrate to the surface at elevated temperatures; however, these elevated temperatures may also lead to sintering of the particles that were already on the surface leading to a lower catalyst activity.

5.5 - Effect of Support Morphology on CO Oxidation Activity

From the initial results obtained it was observed the preparation method used not only has a dramatic effect on catalytic activity but also on the nature of the iron oxide support. It was shown by XRD that the order of addition of the acid and the base determines the phase of the iron oxide support. The addition of acid into base gave rise to a crystalline haematite support material whereas the addition of base into acid gave a much more amorphous ferrihydrite support material. To investigate the effect of the nature of the support material on the catalytic activity of the samples, haematite and ferrihydrite were prepared as support materials by the appropriate preparation methods of varying the order of addition of acid and base. Onto these support materials Au was deposited by a deposition precipitation method described previously in Chapter 2. The XRD diffraction patterns of the catalysts shown in figure 5.5 confirm that samples of both haematite and ferrihydrite were prepared and that the catalysts show no reflections typical of Au, indicating that the Au deposited is in a highly dispersed state.

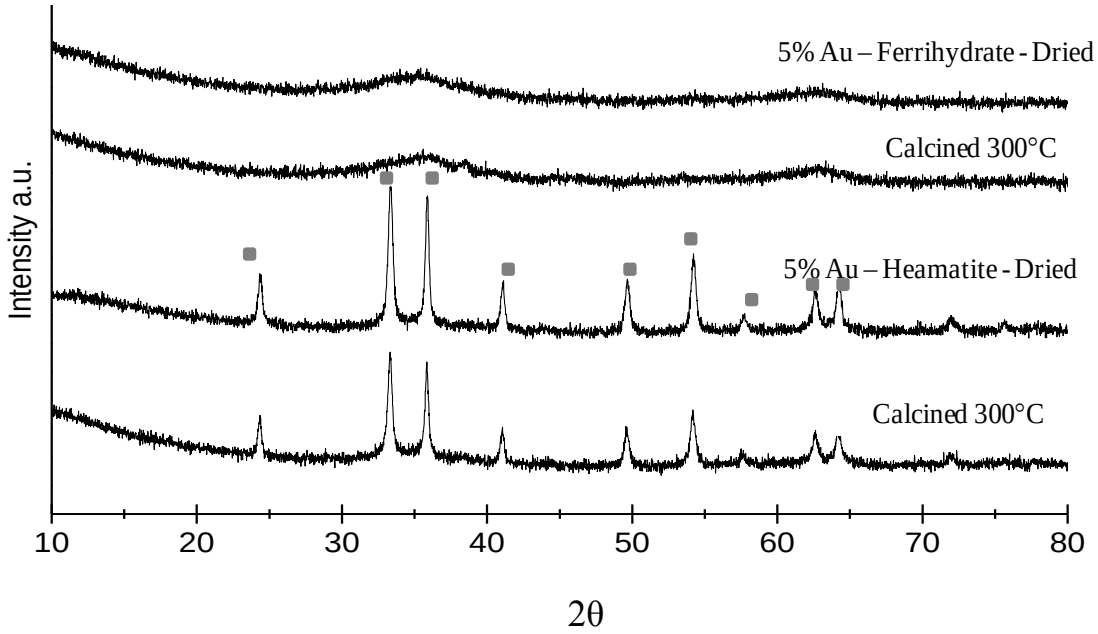

Figure 5.5 - XRD diffraction patterns of 5% Au / FeO_x prepared by a deposition precipitation method on two iron oxide supports, both dried and calcined at 300 ºC for 3 h.

The dried and calcined catalysts were tested for CO oxidation at 50 and 100 ml min^{-1} flow of 0.5% CO / air and the results are shown in table 5.3. The results show that the two catalysts have

almost identical activities at both flow rates used in these experiments. The catalysts show the same behaviour when dried or calcined which gives a strong indication that the nature of the iron oxide support is not crucial in determining the catalytic activity when prepared by deposition precipitation. Based on these results the various catalyst activities seen in the previous section with different preparation methods now seem to be more related to the nature of the Au species present rather than the support that is synthesised by the preparation conditions.

Catalyst	Dried 120 °C / 16 h		Calcined 300 °C / 3 h	
	50 ml min^{-1}	100 ml min^{-1}	50 ml min^{-1}	100 ml min^{-1}
5% Au / Haematite	99 %	92 %	75 %	49 %
5% Au / Ferrihydrite	99 %	89 %	74 %	47 %

Table 5.3 – CO Conversion for the 5% Au / FeO_x catalysts characterised in Figure 5.5. Testing conditions – various flows of 0.5% CO / air, 10 mg catalyst, 25 ºC GHSV = 300,000 – 600,000 h^{-1}.

5.6 – Comparison of Catalysts from Cardiff and Tokyo Metropolitan Universities

5.6.1 - Comparison of Preparation Methods between Tokyo Metropolitan University (TMU) and Cardiff University

It has been shown that the activity of Au / FeO_x towards CO oxidation is very sensitive to the preparation method employed especially when preparing catalysts by co-precipitation. The method previously reported by Hutchings *et al.*[7] was shown to produce highly active catalysts for CO oxidation and this has been confirmed in the initial work carried out in this study. However when this preparation method was compared with the optimum reported by Prof. Haruta[1] it was found to be very different. The most active catalyst prepared in Cardiff was prepared by adding base into acid slowly (drop-wise) and then drying the sample; the catalyst then lost activity on calcination in air at elevated temperatures. In contrast, Haruta *et al.* [1, 2] report that adding acid into base quickly is the best method with the catalyst becoming more active after calcination at 300 °C. A summary of the preparation conditions of the best catalysts is shown in table 5.4

	Cardiff	TMU
Preparation	Base into acid slowly	Acid into base quickly
Aging Time / Temp	1 h / 80 °C	1 h / 80 °C
pH	8.5	8.5
Washing	2 L hot water – Buckner funnel	Centrifuge with hot water
Most Active Catalyst	After drying 110 °C / 16 h	After calcination 300 °C / 3 h

Table 5.4 – Details of the preparation methods used by Cardiff University and Tokyo Metropolitan University.

The activity of catalysts prepared by these two methods, shown in table 5.5, show how sensitive the catalyst activity is to differing preparation methods, It was decided to use this set of catalysts, prepared in Cardiff and Tokyo Metropolitan University (TMU) both dried and calcined, to study the similarities and differences by detailed STEM and characterisation studies and to attempt to correlate them with the observed catalytic activities.

5.6.2 - Origins of Differences Between Cardiff and TMU Catalysts

Attempts were made to reproduce the TMU catalyst preparation in Cardiff. Although we managed to prepare a relatively active catalyst, in contrast to the TMU sample, it lost activity on calcination. To eliminate the chance that the difference was related to the different sources of the starting materials, an attempt was made in Tokyo to prepare a catalyst using starting materials taken from the supplies used in Cardiff. This resulted in a catalyst that matched the activity of the catalyst prepared in TMU, hence eliminating the starting materials as a possible source of difference in the catalyst preparation. A detailed procedure written by Prof. Haruta was followed in Cardiff, including the scale of the preparation and the concentration of starting solutions, and this resulted in a catalyst that was much less active than the catalyst prepared in TMU. The only difference in the preparations that could not be replicated between Cardiff and TMU is the washing of the catalyst sample. The washing by centrifuge in TMU is a much more thorough washing procedure than the Buckner funnel filtration used in Cardiff and it is speculated that this step is crucial in explaining the different behaviours of the two catalysts. Residual impurities such as Cl^- or Na can affect the behaviour of the catalyst particularly during calcinations where Cl^- is known so accelerate the sintering of Au particles[13, 14] which may explain the differences in activity after calcination of the two samples. Higher concentrations of Cl^- and Na were observed

by ICP in the Cardiff samples (Cardiff Catalysts – 412 ppm of Cl and 668 ppm of Na, Tokyo Catalyst 141 ppm Cl and 100 ppm Na)

5.6.3 - Testing of Cardiff and TMU Catalysts

Samples of both dried and calcined catalysts prepared in Cardiff and Tokyo were tested at both institutions under the testing regimes previously described in Chapter 2. The results of the testing in Cardiff are shown in table 5.5 where it can be seen that the dried catalysts show similar activity towards, however it is should be taken into account that at conversion above ~90 % mass transfer must be considered and it is not possible to confidently compare the performance of high activity catalysts, but after calcination the Cardiff catalysts loses activity whereas the TMU catalyst retains its observed activity. One way to avoid mass transfer is to operate in a conversion regime well below 100 % by manipulating reaction conditions such as catalyst mass and flow rate of reactant.

Catalyst	Dried 110 °C / 16 h	Calcined 300 °C / 3h
Au / FeO_x – Cardiff University	99 %	37 %
Au / FeO_x – Tokyo Metropolitan University	97 %	92 %

Table 5.5 - CO Conversion of 5% Au / FeO_x catalysts prepared by co-precipitation methods in Cardiff and Tokyo, both dried and calcined at 300 ºC for 3 h. Testing conditions – 50 ml min^{-1} 0.5% CO / air, 10 mg catalyst, 25 ºC, GHSV = 300,000 h^{-1}.

Experiments were carried out into the stability of the Cardiff and Tokyo catalysts over a reaction period of 5 hours, the results are shown in figure. A flow rate of 100 ml min^{-1} was used to limit the effects of mass transfer. Using this high gas flow rate all of the catalyst samples were shown to be stable over the reaction period. As previously seen the TMU catalyst is highly active and retains its activity after calcinations whereas the Cardiff catalysts loses a substantial amount of activity

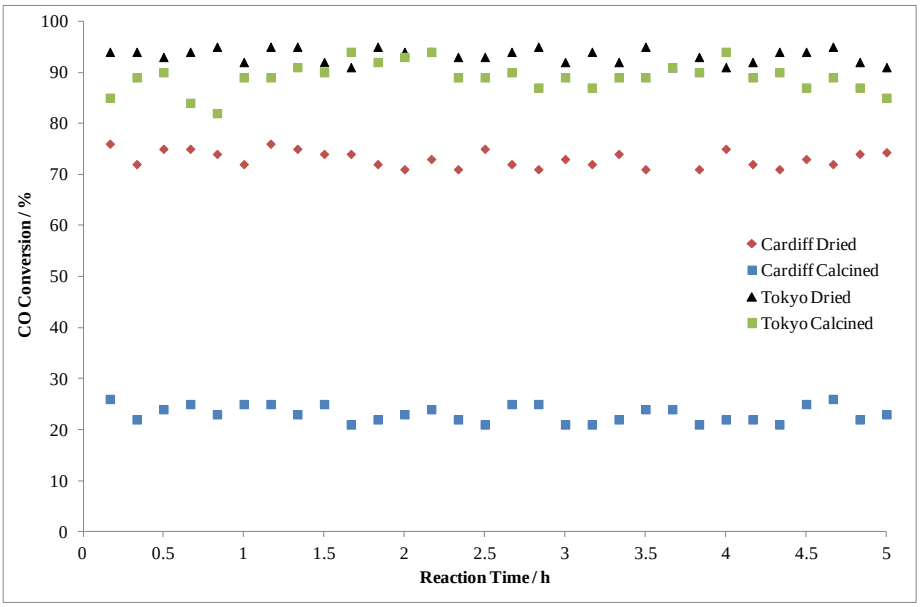

Figure 5.6 - CO Conversion of 5% Au / FeO_x catalysts prepared by co-precipitation methods in Cardiff and Tokyo, both dried and calcined at 300 ºC for 3 h. Testing conditions – 100 ml min^{-1} of 0.5 % CO / air, 10 mg catalyst, various temperatures. GHSV = 600,000 h^{-1}

Testing the catalysts at TMU allows for much more flexible experiments where parameters such as temperature and concentration of reactants can be varied over a much greater range. Experiments were carried out with the dried and calcined catalysts over a large temperature range while keeping the reactant concentration constant; the results are shown in figure 5.7. The testing results from TMU confirm the results for the dried catalysts seen in Cardiff in that the catalysts showing the same activity at ambient temperature with the temperature for 50% conversion being 10 °C. The results also show that the dried catalysts exhibit the same activity over the whole temperature range investigated, down to -60 °C, and reach 100 % conversion at around 25 °C in agreement with the Cardiff tests. The activity of the calcined catalysts at ambient temperature also confirms the observations made in Cardiff that the TMU calcined sample has high activity whereas the Cardiff samples loses a substantial amount of activity. Interestingly, while the Cardiff samples becomes less active over the whole temperature range (temperature of 50 % conversion = 55 °C) the TMU sample becomes more active (temperature of 50% conversion = -40 °C) at sub ambient temperature, a feature that was unable to be tested in Cardiff where it appeared that the activity was retained on calcination and not increased with calcination. These results indicate that the heat treatment causes an evolution in either the

support material or the Au distribution that produces more highly active sites in the TMU catalyst which are capable of catalysing CO oxidation at sub-ambient temperatures

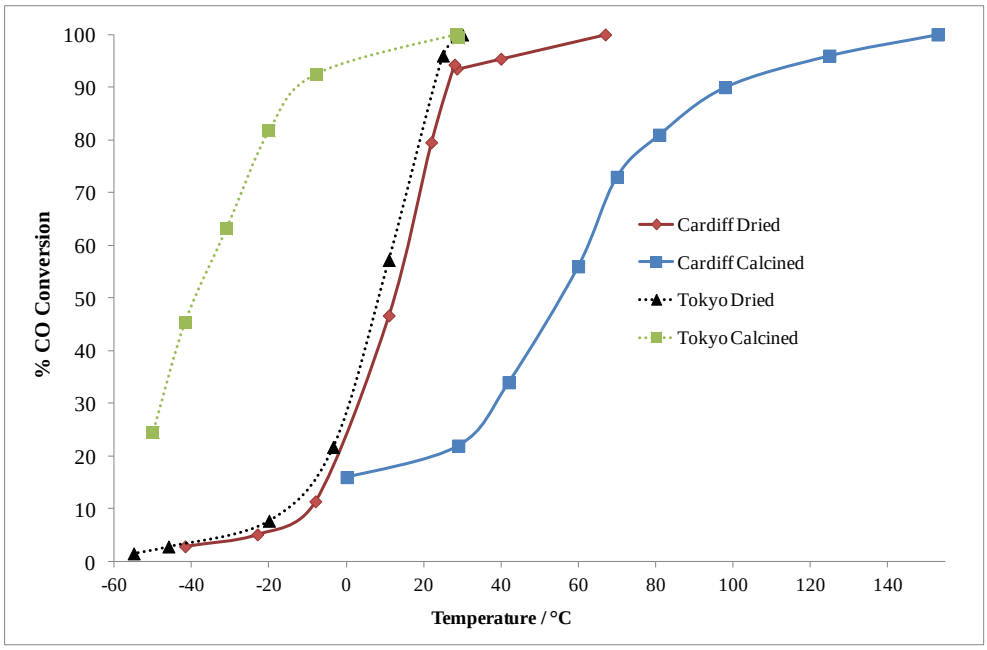

Figure 5.7 - CO Conversion of 5% Au / FeO_x catalysts prepared by co-precipitation methods in Cardiff and Tokyo, both dried and calcined at 300 ºC for 3 h. Testing conditions – 50 ml min^{-1} of 1 % CO / air, 50 mg catalyst, various temperatures. GHSV = 60,000 h^{-1}

5.6.4 - Kinetic Analysis of Cardiff and TMU Catalysts

To investigate the kinetics of the reaction over the different catalysts and determine the activation energy of the reaction, studies were made using the testing equipment at TMU. To allow the determination of kinetic parameters and accurate determination of the activation energy the reactor was modelled as a differential plug flow reactor and the following experimental conditions were used;

1. Small catalyst amounts – to allow the assumption that the reaction rate is constant throughout the bed.
2. Slow reactions – low conversion was achieved by high flow rates which allows the assumption that there are no concentration gradients through the catalyst bed.

By modelling the reactor as a differential reactor it is possible to determine the reaction rate by using equation 5.1

$$\text{Reaction rate} = \frac{\text{CO Flow rate x Conversion}}{\text{Catalyst Bed Volume}} \quad (5.1)$$

Following the determination of the reaction rate the rate constant can be determined and an Arrhenius plot can be constructed by measuring the rate constant at various temperatures and using the Arrhenius equation shown as equation 5.2 to plot ln k *vs* 1/T.

$$k = Ae^{\frac{-E_a}{RT}} \quad (5.2)$$

5.6.5 - Arrhenius Plots

The Arrhenius plot constructed to compare the two dried catalysts sample is shown in figure 5.8. As seen in the experiments previously carried out, the two dried samples show very similar activity although differing behaviour was seen as the temperature was increased. Below 60 °C both catalysts show very similar activity with activation energies of 30 kJ mol^{-1} being measured for the Cardiff sample and 27 kJ mol^{-1} for the TMU sample; above 60 °C differing behaviour was seen. No change in activation energy was seen in the TMU sample, with an activation energy of 27 kJ mol^{-1} being measured over the whole temperature range, whereas the Cardiff dried sample shows a change in activation energy at around 60 °C, from 30 to 15 kJ mol^{-1} which indicates a change in reaction mechanism as the reaction passes through this temperature; a similar feature has been reported for Au / TiO_2 catalysts.[15]

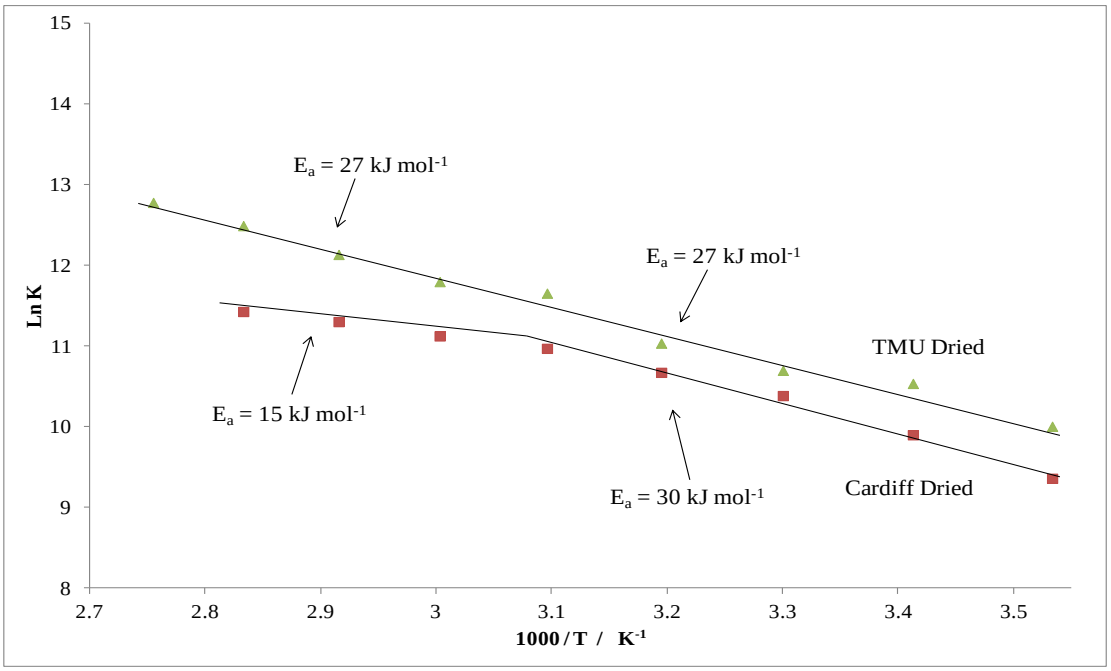

Figure 5.8 – Arrhenius plot of 5% Au / FeO_x catalysts prepared by co-precipitation in Cardiff and Tokyo and dried for 16 h at 110 ºC. Temperature range of Arrhenius plots 10 – 120 ºC.

Arrhenius plots were also constructed for the two calcined samples over the same temperature range as the dried samples and are shown in figure 5.9. The calcined samples behave similarly below 60 °C and exhibit apparent activation energy of around 30 kJ mol^{-1}, similar to the dried catalysts. Above 60 °C an interesting change in behaviour was observed, both calcined samples underwent a change in activation energy but unlike the Cardiff dried sample which showed a decrease in activation energy the calcined samples showed an increase in activation energy. Above 60 °C the rate of reaction increased dramatically with a high activation energy observed of 95 kJ mol^{-1} for the TMU catalyst and 120 kJ mol^{-1} for the Cardiff calcined sample.

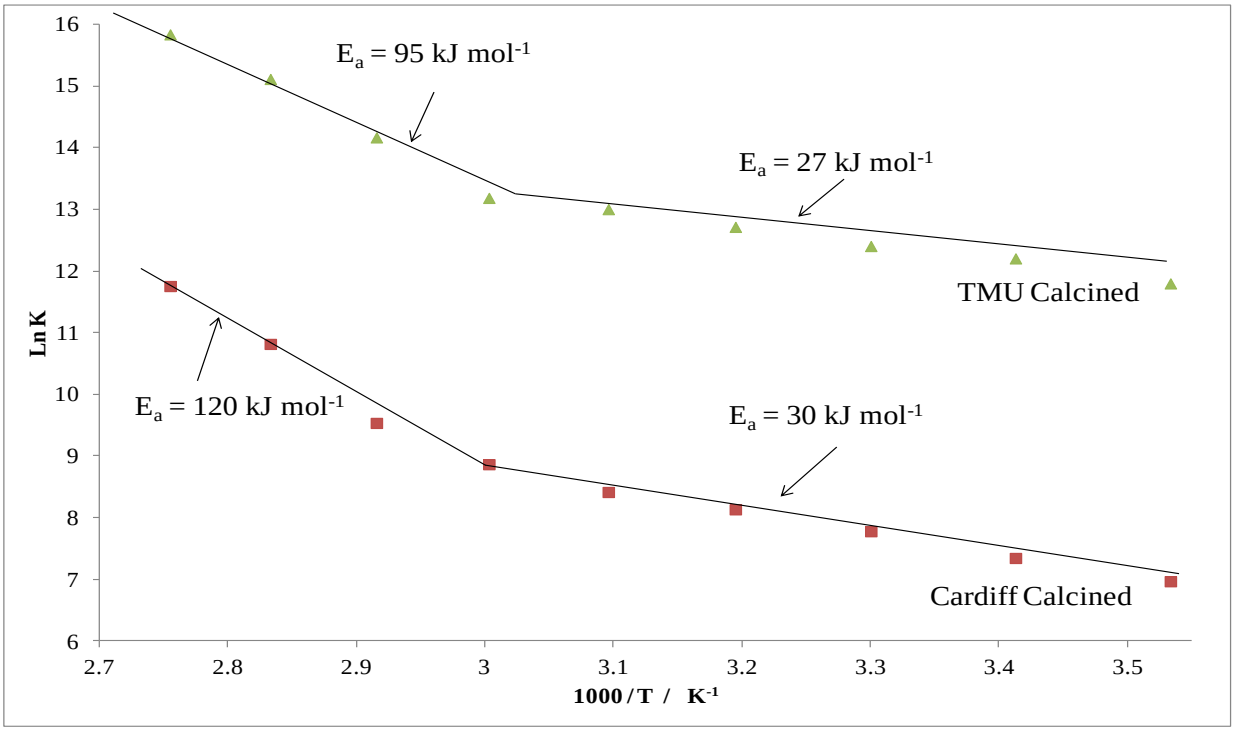

Figure 5.9 - Arrhenius plot of 5% Au / FeO_x catalysts prepared by co-precipitation methods in Cardiff and Tokyo and calcined for 3 h at 300 ºC. Temperature range of Arrhenius plots 10 – 120 ºC.

These activation energies are very large compared to the activation energies reported in the literature for Au / TiO_2 systems above 60 °C [15] and resemble more the activation energies of model Pt group metal catalysts. No previous literature measurements of Au / FeO_x catalysts could be found above 60 °C. This increase in activation energy may be the result of a different active species taking part in the reaction when the temperature is above 60 °C this active site may have a larger barrier to reaction which could come from either less favourable adsorption of the reactants or through its ability to activate the reactants to allow a reaction. The potential for

more than one active species should not be ignored and it should be remembered that the activation energies observed are only empirical activation energies and are a weighted average of the activation energies of all the active species present. This may be the origin of the difference between the values of 95 and 120 kJ mol^{-1}, indicating the TMU calcined sample may contain more species with lower activation energy than the Cardiff calcined sample.

5.6.6 - CO and O_2 Reaction Orders at Various Temperatures

Experiments were carried out at 25 ºC and 70 ºC to determine the order of reaction with respect to O_2 and CO above and below the observed change in activation energy. Experiments were conducted over a large range of reactant concentrations (O_2 5 – 20 vol% and CO 1 – 10 %) by varying one reactant concentration while holding the other constant while measuring the reaction rate. All of the catalysts showed a first order dependence on the concentration of CO both above and below 60 °C at all reactant concentrations. Between 1 – 10 vol % the reaction rate had a first order dependence with respect to O_2 which then became independent of O_2 concentration between 10 and 20 vol %, with the exception of the Cardiff dried catalysts which remained first order up to 20 vol % O_2. The reaction orders at concentrations used in the Arrhenius plots, 20 vol % O_2 and 1 % CO, are summarised below in table 5.6.

Catalyst	**Reaction Order Below 60 °C**		**Activation Energy /** kJ mol^{-1}	**Reaction Order Above 60 °C**		**Activation Energy /** kJ mol^{-1}
	CO	O_2		CO	O_2	
Cardiff Dried	1	0	30	1	1	15
Cardiff Calcined	1	0	30	1	0	120
TMU Dried	1	0	27	1	0	27
TMU Calcined	1	0	27	1	0	95

Table 5.6 – Table summarising the experimentally measured reaction orders with constant catalyst mass, 10 mg, and various concentrations of CO (1 – 10%) and O_2 (1 – 10%) with a constant gas flow of 50 ml min^{-1}.

Below 60 °C all of the catalysts have the same order of reaction with respect to O_2 and CO. This indicates that below 60 °C the rate determining step of the reaction involves a CO molecule

possibly indicating that the adsorption of CO is rate determining as the reaction rate increases with the concentrating of CO. The zero order dependence on O_2 indicates that the slowest step of the mechanism does not involve O_2, indicating that the catalyst has a high concentration of activated O_2 which can react with small activation barrier. Above 60 °C the Cardiff dried catalyst shows a dependence on the concentration of O_2 which indicates that the rate determining step of the mechanism on this catalyst now involves a molecule of both CO and O_2; however the barrier to reaction has reduced. The TMU dried catalyst showed no change in reaction order or activation energy above or below 60 °C indicating that the mechanism is likely to be the same for this catalyst at high and low temperatures.

The calcined samples show the same dependence on CO and O_2 above and below 60 °C, indicating that the rate determining step of the mechanism still involves a CO molecule again possibly involving the adsorption of CO onto the active site of the catalyst. However the observed activation energy increased dramatically above 60 °C, which could indicate that above 60 °C a different active site is able to carry out the reaction either instead of or along with the sites that are already active below 60 °C. The high activation energy indicates that the barrier to reaction is much higher on this site, which could indicate that the adsorption of the reactants is not as favourable but the energy imparted into the system by heating allows the reaction to proceed on this site above 60 °C.

This feature has been previously observed by Haruta for Au / TiO_2[15, 16] where a change in activation energy was observed as the reaction temperature was increased above 60 °C. However, in contrast to the TiO_2 system, where the activation energy reduced to 2-3 kJ mol^{-1}, an increase in activation energy in the calcined FeO_x supported catalyst was observed. The change in mechanism at this temperature is thought to correspond to a change in active site. Below 60 °C in the study by Haruta[15] a correlation with the number of periphery atoms is seen and water is essential to achieve high reaction rates. Above 60 °C no correlation was observed and the reaction became independent of moisture concentration, and it is postulated that the reaction happens completely on the surface of the Au particles above this temperature. The high activation energy for this process on FeO_x catalysts could possibly be a result of different particle morphologies or support particle interactions increasing the barrier to reaction when compared to the Au / TiO_2 system.

5.6.7 - Characterisation of Cardiff and TMU Catalysts

5.6.7.1 - X-Ray Diffraction of Cardiff and TMU Catalysts

Samples of the Cardiff and TMU catalysts were characterised by XRD to determine the bulk structure of the iron oxide support material; the diffraction patterns of the dried and calcined samples are shown in figure 5.10. The diffraction patterns show that the phase of the support materials of the two catalysts is different, with the dried Cardiff sample appearing to be much more amorphous than the TMU sample. The Cardiff sample appears to be mainly ferrihydrite ($Fe_2O_3.0.5H_2O$), which is generated by the base into acid preparation method as previously shown in section 5.4.3.2, whereas the TMU sample was shown to be haematite which is the iron oxide phase generated by the acid into base methodology. On calcination the TMU sample becomes much more crystalline, as indicated by the more intense reflections detected, whereas the Cardiff sample, while still showing ferrihydrite reflections also begins to show weak haematite reflections at 24°. No Au reflections were observed in any of the XRD patterns, suggesting that the Au is highly dispersed in both the dried and calcined catalysts. The same features of haematite and ferrihydrite were also seen using electron diffraction carried out during the STEM analysis which is reported later in this chapter.

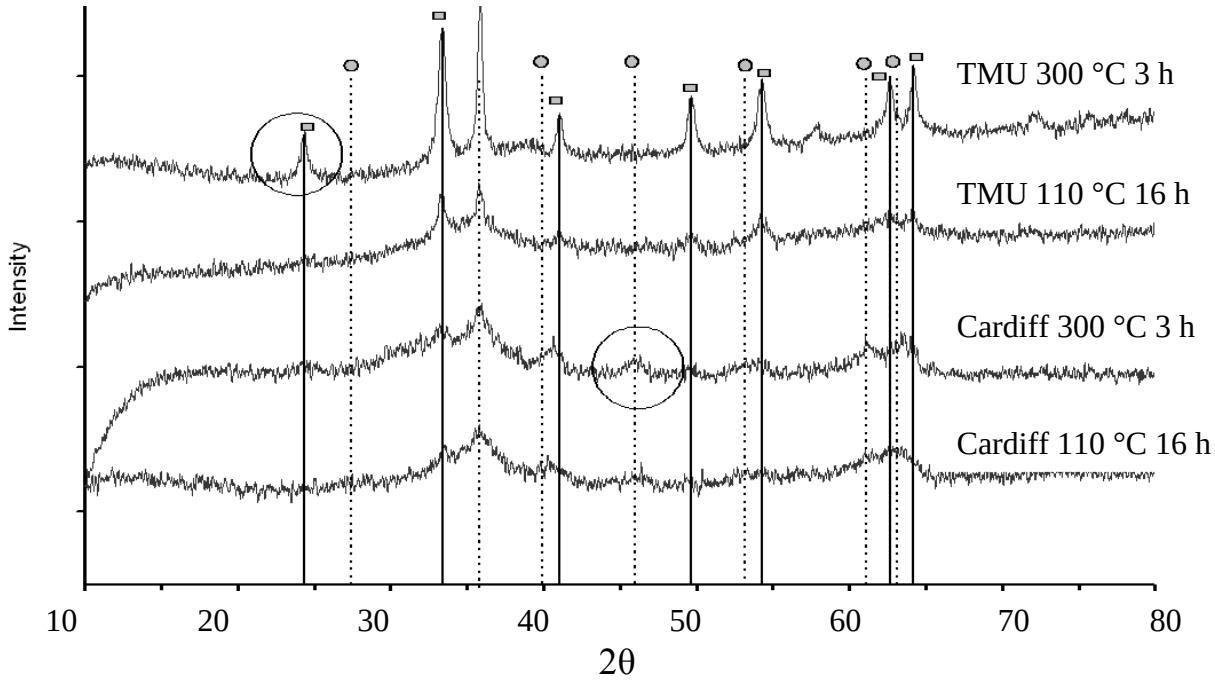

Figure 5.10 – X-ray diffraction patterns of dried and calcined catalysts prepared by co-precipitation in both Cardiff University and Tokyo University, after drying and calcination at 300 °C for 3h. Haematite peaks are indicated by ■ and ferrihydrite peaks by ●.

To monitor the evolution of the support phase through the calcination procedure, *in-situ* XRD was carried out on the samples. A heating program was carried out to mimic the calcination procedure: the sample was heated from room temperature to 300 °C at a ramp rate of 20 °C min^{-1}, and when the sample reached 300 °C it was held there for 5 h to investigate the evolution of the material. It was then heated up to 600 °C at the same ramp rate, 20 °C min^{-1}, XRD patterns being recorded between 20 -55° using a 10 min scan time. The *in-situ* XRD of the Cardiff sample is shown in figures 5.11a and 5.11b.

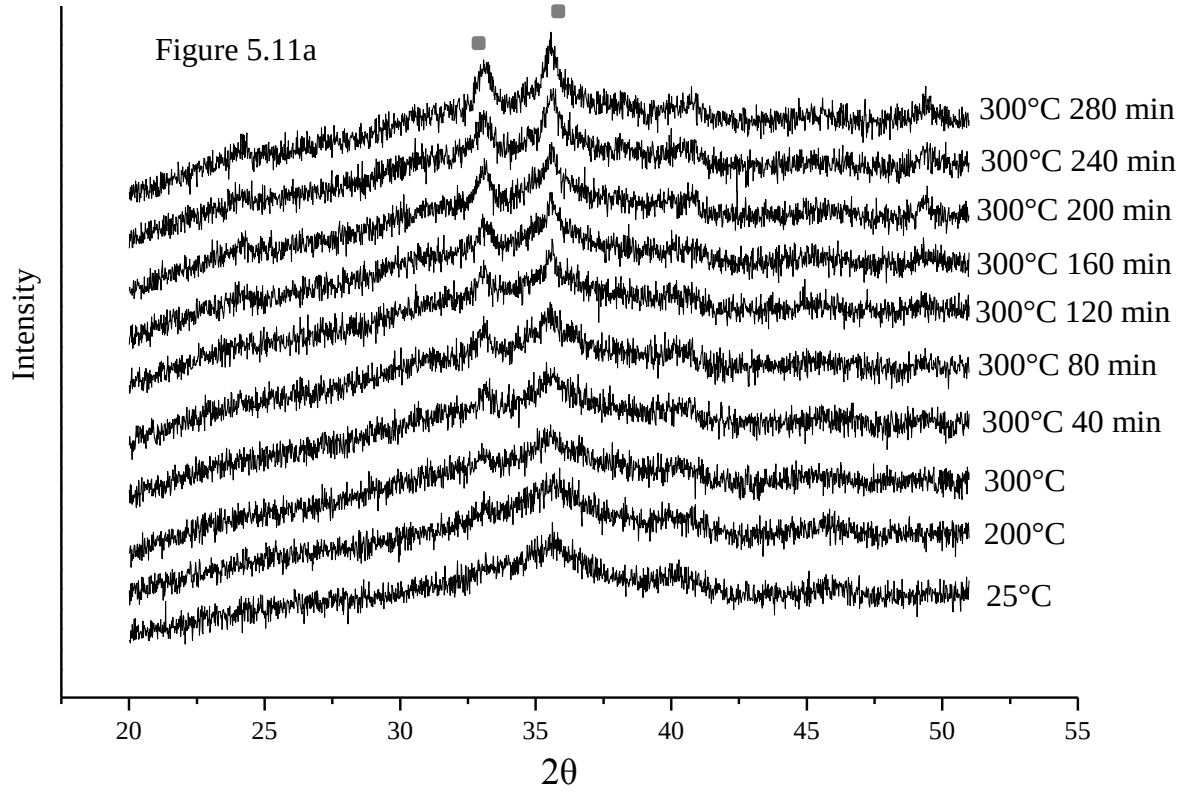

Figure 5.11 - a) *In-situ* XRD patterns of Cardiff dried catalyst during heating to 300 °C and holding at 300°C for 5 h. Haematite peaks are indicated by ■

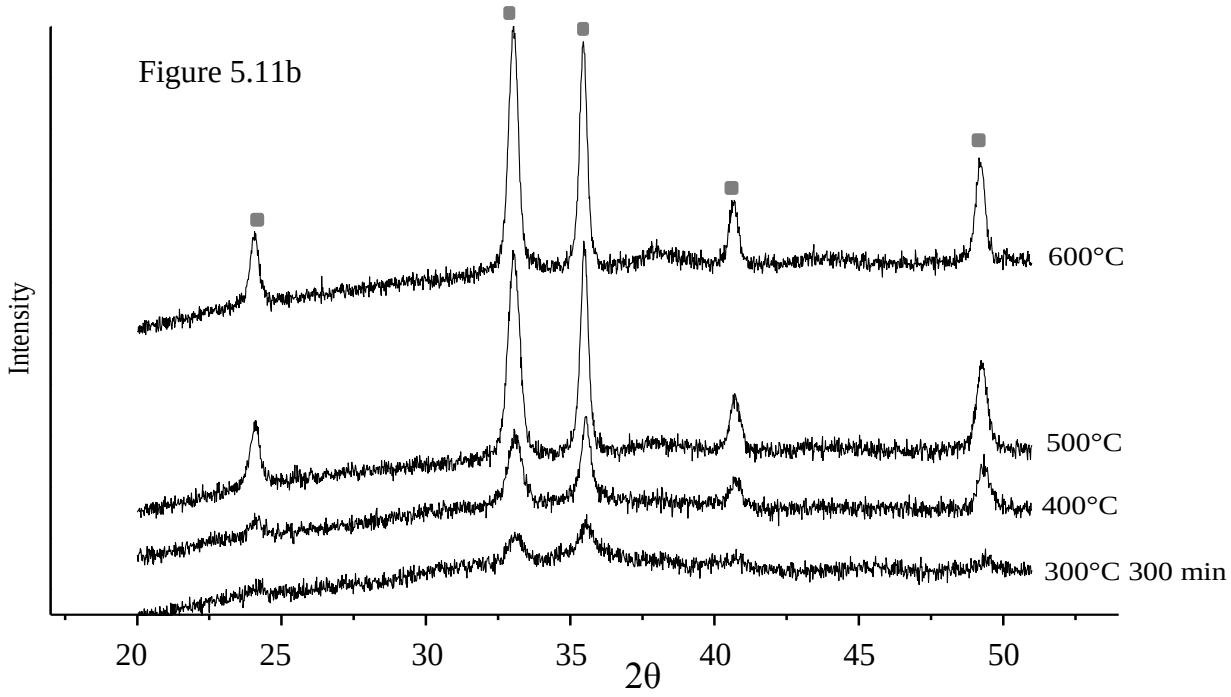

Figure 5.11 - b) XRD patterns of Cardiff dried catalyst during heating from 300 - 600 °C. Haematite peaks are indicated by ■

The Cardiff catalyst is very poorly crystalline initially and remains poorly crystalline after heating up to 200 °C. The catalyst was held at 300 °C for 5 h and haematite reflections can be seen towards the end of this heat treatment, but they remain broad and not well defined during the first 3 h, as was seen for the calcined catalyst. After 5 h at 300 °C the hematite reflections can be seen but they are broad and have low intensity. When the temperature is increased further to 400 °C the emerging haematite reflections become much more defined and intense and this trend continues after heating to 500 and 600 °C, with a faint gold reflection present at 38° after treatment at this high temperature, indicating the sintering of the Au particles.

In contrast the TMU sample shows different behavior and is shown in figures 5.12a and 5.12b. The haematite reflections already present in the dried sample begin to become more defined and more intense even after heating at 200 °C. The phase appears to become more crystalline throughout the 300 °C hold and during heating in the temperature range 400 - 600 °C.

It is clear that the ferrihydrite phase of the Cardiff catalyst cannot be transformed to the haematite phase under the heat treatments used in the preparation by the Cardiff route - even with extended heat treatments at 300 °C only weak haematite reflections can be seen after 5 h. The catalyst prepared by the TMU method shows a dominant haematite phase in the dried sample and begins to become more crystalline from 200 °C as the temperature is increased. The

results of the *in-situ* experiments confirm that the phase of the support is not a result of possible differences in the heat treatments carried out in Cardiff and Tokyo Metropolitan Universities but from differences in the preparation methods, in particular the order of addition of the acid and base.

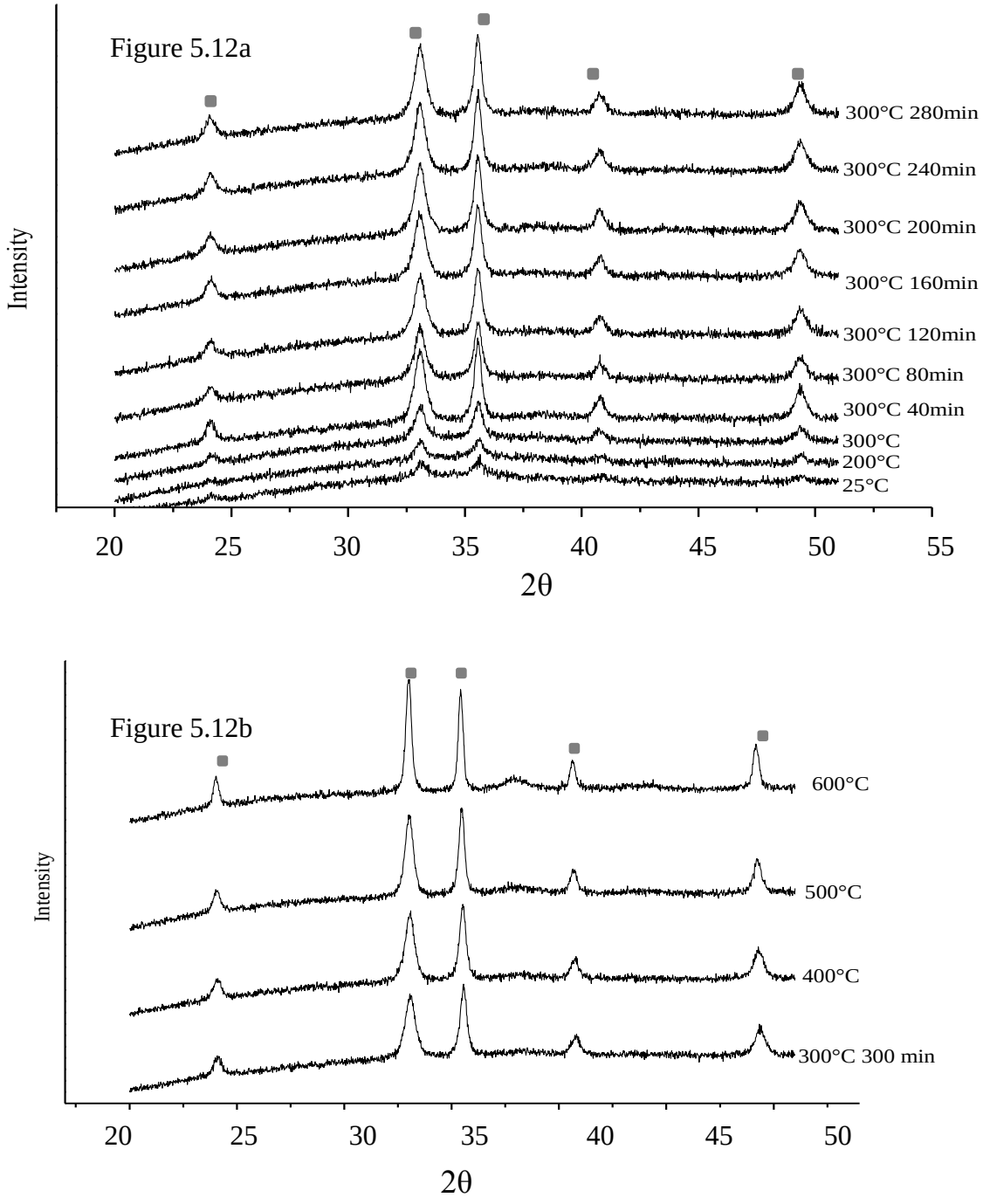

Figure 5.12 - a) *In-situ* XRD patterns of TMU dried catalyst during heating to 300 °C and holding at 300 °C for 5 h b) XRD patterns of TMU dried catalyst during heating from 300 - 600 °C. Haematite peaks are indicated by ■

5.6.7.2 - BET Surface Area of Cardiff and TMU Catalysts

The surface area of the catalysts after various heat treatments was determined using nitrogen adsorption and the BET isotherm and the results are shown in table 5.7. The BET analysis of the samples shows that they have very similar surface areas both after drying and after calcination at 300 °C for 3h, indicating that a large difference in surface area is not the origin of the difference in activity between the two catalysts.

	Surface area / $m^2 g^{-1}$	
Preparation Method	**Dried only**	**300 ºC / 3 h**
Cardiff – Base into acid slowly	253	125
TMU – Acid into base quickly	255	138

Table 5.7 - BET surface areas of 5% Au / FeO_x catalysts prepared by Cardiff and TMU methods after drying and calcination at 300 °C for 3 h.

5.6.7.3 - ICP Analysis of Cardiff and TMU Catalysts

To determine the total Au loading of the two catalysts ICP analysis was carried out on the calcined samples (it was assumed that the dried samples have the same Au content as the calcined samples), and the results are shown in table 5.8.

Preparation Method	**wt % Au**
Cardiff – Base into acid slowly	3.5
TMU – Acid into base quickly	6.0

Table 5.8 – Au content determined by ICP of 5% Au / FeO_x calcined catalysts prepared by Cardiff and TMU methods.

The Cardiff sample was shown to contain only 3.5 wt % Au in total, meaning a loss of 1.5 wt% Au during the catalyst preparation which is typical of precipitation methods. Surprisingly the catalyst supplied by TMU contained 6 wt % Au, which indicates that the preparation method employed in TMU is much more effective in preserving Au content in the catalyst. The higher

weight loading of the TMU catalyst could also be caused by incomplete precipitation of the iron nitrate used in the preparation when a predetermined amount of base is used to precipitate the catalyst.

5.6.7.4 - XPS of Cardiff and TMU Catalysts

XPS of the Cardiff and TMU dried and calcined catalyst was carried out and the spectra are shown below in figure 5.13.

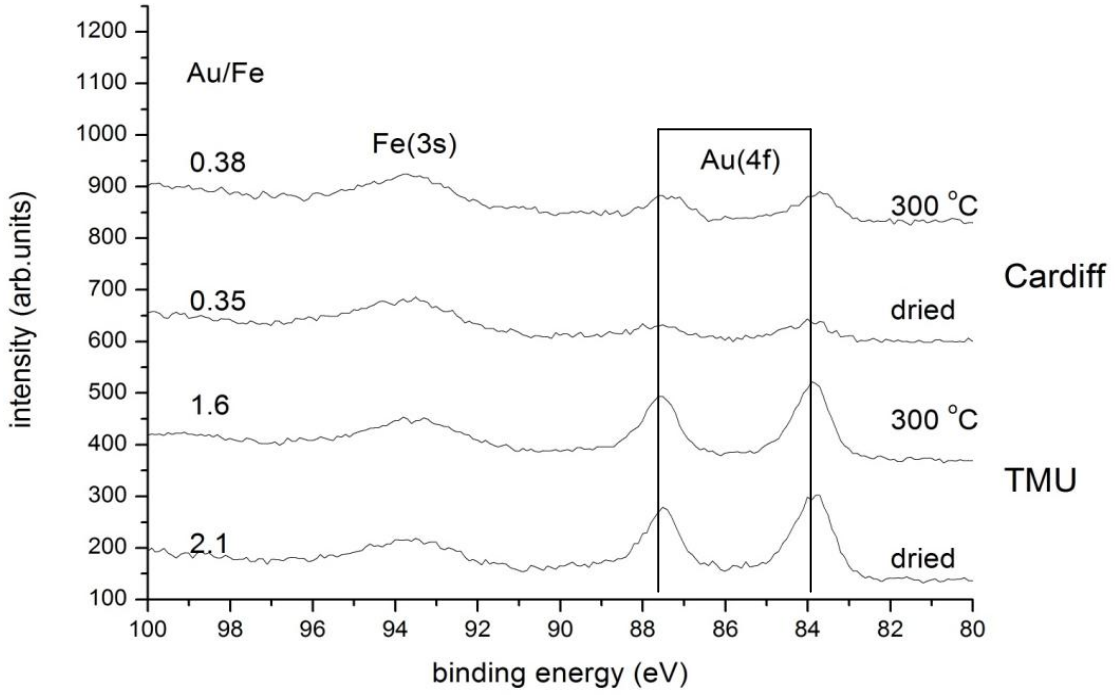

Figure 5.13 – Au (4f) XPS spectra of 5% Au / FeO_x catalysts prepared by Cardiff and TMU methods after drying and calcination at 300 °C for 3 h.

The XPS data clearly confirms that the TMU sample contains a higher Au atomic % at the surface than the Cardiff catalysts. The surface Au : Fe ratio of the TMU catalysts is *c.a.* four times higher than the Cardiff catalyst although from this data alone it is not possible to determine the number of Au sites present on the surface of the catalyst. As XPS has a sampling depth of 5 - 10 nm the TMU catalyst may have many more sub surface Au species than the Cardiff catalyst which would give rise to a stronger Au signal when in fact the number of surface Au sites, which are able to carry out catalysis, may be responsible for the differences in activity. Comparing the Au : Fe ratio of the TMU calcined catalyst and dried catalysts the calcined catalyst has less surface Au detected by XPS, which could indicate sintering of the Au particles to sizes larger than the sampling depth of XPS meaning a loss of signal from the centre of these particles. The

identical binding energies of the Cardiff and TMU samples indicate that, as far as can be detected by XPS, the Au present is the same in both catalysts with a slight shift to higher binding energy indicating a small amount of oxidic Au.

5.7 - Detailed STEM Analysis of Cardiff and TMU Catalysts

5.7.1 - Particle Size Distributions

A detailed STEM analysis of the Cardiff and TMU samples was carried out at Lehigh University, under the supervision of Prof. Kiely. For each sample 50 low magnification images and 100 high magnification images were taken which allowed all particles sizes to be observed from "large" 10 nm Au nanoparticles to atomic Au species. Representative high and low magnification images are shown in figure 5.14.

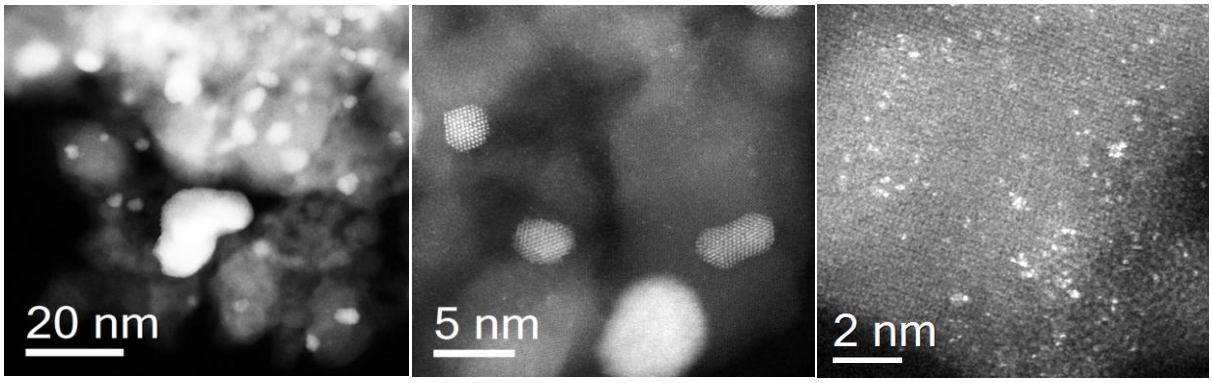

Figure 5.14 – Representative high and low magnification STEM images used to determine populations of nanoparticles, sub nanometer clusters and atomic Au species.

From the collection of images 2000 large particles and 3000 small particles were counted to generate the particle size distributions. An artificial cut-off value of 1.15 nm was used to avoid any particles being counted twice. Particles larger than this cut-off value were counted using the low magnification images and particles smaller than this value were counted in the high magnification images. A number of methods were considered to represent the absolute number of Au sites in the catalyst materials and each method needs a number of assumptions to be made which are summarised in table 5.9

Particle Size Distribution Method	Assumptions Made	Suitability
Compare Number Fraction	Catalysts have similar amounts of particles	Not suitable for large particle size variation seen in these samples
Compare Number Density	Catalysts have the same/similar projected area	Suitable for the current case because larger particles can simply be excluded
Compare the Mass Fraction	Catalysts have known Au loading	Including large particles can result in large errors

Table 5.9 - Table to summarise possible methods to determine the particle size distributions of the catalysts by STEM.

Simply comparing the number fraction of species is not suitable for this case as the catalysts are known from ICP to contain different amounts of Au. As the catalysts have been shown to have similar surface areas, calculating the number density of Au species is a more suitable approximation of the particle size distribution. Using this method it is possible to generate a particle size distribution where large catalytically inactive particles, > 20 nm, can be ignored to avoid large errors in the data. From this distribution the mass fraction of each species can be generated without the inclusion of large Au particles. The number density particle distribution is shown in figure 5.15.

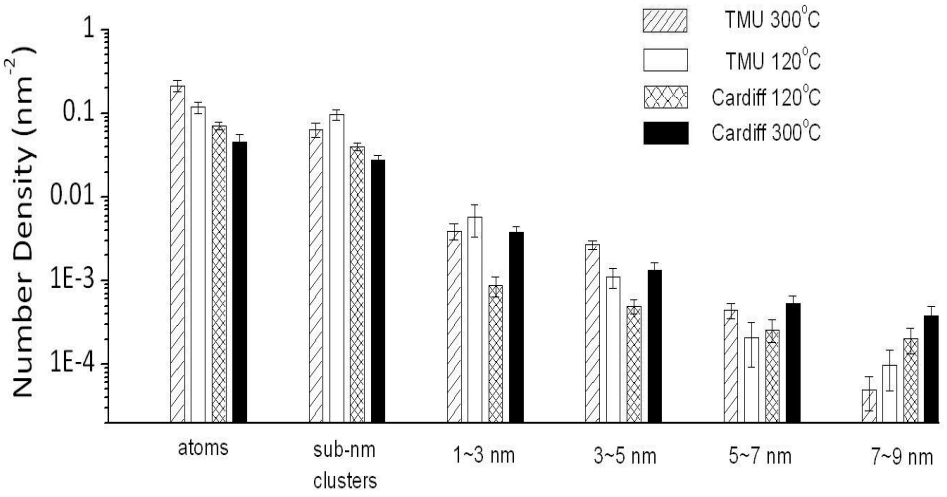

Figure 5.15 - Number density of Au species determined by STEM for catalysts prepared by Cardiff and TMU methods and after drying and calcination at 300 °C for 3 h.

Based on inspection of the kinetic measurements previously carried out in this investigation two distinct behaviours were observed for the catalysts. This may be because there are multiple active species with different specific activity at certain temperatures; the overall CO oxidation activity will therefore be a convolution of an activity distribution with the particle size distribution.

All catalysts behaved similarly at low temperatures; below 60 °C the activation energy of the reaction was measured to be around 30 kJ mol^{-1} whereas above 60 °C the calcined samples showed increased activation energy of 95 – 120 kJ mol^{-1}. Using the particle size distributions we can aim to identify two active species, one of which is active at low temperatures with an activation energy of 30 kJ mol^{-1} whose population should follow the activity of the catalysts at low temperature, TMU calcined > TMU dried > Cardiff dried > Cardiff calcined. The other is active at temperatures above 60 ^{o}C with an activation energy around 100 kJ mol^{-1} whose population should follow TMU calcined > Cardiff calcined > Cardiff dried ~ TMU dried.

From inspection of the population density of the Au species on the most active catalyst, TMU calcined, there is not one particle size that dominates the distribution that is obviously responsible for the activity of the catalyst when compared to the other catalysts. To correlate the kinetic observations to the particle size distribution for the behavior above 60 °C the particle density distribution at particle size of around 5 nm follows the expected trend for this behaviour (TMU calcined > Cardiff calcined > Cardiff dried ~ TMU calcined). This may indicate the

nanoparticles around 5 nm are responsible for the behaviour seen above 60 °C; a higher population of nanoparticles would be expected in the calcined samples because of sintering of small Au particles into larger nanoparticles.

The particle size distribution suggests that 1-5 nm Au particles cannot be the dominant species for low temperature CO oxidation as the Cardiff calcined sample would be more active than the Cardiff dried only sample. At high temperatures the behaviour of the calcined catalysts can be correlated to the populations of particles around 5 nm. It was observed that the TMU catalysts always have more sub nm clusters than the Cardiff samples; however it is not possible to correlate the activity with the populations of these particles as it is possible that these species could be located beneath the surface of the catalyst. The observation that catalysts prepared by deposition precipitation, which is known to produce catalysts with more nanoparticles rather than sub nanometer clusters, are less active than the CP (co-precipitation) catalysts agrees with the assumption that sub-nm clusters are important in co-precipitated catalysts.

Also observed during the STEM analysis of the TMU catalyst was the growth of the catalyst particles after heat treatment, with the particles growing from around 5 nm to 40 nm after calcination at 300 °C for 3 h. During the heating process the Cardiff sample showed much smaller growth than the TMU sample with catalyst particles growing to 15 – 20 nm. The TMU catalyst also showed different morphology changes during the calcination procedure - on heating, internal pores were observed to develop in the catalyst, whereas these pores were not observed in the Cardiff sample.

5.7.2 - Investigation of atomic and sub-nm Au species in Au / FeO_x catalysts

The STEM investigation carried out had sufficient resolution to identify atomic Au and sub nanometer clusters on the catalysts. To further refine the particle size distributions to include the structure of the sub nanometer clusters and classify the amount of monolayers and bilayers, a single atom has to be used as a reference and the brightness of the nearby cluster can then be identified as either a monolayer or bilayer. During this process it was noticed that the brightness of the single atoms varied greatly along with the brightness of the clusters. This indicated that not all of the atomic Au was equivalent and what was thought to be surface atomic Au and clusters may in fact be sub surface or even embedded into the lattice. It has been observed previously that when preparing catalysts by co-precipitation methods Au can become trapped in

the support structure.[11] To investigate the morphology of the bulk of the catalyst particles STEM was carried out by focusing through catalyst particles. It had been previously shown that on calcination the TMU samples formed some internal pores and it was thought that these pores could be where the sub surface Au was located. A number of STEM images were recorded by focusing the beam at different depths through the catalyst particles as shown by the schematic and images in figure 5.16.

As the electron beam is focused through the sample Au species can be seen throughout the sample, indicating that a large amount of Au is trapped in the support material including sub surface atomic Au and also sub surface Au clusters. As the beam is focused into the pore in the centre of the particle it is possible to clearly see the outline of the pore because of the high number of Au species. As the beam is focused through the sample to the underside of the particle Au species on the underside of the particle come into focus. These images indicate that there was a large amount of sub surface Au present in all of the catalysts, much more than was previously thought. The presence of these sub surface Au species makes the identification of monolayers and bilayers challenging as overlap of surface and subsurface Au makes the identification by brightness difficult. The same features were seen across all catalyst samples which indicates that the populations measured for atomic and cluster features are likely to be greatly affected by sub surface species being counted.

From the small number of clusters that could be confidently identified, it was seen that the majority were monolayer structures, agreeing with the work of Han[17] and Olson[18] who showed that the preferred structure of small Au clusters of around 8 atoms is to form planar structures, although not enough clusters could be assigned as monolayer or bilayer to confidently state that monolayers were the most abundant species for Au clusters.

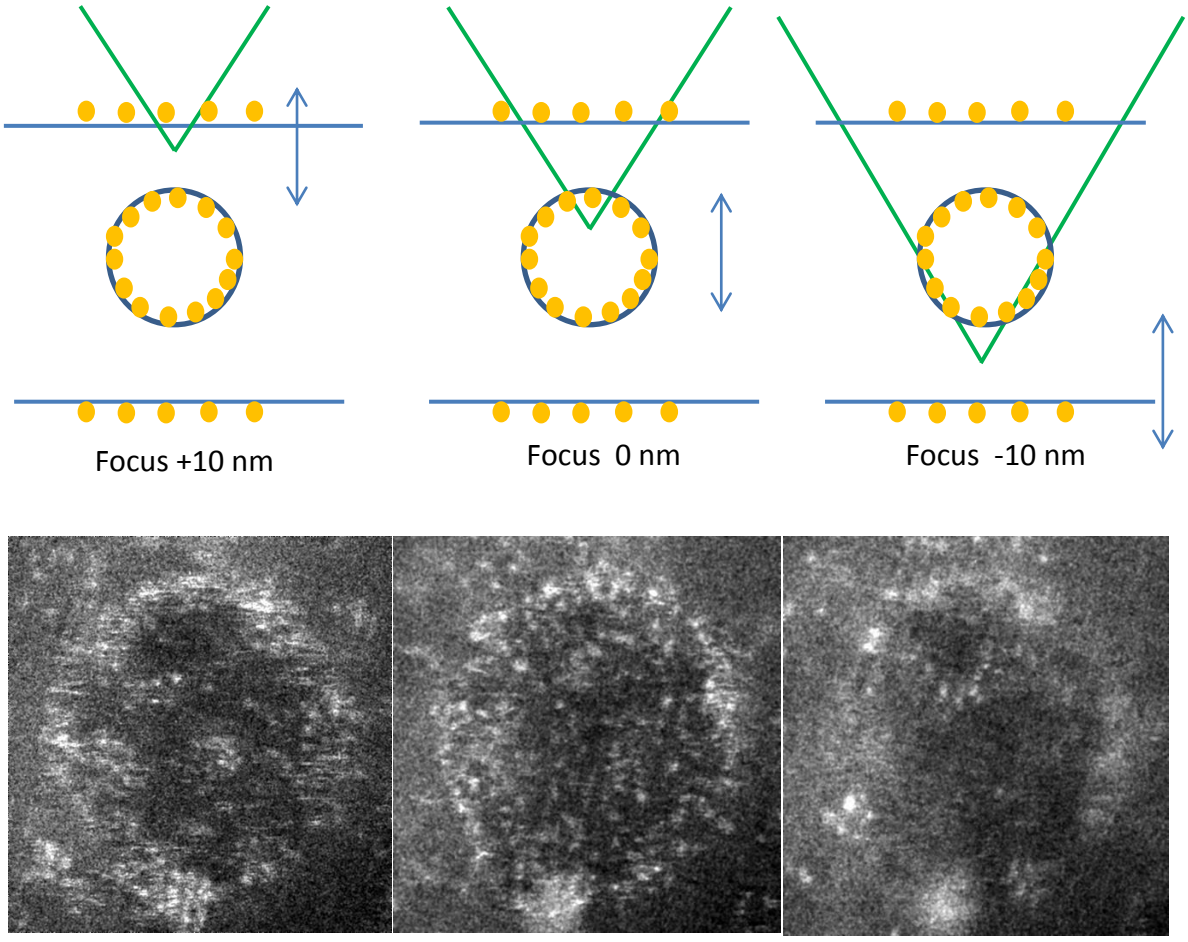

Figure 5.16 - STEM through focus images corresponding to the schematics above of the TMU calcined catalyst showing the distribution of atomic Au through a catalyst particle including an internal pore.

A more detailed analysis of the catalyst surface revealed a number of other Au environments. Along with surface clusters and sub-surface clusters, Au atoms were also observed to be positioned on the Fe sites of the inner support meaning that some atomic Au was substituting the Fe in the lattice, as shown by the red arrows in figure 5.17. These features will also complicate the statistics of the very small particles in the particle size distribution. For example, in terms of atomic Au there are: species trapped in pores which cannot do catalysis and are not counted in the statistics, species substituting Fe in the lattice which cannot do catalysis but which are counted in the statistics, and atomic species on the surface which may be catalytically important. A similar limitation applies to the sub nm clusters, as sub surface clusters either in pores or on the surface may both be counted in the statistics but only the clusters exposed on the surface will

be catalytically active. As nano particles are much less likely to be trapped in the support the particle size distributions for the particles > 1 nm are more reliable.

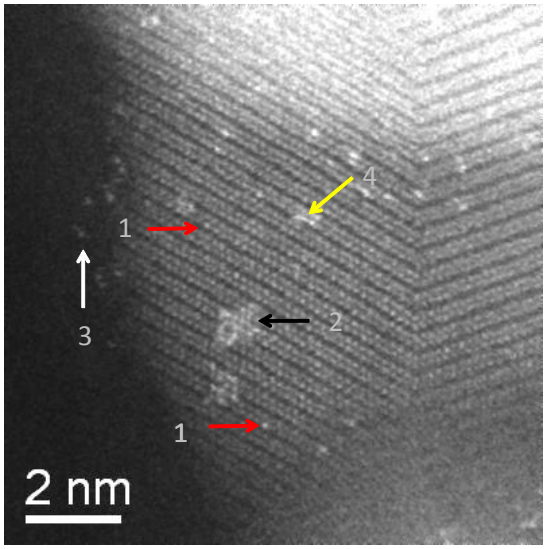

Figure 5.17 – STEM images of the TMU calcined catalyst showing the different atomic Au environments: arrow 1 indicates Au substituted into the lattice, arrow 2 indicates a surface cluster, arrow 3 indicates Au species in an amorphous surface layer and arrow 4 indicates a subsurface cluster.

5.7.3 - Investigation of the surface of Au / FeO_x catalysts

Following the observations that Au species could be observed either on the surface, sub surface or substituted into the surface of the iron oxide support of the catalysts, a more detailed investigation of the catalyst surface was undertaken. The aim was to identify the morphology of the catalyst surface and in particular to identify if a different support morphology was responsible for the identification of apparent Au particles sitting slightly above the observed crystalline phase, as indicated by the white arrow in figure 5.17. Initially XPS analysis was carried out on all four samples to investigate the oxidation state of the Fe in the uppermost surface of the support. The Fe (2p) XPS spectra are shown in figure 5.18 and show that they mainly consist of Fe^{3+} as indicated by the peaks at binding energy 711 and 725 eV. However the main peak at 725 eV shows an asymmetry in all of the samples as indicated by the dashed line at lower binding energy which indicates that there is a small Fe^{2+} component in the surface of the catalyst support. There is little evidence of the development of a satellite for Fe^{2+} expected at 715 eV although this would be very weak and could easily be masked by the Fe^{3+} peak tail. No

evidence has been found in the literature that X-rays can induce the reduction Fe^{3+} to Fe^{2+} in haematite during XPS measurements.

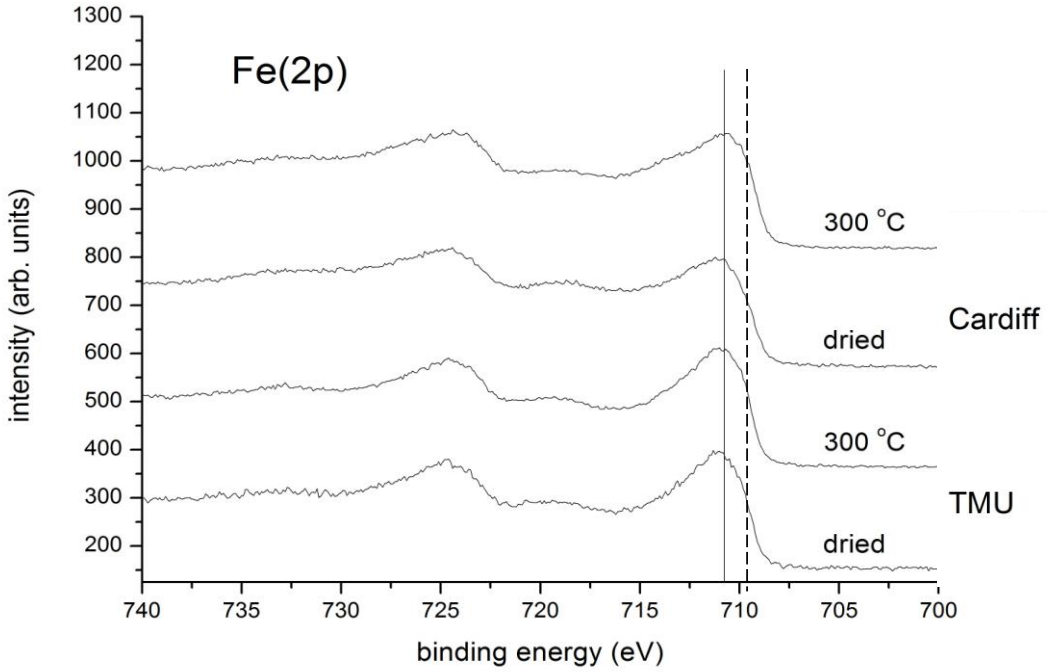

Figure 5.18 - Fe (2p) XPS spectra of 5% Au / FeO_x catalysts prepared by Cardiff and TMU methods after drying and calcination at 300 °C for 3 h.

To confirm the presence of a more reduced Fe species in the surface of the catalyst electron energy loss spectroscopy (EELS) was carried out at Oak Ridge National Laboratory by Dr Wu Zhou. By comparing the ratio of the Fe L_3 : L_2 peaks it is possible to identify if a more reduced surface is present in the catalysts. The EELS spectra of the TMU calcined sample are shown in figures 5.19 - 5.21. The spectra shown in figure 5.19 indicate that the surface spectrum is indeed different from the bulk spectrum. A lower L_3 : L_2 ratio for the surface when compared to the bulk indicates that the surface is likely to contain some Fe^{2+}. The image that the EELS spectra were taken from in fact shows the presence of the surface layer which contains a more reduced form of Fe, as indicated in the white box, and seems to be much more amorphous than the Fe_2O_3 layer identified as the bulk phase by XRD analysis.

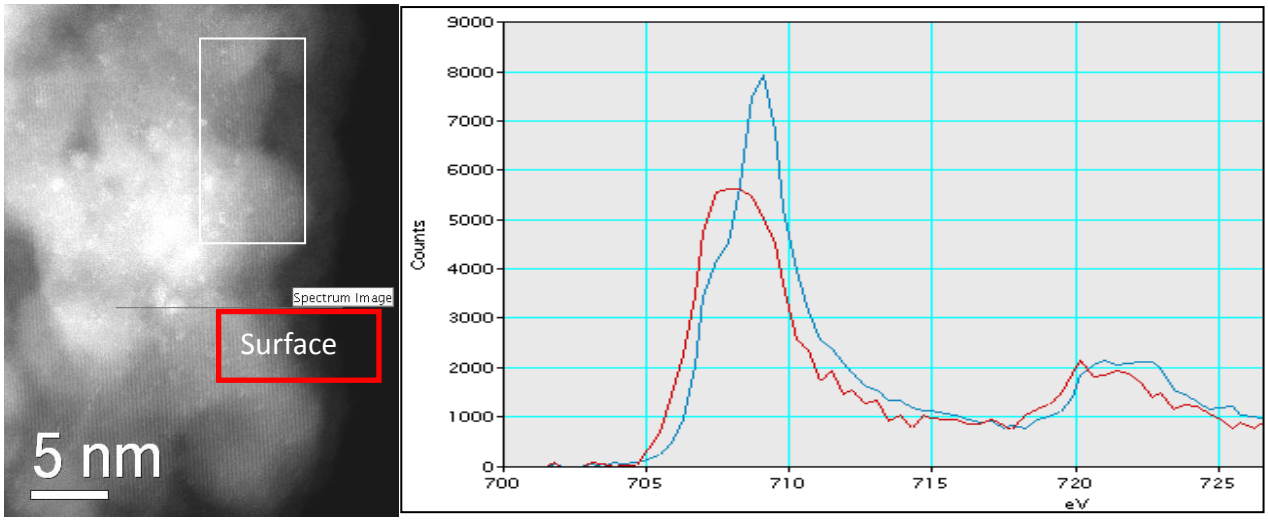

Figure 5.19 – EELS spectra comparing the nature of the surface of the FeO_x support to the bulk for the TMU calcined catalyst. The blue line shows the bulk spectrum and the red line shows the surface spectrum.

To investigate if the bulk structure was effected by the presence of a Au particle on the surface, EELS spectra were recorded of the bulk material both next to and away from an Au nano particle and compared with the surface spectrum of the support. As shown in figure 5.20, the bulk structure was identical both near to and away from the Au nanoparticles and indicated that the material consisted of Fe^{3+}which corresponds to the Fe_2O_3 observed in the bulk techniques such as XRD. The surface was again observed to contain some Fe^{2+} which was an amorphous phase. The layer was measured to be 2-3 nm thick and likely to be FeO – OH when the O_2 fine structure is compared to the literature. [19]

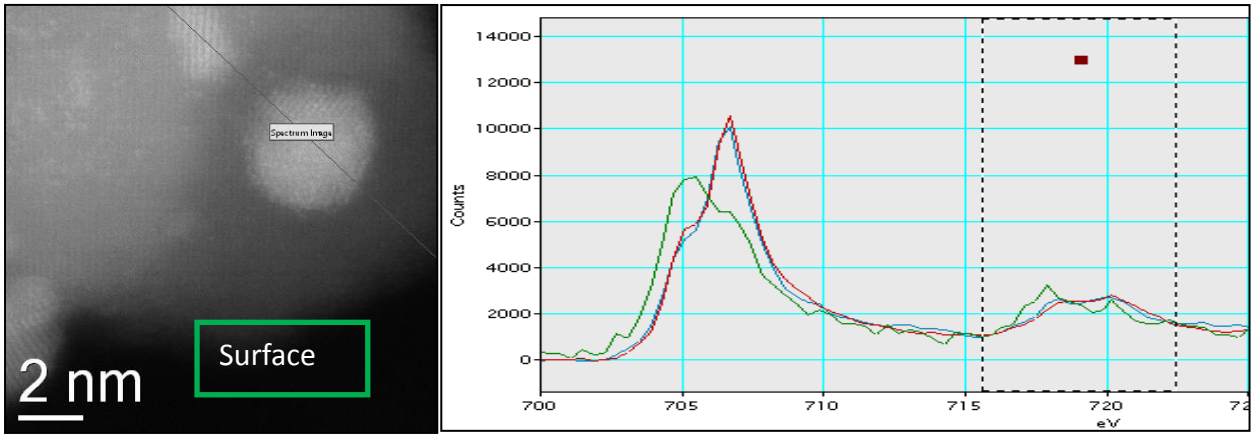

Figure 5.20 - EELS spectra comparing the nature of the surface FeO_x to the bulk either near to or away from a Au nanoparticles of the TMU calcined catalyst. The blue line shows the bulk spectrum near a nanoparticle, the red line shows the bulk spectrum away from a nanoparticle and the green line shows the surface spectrum.

To investigate if the Au particles induced the surface reduction of the FeO_x, EELS spectra were recorded of the surface of the catalyst both near to and away from a Au particle and compared to the bulk; the spectra are shown in figure 5.21. It can be seen that the catalyst surface is uniform and contains Fe^{2+} irrespective of its proximity to the Au nanoparticles. There have been no published reports to indicate the electron beam could be responsible for the surface reduction of the Fe support, and the fact that a shoulder is seen in the XPS spectra of all four samples shows agreement with the EELS spectra and suggests that the surface reduction is not an artefact of the characterisation techniques. These spectral features were seen in all of the catalyst samples investigated, indicating that it was not preparation method dependent. The presence of reduced Fe centres in the surface of the support could be the reason for the high activity of the FeO_x supported catalysts. It has been widely reported in the literature that Au on reducible supports such as TiO_2, CeO_2 and FeO_x are the best CO oxidation catalysts because the catalyst is capable of reversibly activating O_2 using the slightly reduced Fe layer at the surface. The catalytic rate of CO oxidation may be enhanced by the presence of this activated O_2 near the Au nano particles. As has been shown earlier in the kinetic data, the rate determining step in the reaction seems to be the activation of CO, as indicated by the reaction being first order with respect to CO concentration; this indicates that activation of O_2 is fast as the reaction rate does not depend on O_2 concentration. This may be because of the ability of the observed amorphous layers to activate O_2 easily and supply the Au particles with O_2 to carry out the reaction.

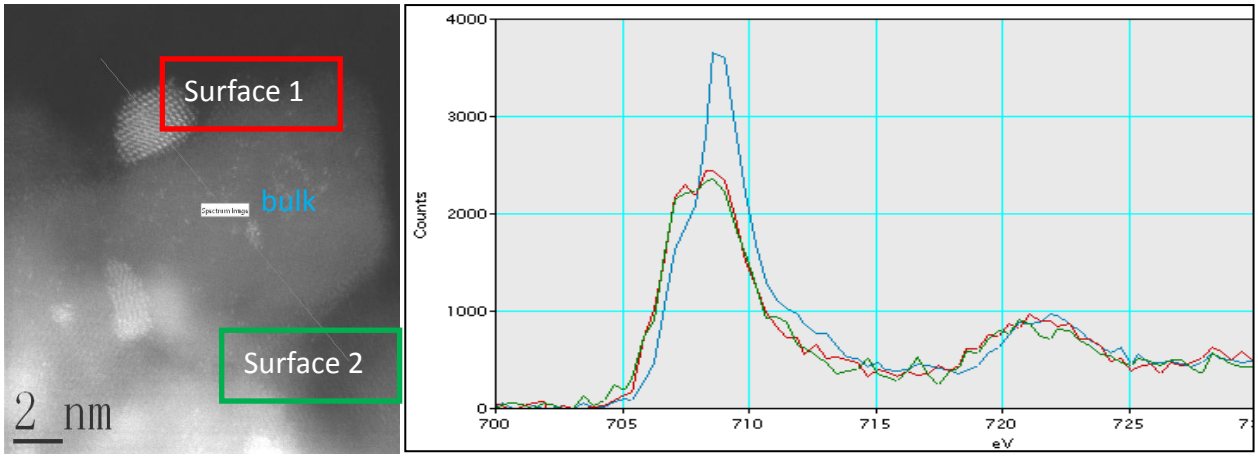

Figure 5.21 - EELS spectra comparing the nature of the surface FeO_x either near to or away from Au nanoparticles with the bulk structure. The blue line shows the bulk spectrum , the red line shows the surface spectrum near a nanoparticle and the green line shows the surface spectrum away from a nanoparticle.

The origin of the reduced layer is uncertain at this point, although it has been shown not to affect the catalytic activity in the catalysts studied. A very active catalyst was calcined for an extended period of time at 300 °C to induce very low activity. EELS measurements were carried out on this sample and the presence of the 2-3 nm amorphous layer was still seen.

5.8 - Discussion and Proposed Explanation

The four catalysts tested were shown to have very different activity for the low temperature oxidation of CO; below 60 °C it has been shown that they all have the same activation energy of around 30 kJ mol^{-1} and the rate of reaction depends linearly on CO concentration and is independent of O_2 concentration. This observation suggests that at low temperatures all of the catalyst samples share the same active site and the populations of the active sites are responsible for the difference in activities. Particle size distributions suggest that above 60 °C it is possible to correlate the populations of nanoparticles of size ~ 5 nm to the CO oxidation activity. No correlation between nanoparticles population could be made for the activity below 60 °C, which suggests that smaller sub nanometer cluster may be the dominant active species at low temperatures.

The problem with correlating the PSDs for the sub nanometer clusters is that some of the sub nanometer clusters and isolated atoms were found trapped in the support lattice but were still

counted in the PSD as is difficult to distinguish surface from sub surface atomic and sub nanometer clusters. However due to the lack of internal pores in the catalysts apart from the calcined TMU catalyst, nanoparticles should be all on the outer surface of the support meaning that the nanoparticle PSDs will not be effected by this problem as it is unlikely that they can form inside internal pores.

It was reported by Allard *et al.*[20] that for Au / FeO_x systems prepared by co-precipitation the evolution of Au particles during heat treatments could play a key role in the catalysis. By studying a leached Au / FeO_x catalyst using an *in-situ* STEM fitted with a sample heater, they firstly observed many sub-surface Au clusters buried in the support and mainly associated with internal pores similar to those observed in the calcined TMU catalyst. Also, many small Au species were also identified without significant sign of internal pores, indicating that they were trapped in the haematite lattice of the support. During heat treatment at 500 °C for various times between 2 – 15 mins, the Au species were seen to migrate toward the surface and re-form small Au nanoparticles on the surface. This explained the observed reactivation of the leached catalysts in this study after heat treatment and also agreed with XPS result showing an increase of Au surface content after heat treatment. [20, 21]

Based on the characterisation and testing data obtained it is possible to suggest a mechanism based on the evolution of sub-surface Au during heat treatment. Due to the different preparation methods employed, the TMU dried catalyst consists of a haematite support with lots of atomically dispersed species; however, as was shown earlier using STEM, by focusing through the catalyst particle many of these are sub surface and therefore do not contribute to the catalysis. Due to a high number of species being sub surface, even though the PSD shows that the TMU dried catalyst has a higher number of clusters than the Cardiff dried sample not all of them may be involved in the catalysis. The Cardiff dried sample in contrast consists of ferrihydrite and has fewer atomic and sub nanometer Au species, meaning that there are less sub surface Au species. The identical activity of the dried samples could arise from having similar numbers of sub nanometer Au species on the surface despite the PSDs showing the TMU sample had a greater number as this included a large number of sub surface species.

On calcination the haematite particles in the TMU dried catalyst start to sinter to form bigger particles with internal pores. Also during heat treatment, atomically dispersed Au species that are buried sub surface in the lattice will diffuse out to the surface of the catalyst particle while a competing sintering process occurs on the surface. Small particles on the surface will start to grow

through agglomeration with other surface particles to generate larger nanoparticles. Some atoms will also diffuse into the internal pores, where they seem to be stabilised, which is the reason for the high particle density inside the pore as seen previously in the through-focus images. The overall result is the presence of more sub nanometer clusters on the surface of the TMU calcined catalyst by migration from the sub surface, and it is these species that are dominant for the oxidation of CO below 0 °C. A schematic is shown in figure 5.22.

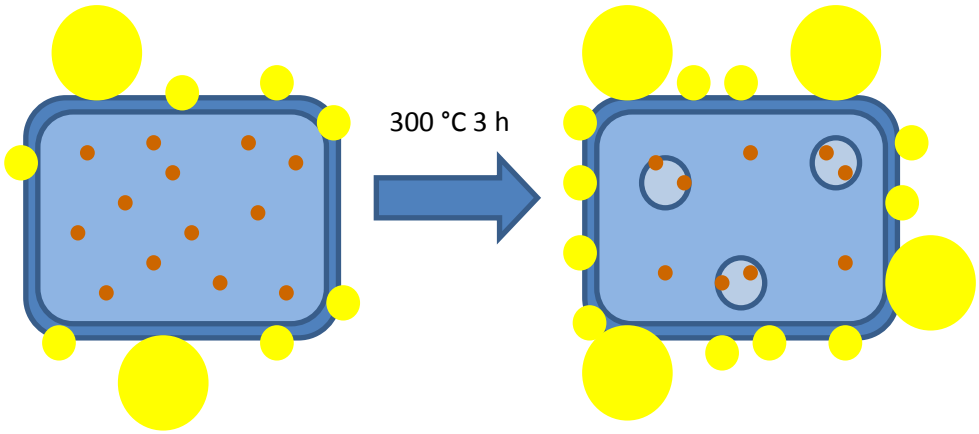

Figure 5.22 - Schematic representation of the evolution of Au species in the TMU catalyst during calcination. ● - Subsurface Au species, ● - Surface Au species, ■ - bulk haematite phase and ■ - surface amorphous Fe phase.

In contrast, the support particle for the Cardiff dried samples does not undergo significant sintering with the formation of no internal pores during heat treatment. As was seen in the PSD the number of atoms and sub nanometer particles is much lower than the TMU catalyst and because of the competing agglomeration during the calcination process the overall number of exposed sub nanometer clusters is much less than in the dried state, with an increase in the number of nano particles > 1 nm. The rate of agglomeration may also be increased by the smaller grain size of the Cardiff catalyst because the sub surface particles will have a shorter distance to migrate to the surface meaning more time to agglomerate into bigger particles when they reach the surface. The hypothesis is illustrated in figure 5.23. This hypothesis fits well with the observed catalytic and characterisation data as well as observations in the literature about the migration of Au and reactivation of catalysts in the literature that have undergone leaching.[20, 21]

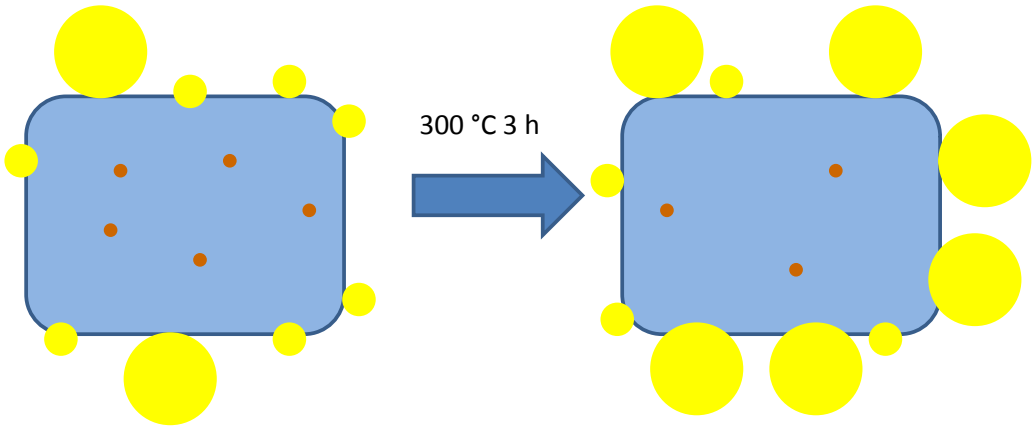

Figure 5.23 - Schematic representation of the evolution of Au in the Cardiff catalyst during calcination. ● - Subsurface Au species, ● - Surface Au species, ■ - bulk haematite phase and ■ - surface amorphous Fe phase.

5.9 – Conclusions

Since the discovery that Au catalysts showed exceptional rates for CO oxidation it has become one of the most studied reactions in heterogeneous catalysis. There has been much debate in the literature about the nature of the active site and this study brought together three leading groups in Au catalysis to try and improve the understanding of CO oxidation in Au / FeO_x systems. This was carried out by undertaking kinetic studies of catalysts prepared in both Cardiff and Tokyo Metropolitan Universities to try and identify similarities and differences. Extensive characterisation using STEM in an attempt to determine complete particle size distributions ranging from 10 nm particles down to single atomic species for a number of catalysts was carried out. Despite numerous attempts the preparation method of Au/FeOx from Tokyo which results in a catalyst that improves on calcination could not be repeated in Cardiff. The only difference in the preparation that could not be repeated is the washing by centrifuge, catalysts prepared in Cardiff were observed by ICP to contain a higher level of chloride and sodium which could be the reason for the deactivation of the Cardiff catalysts due to the promotion of sintering of Au particles. Through a detailed analysis of catalysts prepared in Cardiff and Tokyo using STEM, XPS and EELS a number of new interesting features were observed including the presence of an amorphous slightly reduced iron oxide layer which is present on the outer 2-3 nm of the catalyst particle. A correlation between particles size distributions and activity suggested that the activity above 60 ºC could be correlated with Au particles around 5 nm in size. No correlation between these particles and the activity at sub ambient temperatures could be made which suggests that nanoparticles are not the active species in this temperature regime and questions the published literature which

suggests that nanoparticles ~2-3 nm are the active site. It is speculated that sub nanometer clusters may be the most active species below ambient temperature although in this study sub surface Au made the quantification of these species difficult.

The presence of a high proportion of sub surface Au was observed in the catalysts along with Au species substituting Fe in the lattice. The higher than expected sub surface clusters was proposed as the reason why TMU catalysts become more active as the Au particles migrate to the surface on calcination whereas the Cardiff catalysts, which has many fewer sub surface Au species, lose activity through sintering of Au particles. These results require further experiments to be designed to prove the hypothesis that sub nanometer clusters are the most active species at sub ambient temperatures. These include detailed STEM analysis after catalysts have had their nanoparticles removed by methods such as cyanide leaching. Alternatively preparation methods need to be carefully designed to produce even tighter particle size distributions to deconvolute the activity distribution from the particle size distribution. Another area which should be investigated methodically using STEM is the morphology of the Au particles to try and identify the most stable Au particle shape and also identify any Au particles shape dependency on the reaction rate.

5.10 – References

1. M. Haruta, T. Kobayashi, H. Sano and N. Yamada, *Chem. Lett.*, 1987, 405 - 408.

2. M. Haruta, S. Tsubota, T. Kobayashi, H. Kageyama, M. J. Genet and B. Delmon, *J. Catal.*, 1993, **144**, 175-192.

3. J. K. Edwards, B. Solsona, P. Landon, A. F. Carley, A. Herzing, M. Watanabe, C. J. Kiely and G. J. Hutchings, *J. Mater. Chem.*, 2005, **15**, 4595-4600.

4. N. Lopez, T. Janssens, B. Clausen, Y. Xu, M. Mavrikakis, T. Bligaard and J. Norskov, *J. Catal.* 2004, **223**, 232-235.

5. G. C. Bond and D. T. Thompson, *Gold Bull.*, 2000, **33**, 41-51.

6. M. S. Chen and D. W. Goodman, *Science*, 2004, **306**, 252-256.

7. A. A. Herzig, C. J. Kiely, A. F. Carley, P. Landon and G. J. Hutchings, *Science*, 2008, **321**, 1331 - 1335.

8. U. Landman, B. Yoon, C. Zhang, U. Heiz and M. Arenz, *Top. Catal.* 2007, **44**, 199.

9. Y. Liu, C. J. Jia, J. Yamasaki, O. Terasaki and F. Schuth, *Angew. Chem., Int. Ed.* 2010, *49*.

10. R. Finch, N. Hodge, G. Hutchings, A. Meagher, Q. Pankhurst, M. Siddiqui, F. Wagner and R. Whyman, *Phys. Chem. Chem. Phys.*, 1999, **1**, 485-489.

11. N. Hodge, C. Kiely, R. Whyman, M. Siddiqui, G. Hutchings, Q. Pankhurst, F. Wagner, R. Rajaram and S. Golunski, *Catal. Today*, 2002, **72**, 133-144.

12. J. K. Edwards, B. E. Solsona, P. Landon, A. F. Carley, A. Herzing, C. J. Kiely and G. J. Hutchings, *J. Catal.* 2005, **236**, 69-79.

13. I. Dobrosz-Gomez, I. Kocemba and J. M. Rynkowski, *Appl. Catal. B: Environ.*, 2009, **88**, 83-89.

14. H. H. Kung, M. C. Kung, and C. K. Costello, *J. Catal.* 2003, **216,** 425-431.

15. M. Haruta, *Faraday Discuss.* 2011, **152**, 11-32.

16. M. Date and M. Haruta, *J. Catal.* 2001, **201**, 221-224.

17. Y. Han, *J. Chem. Phys.* 2006, **124**.

18. R. M. Olson, S. Varganov, M. S. Gordon, H. Metiu, S. Chretien, P. Piecuch, K. Kowalski, S. A. Kucharski and M. Musial, *J. Am. Chem. Soc.*, 2005, **127**, 1049-52.

19. D. Mavrocordatos and D. Perret, *J. Microscopy*, 1998, **191,** 83-90.

20. L. F. Allard, A. Borisevich, W. Deng, R. Si, M. Flytzani-Stephanopoulos and S. H. Overbury, *J. Electron Microscopy*, 2009, **58**, 199 - 212.

21. W. Deng, C. Carpenter, N. Yi and M. Flytzani-Stephanopoulos, *Topics in Catal.*, **2007**, *44*, 199-208.

Chapter 6

Conclusions and Future Work

As already discussed in Chapter 1, the current method for the industrial production of H_2O_2 is the anthraquinone process. Although this process displays many advantages such as high H_2 selectivity the required continual replacement of organic solvents and the fact that is uneconomic at small scales is driving the development of a catalytic direct synthesis process. The synthesis of H_2O_2 from molecular H_2 and O_2 represents a challenging catalytic reaction as the subsequent hydrogenation of the synthesised H_2O_2 needs to be avoided to achieve the high selectivities (+ 95%) required for an industrial process. Also the subsequent decomposition of H_2O_2 which may be again catalysed by the same catalysts used to synthesise H_2O_2 needs to be avoided. These problems can be addressed either by catalyst design through careful control of reaction conditions. Both approaches have been investigated in this work through the investigation of alternatives to the best Au-Pd catalysts using Pd – Sn as an alternative (Chapter 3) and the design and construction of a fixed bed reactor to allow the study of reaction conditions independently (Chapter 4). The results obtained in these chapters investigating the direct synthesis of H_2O_2 show very promising results and the conclusions reached in these chapters show that the direct synthesis process is an exciting prospect that has a significant chance of being a successful process in the future as well as providing an interesting and challenging reaction to learn about catalysis.

Chapter 3 reports an investigation into an alternative to the current Au-Pd catalyst system. The methodology developed in this work concerning the catalyst preparation of Sn-Pd catalyst

systems show a big step forward in the development of catalysts for the direct synthesis of H_2O_2 and a number of key milestones in the field were achieved. Firstly the synthesis of catalysts that show activity of similar magnitude to analogue Au-Pd catalysts but have replaced Au with a cheap base metal like Sn, makes the system much more attractive form an industrial perspective in terms of cost. Also the observation that Au is not unique in promoting the reaction could lead to extensive research into other metals that could show similar effects in reducing the hydrogenation activity of Pd catalysts. The use of Sn - Pd to prepare a catalyst on SiO_2 which is stable to multiple uses represents an advantage over using the Au-Pd system which has been shown to lose Au during the reaction and is therefore unstable. The heat treatment cycles developed during this research have been able to generate Sn-Pd species that are stable on SiO_2 to the reaction conditions and multiple cycles of the reaction conditions along with TiO_2 catalysts which are also stable.

Most importantly the catalysts developed in chapter 3 show no hydrogenation/decomposition activity towards H_2O_2 under our reaction conditions. These catalysts are only the second example of this to be reported and the first example on commercially available SiO_2 and TiO_2 supports without prior modification. The fact that the catalysts do not include Au as the means of increasing the selectivity towards H_2O_2 represents a big milestone in the process. As it has now been shown that Au can be replaced in the catalysts future work should be undertaken to identify possible alternatives to Pd, and the approach should be taken to reduce the hydrogenation activity of a catalyst rather than start from materials with low hydrogenation activity. The future possible development of a base metal only catalyst makes the process even more attractive.

The work described in chapter 4 concerns the synthesis of H_2O_2 in a fixed bed flow reactor capable of carrying out synthesis reactions at low pressure (10 bar). During the construction and design of the reactor it was observed that a vertical reactor orientation was preferential in terms of H_2O_2 productivity and reproducibility of results. Reaction conditions were systematically studied with short residence times, low temperatures and high pressures being shown to be beneficial for H_2O_2 synthesis. H_2O_2 productivity showed an asymmetrical dependency on $H_2 : O_2$ as had been previously observed in the batch system as a result of the high hydrogenation activity of the catalyst at high H_2 concentrations. It was shown that it was possible to achieve high selectivity (80 %) by increasing the flow of solvent through the catalyst bed although this reduced the concentration that could be achieved. The reactor set-up also allowed rate constants to be determined for the decomposition, hydrogenation and synthesis reactions and these values were combined into a basic kinetic model to predict the H_2O_2 concentration that would be

obtained. The model was able to give a good prediction of the effect of $H_2 : O_2$ which matched closely the experimental results and also showed that the decomposition reaction had a dramatically limiting effect on the concentration of H_2O_2 that can be synthesised.

Following the construction and operation of the fixed bed reactor a number of further kinetic studies can now be undertaken, including determination of activation energies, isotopic effects in the feed gases and this equipment can be further extended to the study of *in-situ* oxidation of organic spices using the –OOH species generated during reaction. The next phase in the development of the process should focus on the development of a high pressure system to focus on the synthesis of higher concentrations of H_2O_2.

The oxidation of CO using Au catalysts is possibly the most studied reactions in heterogeneous catalysis. Chapter 5 aimed to further investigate the active site for CO oxidation using Au / FeO_x catalysts. This was carried out by undertaking kinetic studies of catalytic activity along with extensive characterisation using STEM in an attempt to determine complete particle size distributions ranging from 10 nm particles down to single atomic species for a number of catalysts. This work was carried out in collaboration with Prof. Haruta of Tokyo Metropolitan University and Prof. Kiely of Lehigh University. Through a detailed analysis of catalysts prepared in Cardiff and Tokyo a number of new interesting features were observed including the presence of an amorphous slightly reduced iron oxide layer which is present on the outer 2-3 nm of the catalyst particle. The presence of a high proportion of sub surface Au was observed in the catalysts along with Au species substituting Fe in the lattice. The higher than expected sub surface clusters was proposed as the reason why TMU catalysts become more active on calcination where as the Cardiff catalysts lose activity through sintering of Au particles. Through a detailed particle size analysis it was possible to correlate activity above 60 °C with the presence of nanoparticles around 5 nm in diameter but not low temperature activity which challenges the theory that nanoparticles are the most active species below ambient temperatures. These results require further experiments to be designed to prove the hypothesis that sub nanometer clusters are the most active species at sub ambient temperatures. These include detailed STEM analysis after catalysts have had their nanoparticles removed by methods such as cyanide leaching. Alternatively preparation methods need to be carefully designed to produce even tighter particle size distributions to deconvolute the activity distribution from the particle size distribution.

Appendix 1 – Determination of Reaction Rate from Flow Reactors

Fundamental Equations for Plug Flow Reactor

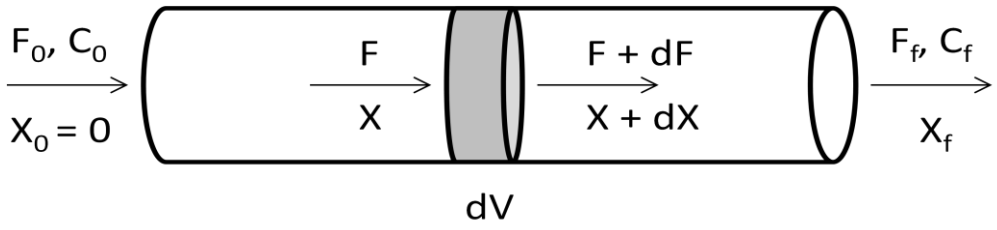

Definitions

F = Flow Rate of Reactant

r = Reaction Rate

C = Concentration of Reactant

V = Volume of Catalyst Bed

X = Conversion of Reactant

$_0$ = initial $_f$ = final

Flow at inlet = Flow at outlet + rate of conversion

$$F = (F + dF) + r\,dV \quad (1)$$

$$F = F_0 (1-X) \quad (2)$$

$$\text{Therefore } dF = d[F_0 (1-X)] = -F_0 dX \quad (3)$$

Substituting equation (3) into (1) gives

$$F_0 dX = r dV \quad (4)$$

Integrating the equation $\int_0^V \frac{dV}{F_0} = \int_0^{X_f} \frac{dX}{r}$ (5) considering that V and F_0 are constant gives

$$\frac{V}{F} = \int_0^{X_f} \frac{dX}{r} \quad (6)$$

where $\frac{V}{F}$ is equal to the reactant catalyst contact time

Assuming a differential reactor model where reaction rate is constant thorough the catalyst bed means that r in equation (6) is constant. Reaction rate may then be determined by integrating equation (6) to give

$$r = \frac{F}{V} . X \quad (7)$$